Paleobathymetry and Sediment Accumulation in the northern North Atlantic and southern Greenland-Iceland-Norwegian Sea

Dissertation

zur Erlangung des Doktorgrades

der Mathematisch-Naturwissenschaftlichen Fakultät

der Christian-Albrechts-Universität

zu Kiel

vorgelegt von

Christopher Ned Wold

Kiel

1992

Table of Contents

Zusammenfassung

Eine neue Methode zur Rekonstruktion der Massen/Alter-Verteilungen innerhalb eines geschlossenen Systems wird anhand veröffentlicher Daten für die globale Sedimentmasse vorgestellt. Die gesamte Sedimentmasse der Erde wird auf 2943.1 x 10^{21} g geschätzt. Die globale Sedimentmasse wird unterteilt in 2082.6 x 10^{21} g im Phanerozoikum, 845.5 x 10^{21} g im Proterozoikum und 15 x 10^{21} g im Archaikum.

Die rekonstruierten Sedimentmassen während des Phanerozoikums scheinen eine Periodizität von 150 Mio. Jahren zu haben mit Maxima im Kambrium, Devon, Perm und der Kreide. Verstärkte Heraushebung und das Klima sind die wichtigsten Faktoren, die die erhöhten Erosions- und Ablagerungsraten kontrollieren. Episoden globaler Heraushebungen und Orogenese sollten in schnelleren Raten des Sedimentrecyclings resultieren, die als Zeiten erhöhter Sedimentionsraten beobachtet werden. Es ist wahrscheinlich, daß die Massen/Alter-Verteilung und die rekonstruierten phanerozoischen Sedimentionsraten den Ausdruck langandauernder Mantelkonvektionen an der Oberfläche darstellen. Die devonischen, permischen und kretazischen Maxima sind alle mit Superplume-Ereignissen korreliert.

Als Datengrundlagen für Testmethoden zur Rekonstruktion der Paleobathymetrie und zur Analyse der Sedimentakkumulation wurde die känozoische Stratigraphie des nördlichen Nordatlantiks und der südlichen Grönland-Island-Norwegen-See auf der Basis eines 1 x 1° Netzes kompiliert. Massen/Alter-Verteilungen im Untersuchungsgebiet geben einen Einblick in seine geologische Geschichte. In diesem Gebiet gab es während des gesamten Känozoikums vier getrennte Tröge für vier verschiedene Herkunftsgebiete. Die vier verschiedenen Tröge erstrecken sich vom Rand des Britischen Schelfs zum Reykjanes-Rücken, vom Reykjanes-Rücken zum Ost-Grönland-Schelf, vom Ost-Grönland-Schelf zum Jan-Mayen-Rücken und vom Jan-Mayen-Rücken zum Faröer-Shetland-Escarpment. Regionale Massen/Alter-Verteilungen zeigen, daß die neogene Sedimentation im Rockall-Trog und im Süd-Island-Becken von der Ablagerung von Sediment-Driftkörpern dominiert wurde. Es gab eine verzögerte Reaktion zwischen dem Beginn des sea-floor spreading und der Zeit des maximalen Sedimenteintrages in das Irminger Becken, verursacht durch die Änderung in der Neigung der regionalen Topographie in Ost-Grönland. Die höchsten känozoischen

Sedimenationsraten traten vor Ost-Grönland am westlichen Rand des Island-Plateaus auf. Die Sedimentationsraten in Norwegen-Becken waren durchgehend die niedrigsten im Untersuchungsgebiet.

Die Paläobathymetrie des Untersuchungsgebietes wurde für die letzten 50 Mio. Jahre rekonstruiert. Die Rekonstruktionen verbinden Backstripping mit plattentektonischer Modellierung. Zwei verschiedene Modelle wurden getestet. Eines unter der Annahme, daß kretazisches Rifting oder Kontinentdehnung den Rockall-Trog und den Faröer-Shetland-Kanal geöffnet hat, das andere unter der Annahme, daß die Rockall-Faröer-Region in der Kreide geriftet wurde und anschließend im oberen Paläozän durch die Erwärmung der Lithosphäre durch den Mantelplume des Island-Hotspots herausgehoben wurde. Die modellierte Paläobathymetrie reagiert sehr sensitiv auf Annahmen bezüglich des thermischen Alters der Lithosphäre. Das hat wichtige Auswirkungen auf die Paläozeanographie. Der Ursprung des Bodenwassers im unteren Oligozän, das begann, den Feni-Driftkörper zu bilden, wurde dem arktischen Mittelschichtwasser zugeordnet, das durch den Faröer-Shetland-Kanal in den Rockall-Trog floß, obwohl eine tiefe Verbindung zwischen der Arktis und der Grönland-Island-Norwegen-See sich nicht vor dem Pliozän öffnete, und die tiefste Passage vom Faröer-Shetland-Kanal über den Grönland-Schottland-Rücken zum Süd-Island-Becken führte. Paläobathymetrische Rekonstruktionen, die auf zwei verschiedenen thermischen Entwicklungen für die Rockall-Faröer-Region basieren, ergeben neue potentielle Herkunftsgebiete für dichtes Wasser in unteren Oligozän. Das thermische Modell, das auf kretazischem Rifting des Rockall-Troges und des Faröer-Shetland-Kanals basiert, sagt einen breiten Schelf nördlich des Rockall-Troges im unteren Oligozän voraus, der ein Gebiet zur Bildung dichten Wassers gewesen sein könnte, falls das Gebiet kalt genug war. Das thermische Modell, das auf paläozäner Heraushebung durch Erhitzung der Lithosphäre beruht, ergibt ein flaches Rockall-Plateau in unteren Oligozän. Wenn hohe Verdunstungsraten über dem Rockall-Plateau bestanden, hätte sich dichtes Wasser durch erhöhte Salinität bilden können. Die Ausdehnung der Driftkörperbildung bis zum Süd-Island-Becken (Hatton-, Gardar- und Bjorn-Driftkörper) und der Westseite des Reykjanes-Rückens (Snorri-Driftkörper) im unteren Mittel-Miozän war wahrscheinlich das Ergebnis der Verlagerung des Bildungsortes des Tiefenwassers zu flacheren Gebieten auf dem Island-Faröer-Rücken. Nach der Bildung des flachen Schelfmeeres nordwestlich von Island hat sich eventuell der Strom durch die

Dänemark-Straße verstärkt, was in der Bildung des Eirik-Driftkörpers vor der Südspitze von Grönland resultierte.

Die Sediment-Driftkörper im nördlichen Nordatlantik haben eine wesentlich größere Ausdehnung als zuvor angenommen. Der Feni-Driftkörper ist der älteste Sediment-Driftkörper in dem Gebiet, der sich im unteren Oligozän bildete. Er wurde gefolgt von der Bildung der Bjorn-, Gardar-, Hatton- und Snorri-Driftkörper in unteren Mittel-Miozän. Eirik- und Gloria-Driftkörper begannen sich im unteren Pliozän zu bilden. Als Alternative zu der Hypothese, daß Wasser aus der Norwegen-See im unteren bis mittleren Miozän über den Island-Faröer-Rücken floß, schlage ich vor, daß sich dichtes Wasser entlang flacher Segmente des Island-Faröer-Rückens bildete und dann in das Süd-Island-Becken floß, um die Ablagerung der Bjorn-, Gardar- und Snorri-Driftkörper zu beginnen. Der Beginn der Bildung des Eirik-Driftkörpers wird zurückgeführt auf die Bildung eines flachen Schelfmeeres nordwestlich von Island vor etwa 5 Mio. Jahren. Dichtes Wasser, das sich auf dem Schelf nordwestlich von Island bildete, floß südlich durch die Dänemark-Straße und hat möglicherweise das Strömungsmuster westlich des Reykjanes-Rückens in der Art verändert, daß die Ablagerung des Gloria-Driftkörpers zur gleichen Zeit begann wie die des Eirik-Driftkörpers.

Megarippel auf Driftkörpern scheinen sich aus breiten, niedrig-energetischen Bodenwasserströmen entwickelt zu haben, während hoch- energetische Ströme in Driftsedimentation ohne Megarippeln resultierte.

Driftsedimentation dominierte die Art der Sedimentakkumulation zwischen dem Grönland-Schottland-Rücken und der Charlie-Gibbs-Fracture-Zone während des Quartärs und dem Pliozän. Während des oberen und mittleren Miozäns war die Driftsedimentation auf relativ kleine Gebiete des Süd-Island-Beckens und der Westseite des Rockall-Troges beschränkt. Während des unteren Miozäns und des Oligozäns war die Driftsedimentation auf die östlichen und südlichen Ränder des Rockall-Plateaus beschränkt. Während dieser Zeit ereigneten sich die überdurchschnittlichen Sedimentakkumulationen hauptsächlich auf dem sich entwickelnden mittelatlantischen Reykjanes-Rücken und dem Rockall-Plateau. Im Eozän waren die einzigsten Gebiete mit überdurchschnittlichen Sedimentationraten die regionalen Hauptsenken, der Rockall-Trog, die Porcupine-Tiefsee-Ebene und das Irminger-Becken.

Abstract

A new method for reconstructing sediment mass/age distributions within a closed system is demonstrated on published data for the global sediment mass. The total mass of sediment on the Earth is estimated at 2943.1 x 10^{21} g. The global mass is subdivided into 2082.6 x 10^{21} g of Phanerozoic, 845.5 x 10^{21} g of Proterozoic and 15 x 10^{21} g of Archaean sediments.

Reconstructed sediment fluxes during the Phanerozoic appear to have a 150 m.y. periodicity with maximum values in the Cambrian, Devonian, Permian and Cretaceous. Increased elevation and climate are the most important factors controlling increased rates of erosion and deposition. Global episodes of uplift and mountain building would result in more rapid rates of sediment recycling, observed as times of increased sediment flux. It is likely that the mass/age distribution and reconstructed fluxes of Phanerozoic sediment represent the surface expression of long-term mantle convection. The Devonian, Permian and Cretaceous peaks are all correlated to mantle superplume events.

To provide a database for testing methods of reconstructing paleobathymetry and analyzing sediment accumulation, the Cenozoic stratigraphy of the northern North Atlantic and southern Greenland-Iceland-Norwegian Sea was compiled on a 1 x 1° gridded database. Sediment mass/age distributions for the study area provide insight into its geological history. In this area there have been four separate sinks for four different source areas throughout the Cenozoic. The four different basins are the edge of the British shelf to Reykjanes Ridge, Reykjanes Ridge to the East Greenland shelf, the East Greenland shelf to Jan Mayen Ridge, and Jan Mayen Ridge to the Faeroe-Shetland Escarpment. Regional mass/age distributions show that Neogene sedimentation in the Rockall Trough and South Iceland Basin was dominated by deposition of sediment drifts. There was a delayed response from the initiation of sea-floor spreading to the time of maximum sediment input into the Irminger Basin, related to a change of slope of the regional topography in East Greenland. The highest Cenozoic sedimentation rates occurred off East Greenland on the western margin of the Iceland Plateau. Sedimentation rates in the Norway Basin were consistently the lowest of the study area.

The paleobathymetry of the study area has been reconstructed from 50 Ma to present. The reconstructions combine backstripping with plate tectonic modelling. Two different models were tested, one assuming Cretaceous rifting or continental extension that opened the Rockall Trough and Faeroe-Shetland Channel, and the other model assuming the Rockall-

Faeroe region rifted in the Cretaceous and was then uplifted in the late Paleocene due to heating of the lithosphere by the mantle plume of the Iceland Hotspot. The modelled paleobathymetry is very sensitive to assumptions regarding the thermal age of the lithosphere. This has important implications for paleoceanography. The source of early Oligocene bottom water that started forming Feni Drift has been attributed to Arctic intermediate water flowing through the Faeroe-Shetland Channel into Rockall Trough, although a deep connection between the Arctic and Greenland-Iceland-Norwegian Sea did not open until the Pliocene, and the deepest passageway from Faeroe-Shetland Channel across the Greenland-Scotland Ridge leads to the South Iceland Basin. Paleobathymetric reconstructions assuming two different thermal histories for the Rockall-Faeroe region offer new potential source areas for dense water in the early Oligocene. The thermal model based on Cretaceous rifting of the Rockall Trough and Faeroe-Shetland Channel without uplift in the Paleocene predicts a broad shelf north of Rockall Trough in the early Oligocene that could have been a site of dense water formation if the area were cold enough. The thermal model based on Paleocene uplift from reheating of the lithosphere, reconstructs a shallow Rockall Plateau in the early Oligocene. If high evaporation rates existed over Rockall Plateau dense water could have been formed through increased salinity. The expansion of drift formation to the South Iceland Basin (Hatton, Gardar and Bjorn Drifts) and west side of Reykjanes Ridge (Snorri Drift) in the early Middle Miocene was probably the result of a shift in the site of deep water formation to shallow areas on the Iceland-Faeroe Ridge. After development of the shallow shelf sea northwest of Iceland, flow through the Denmark Strait may have strengthened resulting in the formation of Eirik Drift off the southern tip of Greenland.

The northern North Atlantic sediment drifts have a much greater areal extent than has previously been indicated. Feni Drift is the oldest sediment drift in the region, originating in the Early Oligocene. It was followed by accumulation of Bjorn, Gardar, Hatton, and Snorri Drifts in the early Middle Miocene. Eirik and Gloria Drifts began to form in the Early Pliocene. As an alternative to the hypothesis of Norwegian Sea water overflowing the Iceland-Faeroe Ridge in the early-middle Miocene, I suggest that dense water formed along shallow segments of the Iceland-Faeroe Ridge and then flowed into the South Iceland Basin to begin accumulation of Bjorn, Gardar and Snorri Drifts. The initiation of sediment accumulation on Eirik Drift is attributed to the formation of a shallow shelf sea northwest of Iceland approximately 5 Ma. Dense water that formed on the shelf northwest of Iceland flowed south

through the Denmark Strait and may have altered circulation patterns west of the Reykjanes Ridge such that accumulation of Gloria Drift was initiated at the same time as Eirik Drift.

Sediment waves on the surface of drifts appear to be developed from more dispersed, low-energy bottom water flowing, while more energetic flow results in drift sedimentation without sediment waves.

Drift sedimentation has dominated the pattern of sediment accumulation between the Greenland-Scotland Ridge and the Charlie Gibbs Fracture Zone during the Quaternary and Pliocene. During the Late and Middle Miocene drift sedimentation was restricted to relatively small areas of the South Iceland Basin and to the western side of Rockall Trough. During the Early Miocene and Oligocene drift sedimentation was limited to the eastern and southern margins of Rockall Plateau. At this time the greater-than-average sediment accumulations occurred mostly on the developing mid-ocean Reykjanes Ridge and on Rockall Plateau. In the Eocene the only areas that had above-average sediment accumulation rates were the major regional depressions, Rockall Trough, Porcupine Abyssal Plain, and Irminger Basin.

Introduction

This work represents part of a project to understand the development of the North Atlantic and its adjacent seas. The ultimate goal is to reconstruct the configuration of the ocean basins and the adjoining continents through the Mesozoic and Cenozoic, and to determine the history of erosion and sedimentation throughout the region. The goal will be achieved in a series of stages, through creation of appropriate databases for the region and a modular computer program (BalPal) designed to analyze and perform operations on the data. BalPal is a collection of functions for balanced paleogeographic reconstruction. The software is written in the C-programming language and implemented with the UNIX computer operating system. The BalPal software package consists of separate modules that perform different tasks for paleogeographic modelling. The project consists of the following sequence of stages: 1) demonstrate that it is in principle possible to reconstruct ancient sediment fluxes within a closed system from the present mass/age distribution, in accordance with the law of conservation of mass; 2) compile and analyze a gridded stratigraphic database to determine mass/age distributions; 3) reconstruct regional paleobathymetry; 4) reconstruct the sedimentation history; 5) reconstruct the paleotopography and erosion history of the land areas; 6) reconstruct regional paleogeologic maps. This study is concerned with the first four topics; the last two have been worked out in theory but have not yet been programmed (Wold et al., in press; Hay and Wold, in press). Each chapter represents one of the stages listed above. The analysis at the end of each stage suggests how the next stage should be accomplished.

Reconstruction of paleobathymetry and paleotopography depends on knowledge of sediment fluxes in the past. If there is to be a closed solution to the problem of reconstructing ancient fluxes, it must be demonstrated that there is a unique and exact solution to the problem that adheres to the conservation of mass. In Chapter 1, "Reconstructing Ancient Mass/age Distributions and Sediment Fluxes," I develop a new method for determining the masses of sediment eroded and deposited through geologic time. The method requires that the erosion and deposition take place within a closed system. It is demonstrated using previously published global data sets for Phanerozoic sediments.

To determine how best to construct a database, I selected an oceanic area between Greenland and Europe to serve as a pilot study. This region comprises the northern North Atlantic, the Greenland-Scotland Ridge and the southern Greenland-Iceland-Norwegian (GIN) Sea. It was chosen because it is a passive margin environment with a complex history. It includes basins that formed at different times, from Cretaceous (Rockall Trough) to Cenozoic (South Iceland Basin, Irminger Basin, Iceland Plateau and Norwegian Basin). It includes three major sediment source regions: Western Europe-Scandinavia, Greenland, and the Greenland-Scotland Ridge. It has also had a complex sedimentary history, with pelagic and hemipelagic sediments occurring over much of the region and sediment drifts formed by bottom currents on the margins of the basins south of the Greenland-Scotland Ridge. Because of these complexities this region serves well as a base to test the computer modelling program (BalPal) for reconstructing the geographic and sedimentologic history.

Sediment mass/age distributions provide a synopsis of the geologic history of a region. Compilations of mass/age distribution data have usually relied on isopach maps for all of the stratigraphic units in a given region. Although this kind of information exists for large areas of some continents, it is only available for a few areas in the ocean basins. In Chapter 2, "Compilation and Analysis of Sediment Mass/age Distributions," I describe a method for compiling a gridded data base for estimating the masses of sediment of different ages. The gridded data base is constructed so that it will be compatible with methods to produce maps showing paleobathymetry and distributions of sediment within the region. Using the gridded data base I compile and analyze mass/age distributions for a number of regions in the study area. The pilot study area does not represent a closed system, so the method for reconstructing sediment fluxes developed in Chapter 1 cannot be applied. I demonstrate that each of the individual basins has a different mass/age distribution and that there are five main sinks for sediment within the region; most of these have been independent of each other throughout their history.

In order to visualize the changes that have taken place in this area in the past it is necessary to have a series of maps of the configuration and paleobathymetry of the region in the past. In Chapter 3, "Paleobathymetric Reconstruction on a Gridded Database," I describe a new palinspastic plate tectonic reconstruction method for the study area with four lithospheric plates. Using paleogeographic modelling software (BalPal) the gridded data is rotated according to the parameters of a plate tectonic model to its geographic position in the

past. The paleobathymetry of the region is then reconstructed by backstripping layers of sediment, restoring the underlying sediment to its condition prior to loading, removing the effects of thermal subsidence, taking into account eustatic sea level change, and ensuring that the reconstruction is in isostatic equilibrium. Two models for the thermal history are compared, the first assuming that the crust of the Rockall-Faeroes-Shetland area was heated only once, during the rifting episode in the Cretaceous, and the second assuming that the region was reheated shortly in the early Tertiary.

To evaluate the effects of the changes in plate tectonic configuration and paleobathymetry of the region on the sedimentary history, I interpret the history of the sediment drifts in Chapter 4, "Cenozoic Sediment Accumulations." Here I describe the modern bottom water circulation and then explore possible circulation patterns from the present to early Oligocene to test some of the conclusions reached in Chapter 3. Some of the best clues for pre-Pleistocene bottom water circulation in the North Atlantic can be obtained by studying sediment drifts. The largest sediment drifts in the study area are described in detail. Using the paleobathymetric reconstructions developed in Chapter 3, I model the distribution of sediment drifts through time. Finally the sedimentation history of the region is investigated using maps of the "apparent accumulation rates" of sediment. The apparent accumulation rate of sediment is the observed accumulation rate corrected for sea-floor spreading.

Summary of Main Conclusions

The new model for reconstructing sediment mass/age distributions in a closed system also reconstructs the original sediment fluxes exactly while conserving the total sediment mass. The new method is demonstrated on published data for the global sediment mass assuming that the Earth approximates a system closed to sediment recycling. This is reasonable if additions of new material from erosion of igneous and crystalline metamorphic rocks are exactly offset, on a timescale of millions of years, by the loss of sediment from the system to subduction and metamorphism. The total mass of sediment on the Earth is estimated at 2943.1×10^{21} g. The global mass is subdivided into 2082.6×10^{21} g of Phanerozoic, 845.5×10^{21} g of Proterozoic and 15×10^{21} g of Archaean sediments.

Reconstructed sediment fluxes during the Phanerozoic appear to have a 150 m.y. periodicity with maximum values in the Cambrian, Devonian, Permian and Cretaceous. Increased elevation and climate are the most important factors controlling increased rates of erosion and deposition. Global episodes of uplift and mountain building would result in more rapid rates of sediment recycling, observed as times of increased sediment flux. It is likely that the mass/age distribution and reconstructed fluxes of Phanerozoic sediment represent the surface expression of long-term mantle convection. There are two hypotheses concerning uplift and mantle convection: first, that uplift results from insulation of the mantle by supercontinents and second, that interactions at the core-mantle boundary create mantle superplumes that cause uplift. Both of these could result in long periods of broad continental and oceanic uplift and climate change. The Devonian, Permian and Cretaceous peaks are all correlated to mantle superplume events.

Regional sediment mass/age distributions show the timing of depositional and erosional events within a basin and its source areas. In most areas the stratigraphic data used to compile the sediment volumes must be interpolated from seismic data supplemented by "ground truth" from outcrops and drill holes. The conversion from sediment volumes to masses of sediment depends to a large extent on estimates of the solidity (100% - porosity) of the sediment. From comparison of empirical curves that describe the increase of solidity with increasing burial depths, I concluded that the compaction of shales and sands is best modelled by exponential decay equations and compaction of limestones as a power-law function.

The region chosen as a pilot study for paleobathymetric reconstruction and sediment accumulation analysis is the northern North Atlantic and southern GIN (Greenland-Iceland-Norwegian) Sea. In this area there have been four separate sinks for four different source areas during the Cenozoic. The four different basins are the edge of the British shelf to Reykjanes Ridge, Reykjanes Ridge to the East Greenland shelf, the East Greenland shelf to Jan Mayen Ridge, and Jan Mayen Ridge to the Faeroe-Shetland Escarpment. The mass/age distributions for the basins east and west of Reykjanes Ridge show a different uplift and subsidence history of western Europe compared to that of East Greenland. Sediment mass/age distributions for the basins east of Reykjanes Ridge have relatively constant masses per unit time which is uncharacteristic of a sea-floor spreading depositional environment. The mass/age distributions indicate uninterrupted sedimentation in Rockall Trough during the Cenozoic. Mass/age distributions for the western basins south of the Greenland-Scotland Ridge indicate a large input of sediment in the Eocene and Early Oligocene. The time lag between the separation of the continental blocks and the time of maximum sediment input is probably related to the reversal of drainage on land that occurred as the uplifted East Greenland margin subsided. The sediment mass/age distribution for the Iceland Plateau is directly related to the age of young ocean crust formed east of Scoresby Sund after the separation of Jan Mayen Ridge from Greenland in the Oligocene. The large mass of Neogene sediment reflects the newly created accommodation space on the Iceland Plateau that could store large amounts of detrital sediment eroded from Greenland. In the Paleocene, less sediment was transported from Greenland to offshore eastern basins as reflected by relatively small sediment masses in the Norway Basin.

The paleobathymetric reconstructions combine backstripping, including decompaction of sediment, with plate tectonic reconstructions. The modelled paleobathymetry is very sensitive to assumptions regrading the thermal age of the lithosphere. This has important implications for paleoceanography. For example, it has been suggested that the initiation of Feni Drift at the beginning of the Oligocene was in response to unusually dense water flowing from the Arctic into the Norwegian Sea, and from there through Faeroe-Shetland Channel into Rockall Trough. However, the deepest passage out of Faeroe-Shetland Channel is through Faeroe Bank Channel into the South Iceland Basin where drift formation did not start until the middle Miocene. Furthermore, plate tectonic reconstructions indicate that deep water connections between the Arctic Ocean and GIN Sea did not exist in the Oligocene.

Paleobathymetric reconstructions assuming two different thermal histories for the Rockall-Faeroe region offer new potential source areas for dense water in the early Oligocene. The thermal model based on Cretaceous rifting of the Rockall Trough and Faeroe-Shetland Channel without uplift in the Paleocene predicts a broad shelf north of Rockall Trough in the early Oligocene. This could have been a site of dense water formation if the area were cold enough. The thermal model based on Paleocene uplift from reheating of the lithosphere due to the Iceland Hotspot, reconstructs a shallow Rockall Plateau in the early Oligocene. There is evidence for extreme aridity at this time in the Rhine Graben, so it is possible that high evaporation rates could have existed over Rockall Plateau creating dense water through increased salinity. The expansion of drift formation to the South Iceland Basin (Hatton, Gardar and Bjorn Drifts) and west side of Reykjanes Ridge (Snorri Drift) in the early Middle Miocene was probably the result of a shift in the site of deep water formation to shallow areas of the Iceland-Faeroe Ridge. After development of the shallow shelf sea northwest of Iceland, flow through the Denmark Strait may have strengthened resulting in the formation of Eirik Drift off the southern tip of Greenland.

Sediment drifts in the northern North Atlantic have a much greater areal extent than has been indicated by previous authors. The first to form, Feni Drift on the eastern and southern margins of Rockall Plateau, has not increased in size since its origin in the early Oligocene. Although sedimentologists have cited the fact that sediment waves are no longer migrating on Feni Drift as evidence that it is not actively forming, sedimentation rates on it during the last 1 m.y have been higher than the regional average. Hatton Drift, on the western margin of Rockall Plateau, began to form in the early Middle Miocene. At the same time Feni Drift showed an increase in accumulation rate. Gardar and Bjorn Drifts started to form in the late Early Miocene and have expanded gradually but continuously since then. During the early Pliocene (3-4 Ma) accumulation on Gardar Drift increased by a factor of more than six over earlier rates, while the accumulation rates on Bjorn Drift doubled. The rate of sediment accumulation on both decreased from the Pliocene to Quaternary. The area of accumulation of Snorri Drift has increased steadily since the Middle Miocene. Both Eirik and Gloria Drifts appeared abruptly in the late Miocene-early Pliocene, but each was deposited by a different contour-following bottom current.

Sediment waves on the surface of drifts appear to be developed from more dispersed, low-energy bottom water flowing, while more energetic flow results in drift sedimentation

without sediment waves. Sediment drifts covered by sediment waves include Gloria Drift, southeastern Gardar Drift and South Feni Drift, and are in areas of weaker bottom current flow. The lack of sediment waves on the northern part of Gardar Drift, on Bjorn Drift, and on Eirik Drift appears to be a response to the much stronger flow of bottom water over these bodies.

In summary, drift sedimentation has dominated the pattern of sediment accumulation between the Greenland-Scotland Ridge and the Charlie Gibbs Fracture Zone during the Quaternary and Pliocene. During the Late and Middle Miocene drift sedimentation was restricted to relatively small areas of the South Iceland Basin and to the western side of Rockall Trough. During the Early Miocene and Oligocene drift sedimentation was limited to the eastern and southern margins of Rockall Plateau. At this time the greater-than-average sediment accumulations occurred mostly on the developing mid-ocean Reykjanes Ridge and on Rockall Plateau. In the Eocene the only areas that had above-average sediment accumulation rates were the major regional depressions, Rockall Trough, Porcupine Abyssal Plain, and Irminger Basin.

CHAPTER 1. Reconstructing Ancient Mass/age Distributions and Sediment Fluxes

1.1 Introduction

A major problem in geology is determining the magnitude of material fluxes at different times in the geologic past. If the masses of sediment eroded and deposited are known, it is in principle possible to reconstruct paleotopography and paleobathymetry (Hay et al., 1989a, 1989b; Shaw and Hay, 1989). In order to determine the history of erosion of sedimentary materials from their sources to sites of deposition it is necessary make accurate estimates of the magnitude of fluxes at different times in the geologic past. Unless it is possible to make quantitative estimates of material fluxes in the past, historical geology must remain a qualitative interpretive aspect of the science and the details of Earth's history can never be known. The hypothesis of sediment cycling suggests that it should be possible to determine the masses of sediment eroded and deposited through geologic time. As discussed below, there have been several attempts to describe sedimentary cycling in quantitative terms, but they have either involved too many simplifying assumptions or have failed to take into account the principle of conservation of mass. The new method developed here is a rigorous description of sedimentary recycling that conserves mass. Because it does conserve mass, it requires that the erosion and deposition take place within a closed system. The reconstruction method is demonstrated using previously published global data sets for Phanerozoic sediments.

1.1.1 Sediment Recycling and Mass/Age Distributions

Veizer and Jansen (1979) have reviewed the development of ideas regarding cycling of sedimentary rocks in the introduction to their paper on basement and sediment recycling and continental evolution. They noted that since the turn of the century it had been recognized that the existing mass of sedimentary rock per unit time approximates an exponential decay curve with increasing age of the deposit.

This was first discovered in terms of maximum preserved thickness of stratigraphic units (Barrell, 1917; Schuchert, 1931) and was interpreted as a reflection of increasing rate of tectonism through geologic time. It was Gilluly (1949), who recognized that the exponential relationship is an expression of the more complete preservation of younger deposits. Gregor (1968, 1970) used the compilations of Ronov (1968) and Holmes (1965) to calculate the rate of denudation of the continents which would produce the results observed. Garrels and Mackenzie (1971a) presented the first extensive discussion of sedimentary cycling, developing models for constant sedimentary mass and for linear accumulation of the sedimentary mass. Veizer and Jansen (1979) have shown that the exponential relationship holds for the age distribution of the area continental basement, the thickness of sedimentary and volcanogenic units, the thickness, area, and volume of sedimentary rocks, and even the cumulative reserves of most mineral commodities. They concluded that "the described exponential relationship is a fundamental law of present day age distribution of geological entities" (p. 342). As such, it obviously has significant ramifications for the interpretation of geologic history.

The papers written in the 1960's and 70's did not take into account the mobility of the earth's crust implied by the theory of plate tectonics. Garrels and Mackenzie (1971b) assuming permanence of continents and ocean basins, thought that the total mass of sediment (TSM) existing on the earth is about 3200 x 10^{21}g, of this 44% would be Precambrian, 23% Paleozoic and 33% Mesozoic-Cenozoic. Southam and Hay (1981) reviewed previous work and prepared new estimates of sediment volumes and masses in major sediment reservoirs for an estimated total Phanerozoic sedimentary mass of 2485 x 10^{21}g. Of this Phanerozoic sedimentary mass (PSM), they determined 35% to be Paleozoic and 65% to be Mesozoic-Cenozoic. The first attempt to work out the total mass/age distribution of all Phanerozoic sediments was that of Gregor (1985) who estimated the PSM to be 2100 x 10^{21} g. Gregor (1985) compiled sediment masses for the three major reservoirs; the cratons, continental margins and ocean basins. He plotted his mass/age distribution of the Phanerozoic sediments in terms of the duration of geologic Periods. The general shape of the exponential decay can be recognized as well as a peak in the mass of Devonian sediment, but finer details in the mass/age distribution are not apparent.

Figure 1.1 shows a mass/age distribution of existing Phanerozoic sediments similar to that compiled by Wold and Hay (1990), but including Quaternary sediments. The estimates of Budyko et al. (1987) were used for sediments of Pliocene to Middle Jurassic age. Masses of older sediments were compiled from the data of Ronov (1982). For the masses of Quaternary sediments I used the estimate of Hay (1993). The distribution is plotted using the timescales of Berggren et al. (1985), McKerrow et al. (1985) and Snelling (1985). The new estimate of the total mass of Phanerozoic sediments is 2082.6 x 10^{21} g. The mass/age distribution of Cenozoic sediments including the Quaternary is shown in Figure 1.2.

1.2 Reconstruction of Original Sediment Flux Rates

The reconstruction of ancient sediment mass is based on the assumptions that young sediment is generally unconsolidated, has the greatest areal exposure and thus has the greatest probability of being eroded. Young sediment is therefore recycled more rapidly than old sediment which is more consolidated and has a smaller areal exposure. This assumption is the fundamental principle underlying the theory of sediment recycling.

Previous attempts to determine ancient sediment fluxes from modern mass/age distributions (Wold et al, 1986; Wold and Hay, 1990) have not required that mass be conserved. Wold and Hay (1990) presented a practical method for reconstructing ancient sediment flux rates. They approximated original Phanerozoic sediment fluxes by fitting an exponential decay curve to the observed mass/age distribution of sediments, then multiplying the ratio of the observed mass to the exponential decay curve mass by the zero-age flux rate predicted by the exponential decay curve. Their method was a good first approximation of the original fluxes and will be compared to the new method discussed below.

1.2.1 A New Method for Reconstructing Ancient Mass/age Distributions and Estimating Original Sediment Flux Rates

Following Wold and Hay (1990) it is assumed that on a global scale the sedimentary system is in steady state and has a mass that remains constant because most younger sediments are derived from cannibalization of older sediments through erosion. This implies that gains of sediment mass from weathering, erosion, and deposition of igneous and

crystalline metamorphic rocks are exactly offset by losses to subduction and metamorphism. It is also assumed that no significant masses of sediment can be stored in ocean water or in the atmosphere.

The general decline of sediment mass with age resulting from recycling of older sediment to become younger sediment may be approximated by a simple exponential decay

$$y = Ae^{-bt} \qquad (1.1)$$

where y is the remnant of the original sediment flux at time t, that would be observed today after t m.y. of recycling at a constant rate of erosion b ("average recycling proportionality parameter" of Veizer and Jansen, 1985), and a constant depositional rate, A (the rate at which sediment is being deposited at present).

Eqn. (1.1) is the average rate of sediment recycling over the time represented by the mass/age distribution. The observed sediment masses in Figure 1.1 have been normalized to 10 m.y. intervals and are shown in Figure 1.3. The existing mass of sediment in each 10 m.y. interval was calculated by determining the existing mass per million years for each of the traditional geologic intervals recognized by Ronov (1982) or Budyko et al. (1987) and summing the mass increments from the portion of each traditional geologic interval within the 10 m.y. interval.

The average rate of sediment recycling and zero-age sediment flux rate were calculated from a least-squares fit of an exponential curve (Eqn. 1.1) to the normalized data (Fig. 1.3). Because the mass of Quaternary sediments could be included, it was possible to determine the average Phanerozoic zero-age flux rate to be 5.756×10^{21} g m.y.$^{-1}$ and the average rate of sediment recycling to be -2.062×10^{-3} m.y.$^{-1}$. A is slightly greater than the value of 5.735×10^{21} g m.y.$^{-1}$ calculated by Wold and Hay (1990) and b is more positive than their value of -2.102×10^{-3} m.y.$^{-1}$. This indicates that the average Phanerozoic recycling rate is slower than what they calculated, although the average zero-age flux rate in our new compilation is higher. The new exponential decay curve ($y = 5.756\ e^{-0.002062t}$]) is a more accurate representation of the average Phanerozoic flux and recycling rates.

The new reconstruction method keeps the sediment mass constant. The total sediment mass (TSM) includes both the documented Phanerozoic sediment and an estimate of the mass of Proterozoic and Archaean sediments. The older sediment masses were calculated from the area under the exponential decay curve. These are 845.5×10^{21} g for the Proterozoic (570 to

2500 Ma) and 15.0 x 10^{21} g for the Archaean (2500 to 3800 Ma) sediments, as shown in Figure 1.4). The original sediment flux during each of the 10 m.y. intervals in the Phanerozoic can be estimated by successively reconstructing each of the older mass/age distributions. For any given mass/age distribution we can number the normalized intervals from 0 to n, where there are n+1 intervals in the mass/age distribution. We can refer to the mass of sediment in the youngest interval as mass[0] and the mass in the oldest interval mass[n]. Then the total mass of sediment would be the sum of all the interval masses from mass[0] to mass[n]

$$TSM = \sum_{i=0}^{n} m[i], \qquad (1.2)$$

and the mass of sediment in the youngest interval (mass[0]) is the sum of all the sediment that was eroded from each of the older intervals (mass[1] through mass[n]) during the time interval in which mass[0] was deposited

$$mass[0] = \sum_{i=1}^{n} m[i]_{eroded}. \qquad (1.3)$$

The mass of sediment eroded from each of the older masses during interval 0 is

$$m[i]_{eroded} = m[0] \; x \; \frac{m[i]}{TSM - m[0]}. \qquad (1.4)$$

The youngest mass is subtracted from TSM in Eqn. (1.4) so that the total proportion of all the older masses will equal one, but TSM remains constant.

The method is illustrated in Figure 1.5 by a series of reconstructed mass/age distributions, the length of each is kept constant at 570 m.y. (the duration of the Phanerozoic). In each older reconstruction, the sediment masses in corresponding 10 m.y. intervals are greater as illustrated by the increasing height of the major peaks in sediment flux during the Cretaceous (K), Permian (P), Devonian (D) and Cambrian (C). The part of each mass/age distribution older than 570 Ma is represented by the exponential curve because there are no compilations of Precambrian sediment masses. Figure 1.6 shows the original fluxes estimated from reconstruction of the sediment mass/age distributions at the time of each of the 56 older age intervals.

1.3 Discussion

The most striking feature of the reconstructed global sediment flux for the Phanerozoic is the regular recurrence of peaks of erosion and deposition at 150 m.y. intervals, first noted by Hay and Wold (1986). The peaks of sediment flux occur in the Cretaceous, Permian, Devonian, and Cambrian. Wold and Hay (1990) argued that because most (approximately 80%) sediment is detrital and because the erosion of detrital sediment is most strongly dependent on elevation, the peaks of sediment flux must represent times of uplift and mountain building. They also suggested that because the increases in sediment flux are paralleled by increases in volcanic flux it was likely that the peaks represent times when plate tectonic processes were especially rapid. Wold et al. (1987) associated the Devonian, Permian and Cretaceous peaks in reconstructed sediment flux with major collisions and reorganization of lithospheric plates. Hay and Wold (1990) noted that the times of low global sediment flux correspond to times of deposition of iron oolites and phosphorites, and that times of high global sediment flux correspond to times of potash deposition. They suggested that these are probably related to different climatic and weathering regimes when the earth has high continents and when the landmasses are low.

Eustatic (globally uniform) sea level rises are directly related to increased rates of sea-floor spreading (Kominz, 1984). However, epeirogenic motions (large-scale vertical motions of continental regions relative to one another) are as important as eustasy in explaining the relative rise and fall of sea level (Gurnis, 1992). Epeirogenic continental uplift of 500 to 1000 m can be generated within 100 m.y. (Gurnis, 1992) from insulation of the mantle by a supercontinent (Anderson, 1982) resulting in long-wavelength temperature gradients within the mantle that cause mantle convection (Gurnis, 1992). Dynamic modelling with rudimentary oceanic and continental plates has shown that as a continental plate breaks up over a hot portion of the mantle (elevated region of the geoid), its fragments move towards cooler regions of the mantle (depressed regions of the geoid; Gurnis, 1992). This process of continental dispersion and accretion is cyclic with a periodicity of approximately 440 m.y. and can be traced as far back as 2 Ga (Worsley et al., 1984).

The peaks of reconstructed sediment flux in the Phanerozoic (Fig. 1.6) correspond to times when reversals of the Earth's magnetic field have ceased (Molostovsky and Khramov, 1984; Courtillot and Besse, 1987; Larson and Olson, 1991). The Cretaceous peak corresponds

to the "mid-Cretaceous" superplume of Larson and Olson (1991). Mantle plumes represent another type of mantle convection related to processes at the core-mantle boundary (Courtillot and Besse, 1987; Larson, 1991). The Pennsylvanian-Permian peak may also correspond to a superplume event (Larson, in press), and the Devonian peak corresponds to a superplume event postulated by Wajsprych (1992). It seems likely that there is a relation between events at the core-mantle boundary, the development of superplumes, insulation of the mantle by supercontinents, the rate of sea-floor spreading, subduction, mountain-building, epeirogeny and climate. The global Phanerozoic sediment mass/age distribution may well represent the response of materials on the Earth's surface to these interrelated processes and could serve as an important tool for deciphering the history of mantle convection.

It has been suggested that some sediments, such as evaporites, are recycled more readily than others, and that sediments of some ages are specially protected against erosion (Garrels and Mackenzie, 1971b). On a global basis stratigraphic units are always very thin compared with their areal extent and can only be eroded sequentially. Although evaporites are more soluble than other rocks and can be dissolved by groundwaters in the subsurface, their removal means that the overlying strata must collapse, and this does not appear to have happened often. Halite is very light and mobile, and may push upward through other sediments to reach the region of active groundwater flow, but only a small part of the deposit can be lost through dissolution of diapirs. In fact, it could be argued that evaporites are the best candidates for rocks that are preferentially preserved, because they are often deposited in rifts early in the development of passive margins, and hence tend to be deeply buried. As Hay and Wold (1990) noted, the greatest masses of evaporites correspond to the greatest sediment masses. The greatest sediment masses mean that large amounts of detrital sediment are being deposited. The flux of detrital sediment is a function of elevation, and the presence of mountains and plateau uplifts causes the earth to have more differentiated climate. Because of these interrelations, they concluded that the deposition of evaporites occurred at times when the relief was maximal, and when maximal aridity might occur.

The idea that sediments of a particular age might be selectively preserved rests on the assumption that at certain times most sediment is deposited in continental margins where they become deeply buried and hence are selectively preserved. The Devonian peak which was recognized by Garrels and Mackenzie (1971b) as a major anomaly, has been considered as possibly due to selective preservation. The hypothesis of selective preservation of sediments

in continental margin settings can be tested using the data of Budyko et al. (1987) and Ronov (1982). They separated deposits associated with the continents into two major categories, "platform" and "geosynclinal". The used the term "platform" for the relatively undeformed sediments on the cratonic interior of the continental blocks and the term "geosynclinal" for the deposits of mountain belts and continental margins (edge of continental cratons). If it is true that continental margin sediments are selectively preserved, then the ratio of "geosynclinal" to "platform" sediments should increase with age. Figure 1.7 shows the ratio of the masses of sediment in preserved in "geosynclines" to the masses preserved on "platforms". The scatter of points is striking, but it might be argued that there is a general trend that can be interpreted as favoring a slightly greater chance toward preservation of Paleozoic sediments in the "geosynclinal" regions. The Devonian does not stand out relative to the rest of the Paleozoic as being a time of unusually large amounts of sediments being concentrated in the "geosynclines". The times when the ratio of "geosyncline" to "platform" sediment masses are greatest and least do not correspond to times when preserved total sediment masses are greatest or least, but any relationship appears to be random.

The rapid increase in sediment masses during the Cenozoic is to a large extent a reflection of the distribution of sediments on the ocean floor. The creation and subduction of ocean crust produces an area-age distribution that resembles a linear decay of cumulative area with increasing age (see Fig. 4.18 for example). Because of the mass/age distribution of ocean crust, and because at any given time a significant proportion (± 10%) of the global sedimentary mass resides on ocean crust, there will always appear to be an unusually large amount of sediment having an age less than 50 m.y. However, as discussed by Hay (1993) even if this is taken into account the Quaternary rates of sediment cycling are high compared to older cycling rates. Much of the Quaternary sediment mass resides on the ocean floor and is not likely to be recycled soon. The very large masses of Quaternary sediment are related to the frequent changes of climate that accelerates weathering, or to late Cenozoic uplift in many parts of the world that may be the cause of development of the northern hemisphere ice sheets, or to offloading of older sediment from the continental shelves in response to lower sea levels during glacial times, or to a combination of all of these factors.

The original sediment flux rates for each 10 m.y. interval are shown reconstructed using the new and old methods in Figure 1.8. The difference between the flux rates reconstructed using both methods is also shown in Figure 1.8. The new reconstruction method is a fine-adjustment of the old method (Wold and Hay, 1990) with differences in reconstructed sediment fluxes that are less than $\pm 0.5 \times 10^{21}$ g my^{-1} per 10 m.y. interval (Fig. 1.8).

1.4 Conclusions

The old method (Wold and Hay, 1990), although a good first-approximation, depended almost entirely on the average rates predicted by the exponential decay curve. The zero-age flux rate (A) was held constant and the rate of sediment cycling (b) during each time interval was always proportional to the average rate of sediment cycling. In the new method TSM is initially calculated and then held constant throughout the reconstructions. The original flux rate (A) and sediment cycling rate (b) for each interval varies proportionally to TSM and the young flux being used to reconstruct the mass/age distribution. The sediment flux and cycling rates are more dynamic in this new model and can predict original sediment fluxes exactly while conserving the total sediment mass.

The new total sediment mass for the Phanerozoic is 2082.6×10^{21} g. Based on a least squares fit of an exponential decay curve to the data, the average zero-age flux rate of Phanerozoic sediment is 5.756×10^{21} g $m.y.^{-1}$ and the average rate of sediment recycling is -2.062×10^{-3} $m.y.^{-1}$. The new estimate of the mass of Proterozoic sediment is 845.5×10^{21} g and that of Archaean sediment is 15.0×10^{21} g.

It has been suggested that some lithologies are recycled more rapidly than others (Garrels and Mackenzie, 1971b). On the scale of continental platforms and major ocean basins (i.e. global scale), sedimentary layers are thin horizontal sheets that can only be eroded sequentially, thus prohibiting selective preservation based on lithology. It has also been suggested that Devonian sediments are selectively preserved because they were deposited in geosynclines. The Devonian does not stand out as a time of maximum sediment preservation. The masses of Paleozoic sediments in "geosynclines" are generally greater than Cenozoic and Mesozoic sediments but there is no correlation between the proportion of sediment in "geosynclines" versus platforms and the mass/age distribution of Phanerozoic sediments.

The interrelationship between mantle convection and plate tectonics is growing into a unified theory (eg. Gurnis, 1992) that may explain global fluctuations in sediment mass as well as long-term climate and eustatic changes. This interrelationship is expressed in the record of mantle "superplumes" (Larson and Olson, 1991; Larson, in press; Wajsprych, 1992), models of eustasy (Kominz, 1984; Gurnis, 1990a), epeirogeny (Gurnis, 1990b), the frequency of magnetic reversals related to core-mantle coupling (Courtillot and Besse, 1987; Larson and Olson, 1991) and changes in global sediment flux (Hay and Wold, 1986; Wold et al., 1987; Hay and Wold, 1990; Wold and Hay, 1990).

1.5 Figure Captions

Figure 1.1. The observed mass/age distribution of existing Phanerozoic sediments compiled from the estimates of Budyko et al. (1987) for the Pliocene to Middle Jurassic, Ronov (1982) for the Middle Jurassic to Cambrian and the new estimate of Hay (1993) for Quaternary sediments. The new estimated total mass of Phanerozoic sediments is 2082.6 x 10^{21} g. The total mass per million years of Quaternary (25.61 x 10^{21} g m.y.$^{-1}$) and Pliocene (14.89 x 10^{21} g m.y.$^{-1}$) are not shown so that the pre-Pliocene variations in the mass/age distribution are better resolved. The timescales of Berggren et al. (1985), McKerrow et al. (1985) and Snelling (1985) were used to display the data and are shown on the bottom of the diagram.

Figure 1.2. The mass/age distribution of Cenozoic sediments including the mass per m.y. of Quaternary sediments from Hay (1993). On the bottom of the diagram is the geologic timescale for the Cenozoic after Berggren et al. (1985), McKerrow et al. (1985) and Snelling (1985).

Figure 1.3. The observed sediment masses normalized to 10 m.y. intervals. The exponential decay curve fit to the data represents the average rate of sediment cycling during the Phanerozoic and the zero-intercept of the curve on the y-axis is the average sediment flux rate per m.y. during the Phanerozoic. The exponential decay has the form $y = A\ e^{-bt}$ where y is the amount of the original sediment flux at time t remaining after t m.y. of recycling at a constant rate of erosion b (-2.062 x 10^{-3} m.y.$^{-1}$) and a constant rate of deposition, A (5.756 x 10^{21} g m.y.$^{-1}$). On the bottom of the diagram is the geologic timescale for the Phanerozoic after Berggren et al. (1985), McKerrow et al. (1985) and Snelling (1985).

Figure 1.4. The total sediment mass/age distribution includes the documented mass/age distribution of Phanerozoic sediment and an estimate of the mass of Proterozoic (845.5 x 10^{21} g) and Archaean (15 x 10^{21} g) sediments. The older sediment masses were estimated directly from the area under the exponential decay curve and the estimated global mass of existing sediment is 2943.1 x 10^{21} g).

Figure 1.5. A series of reconstructed mass/age distributions where the length of each is kept constant at 570 m.y. (the duration of the Phanerozoic). The part of each mass/age distribution older than 570 Ma is represented by the exponential curve because of the lack of data on Precambrian sediment masses. In each older reconstruction, the sediment masses in corresponding 10 m.y. intervals are greater as illustrated by the increasing height of the major peaks in sediment flux for each older reconstruction. Each peak in the rate of sediment flux and recycling rate is indicated by the letters: K - Cretaceous; P - Permian; D - Devonian; and C for the Cambrian.

Figure 1.6. The observed and original sediment flux rates during the Phanerozoic. The observed sediment fluxes are shaded dark gray on the lower part of the diagram and the initial fluxes are equal to the total height of each bar. The original fluxes have been estimated from the successive reconstruction of sediment mass/age distributions. On the bottom of the diagram is the geologic timescale for the Phanerozoic after Berggren et al. (1985), McKerrow et al. (1985) and Snelling (1985).

Figure 1.7. The top of the diagram shows the ratio of the global Phanerozoic sediment in continental platforms vs. geosynclines. In the middle is the geologic timescale for the Phanerozoic after Berggren et al. (1985), McKerrow et al. (1985) and Snelling (1985) and on the lower part of the diagram is the normalized and reconstructed Phanerozoic sediment masses.

Figure 1.8. The observed and original sediment flux rates for each 10 m.y. interval reconstructed using the new and old methods. The observed sediment fluxes are shaded dark gray on the lower part of the upper two diagrams and the initial fluxes are equal to the total height of each bar. The difference between the flux rates reconstructed using both methods is shown on the bottom of the diagram. The differences in reconstructed sediment fluxes that are less than $\pm 0.5 \times 10^{21}$ g m.y.$^{-1}$ per 10 m.y. interval.

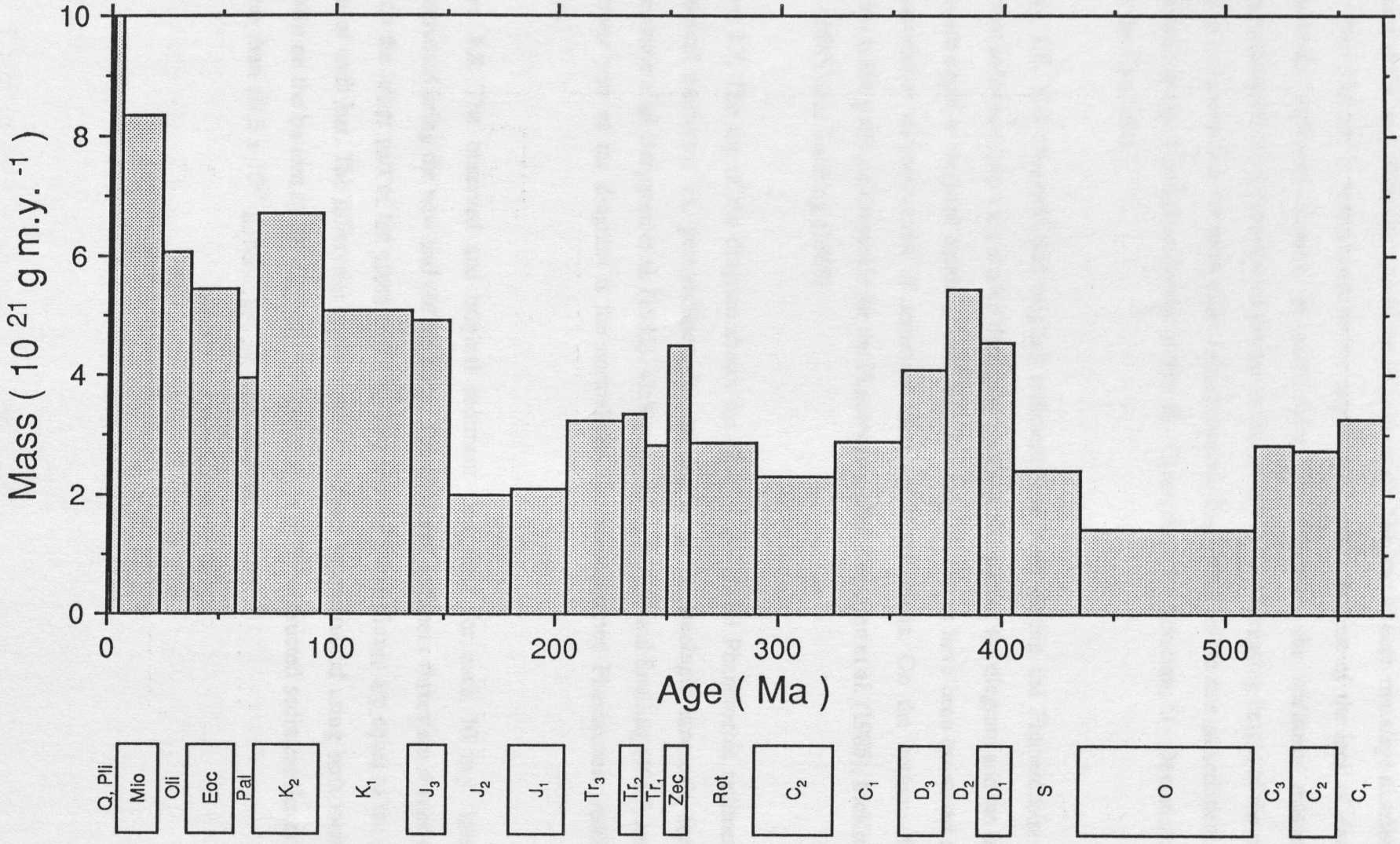
Mass (10 21 g m.y. -1)
10
8
6
4
2
0
0
100
200
300
400
500
Age (Ma)
Q, Pli
Mio
Oli
Eoc
Pal
K2
K1
J3
J2
J1
Tr3
Tr2
Tr1
Zec
Rot
C2
C1
D3
D2
D1
S
O
C3
C2
C1

Figure 1.1

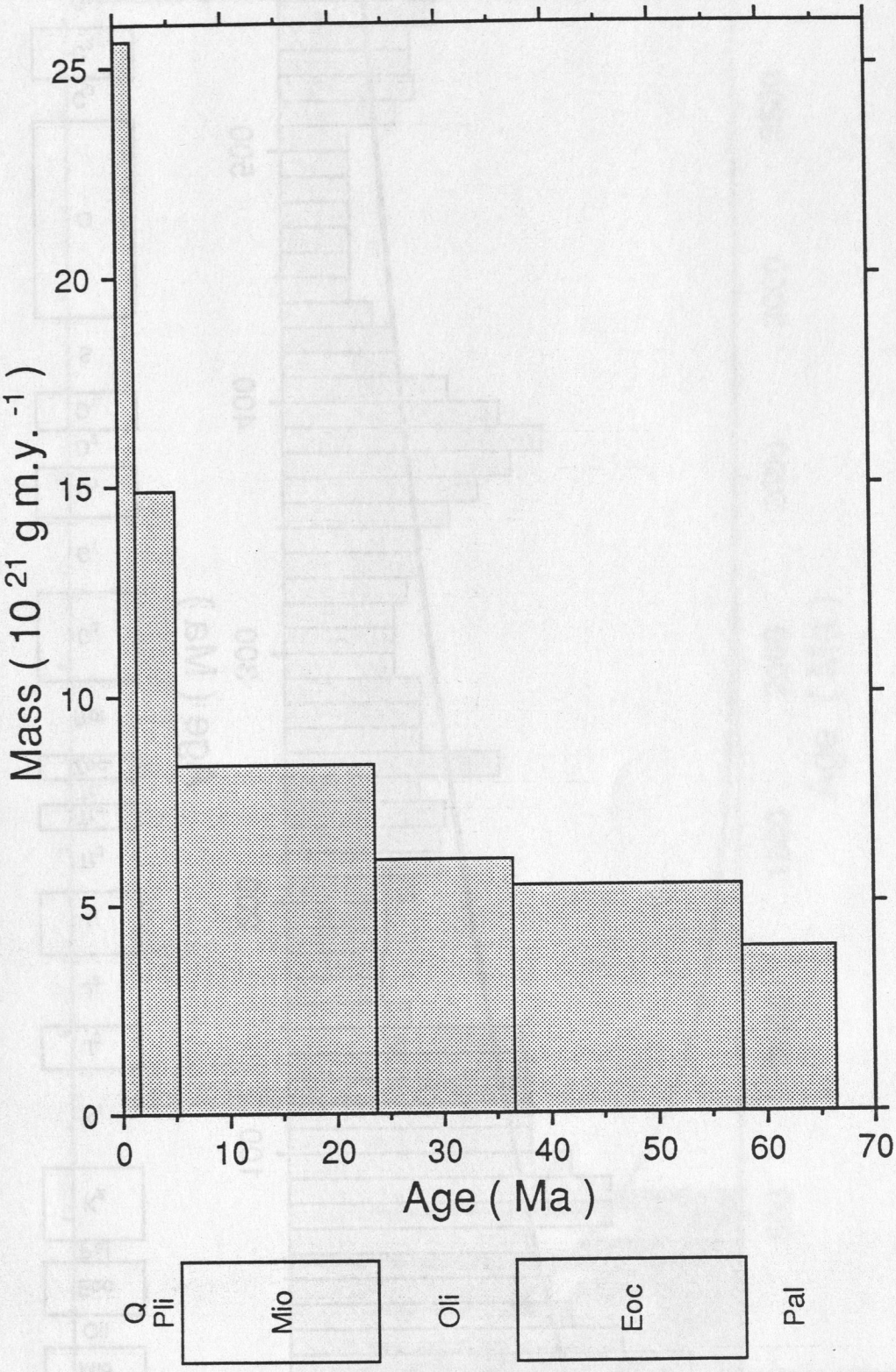
Mass (10 21 g m.y. -1)
25
20
15
10
5
0
0
10
20
30
40
50
60
70
Age (Ma)
Q
Pli
Mio
Oli
Eoc
Pal

Figure 1.2

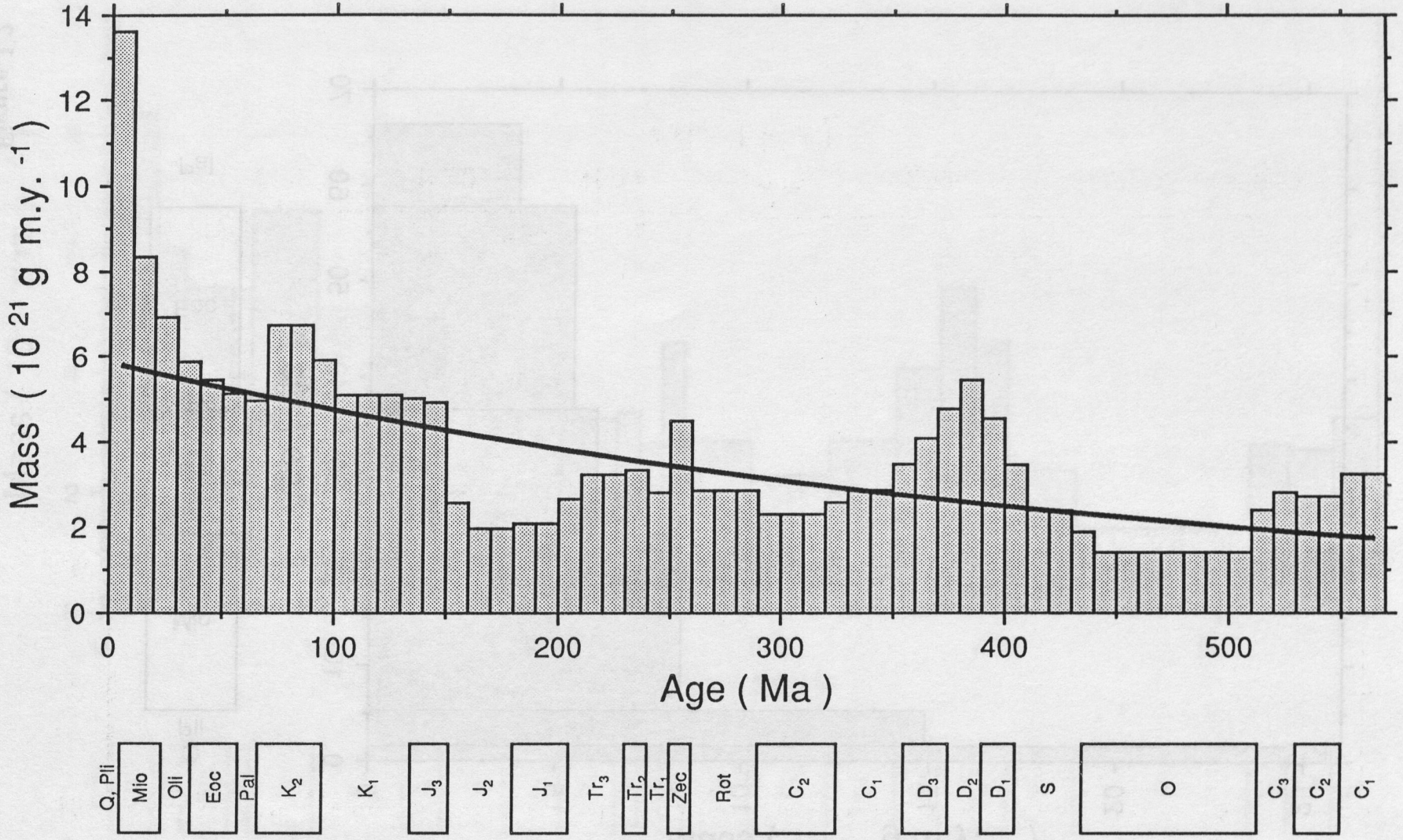
Mass (10 21 g m.y. -1)
0
2
4
6
8
10
12
14
0
100
200
300
400
500
Age (Ma)
Q, Pli
Mio
Oli
Eoc
Pal
K2
K1
J3
J2
J1
Tr3
Tr2
Tr1
Zec
Rot
C2
C1
D3
D2
D1
S
O
C3
C2
C1

Figure 1.3

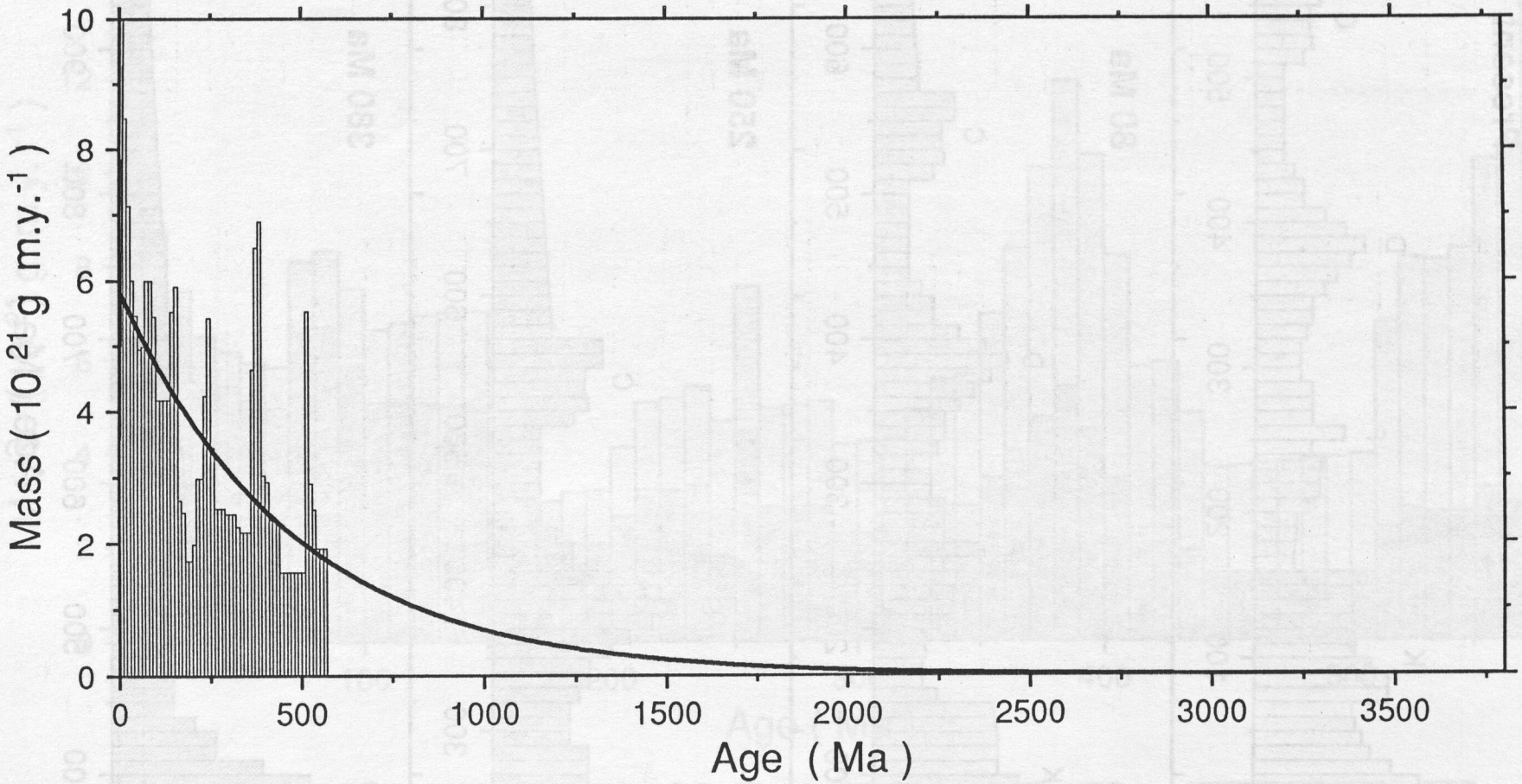
Mass (10 21 g m.y.-1)
10
8
6
4
2
0
0
500
1000
1500
2000
2500
3000
3500
Age (Ma)

Figure 1.4

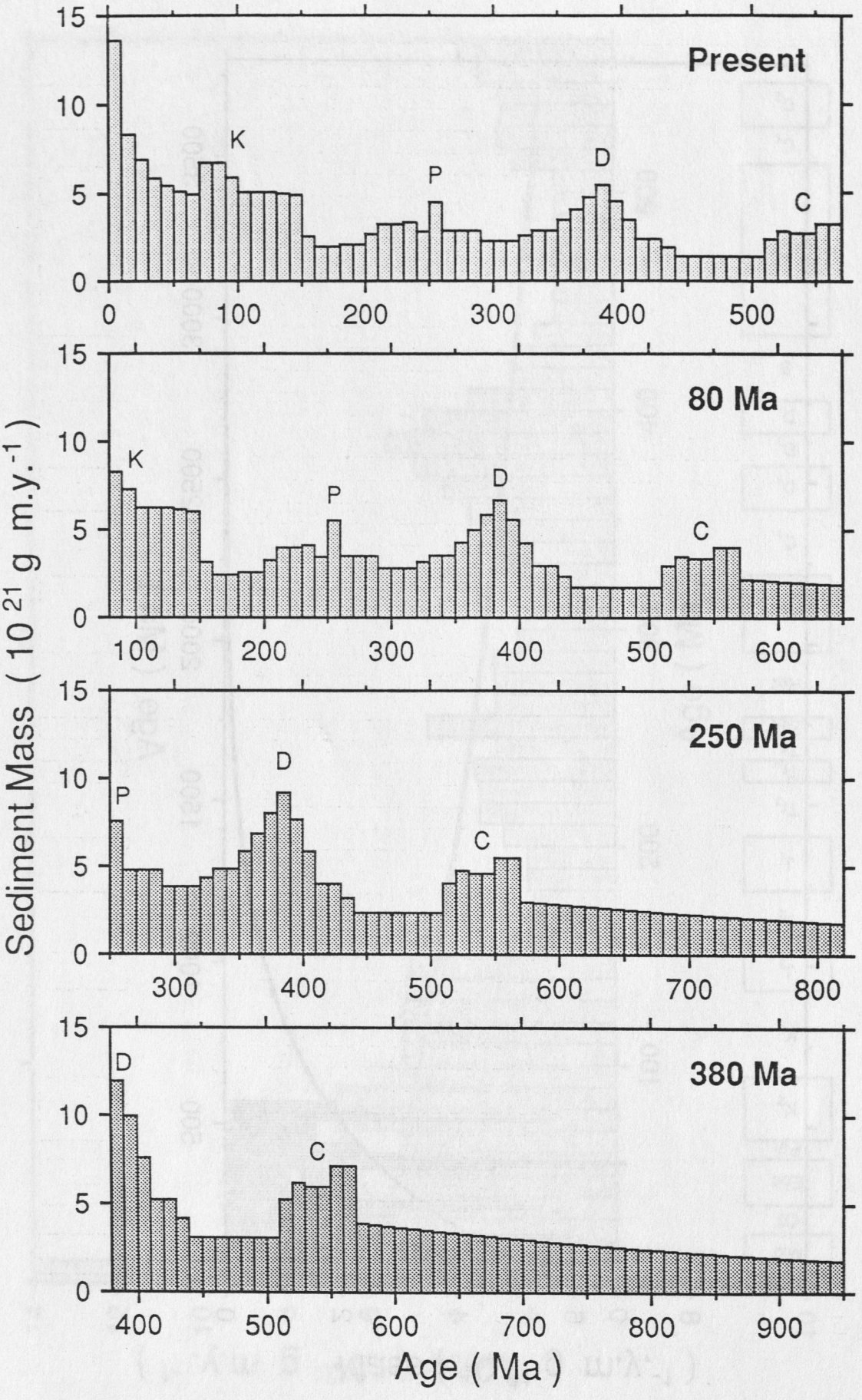
Present
80 Ma
250 Ma
380 Ma
K
P
D
C
Sediment Mass (10 21 g m.y.-1)
Age (Ma)

Figure 1.5

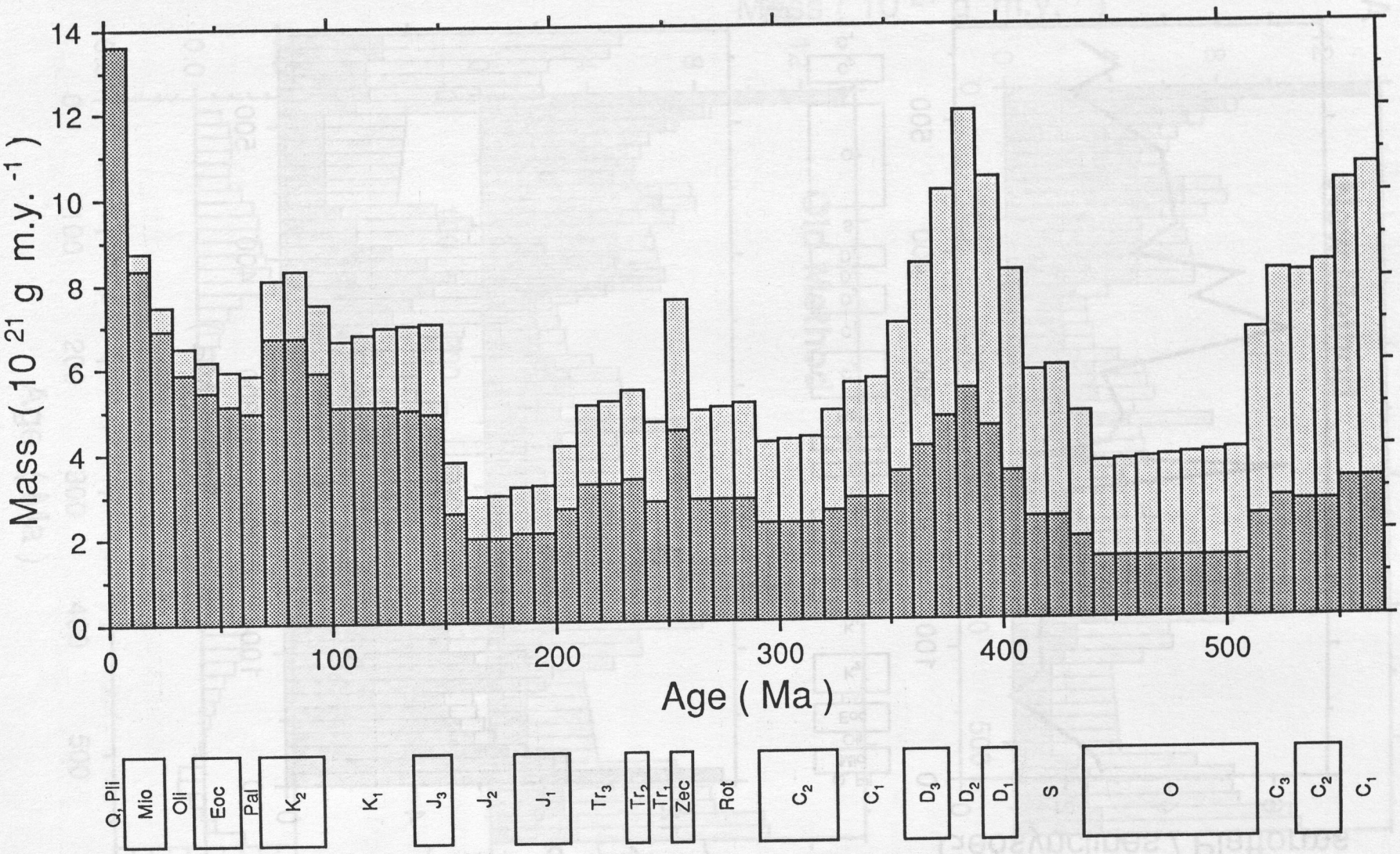
Mass (10 21 g m.y. -1)
0
2
4
6
8
10
12
14
0
100
200
300
400
500
Age (Ma)
Q, Pli
Mio
Oli
Eoc
Pal
K2
K1
J3
J2
J1
Tr3
Tr2
Tr1
Zec
Rot
C2
C1
D3
D2
D1
S
O
C3
C2
C1

Figure 1.6

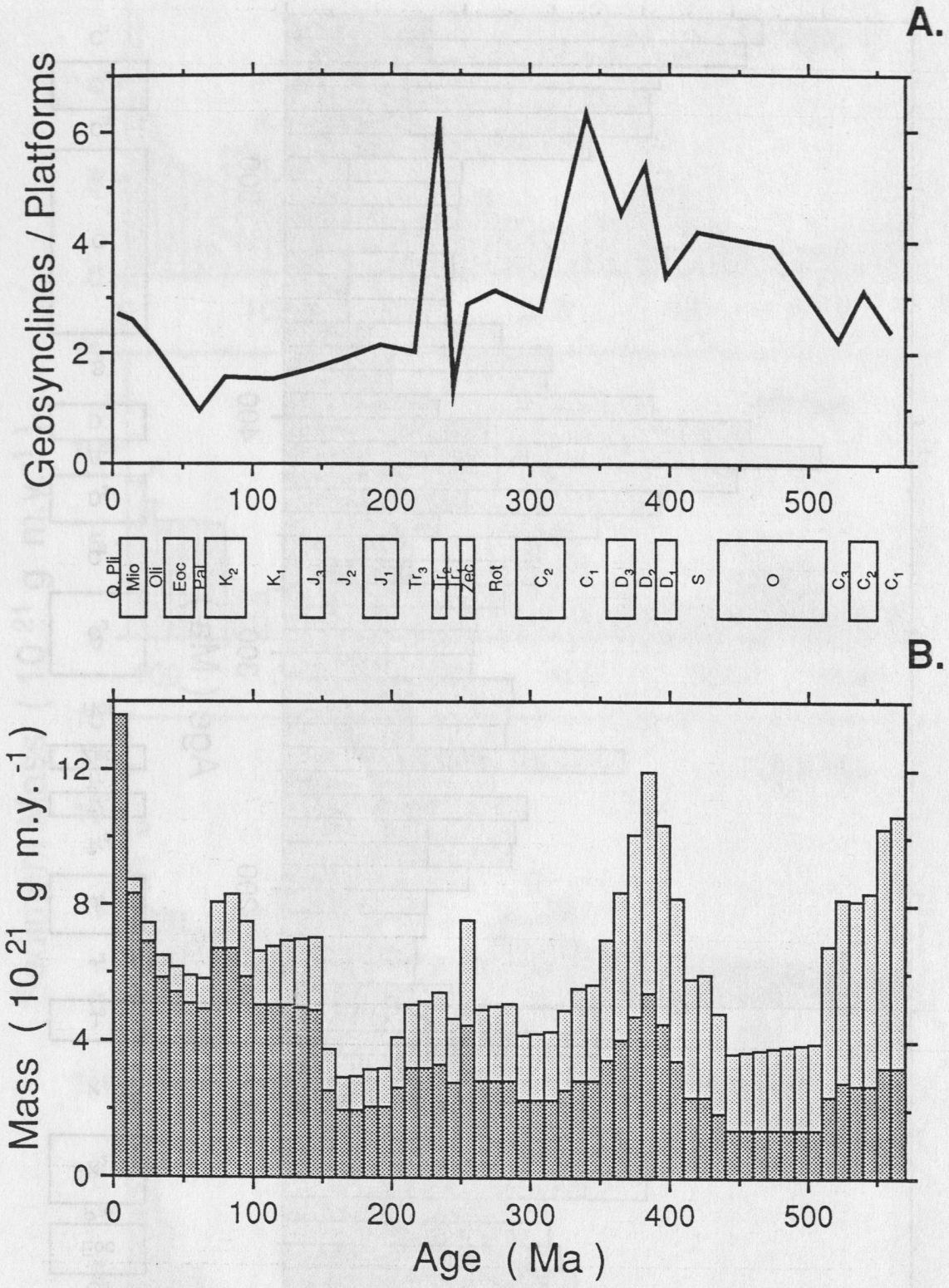
A.
Geosynclines / Platforms
0
2
4
6
0
100
200
300
400
500
Q Pli
Mio
Oli
Eoc
Pal
K2
K1
J3
J2
J1
Tr3
Tr2
Tr1
Zec
Rot
C2
C1
D3
D2
D1
S
O
C3
C2
C1
B.
Mass (10 21 g m.y. -1)
0
4
8
12
0
100
200
300
400
500
Age (Ma)

Figure 1.7

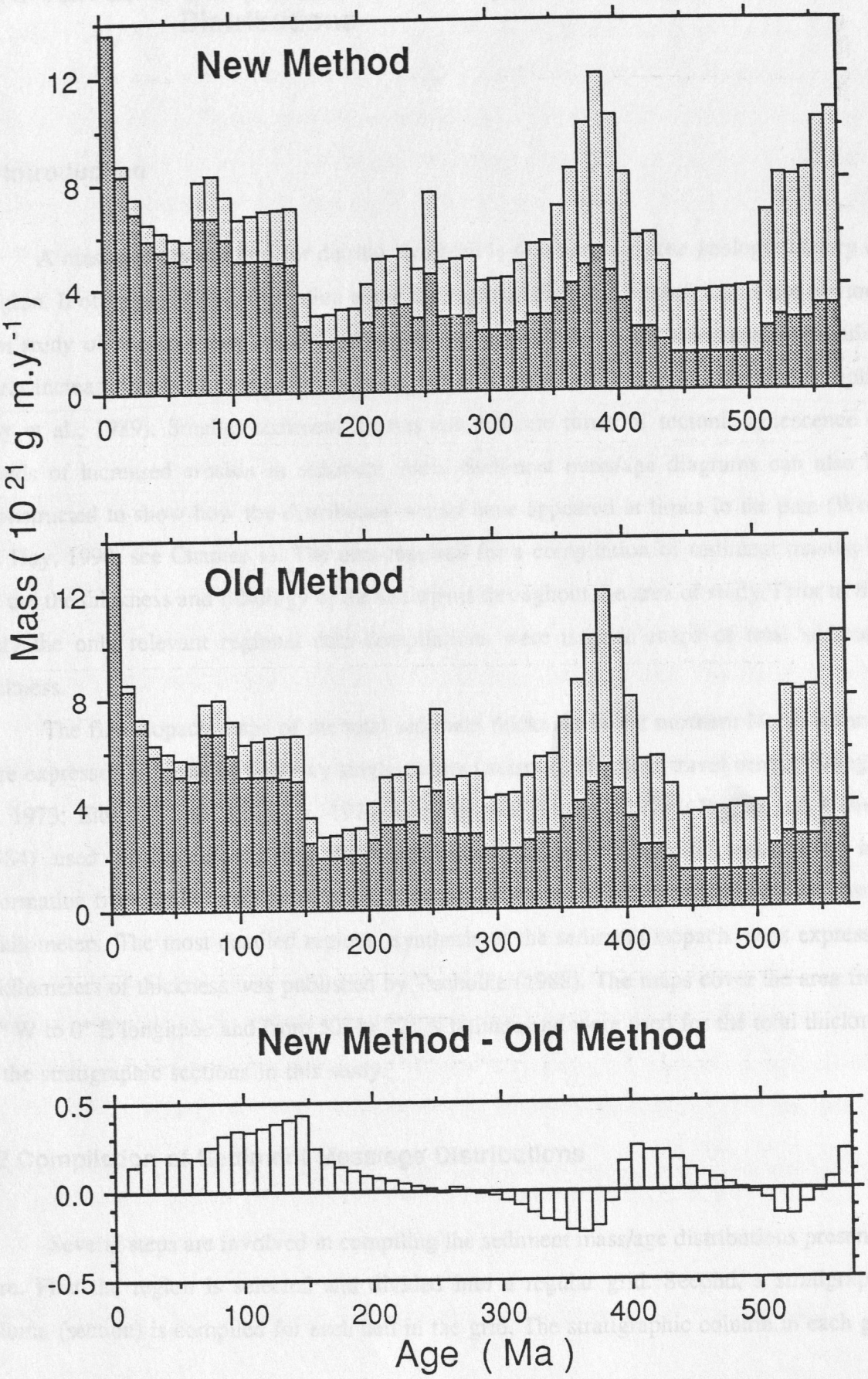
New Method
Old Method
New Method - Old Method
Mass (10 21 g m.y.-1)
Age (Ma)
0
4
8
12
0
100
200
300
400
500
0.5
0.0
-0.5

Figure 1.8

CHAPTER 2. Compilation and Analysis of Sediment Mass/age Distributions

2.1 Introduction

A mass/age distribution for detrital sediment is an abstract of the geologic history of a region. It often provides information about the regional geologic history that is not obvious from study of one or a few local stratigraphic sections. Peaks in the mass/age distribution reflect increased rates of erosion in sediment source areas often in response to tectonic uplift (Hay et al., 1989). Smaller sediment masses can indicate times of tectonic quiescence or periods of increased erosion in sediment sinks. Sediment mass/age diagrams can also be reconstructed to show how the distribution would have appeared at times in the past (Wold and Hay, 1990; see Chapter 1). The data required for a compilation of sediment masses by age are the thickness and lithology of the sediments throughout the area of study. Prior to this study the only relevant regional data compilations were isopach maps of total sediment thickness.

The first isopach maps of the total sediment thickness in the northern North Atlantic were expressed in terms of two-way single-channel seismic reflection travel times (Ewing et al., 1973; Eldholm and Windisch, 1974; Grønlie and Talwani, 1978). Emery and Uchupi (1984) used the calculated time-depth relationship from seismic refraction data and information from DSDP drill sites to publish maps of the total sediment thickness expressed in kilometers. The most detailed regional synthesis of the sediment isopach maps expressed in kilometers of thickness was published by Tucholke (1988). The maps cover the area from 65° W to 0° E longitude and from 50° to 72° N latitude and were used for the total thickness of the stratigraphic sections in this study.

2.2 Compilation of Sediment Mass/age Distributions

Several steps are involved in compiling the sediment mass/age distributions presented here. First the region is selected and divided into a regular grid. Second, a stratigraphic column (section) is compiled for each cell in the grid. The stratigraphic column in each grid

cell is divided into layers of sediment; a layer can be defined by age, lithology or both. Third, the mass of the solid-phase of the sediment per unit volume in a grid cell is calculated using a lithology-dependant curve that describes the solidity of sediment at different burial depths and from the grain densities for the lithologies. The mass of sediment of a given age in a grid cell is the sum of the masses of all the layers of that age in the column. The mass within the grid cell is the mass per unit volume times the area of the grid cell. The mass within a region is the sum of the masses in all of the grid cells in the region. Finally the masses of sediment that were compiled in terms of geologic age intervals are normalized to age intervals of equal length.

2.2.1 The Study Region and Data Grid

The study area is shown in Figure 2.1, a bathymetric map compiled from ETOPO5 (1986). ETOPO5 (1986) is a digital data set of global elevation on a 5 x 5' grid, and is the resolution at which the sheets of the General Bathymetric Chart of the Oceans (GEBCO, 1982) were compiled. The bathymetry shown in Figure 2.1 was averaged to a 10 x 10' grid from ETOPO5 (1986) data. The western edge of the region described in this chapter is defined by the continent-ocean boundary along the East Greenland margin. The eastern edge is the shelf break to the west and northwest of the United Kingdom and west of the Mφre High. The northern margin is the Jan Mayen Fracture Zone and the southern margin is the Charlie Gibbs Fracture Zone. North of the Greenland-Scotland Ridge the region belongs to what has come to be called the Greenland-Iceland-Norwegian (GIN) Sea. I follow the terminology of Coachman and Aagaard (1974), in referring to the region between Greenland, Jan Mayen and Spitsbergen as the Greenland Sea, the region between Greenland, Jan Mayen and Iceland as the Iceland Sea, and the remainder as the Norwegian Sea; the entire ocean area between Greenland-Scotland Ridge and the Fram Strait is referred to as the GIN Sea. All of the Iceland Sea, the southern half of the Norwegian Sea, and very little of the Greenland Sea is included in the study area.

The study region has been divided into a 1 x 1° latitude-longitude grid consisting of 668 cells, shown in Figure 2.2. The 1 x 1° grid realistically reflects the availability of geologic data but it degrades the bathymetric detail.

Figure 2.3 is the ETOPO5 (1986) bathymetry averaged to the 1 x 1° grid used here. Figure 2.3 shows the general bathymetric features of the region but some of the features seen in Fig. 2.1 are not resolved when the bathymetric data is averaged to a 1 x 1° grid. Conforming to the density of seismic lines in this region, the stratigraphic data used in this study were compiled on a 1 x 1° grid and the difference between Figs. 2.1 and 2.3 illustrates what is not seen on the coarser grid. Features seen in Fig 2.1 that are not resolved in Fig. 2.3 include: the Wyville-Thompson Ridge, Faeroe Bank Channel, Faeroe Bank, Bill Bailey's Bank, Rosemary Bank, George Bligh Bank, the Anton Dohrn Seamount, Hebrides Terrace Seamount, Edoras Bank, Eriador Seamount and Eirik Ridge. Lousy Bank is a relatively small-scale feature that can be seen on both Figures 2.1 and 2.3. In Fig. 2.1 the Faeroe-Shetland Channel (just north of the Wyville-Thompson Ridge) is shown having a depth > 750 m, but at the coarser resolution of the 1 x 1° grid (Fig. 2.3) the channel appears to be blocked by a ridge slightly less than 500 m deep. The sill from the Faeroe-Shetland Channel into the South Iceland Basin lies in the Faeroe Bank Channel between Faeroe Bank and the Faeroe Shelf on which the Faeroe Islands are located. The minimum depth in Faeroe Bank Channel is about 850 m. At the 10 x 10' resolution of Figure 2.1 Faeroe Bank Channel appears to be only slightly more than 500 m deep, and at the 1 x 1° resolution of Figure 2.3 Faeroe Bank Channel cannot be discerned. The area where it is located appears to be between 250 and 500 m deep. The sill depth over the WNW-ESE trending Wyville-Thompson Ridge is 650 m. It is correctly portrayed as between 500 and 750 m in Figure 2.1, but Figure 2.3 shows a N-S trending ridge between Faeroe Shelf and Scotland with a sill depth slightly less than 500 m. The general morphology of the Denmark Strait and Iceland-Faeroe Ridge are relatively well-preserved in the coarser grid, where the sill depths of approximately 600 and 500 m respectively are seen in both Figs. 2.1 and 2.3. The shelf margin of Iceland that is well-defined by the 250 m bathymetric contour in Fig. 2.1 is lost in Fig. 2.3. The sinuous shape of Jan Mayen Ridge seen in Fig. 2.1 is also obscured in Fig. 2.3. The entire irregularity of the seafloor seen in Fig. 2.1 is smoothed-out when plotted at the coarser grid resolution of Fig. 2.3.

2.2.2 Compilation of Stratigraphic Sections

The regional data are compiled from stratigraphic sections representative of the area within each grid cell. The stratigraphic section in each grid cell is referred to as a grid column and each of the stratigraphic-lithologic units in a column is called a layer. The stratigraphic columns are recorded as ASCII files. Each file represents the stratigraphy and lithology of a sediment column in a grid cell. All of the files together form a stratigraphic database. A column is divided from top to bottom by age and lithology. The minimum amount of information required to represent a column is the age of the top and bottom surfaces and a single lithology. Such a column would be said to consist of a single layer. The level of an unconformity may also be stored in the ASCII file but the age boundaries of the unconformity must be defined. Age boundaries (event surfaces) in a column can be entered as absolute ages or as the boundary of a geologic interval. The geologic intervals are converted to absolute ages from a reference timescale. The reference timescale used for this study is that of Berggren et al. (1985) and Kent and Gradstein (1986).

When the program (BalPal) reads a stratigraphic column from an ASCII file, it uses the reference timescale to define numeric ages for the top and bottom of each layer. Then it distributes the sediment mass in the column assuming constant accumulation rates between the age datums. An interval between datums can be any length of time, but for most compilations the shortest interval is not less than 1 m.y.

A stratigraphic section has been compiled for each grid cell. Within this area the total sediment thickness for each grid cell was interpolated from isopach maps of Tucholke (1988). Stratigraphy was interpreted from 22 Deep Sea Drilling Project (DSDP) and Ocean Drilling Project (ODP) Site reports, other literature sources and from seismic reflection profiles. Some published multichannel seismic profiles were used for this compilation but most of the data were taken from single-channel seismic reflection profiles available from the NOAA (U.S. National Oceanographic and Atmospheric Administration) National Marine Geophysical Data Center (Boulder, Colorado, U.S.A.). Figure 2.4 shows the distribution of single-channel seismic reflection profiles and the DSDP-ODP site locations used to compile the stratigraphic database. Most of the area between the Charlie Gibbs Fracture Zone and Greenland-Scotland Ridge has good seismic coverage with the exception of the South Iceland Basin from 35° to 20° W longitude and from 55° to 60° N latitude. The coverage is also sparse north of 60° N

latitude in the Irminger Basin. Stratigraphy for these less well-known regions was interpolated from the surrounding areas.

Figures 2.5 through 2.9 illustrate the quality of the single-channel seismic data used in the stratigraphic compilation. Figure 2.5 is a northwest to southeast profile through the Hatton-Rockall Basin. Seismic reflectors in this basin were correlated to DSDP Sites 116 and 117 (Laughton, Berggren et al., 1972). The data were collected in 1970 from the Lamont-Doherty ship R/V "Vema". A typical profile across the Reykjanes Ridge is shown in Figure 2.6 that runs from southwest to northeast. It is apparent that sediment is very thin across the ridge. The profile in Figure 2.6 was taken in 1978 aboard the Lamont-Doherty ship R/V "Robert Conrad". The continental margin along East Greenland has a very thick accumulation of sediment that can be partially seen in the single-channel profile shown in Figure 2.7. Seismic reflectors in Figure 2.7 were correlated to those from multichannel seismic profiles published by Larsen (1990). The Iceland Plateau to the west of the Jan Mayen Ridge in Figure 2.8 has a relatively thin sediment cover. The southern ridge complex of the Jan Mayen Ridge is shown in Figure 2.8, it forms a boundary between the shallow Iceland Plateau to the west and the deeper Norway Basin to the east. The Norway Basin (Figure 2.9) is the deepest ocean basin in the study area. In the center of the Norway Basin is Aegir Ridge. It was the initial center of seafloor spreading in this region and became extinct approximately 25 Ma when spreading shifted entirely to the Kolbeinsey Ridge on the Iceland Plateau.

Studies of sediment thickness show that the distribution of sediments in the North Atlantic and the GIN Sea is primarily controlled by plate tectonic processes and bottom currents. The total sediment thicknesses in the study area are shown in Figure 2.10. Sediments are very thin or absent on the crest of the modern active spreading centers. Over the central portion of Reykjanes Ridge sediments are less than 100 m thick but are closer to 200 m thick over the axis of Kolbeinsey Ridge. Sediments are thinner over extinct spreading centers in the Labrador Sea and the Norwegian Sea (Aegir Ridge). The position of the extinct Aegir spreading center is apparent from symmetric thinning of the sediment in the center of the Norway Basin. Sediment cover is also thin over the Greenland-Scotland Ridge. Sediment is absent on Iceland, only about 100 m thick on the Iceland-Faeroe Ridge and up to 1000 m thick in the Denmark Strait. Sediments increase in thickness to about 1500 m in regions of older crust. The largest accumulations of sediment are off Scoresby Sund, in Rockall Trough and the Faeroe-Shetland Channel. South of the Greenland-Scotland Ridge sediments have

been reworked by abyssal currents resulting in regional unconformities and the related deposition of sediment drifts. Sediment drifts are elongate bodies of fine-grained sediment that are deposited along bathymetric contours by deep-sea bottom currents. They may range from 200 to 2000 m in thickness and have lengths of up to hundreds of kilometers (Johnson and Schneider, 1969). A sediment drift can be recognized in seismic reflection profiles by characteristic morphologic features: sediment waves on the surface of the drift (eg. Feni, Gardar and Gloria Drifts) and multiple high-amplitude parallel to subparallel internal reflectors (eg. Eirik Drift). Sediment drifts make up about 18% of the total volume of sediment between the Charlie Gibbs Fracture Zone and Greenland-Scotland Ridge. An analysis of the masses of sediment of different ages provides insight into the history of sedimentation.

Seismic stratigraphic markers are key elements in extending the stratigraphy from DSDP and ODP drill sites over a broader region. In the areas discussed below certain DSDP and ODP Sites and widely recognized seismic stratigraphic markers are critical to interpretation of the regional stratigraphy.

2.2.2.1 Rockall Plateau-Rockall Trough

Roberts (1975) first recognized a prominent reflector observed in most seismic reflection profiles on Rockall Plateau, in Rockall Trough, and around the Wyville-Thompson Ridge and Faeroe Basin. The reflector was named "R4" and Roberts et al. (1981) further delineated its extent. In Rockall Trough the R4 equivalent was called the Challenger reflector by Dingle et al. (1982). It is the "green reflector" of Masson and Kidd (1987). On Rockall Plateau R4 represents an unconformity at the base of the Oligocene. At DSDP Site 117 on the eastern margin of the Hatton-Rockall Basin, the unconformity lasts from the Lower Eocene to Lower Oligocene. Towards the center of the basin near DSDP Site 116, the length of the unconformity decreases to Lower to Upper Oligocene (Laughton, Berggren et al., 1972). At DSDP Sites 404 and 405 (Montadert, Roberts et al., 1979) on the southwest margin of Rockall Plateau the unconformity marked by R4 represents the Middle Eocene to Lower Oligocene. At DSDP Site 406, only 5 nautical miles south of Site 405, it lasts from Upper Eocene to Middle Oligocene (Roberts et al., 1979). The sediment above reflector R4 is mostly calcareous ooze and below it are limestones and mudstones (Laughton, Berggren et al., 1972).

From drilling at DSDP Site 610 in southern Rockall Trough, Masson and Kidd (1987) reinterpreted the age and nature of reflector R4 to be a upper Lower Miocene "regional oceanographic event" and described it as an episode of increased production of biogenic silica.

Feni Drift (Johnson and Schneider, 1969; Jones et al., 1970) is located on the southern and eastern flanks of Rockall Plateau (Figs. 2.1 and 4.4). Drilling at DSDP Site 610 (Ruddiman, Kidd, Thomas et al., 1987) just reached the upper Lower Miocene "green reflector" of Masson and Kidd (1987). From multichannel seismic data Kidd and Hill (1987) interpreted the onset of sedimentation on Feni Drift to correspond to their "brown reflector" which they believed to be upper Eocene or lower Oligocene. By correlating the stratigraphy at DSDP Site 610 with multichannel seismic reflection profiles, Masson and Kidd (1987) concluded that the drift began to form just after the end of the Eocene and has been accumulating ever since.

The stratigraphy of older sediments in Rockall Trough is not well known because of the difficulty in imaging the deeper strata and because the deeper strata have never been penetrated by the drill. It is assumed that the oldest sediments in southern Rockall Trough are Late Cretaceous or older (Roberts et al., 1981; Masson and Kidd, 1987).

Hatton Drift (Ruddiman, 1972) lies on the western margin of Rockall Plateau (Figs. 2.1 and 4.4). Stow and Holbrook (1984) concluded that from the Early Eocene until the mid-Miocene bottom currents were too strong to allow a drift to accumulate in this area. They believed the age of initiation of Hatton Drift is thus assumed to be early Middle Miocene.

Bjorn and Gardar Drifts lie on the eastern flank of Reykjanes Ridge (Figs. 2.1 and 4.4). Bjorn Drift (Laughton, Berggren et al., 1972) has an average depth of 1800 m and Gardar Drift (Johnson and Schneider, 1969) lies below it at a depth of about 2800 m. Their crests merge to the south. Bjorn Drift was drilled on DSDP Leg 12 at Site 114 (Laughton et al., 1972) and the southern tip of Gardar Drift was drilled during DSDP Leg 94 at Site 611 (Ruddiman, Kidd, Thomas et al., 1987). Single-channel seismic profiles indicate that Gardar Drift overlies the late Early Miocene "IR" seismic reflector of Ruddiman (1972) which corresponds to the R2 reflector of Miller and Tucholke (1983).

2.2.2.2 The East Greenland Margin and Irminger Basin

On the southeast Greenland margin near 63° N latitude, Larsen (1990) recognized three seismic sequences representing Late Paleocene to Eocene, Eocene to Early Oligocene and Miocene to Plio-Pleistocene. He had profiles extending from the continental shelf to the Irminger Basin over oceanic crust. Based on seismic profiles published by Larsen (1990), I have assumed that there is a Lower Oligocene to Miocene unconformity along the southeastern Greenland margin and eastern Irminger Basin.

The three major sediment drifts in the Irminger Basin and southern Labrador Sea are the Snorri (Egloff and Johnson, 1979) on the west flank of Reykjanes Ridge, Eirik (Johnson and Schneider, 1969) which extends out from the southern tip of Greenland, and Gloria (Egloff and Johnson, 1975) which is located in the northern Western North Atlantic Basin (Figs. 2.1 and 4.4). The areal extent of Snorri Drift on the western flank of Reykjanes Ridge was difficult to determine because of poor seismic coverage and because the drift does not have the distinctive morphology that would make it easy to recognize.

Eirik Drift can be distinguished from the surrounding sediment by the reflection characteristics of its seismic sequences and by the pronounced increase in sediment thickness compared to the surrounding region. In single-channel seismic reflection profiles Eirik Drift displays numerous parallel to subparallel internal reflectors. Sediment waves on the surface of Gloria Drift are obvious in seismic reflection profiles and serve to distinguish it from the surrounding sediments.

Drilling at ODP Site 646 on the southwestern flank of Eirik Drift demonstrated that drift accumulation did not begin until the Early Pliocene. The drift was built mostly during the Pliocene and is composed of clays and silts (Srivastava, Arthur, Clement, et al., 1987). Initiation of drift accumulation is marked by seismic reflector R2 of Arthur et al. (1989).

2.2.2.3 The Iceland Plateau

This region lies north of Iceland between Greenland and the Jan Mayen Ridge complex. The only direct information about the stratigraphy of this region comes from DSDP Site 348 from Leg 38 (Talwani, Udintsev et al., 1976). In the Initial Report for Site 348, Talwani, Udintsev et al. (1976) showed an unconformity between the Pliocene and Upper

Miocene. Reanalysis of the data by Pearson and Jenkins (1986) indicated that there are no unconformities at Site 348, and their interpretation is followed here. The stratigraphy at Site 348 was extrapolated to the surrounding grid cells within a radius of about 100km. The age of the top of each sediment column in the rest of the Iceland Plateau region is assumed to be Quaternary and the age of the base of each sediment column is assumed to be the same as the crustal age determined from plate tectonic modelling (Chapter 3).

2.2.2.4 Greenland-Scotland Ridge

The thin sediment cover on the insular shelf of Iceland has been interpreted as Pleistocene and Pliocene glacial deposits, the older sediments having been eroded by glaciers during lowstands of sea level (Vogt et al., 1980). Pleistocene sediments have been analyzed offshore of the Vatnajökull Glacier and were found to consist dominantly of glacial tills (Boulton et al., 1988). Based on this information the thin sediment cover on the Icelandic shelf is interpreted here as Pleistocene and Pliocene till.

Ridd (1983) outlined the Tertiary geology of the Faeroe-Shetland Channel based on previous work (Ridd, 1981) and commercial well information from the Faeroe Basin. Above Cretaceous shales on the southeast side of the basin there is an unconformity in the Lower Paleocene and another unconformity between the Miocene and Lower Oligocene. The oldest sediment in the Faeroe-Shetland Channel is Lower Cretaceous (Ridd, 1983) and the last phase of crustal extension took place in the Late Paleocene (Ridd, 1983). Around the Wyville-Thomsom Ridge, reflector R4 (Roberts, 1975; Roberts et al., 1981) represents a regional unconformity of Eocene-Oligocene age. Post R4 seismic sequences are characterized by frequent unconformities while pre R4 seismic sequences are transparent indicating a lack of unconformities (Roberts et al., 1983).

2.2.2.5 Jan Mayen Ridge to Aegir Ridge

The northern Jan Mayen Ridge was drilled at DSDP Sites 346, 347, and 348 and the Southern Ridge Complex at Site 350 during Leg 38 (Talwani, Udintsev et al., 1976). The remaining part of the region east of the Jan Mayen Ridge complex to the extinct Aegir Ridge has not been drilled. The stratigraphic compilation for this region is based on extrapolation

of the stratigraphy and lithology described at the DSDP sites along single-channel seismic reflection profiles. The single-channel seismic reflection profiles were correlated with multichannel seismic reflection profiles published by Gudlaugsson et al. (1988). The Lower Oligocene unconformity drilled at DSDP Sites 346, 347 and 349 occurs between seismic sequences 2 and 3 of Gudlaugsson et al. (1988) and can be recognized in single-channel seismic reflection profiles. An unconformity from the Upper Oligocene to Middle Miocene was drilled at DSDP Site 350 on the eastern side of the Southern Ridge Complex of Jan Mayen Ridge (Talwani, Udintsev et al., 1976).

2.2.2.6 Aegir Ridge to North European COB

In the southern part of this region, on the north flank of the Iceland-Faeroe Ridge, an unconformity from the Upper Oligocene to Lower Pliocene has been interpreted from drilling at DSDP Site 336 (Talwani, Udintsev et al., 1976) and from seismic data (Krawczyk, 1990). In the north the grid cell stratigraphy was extrapolated from ODP Leg 104, Site 643 (Eldholm, Thiede, Taylor et al., 1987). At site 643, Wolf and Thiede (1991) reported a Middle to Upper Miocene unconformity (13.7 to 8.8 Ma), another unconformity in the Upper Miocene (6.9 to 6.0 Ma) and an unconformity at the Miocene-Pliocene boundary (5.6 to 4.2 Ma). On top of a rift mountain on the eastern flank of Aegier Ridge at DSDP Site 337 (Talwani, Udintsev et al., 1976), Thiede et al. (1986) reported continuous sedimentation from the Lower Oligocene to Present. They derived linear sedimentation rates, sediment thickness divided by basement age, for Site 337 and found an average rate of approximately 2 m / m.y. from Lower Oligocene to Pliocene and 9 m / m.y. for the Pliocene and Quaternary. Deep sea drilling in the Norway Basin has only been on top of topographic highs and the existing information from the DSDP-ODP drill sites does not reflect the true nature of the majority of sediment in the basin. It is difficult to extrapolate stratigraphy from the margins to the center of the basin from seismic data and the stratigraphy of most of the basin remains unknown.

2.2.3 Estimating the Masses of the Solid-Phase of the Sediment

Most discussion of the compaction of sediment with burial are presented in terms of the reduction of porosity with depth. The porosity of sediment is the proportion of the volume of sediment taken up by pore-space between the sediment grains. Porosity is expressed as a percentage of the total volume of the sediment. In calculating the masses of the solid phases sediment, the solidity of the sediment must be used. The solidity (S) is related to porosity by

$$S = 100\% - \text{porosity}. \quad (2.1)$$

The most complete discussions of the decrease of porosity or increase of solidity with depth are those of Baldwin and Butler (1985) and Huang and Gradstein (1990). Baldwin and Butler (1985) compared previously published compaction curves for argillaceous sediments, limestones and sandstones. They derived new equations to describe the increase of solidity with depth for each of these lithologies, using power-law equations of the form

$$Z = Z_{max}S^{\alpha} \quad (2.2)$$

where Z is the burial depth and $S^{\alpha}$is the solidity raised to the power α, or exponential equations of the form

$$P = P_0e^{-bz} \quad (2.3)$$

where P is the porosity, P_0 is the average porosity at the surface, b is a constant, and z is the burial depth. Huang and Gradstein (1990) calculated depth-porosity equations for sediments on the ocean floor. Their database consisted of porosity data collected from 31 Deep Sea Drilling Project (DSDP) and Ocean Drilling Project (ODP) drill sites from the Atlantic, Indian and Pacific Oceans. To model the decrease of porosity with increasing depth they used the least squares method to fit five different types of curves to the data and chose the one with the lowest residual sum of squares. Both Baldwin and Butler (1985) and Huang and Gradstein (1990) discussed the porosity-solidity relation to depth in terms of kilometers. I follow that convention here, but it should be noted that all calculations performed with the paleogeographic modelling software (BalPal) are done in meters, so that the programmed equations differ numerically from those presented here.

Baldwin and Butler (1985) compared a number of empirical equations for the decrease of porosity versus depth in shales (Athy, 1930; Dickinson, 1953; Baldwin, 1971; Durmish'yan, 1974; Magara, 1976; and Hunt, 1979). They concluded that the increase of solidity with increasing depth is best modelled using two different equations; one for shales

with a thickness less than 200 m ("normal") and one for shales with thickness greater than 200 m ("undercompacted"). The solidity versus depth equations for shales are applicable to clay, claystone, mud, mudstone and shale. Baldwin and Butler (1985) modelled the compaction of shales with a thickness less than 200 m (their "normal" shales) using a power law equation,

$$D = 6.02 \times S^{6.35}, \quad (2.4)$$

where D is the burial depth in meters. They stated that shales with a thickness greater than 200 m tend to be undercompacted because they do not lose water readily. Their best-fit curve for undercompacted shales was also calculated from a power law equation,

$$D = 15 \times S^{8}. \quad (2.5)$$

Although a power law equation may represent the best fit to most of the observed data, the endpoints of the curve predict unrealistic porosities and solidities. Power law equations predict 0% solidity for sediment at the surface and reach 100% solidity at some fixed depth with solidity increasing beyond 100% at greater depths. To avoid these problems the values of solidity between 0 and 1 m depth and below the maximum depth are kept constant.

Huang and Gradstein (1990) grouped clay, claystone, mud, mudstone and shale together as the lithologies that compact like claystone. Their porosity versus depth equation for claystone is exponential and was given as

$$\phi = 0.707 \times e^{(-0.633 \times D)}, \quad (2.6)$$

where ϕ is the porosity. From Eqn. (2.1) we can convert Eqn. (2.6) into a solidity versus depth equation where

$$S = [1.0 - (0.707 \times e^{-0.633 \times D})] \times 100\% \quad (2.7)$$

and the solidity is expressed as a percent (Fig. 2.11). Because Huang and Gradstein (1990) exclusively analyzed deep sea sediments, their curves are more applicable to the northern North Atlantic database described in Section 2.2.2. However, Huang and Gradstein (1990) were only able to analyze data between the seafloor and 1700 m burial depth. They did not recommend that their curves be used for greater depths. For the upper 1700 m of the sediment column the Huang and Gradstein (1990) compaction curve for shale predicts solidities that are 10 to 15% less than those predicted by the Baldwin and Butler (1985) curves (Fig. 2.11). The extrapolation of the Huang and Gradstein (1990) curve below 1700 m appears to be a good approximation of solidity at greater depths. It coincides with the Baldwin and Butler

(1985) curve below 3000 m and lies between the two Baldwin and Butler curves between 1700 and 3000 m burial depth. Because of its general applicability, this study uses the Huang and Gradstein (1990) curve to model the solidity versus depth for clays and shales.

The decrease of porosity with increasing depth in limestones was described by Baldwin and Butler (1985) with the same power law equation they used for "normal" shale. Eqn. (2.4) applied to limestone includes unlithified calcareous ooze, semi-lithified chalk and lithified limestone.

Huang and Gradstein (1990) modelled the solidity versus depth behavior of limestones using a power law equation for porosity

$$\phi = 1 - 0.755 \times D^{0.254} \qquad (2.8)$$

and rewriting Eqn. (2.8) for solidity

$$S = 0.755 \times D^{0.254}. \qquad (2.9)$$

Eqn. (2.8) was calculated from porosity data for unlithified calcareous ooze, semi-lithified chalk and lithified limestone in the upper 1700 m of a sediment column. In order to incorporate the lower solidities predicted at shallower depth by Eqn. (2.9) with those at greater depth, Eqn. (2.4), I devised a "modified" curve

$$S = [(D / 6.02)^{0.185}] \times 100\%. \qquad (2.10)$$

Differences between the curves calculated from Eqns. (2.4, 2.9 and 2.10) are illustrated in Figure (2.12).

For sandstones, Baldwin and Butler (1985) used the data of Maxwell (1964) to model the solidity versus depth relationship. The data from Maxwell (1964) were primarily from quartz sandstones in oil and gas reservoirs. Baldwin and Butler (1985) found that the data were best fit by the Sclater and Christie (1980) equation for porosity versus depth in North Sea sandstones. The equation from Baldwin and Butler (1985) is

$$D = 3.7 \times \ln[0.49 / (1 - S)] \qquad (2.11)$$

or when solved for solidity

$$S = \{1 - [0.49 / e^{(D / 3.7)}]\} \times 100\% \qquad (2.12)$$

From analysis of DSDP and ODP drill site porosity data Huang and Gradstein (1990) found that between 150 and 1500 m burial depth the reduction of porosity in sandstones was best represented by a linear decay equation

$$\phi = 0.574 - 0.202 \times D. \qquad (2.13)$$

The linear increase of solidity with depth predicted by the Huang and Gradstein (1990) curve is less than that of Baldwin and Butler (1985) in the top 1000 m of the sediment column (Fig. 2.13). Below this depth the curves of Baldwin and Butler (1985) and Sclater and Christie (1980) predict lower solidities. It would be unrealistic to extend the Huang and Gradstein (1990) curve to greater burial depths because it would predict solidities greater than 100%. It is also unrealistic to assume that sandstone solidities would ever reach 100%. Hence, the solidity versus depth relationship predicted by an exponential decay curve is preferred. I devised a modification of Eqn. (2.13) to incorporate both the lower solidities of deep sea sediments in the upper 1000 m of the sediment column (Huang and Gradstein, 1990) and the values predicted at greater depths by an exponential curve (Baldwin and Butler, 1985; Sclater and Christie, 1980).

$$S = \{1 - [0.574 / e^{(D / 3.1)}]\} \times 100\% \qquad (2.14)$$

Sandstone compaction curves calculated from Eqns. (2.12, 2.13 and 2.14) are shown in Figure 2.13.

Because the database is limited, generalized compaction curves for the wide variety of different types of sediment have not been published. Different lithologies assumed to have similar compaction properties are therefore grouped together and modelled to lose porosity with increasing burial depth in a fashion similar to shales, limestones or sandstones (Fig. 2.14). The solidities of different sediments are thus estimated according to one of three empirical equations (2.7, 2.10 or 2.14) representing shales, limestones and sandstones as indicated in Table 2.1.

2.2.4 The Mass of Sediment of a Given Age

The mass of sediment of a given age interval in a region is the sum of the masses of the solid-phase sediment of that age in all of the grid cells, and is calculated in a series of steps.

The mass of the solid-phase per unit volume of sediment (M_{SP}) in a layer is the product of the grain density (ρ_G) expressed in terms of the unit volume multiplied by the solidity of the sediment

$$M_{SP} = \rho_G \times S. \qquad (2.15)$$

To calculate the mass of a layer of sediment M_L in a grid column, the mass of the solid-phase per unit volume is multiplied by the volume of the layer

$$M_L = M_{SP} \times T \times A. \quad (2.16)$$

The volume of a layer of sediment in a grid column is product of the area of the grid cell (A) multiplied by the thickness of the layer (T). Because a spherical grid (latitude-longitude) is used in this model, the area of each cell decreases from a maximum value at the equator to a minimum at the pole. Latitude is specified relative to the center of a grid cell and the area of a grid cell at some latitude (lat) is given by

$$A = [12309 - lat^{(2.201 - 0.0012 \times lat)}] \times L^2, \quad (2.17)$$

where L^2 is the square of the arc-length of one side of a grid cell. The arc-length is expressed as a decimal degree value, eg. for a 1 x 1° grid cell the arc-length = 1.0 and for a 1/2 x 1/2° grid cell the arc-length = 0.5. A 1 x 1° grid cell centered on the equator (lat = 0) has an area of 12,309 km^2. In Eqn. (2.17), 1° of latitude and longitude are equal to approximately 111 km at the equator.

The masses of the all layers or portions of layers of a given age interval in each grid cells are then summed and these sums for all of the grid cells are added to give the mass of the solid-phase of the sediment of a given age for the entire region.

2.3. Regional Mass/age Compilations

The study area contains two basinal areas, the northern North Atlantic and southern GIN Sea, separated by a shallow barrier, the Greenland-Scotland Ridge. To facilitate interpretation of the sediment mass/age distributions, the area has been divided into subregions of similar stratigraphy, shown in Figure 2.15. Comparison of the mass/age distributions of different subregions and groupings of subregions can show whether the same events are found throughout the region or whether the individual basins have different sediment sources and histories. At the stratigraphic resolution available on the seismic profiles used to compile the database, the sediments throughout the study area are predominantly detrital. For this reason the mass/age distributions are not subdivided by lithology. Because of the significance of drift sedimentation south of the Greenland-Scotland Ridge, the distributions in that area are divided into total sediment, drift sediment, and total minus drift sediment. The summary data for areas, volumes and masses of sediment in each region is given in Table 2.2.

Neither the whole nor any of the subregions of the study area constitutes a closed system, so the method for reconstructing past sediment fluxes described in Chapter 1 cannot be applied here. The four basin areas shown in Figure 2.15 each have a separate source area, and each appears to be a separate sediment sink at present.

2.3.1 The Entire Study Area: Between the Charlie Gibbs and Jan Mayen Fracture Zones and between Greenland and the British and Norwegian Margins

South of the Greenland-Scotland Ridge the study region includes Rockall Trough, Rockall-Hatton Bank, the South Iceland Basin, Reykjanes Ridge, Irminger Basin, and the East Greenland margin. North of the Greenland-Scotland Ridge the study area includes the Iceland Plateau including the Kolbeinsey Ridge, the Jan Mayen Ridge and the Norway Basin with the extinct Aegir Ridge in its center.

The mass/age distributions for all sediment in the study region is shown at the top of Figure 2.16 (labelled CGFZ to JMFZ). The total sediment mass/age distribution has the form of an exponential decay. This is most readily explained by seafloor spreading (see Chapter 4) where the overall sediment mass increases with time as the area of seafloor increases. The masses generally decay from the Present through the Late Oligocene. They rise in the Late Eocene and Early Oligocene and then decay gradually to the Paleocene. As will be addressed in Section 2.4 Discussion, this pattern may be a result of reversal of drainage along the Greenland margin 20 to 30 m.y. after sea-floor spreading between Rockall Plateau and Greenland began.

Following the late Eocene-early Oligocene sediment mass peak is a decrease in observed sediment mass and a gradual increase to the present. The increase from mid-Oligocene to Present has the general shape of an exponential decay curve and could be due to the increase of the area of the seafloor with time. If the sediment mass were dominantly pelagic then the observed mass would increase simply because there is a larger area of seafloor upon which to deposit sediment.

2.3.2 The Northern North Atlantic: Between the Greenland-Scotland Ridge and Charlie Gibbs Fracture Zone and between Greenland and the British Isles

The northern North Atlantic region includes Rockall Trough, Rockall-Hatton Bank, the South Iceland Basin, Reykjanes Ridge, Irminger Basin, and the East Greenland margin. It includes Feni, Hatton, Bjorn, Gardar, Snorri, Eirik and Gloria Drifts.

The mass/age distributions for sediment between the Greenland-Scotland Ridge and the Charlie Gibbs Fracture Zone is shown in the center of Figure 2.16 (labelled CGFZ to GSR). Overall, the total sediment mass/age distribution has the form of an exponential decay, but with a sharp increase since the middle of the Late Miocene. The masses decay gradually from the Late Miocene through the Late Oligocene. They rise in the Late Eocene and Early Oligocene and then decay gradually to the Paleocene. These increases and decreases in the mass/age distribution through time will be discussed separately for the regions to the east and west of Reykjanes Ridge.

2.3.3 Reykjanes Ridge to Rockall Trough

This region includes Faeroe Basin, the area around Wyville-Thompson Ridge, Rockall Trough, Rockall-Hatton Basin, the South Iceland Basin, and the eastern side of Reykjanes Ridge. It includes Feni, Hatton, Bjorn and Gardar Drifts. The sediment mass/age distribution for this region is shown on the top of Figure 2.17. The distribution for the total sediment is a remarkably even, almost constant, decay from the Late Miocene to the Late Paleocene. There is no appreciable increase in the mass of Late Eocene and Early Oligocene sediment. This partially due to the fact that approximately half of the region is underlain by continental crust and the resulting mass/age distribution has not been affected by seafloor-spreading. The other factor is the type of sediment input to the basin, this must have been mostly detrital sediment with relatively constant rates of input during the Tertiary. The overall mass/age distribution shows a major increase in sedimentation rates in the Pliocene to Quaternary. The mass of sediment not in drifts (center of Fig. 2.17) is very nearly constant, with a small increase in the Late Pliocene and Quaternary. The accumulation of sediment in drifts (bottom of Fig. 2.17) began at the end of the Eocene, and comprised about 20% of the total sediment throughout the Oligocene and early Early Miocene. In the late Early Miocene the drift

sedimentation in this region increased to one-third the total sedimentation and continued at this rate through the Late Miocene. In the Pliocene drift sedimentation was the dominant process in the region and accounts for the Pliocene to Quaternary peak in the overall mass/age distribution (top of Fig. 2.17).

2.3.3.1 Feni Drift

Feni Drift apparently began to accumulate at the beginning of the Oligocene (36 Ma) and has remained essentially constant since that time with a slight decrease in the Early Miocene and then an 18% increase in the early Middle Miocene over Oligocene masses (Fig. 2.18). This suggests that the drift has been accumulating at a relatively constant rate, and has not suffered any significant episodes of erosion. It also attests to the fact that Feni Drift is younger than the lithosphere, i.e. its mass/age distribution does not have the shape of an exponential decay due to seafloor spreading.

2.3.3.2 Gardar Drift

Gardar Drift began to accumulate at the end of the Early Miocene (18 Ma). At the beginning of the Pliocene the sediment mass tripled and then increased to over 6 times that of the Miocene in the middle Pliocene (Fig. 2.18). In the Quaternary the mass declined to half the middle Pliocene maximum. The shape of the curve might suggest that the Miocene sediments of Gardar Drift have been eroded to produce part of the Pliocene and Quaternary drift sediment. However, the pattern for the Miocene is so flat that it is hard to imagine that erosive processes in the Early Pliocene could have attacked Miocene sediment of all ages equally. It is more likely that the drift has suffered little erosion, and that the rapid increase in Pliocene and Quaternary represents sediment introduced from an outside source. The increased sediment supply was probably from increased erosion of Iceland and the Iceland-Faeroe Ridge. The Miocene masses in Gardar Drift are only slightly less than those in Feni Drift.

2.3.3.3 Bjorn Drift

Like Gardar Drift, Bjorn Drift began to form at the end of the Early Miocene (18 Ma). However, in this case the mass/age distribution (Fig. 2.19) shows some small fluctuations that might represent either changes in the sediment supply or minor erosive episodes. For the Pliocene and Quaternary the sediment masses are double the Miocene average. In this case it is possible that the Pliocene-Quaternary increase could come from erosion of older sediments in Bjorn Drift, but from comparison with the adjacent Gardar Drift it seems more likely that the increase is a result of increased sediment supply. Again the source of sediment for Bjorn Drift was most likely the same as that for Gardar Drift, i.e. Iceland and the Iceland-Faeroe Ridge.

2.3.3.4 Hatton Drift

The mass/age distribution for Hatton Drift (Fig. 2.20) indicates that it began to form at the beginning of the Middle Miocene, 16 Ma. Like that for Feni Drift on the other side of Rockall Plateau, the distribution is remarkably constant, showing only a slight increase for the Pliocene and Quaternary.

2.3.4 Greenland to Reykjanes Ridge

This region includes the western flank of Reykjanes Ridge, the Irminger Basin, and the eastern margin of Greenland. It includes Snorri, Eirik and Gloria Drifts. The mass/age distribution for this region is shown in Figure 2.21. For the total sediment mass, the distribution resembles two successive exponential decays, one starting from the present and decaying sharply to a low level the Middle Miocene, and continuing to decay gradually until the middle of the Oligocene. The older sediments show a maximum in the Late Eocene and a decay back to the Paleocene. As discussed above, the Late Eocene to Early Oligocene sediment maximum may be the reflection of erosion of terrigenous sediment from Greenland in response to reversal of drainage after the separation of the Iceland platform from Greenland. The mass/age distribution for sediment not in drifts is similar to that for the total sediment except for the Pliocene and Quaternary. In this region the sediment in drifts is

wholly latest Miocene and younger. During the Pliocene and Quaternary about 40% of the sediment deposited in this region is in drifts.

2.3.4.1 Eirik Drift

The mass/age distribution for Eirik Drift (Fig. 2.19) is the opposite of what is usually expected from a mass/age distribution, showing a sharp increase in masses from Quaternary through Pliocene. The shape of this distribution argues against erosion of the older material in the Drift, and suggests that it represents a changing sediment supply. It had its origin at the beginning of the Pliocene, and sediment supply immediately reached its maximum. The sediment supply has been declining ever since.

2.3.4.2 Snorri Drift

Sediment masses in Snorri Drift show a general and almost even increase to present (Fig. 2.20). The oldest drift sediments are 16 Ma, early Middle Miocene. The distribution has the classic form of an exponential decay, suggesting that Snorri Drift may be undergoing erosion and redeposition. The alternative explanation is that the sediment supply to Snorri Drift has been steadily increasing, a condition not observed on any other drift in this region.

2.3.4.3 Gloria Drift

Like Eirik Drift, Gloria Drift (Fig. 2.20) began to form at the beginning of the Pliocene, about 5 Ma. Unlike Eirik drift, the distribution shows masses decreasing from Quaternary to Early Pliocene. Although some of the Early Pliocene drift sediment might have been subsequently eroded, it is most likely that the distribution for Gloria Drift represents a sediment supply that has been increasing with time.

2.3.5 The Southern GIN Sea: From Greenland-Scotland Ridge to Jan Mayen Fracture Zone, and From Greenland to the Norwegian Margin

The southern GIN Sea region includes the eastern Greenland margin between the Greenland-Scotland Ridge and Jan Mayen Fracture Zone, the Kolbeinsey, Jan Mayen and Aegir Ridges, the Iceland Plateau and the Norway Basin. Figure 2.16 shows the mass/age distribution for sediment in this region. The sediment mass/age distribution has the shape of an exponential decay curve characteristic of control by seafloor spreading.

2.3.6 Greenland to Jan Mayen Ridge

This area, between the Denmark Strait and Jan Mayen Fracture Zone, and between the Greenland Margin and Jan Mayen Ridge, includes the present active spreading center, Kolbeinsey Ridge, and the Iceland Plateau. Because ocean floor did not begin to form in this area until the Middle Eocene, the mass/age distribution (top of Fig. 2.22) decays from large Neogene values to zero in the Middle Eocene. The mass of sediment increases gradually from the Middle Eocene until the Miocene, when masses start a more rapid rise that culminates in the early Late Miocene. After a slight decline in the Pliocene, the masses increase through the Pliocene and Quaternary. The large mass of sediment from the Present through late Middle Miocene is primarily due to the very thick and relatively young sediment seaward of Scoresby Sund.

2.3.7 Jan Mayen Ridge to Faeroe-Shetland Escarpment

This area comprises the entire Norway Basin. The mass/age distribution represents a relatively constant rate of sediment input with a major interruption in the Miocene (bottom of Fig. 2.22). Pre-Miocene sediment masses are similar to those in the Plio-Pleistocene. During the Miocene the observed sediment mass decreases due to numerous wide-spread unconformities (eg. Talwani, Udintsev et al, 1976; Pearson and Jenkins, 1986; Krawczyk, 1990; Wolf and Thiede, 1991). This could represent a period of increased erosion and redistribution of sediment by bottom-water currents or decreased sediment supply. The stratigraphy compiled for the Norway Basin remains however speculative, because only

topographic highs within the basin have been drilled and the majority of Cenozoic sediment within the deep basin remains unsampled.

2.4 Discussion

A measure of the overall sedimentation in a region is given by normalizing the sediment mass to the size of the basin, expressed by the ratio of mass to area as shown in Table 2.2. The largest supply of sediment has been to the region from Reykjanes Ridge to Rockall Trough. The least accumulation in relation to their area has been in the Greenland to Reykjanes Ridge (Irminger Basin) and Jan Mayen Ridge to Norway (Norway Basin) regions. Supply of sediment to the region between Greenland and Jan Mayen Ridge (Iceland Plateau) was intermediate between those to the other basins.

The shapes of mass/age distributions offer clues to the erosional-depositional history of a region. Mass/age distributions can be expected to show a gradual exponential decay reflecting sediment recycling, if part of the region is undergoing erosion and another part of the region is a site of deposition. A mass/age distribution may show a more rapid apparent exponential decay with increasing age if the region is one where sea-floor spreading is occurring. Assuming a constant pelagic sediment input per unit area, the increase in the area of ocean floor with time means that the mass of sediment accumulating on it must increase with time. If the distribution represents an area that has remained constant in size and has been only a sediment sink that underwent no erosion, the masses of sediment are a direct reflection of the sediment flux into the sink. A number of these possibilities are illustrated by the mass/age distributions for the basins in the study area.

Comparison of the mass/age distributions for the whole study area, the areas north and south of the Greenland-Scotland Ridge, and for the major basins in the study area suggests that the local mass/age distributions contain important information on the geologic history of the area. The distribution for the whole area and the areas north and south of Greenland-Scotland Ridge show a general increase of preserved sediment through time as would be expected for an ocean basin that is increasing in size. South of the Greenland-Scotland Ridge the late Eocene-early Oligocene sediment peak is suggestive of a basinwards change in direction of the slope of the borderlands resulting in increased delivery of detrital sediment to the ocean basin approximately 20 m.y. after initial separation of the continents.

The importance of the reversal of drainage in the borderlands from away from the rift to towards the rift was recognized by Hay (1981), Hay and Behensky (1981), and Southam and Hay (1981) in the context of the broad pattern of development of passive margins. They suggested that as a continent ruptures, the region surrounding the site of a future ocean basin is uplifted for a long period before continental separation occurs. They attributed this to the effect of a relatively light mantle plume rising through more dense lithosphere, and thought that uplift from this process might start as early as 60 to 80 m.y. prior separation of the continental blocks. During this phase, detritus eroded from the uplifted region is transported away from the site of the future ocean. About 30 m.y. before continental separation a graben develops along the site of the future ocean as the rising mantle plume replaces continental crust. By 10 m.y. prior to separation the graben has subsided to sea level. Lacustrine and fluvial sedimentation occurs in the graben as it forms, but most of the sediment from the bordering uplifted shoulders is transported away from it. During the 10 m.y. prior to continental separation, rifting and subsidence continue. Restricted connections may allow the ocean to enter the graben. In low latitudes this results in development of hypersaline conditions and lagoonal circulation. Extensive evaporite deposition may occur. At high latitudes it could result in the young ocean having a lower salinity and estuarine circulation. The restricted connection to the ocean and differentiation of the waters in the young ocean from those of the open ocean continue for about 10 m.y. after separation of the continents and initiation of seafloor spreading. Sometimes these narrow ocean basins are restricted from larger ocean basins by shallow sills (eg. Greenland-Scotland Ridge). Because the ocean crust is so young the new ocean basin is much shallower than older adjacent oceans and can only be filled by surface to intermediate water masses from the open ocean (Thiede, 1978). For the next 20 m.y. the young ocean exists as a narrow seaway, but the slope of the adjacent borderlands is still away from young ocean. During the next 20 m.y., from 30 to 50 Ma after separation, erosion and thermal subsidence cause the continental margins to subside to sea level. By 30 m.y after separation of the continents the drainage on the adjacent borderlands has begun to reverse, bringing detrital sediment to the young ocean basin. As the reversal of slope proceeds, there is a large input of detrital sediment to the new ocean basin.

Seafloor spreading between Greenland and Eurasia began 57.5 Ma (Eldholm, 1991), and the oldest peak in Tertiary sediment mass occurs in the late Eocene-early Oligocene 20 to 30 m.y. after seafloor spreading started. Reversal of drainage of the adjacent continental

borderlands in response to thermal subsidence could account for this peak in preserved sediment mass so long after the continental separation occurred.

The increased delivery during the Eocene is observed only in the western basins along the Greenland margin. The eastern basins do not show any appreciable change in sediment flux. The suggestion is that the Greenland margin was uplifted more by the rifting process than the European margin.

The beginning of the decrease in preserved sediment in the Early Oligocene could be due to a decreased terrigenous sediment supply or to initiation of extensive erosive activity by bottom-water currents. South of the Greenland-Scotland Ridge this time corresponds to the initiation of sediment accumulation in Feni Drift. North of the Greenland-Scotland Ridge the sediment mass/age distribution appears primarily to reflect pelagic sedimentation in a growing ocean basin.

Throughout its history the Norway Basin has been one of the deepest basins north of the Greenland-Scotland Ridge (see Chapter 3). As such it may have acted as a sediment sink during the Cenozoic. It is thus difficult to imagine where sediment eroded in the Norway Basin could be transported to since it has always been deep and is bounded to the west, south and east by rises. The only path for sediment to be transported out of the basin is to the north through the Jan Mayen Fracture Zone and into the Greenland or Lofoten Basins. Based on linear sedimentation rates for the Cenozoic, Thiede et al. (1986) showed the lowest sedimentation rates along mid-ocean ridges and fracture zones in the Norwegian-Greenland Sea. This could support the hypothesis that the Jan Mayen Fracture Zone was a region of sediment transport by bottom-water currents carrying sediment out of the Norwegian Basin. However, until further stratigraphic compilations are made, and the paleobathymetry of the Lofoten and Greenland Basins is reconstructed, it will remain unclear whether the Norway Basin was an isolated sediment sink or if transport out of the Norway Basin towards the north might have been possible.

The mass/age distributions of the sediment drifts offer significant clues to the history of bottom currents and sediment sources in the area. They indicate that Feni drift originated at the beginning of the Oligocene and was accumulating continuously during the Oligocene with a slight increase in the Miocene. There is little evidence of either a change in the sediment supply or bottom current regime. Hatton, Gardar, Bjorn and Snorri Drifts all had their origin in the early Middle Miocene. Sediment supply to them increased during the

Pliocene-Quaternary. Hatton Drift is "downstream" from Feni Drift. The time of its formation appears to correlate with the increased rate of sediment accumulation on Feni Drift, 16 Ma. The average mass per million year age increment in Hatton Drift is 1×10^{18} g and that of Feni Drift for the same time interval is 5.8×10^{18} g. In the Oligocene the average sediment mass per million years in Feni Drift is 4.9×10^{18}. The same increase in sediment mass in Feni Drift (1×10^{18} g m.y.$^{-1}$) is observed as the total mass per million years in Hatton Drift indicating a bottom-water current that carried 40 percent more sediment than the Oligocene current. The ultimate sediment source for Gardar, Bjorn and Snorri Drifts must have been the Iceland-Faeroes segment of the Greenland-Scotland Ridge. The current forming them would have come down the southern slope of the Greenland-Scotland Ridge into the South Iceland Basin and then have crossed Reykjanes Ridge to be turned back north by the Coriolis force. Accumulation of Eirik and Gloria Drifts began at the beginning of the Pliocene, and they have acquired their mass in a short period of geologic time. The sediment sources must have been the Denmark Strait or along the East Greenland margin and the bottom current that produced them must have come through the Denmark Strait.

2.5 Summary and Conclusions

I have compared different published empirical equations that model the loss of porosity (increase of solidity) in sediment with increasing burial depth. The increase of solidity with increasing burial depth for sediments that compact like shale (clay, claystone, mud and mudstone) and sands is best described as exponential decay functions (Eqns. 2.7 and 2.14 respectively). The increase of solidity with increasing burial depth for sediments that compact like limestones (unlithified calcareous ooze, semi-lithified chalk and lithified limestone) is best described by a power-law function (Eqn. 2.10).

Sediment masses normalized to equal age intervals and expressed as mass/age distributions offer a unique view of regional and long-term geologic history. The regional mass/age distributions indicate that each of the four basinal areas, the British margin to Reykjanes Ridge, Reykjanes Ridge to the East Greenland margin, the East Greenland margin to Jan Mayen Ridge, and Jan Mayen Ridge to the Faeroe-Shetland Escarpment, had an independent history. They served as four separate sinks for four different source areas throughout most of their history. The constant character of the mass/age distribution from

Reykjanes Ridge to the British continental shelf reflects a different overall uplift and subsidence history of the West European margin compared to that of East Greenland. The Reykjanes Ridge to British continental shelf sediment mass/age distribution also shows that sedimentation in Rockall Trough was relatively uninterrupted during the early Tertiary rifting. The East Greenland continental margin and Irminger Basin experienced a large pulse of sediment input in the Eocene and Early Oligocene that indicates that sediment supply from the East Greenland margin lagged separation and the initiation of seafloor spreading. The lag is probably related to the reversal of drainage that occurred on land areas as the uplifted East Greenland margin subsided. Neogene sediment accumulation on the Iceland Plateau was dominated by accumulation of detrital sediments from Greenland. The area around Scoresby Sund has been a major point of delivery of sediment eroded from Greenland to the Iceland Plateau since the Middle Miocene. The Norway Basin experienced continually low rates of sediment accumulation during the Cenozoic with especially small accumulations during the Miocene.

The region between the Reykjanes Ridge and British continental shelf received the largest sediment mass per unit area during the Cenozoic (Table 2.2). The area from Greenland to Jan Mayen Ridge received the second largest mass of sediment per unit area, which was the same as the average mass per unit area for the entire study area from the Charlie Gibbs to Jan Mayen Fracture Zones. The average sediment mass per unit area during the Cenozoic in the Norway Basin was less than the average for the study area but greater than on the East Greenland continental shelf and in the Irminger Basin.

Mass/age distributions for the sediment drifts show that drift sedimentation started in the Early Oligocene in Rockall Trough (Feni Drift). It spread to the South Iceland Basin (Hatton, Bjorn and Gardar Drifts) and the west side of Reykjanes Ridge (Snorri Drift) in the Middle Miocene. At the beginning of the Pliocene drift sedimentation began to occur off the southern tip of Greenland (Eirik Drift) and in the southern Irminger Basin (Gloria Drift).

2.5 Figure Captions

Figure 2.1. The study area between Charlie Gibbs Fracture Zone (CGFZ), Jan Mayen Fracture Zone (JMFZ), Greenland and Europe. Bathymetric contours are every 250 m. The map was constructed from the ETOPO5 (1986) data set using 10 x 10' average elevations. Longitude is negative towards the west and latitude is positive towards the north. Geographic features mentioned in the text are: ADS = Anton Dohrn Seamount, AR = Aegir Ridge, BBB = Bill Bailey's Bank, BD = Bjorn Drift, BI = British Isles, DS = Denmark Strait, EB = Edora Bank, ED = Eirik Drift, ES = Eriador Seamount, FB = Faeroe Bank, FBC = Faeroe Bank Channel, FD = Faeroe Drift, FI = Faeroe Shelf and Islands, FSC = Faeroe-Shetland Channel, FSE = Faeroe-Shetland Escarpment, GBB = George Bligh Bank, GD = Gardar Drift, GLD = Gloria Drift, HAD = Hatton Drift, HAT = Hatton Bank, HTS = Hebrides Terrace Seamount, IB = Irminger Basin, ID = Isengard Drift, IFR = Iceland-Faeroe Ridge, IP = Iceland Plateau, IR = Ireland, JMR = Jan Mayen Ridge, KR = Kolbeinsey Ridge, LB = Lousy Bank, NB = Norway Basin, PA = Porcupine Abyssal Plain, RB = Rosemary Bank, RCK = Rockall Bank, RP = Rockall Plateau, RR = Reykjanes Ridge, RT = Rockall Trough, SC = Scotland, SD = Snorri Drift, SI = Shetland Islands, SIB = South Iceland Basin, SS = Scoresby Sund and WTR = Wyville-Thompson Ridge.

Figure 2.2. The 1 x 1° grid applied to the area for compilation of the stratigraphic database. Contour lines are shown for reference at 500 m intervals below sea level. There are 668 grid cells in the database.

Figure 2.3. Map of the study area between Charlie Gibbs Fracture Zone, Jan Mayen Fracture Zone, Greenland and Europe constructed from the ETOPO5 (1986) data set using 1 x 1° average elevations. Bathymetric contours are every 250 m and depths are given in kilometers below sea level.

Figure 2.4. The distribution of single channel seismic reflection profiles and DSDP/ODP sites used in the stratigraphic-lithologic compilation. DSDP and ODP drill sites are shown as solid black circles and the seismic profiles are shown as solid lines. Coastlines and the 500, 1000, 2000, 3000, 4000 and 5000 meter bathymetric contours are shown for reference.

Figure 2.5. Single-channel seismic reflection profile across the Hatton-Rockall Basin on Rockall Plateau. Depth is given in seconds of two-way travel time. This profile was taken in 1970 from the Lamont-Doherty Geological Observatory (Columbia University, Palisades, N.Y.) ship R/V "Vema".

Figure 2.6. Single-channel seismic reflection profile across Reykjanes Ridge. Depth is given in seconds of two-way travel time. This profile was taken in 1978 from the Lamont-Doherty Geological Observatory (Columbia University, Palisades, N.Y.) ship R/V "Robert Conrad".

Figure 2.7. Single-channel seismic reflection profile across the East Greenland margin and Irminger Basin. Depth is given in seconds of two-way travel time. This profile was taken in 1973 from the Lamont-Doherty Geological Observatory (Columbia University, Palisades, N.Y.) ship R/V "Vema".

Figure 2.8. Single-channel seismic reflection profile across the Iceland Plateau and Norway Basin. Depth is given in seconds of two-way travel time. This profile was taken in 1978 from the Lamont-Doherty Geological Observatory (Columbia University, Palisades, N.Y.) ship R/V "Robert Conrad".

Figure 2.9. Single-channel seismic reflection profile across Norway Basin showing the Aegir Ridge. Depth is given in seconds of two-way travel time. This profile was taken in 1970 from the Lamont-Doherty Geological Observatory (Columbia University, Palisades, N.Y.) ship R/V "Vema".

Figure 2.10. Areal distribution of sediment in the northern North Atlantic and southern GIN Sea digitized from Tucholke (1988). The total sediment thickness is given in kilometers. The greatest thicknesses of sediment are off Scoresby Sund, in Rockall Trough and in the Faeroe-Shetland Channel. Sediment is absent on Iceland, only about 100 m thick on the Iceland-Faeroe Ridge and thicker in the Denmark Strait. Over the central portion of Reykjanes Ridge sediments are less than 100 m thick but are closer to 200 m thick over the axis of Kolbeinsey Ridge. The position of the extinct Aegir spreading center is apparent from symmetric thinning of sediment in the center of the Norway Basin. Some geographic features are labelled for reference: AR = Aegir Ridge, JMR = Jan Mayen Ridge, KR = Kolbeinsey Ridge, RP = Rockall Plateau and RR = Reykjanes Ridge.

Figure 2.11. The increase of solidity in shales with increasing burial depth. The dotted line ("Normal B&B 85) is the curve calculated from Eqn. (2.4) published by Baldwin and Butler (1985) for "normal" shales (less than 200 m thick). The dashed line ("Undercompacted" B&B 85) is the curve calculated from Eqn (2.5) from Baldwin and Butler (1985) for "undercompacted" shales (at least 200 m thick). The solid line (H&G 90) is the curve calculated from Eqn. (2.6) from Huang and Gradstein (1990) that was chosen to model the compaction of shales in this study.

Figure 2.12. The increase of solidity in limestones with increasing burial depth. The dotted line (B&B 85) is the curve calculated from Eqn. (2.4) from Baldwin and Butler (1985) for "normal" shales and limestones. The solid line (H&G 90) is the curve calculated from Eqn. (2.8) from Huang and Gradstein (1990) for limestones. The dashed line ("Modified") is the curve calculated from Eqn. (2.10) chosen to model the compaction of limestones in this study.

Figure 2.13. The increase of solidity in sandstones with increasing burial depth. The dotted line (B&B 85) is the curve calculated from Eqn. (2.12) after Baldwin and Butler (1985) and Sclater and Christie (1980). The solid line (H&G 90) is the reciprocal of Eqn. (2.13) from Huang and Gradstein (1990) for sandstones. The dashed line ("Modified") is the curve calculated from Eqn. (2.14) chosen to model the compaction of sandstones in this study.

Figure 2.14. The three compaction curves used in this study expressed in terms of the increase of solidity with increasing burial depth for shales (dotted line; Eqn. 2.7), limestones (dashed line; Eqn. 2.10) and sandstones (solid line; Eqn. 2.14).

Figure 2.15. Subregions of the northern North Atlantic and southern GIN Sea used for compiling sediment mass/age distributions. The regions shown are the Iceland Plateau (ICP), Norway Basin (NOR), Greenland to Reykjanes Ridge (G2R), Reykjanes Ridge to the European continent (R2E).

Figure 2.16. Mass/age distributions of Late Paleocene to Quaternary sediments for the entire study area from the Charlie Gibbs to Jan Mayen Fracture Zones and between Greenland and the British Isles (top diagram). The study area is subdivided into two subregions, one south (middle diagram) and one north of the Greenland-Scotland Ridge (lower diagram).

Figure 2.17. Mass/age distribution of Late Paleocene to Quaternary sediments from the Charlie Gibbs Fracture Zone to the Greenland-Scotland Ridge between the Reykjanes Ridge and the British Isles including the Rockall Trough and Faeroe-Shetland Channel (top diagram). The mass/age distribution excluding sediment drifts is shown in the middle diagram and the total mass/age distribution of sediment drifts in the region is shown on the bottom.

Figure 2.18. Mass/age distribution of Late Paleocene to Quaternary sediments from the Charlie Gibbs Fracture Zone to the Greenland-Scotland Ridge between Greenland and the Reykjanes Ridge (top diagram). The mass/age distribution excluding sediment drifts is shown in the middle diagram and the total mass/age distribution of sediment drifts in the region is shown on the bottom.

Figure 2.19. Mass/age distribution of Late Paleocene to Quaternary sediments between the Greenland-Scotland Ridge and Jan Mayen Fracture Zone from Greenland to Jan Mayen Ridge (top diagram) and from Jan Mayen Ridge to the Faeroe-Shetland Escarpment (bottom diagram).

Figure 2.20. Mass/age distributions of Late Paleocene to Quaternary sediments in Feni and Gardar Drifts.

Figure 2.21. Mass/age distributions of Late Paleocene to Quaternary sediments in Bjorn and Eirik Drifts.

Figure 2.22. Mass/age distributions of Late Paleocene to Quaternary sediments in Snorri, Hatton, and Gloria Drifts.

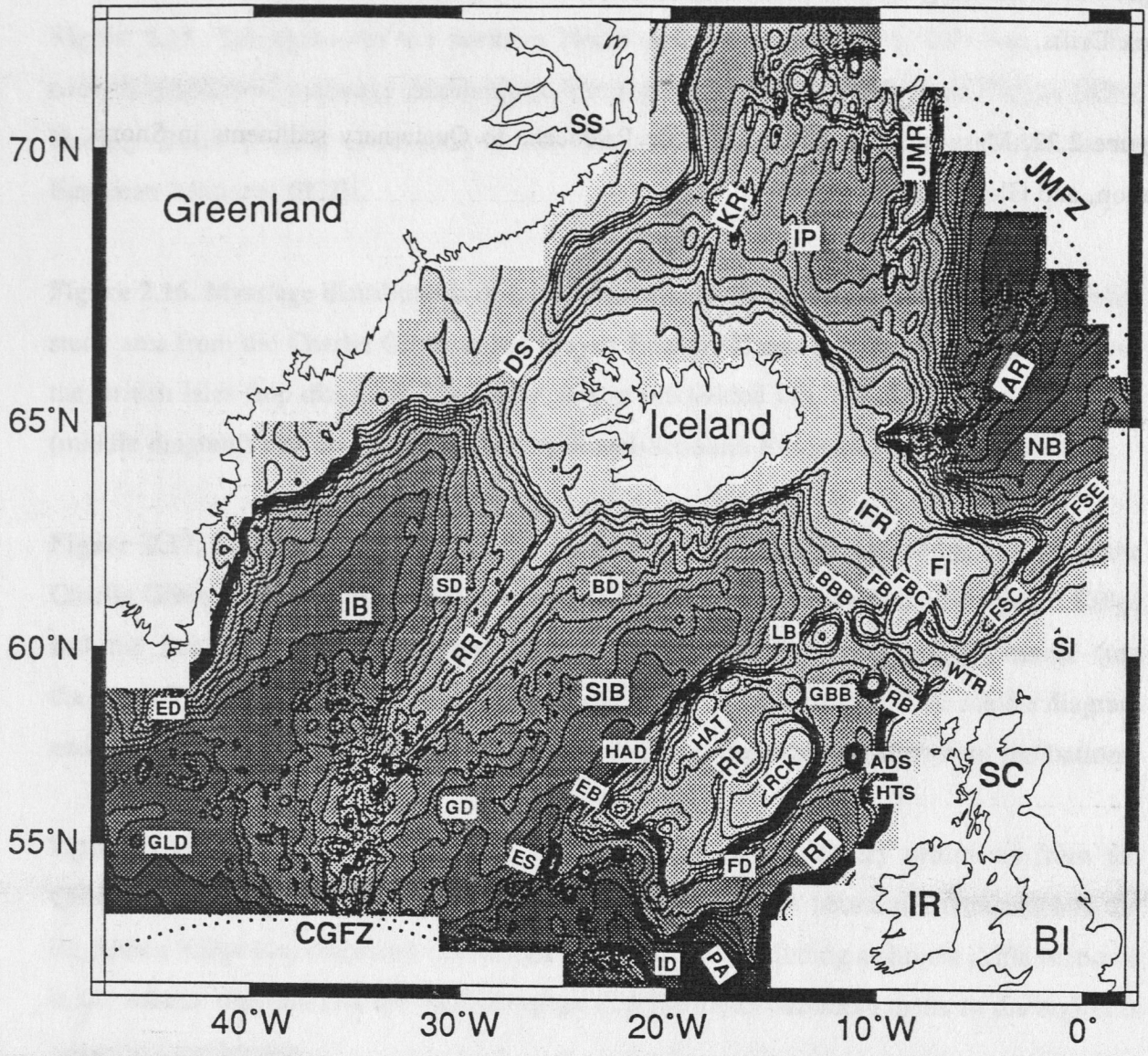
70°N
65°N
60°N
55°N
40°W
30°W
20°W
10°W
0°
Greenland
Iceland
SS
JMR
JMFZ
KR
IP
DS
AR
NB
IFR
FSE
FI
SD
BD
BBB
FBL
FBC
FSC
IB
RR
LB
SI
WTR
ED
SIB
GBB
RB
HAT
HAD
RP
RCK
ADS
HTS
SC
EB
GD
GLD
ES
FD
RT
IR
BI
CGFZ
ID
PA

Figure 2.1

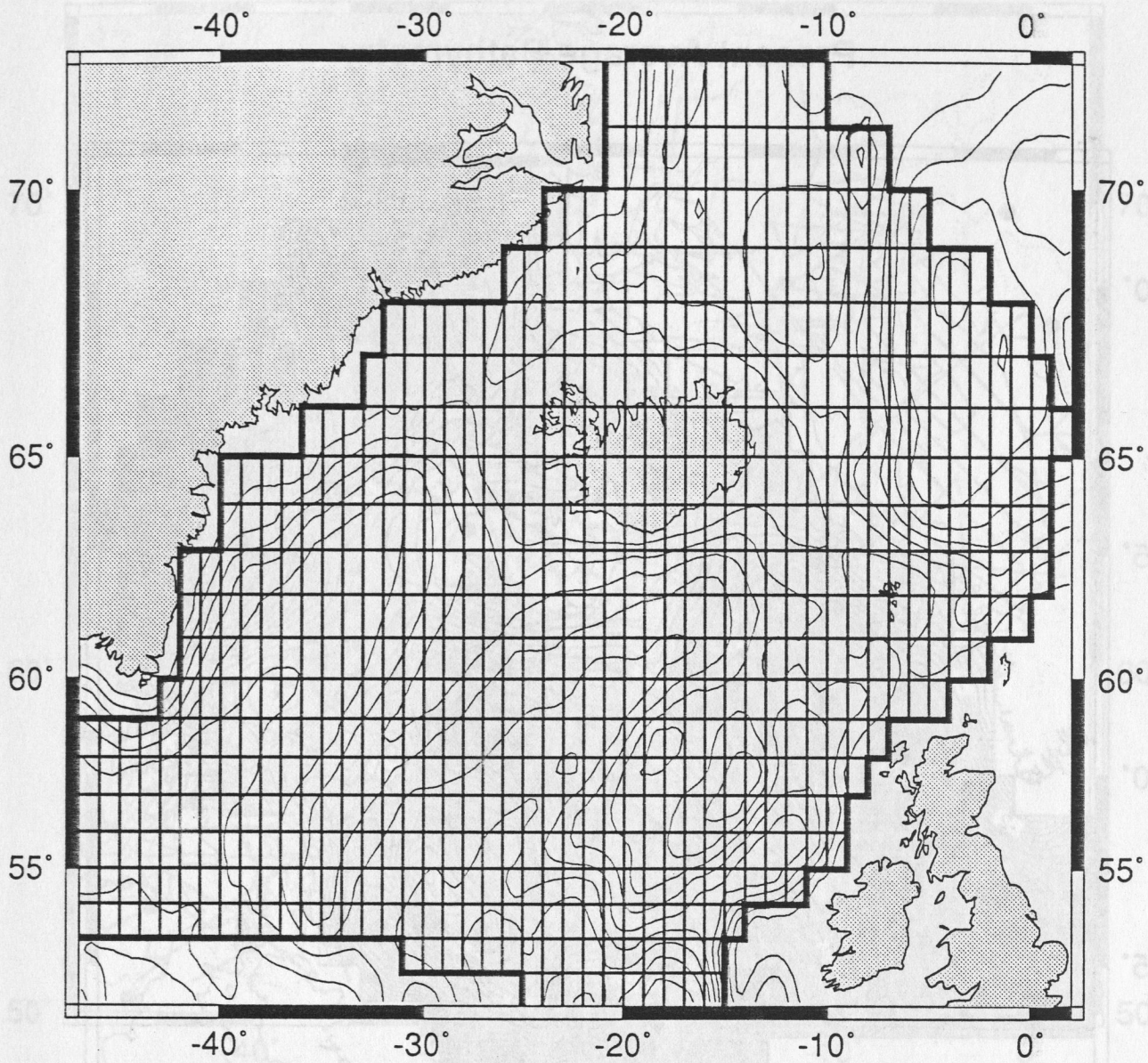

Figure 2.2

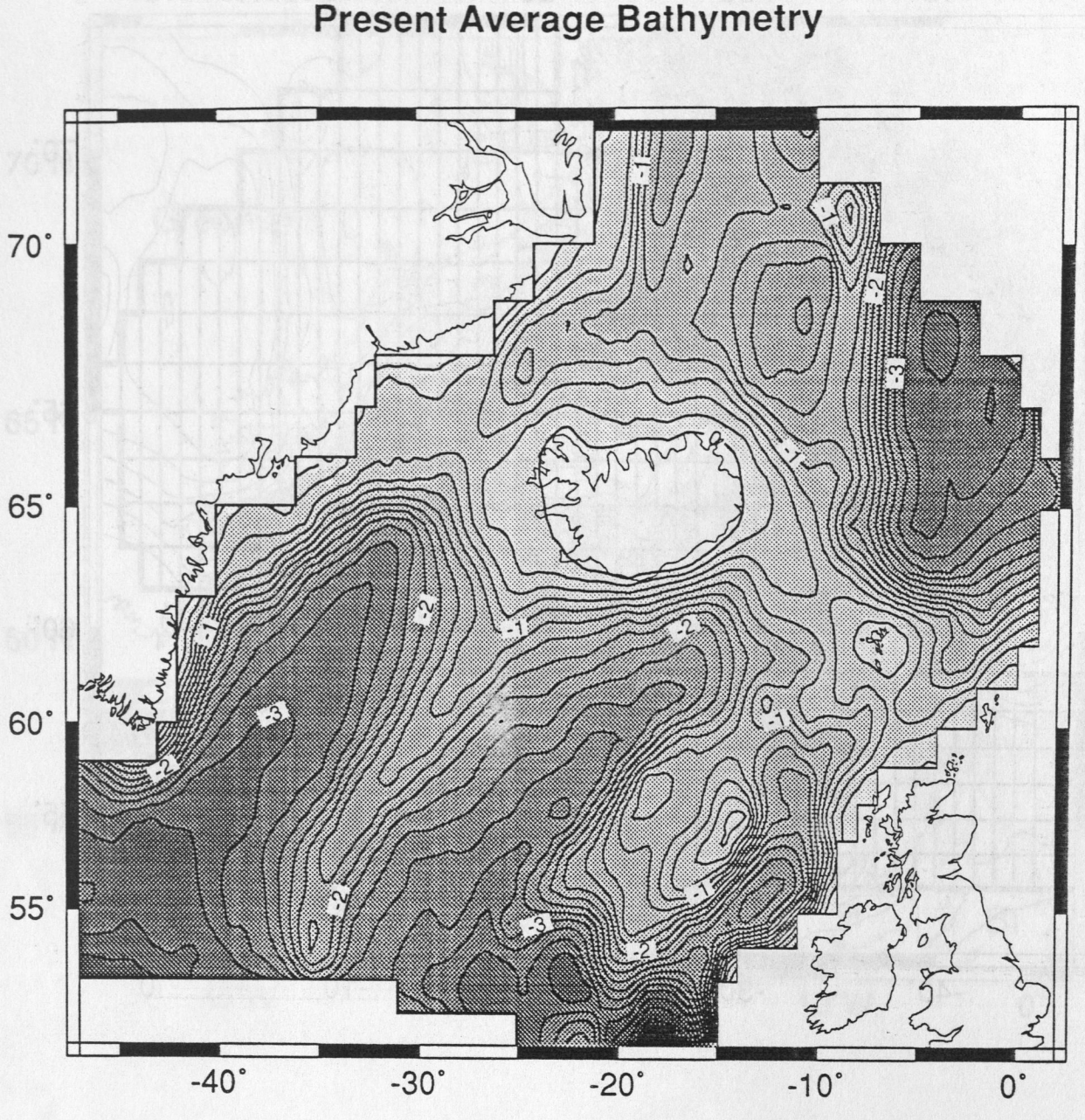

Figure 2.3

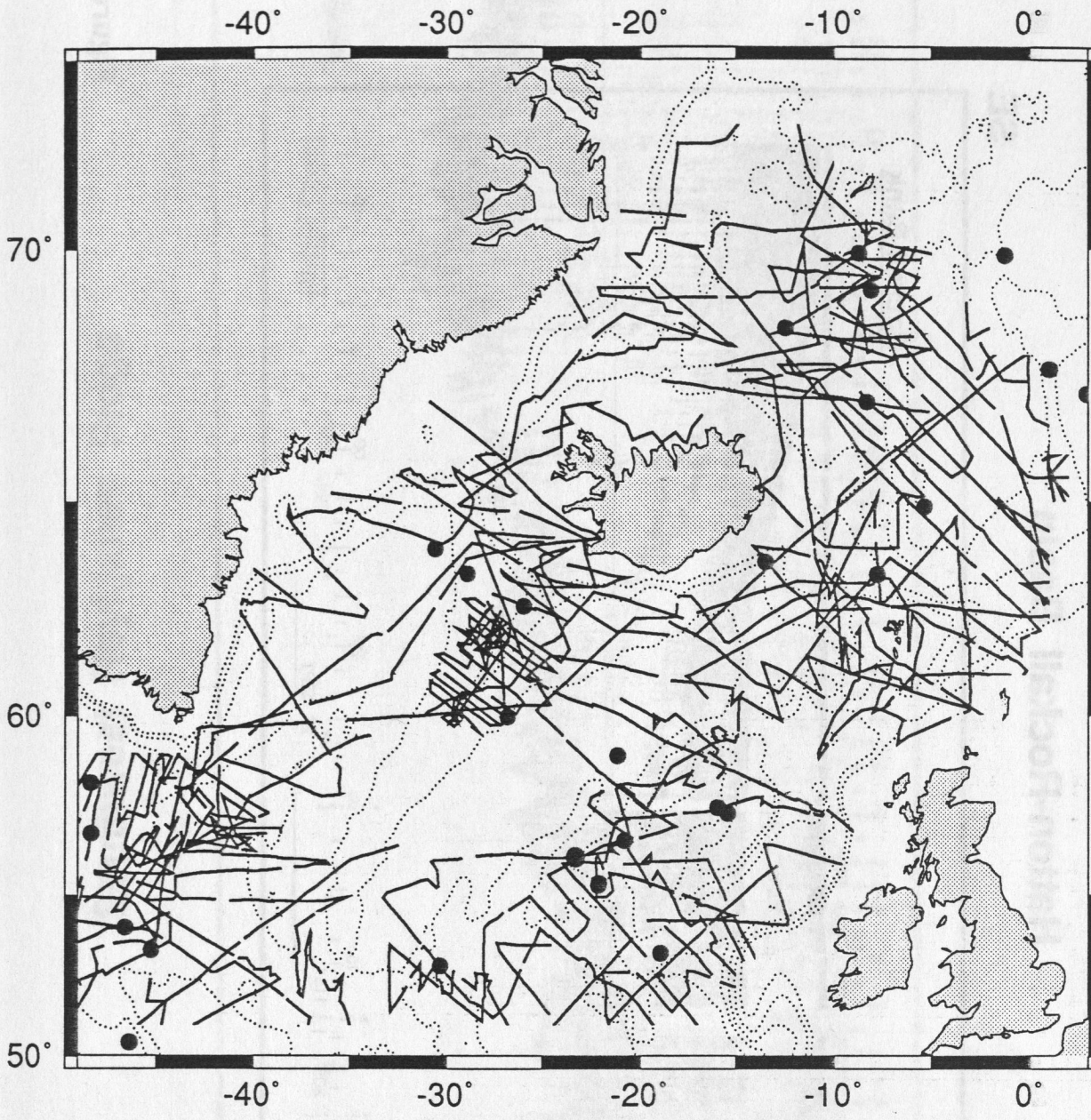

Figure 2.4

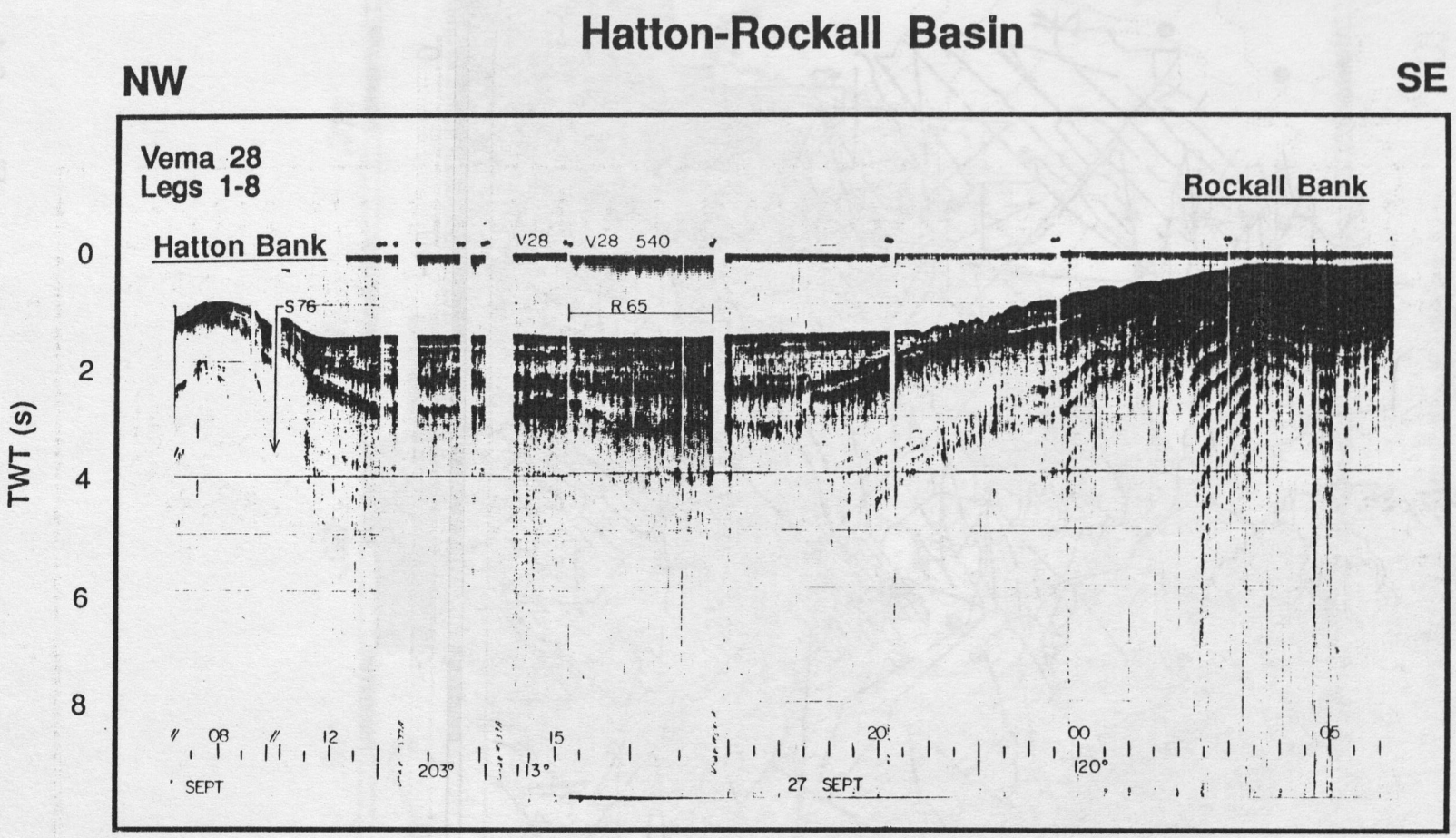
Hatton-Rockall Basin
NW
SE
Vema 28
Legs 1-8
Hatton Bank
Rockall Bank
V28
V28
540
S76
R65
TWT (s)
0
2
4
6
8
08
12
15
20
00
05
203°
113°
120°
SEPT
27 SEPT

Figure 2.5

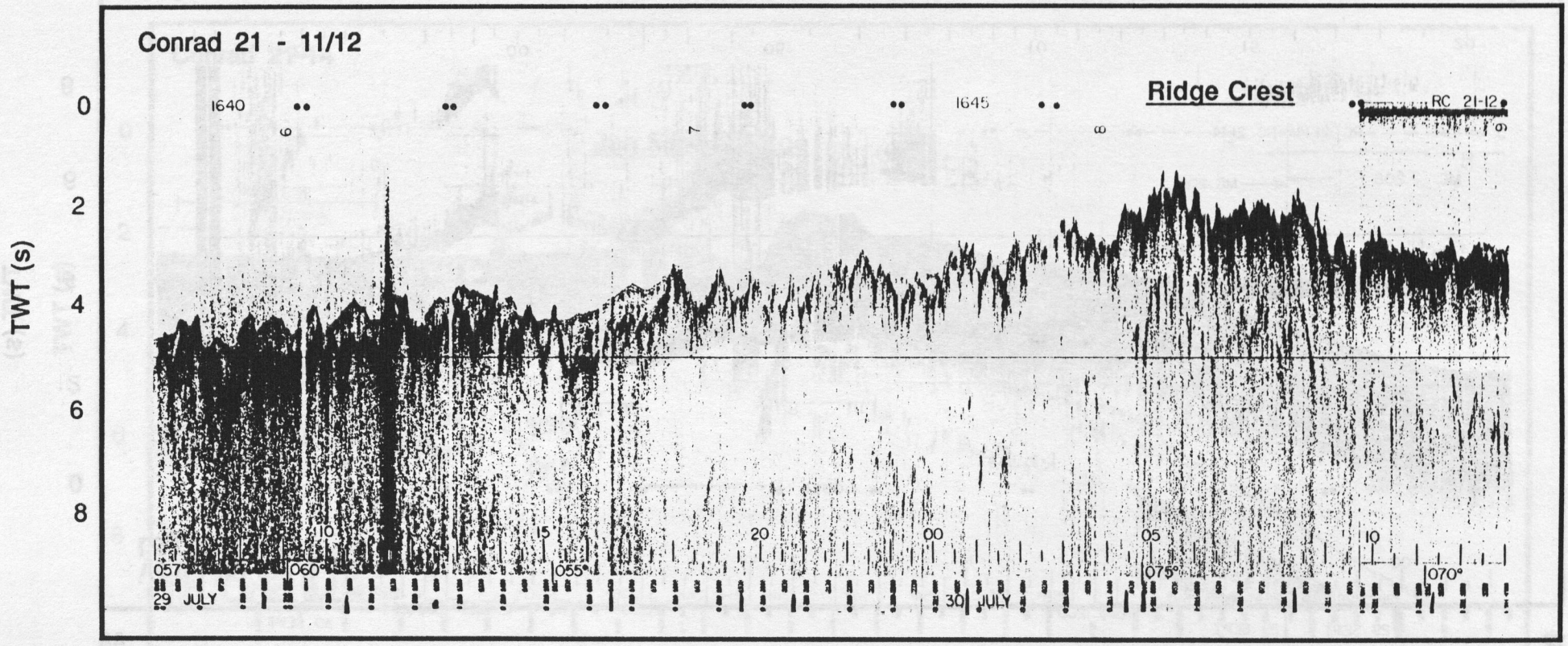
Southwest Reykjanes Ridge
SW
NE
Conrad 21 - 11/12
Ridge Crest
RC 21-12
1640
1645
TWT (s)
0
2
4
6
8
10
15
20
00
05
10
057°
060°
055°
075°
070°
29 JULY
30 JULY

Figure 2.6

East Greenland Margin and Irminger Basin

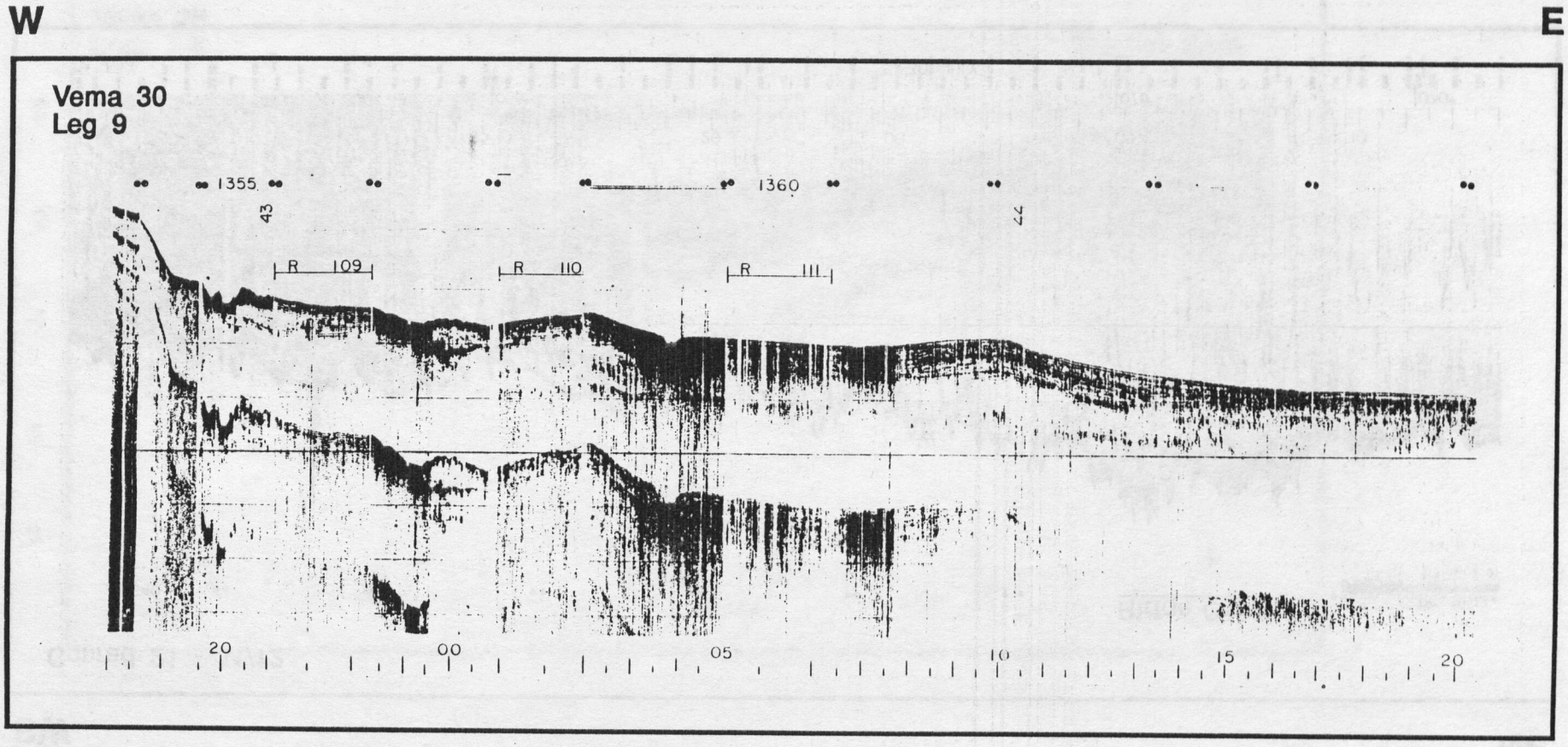

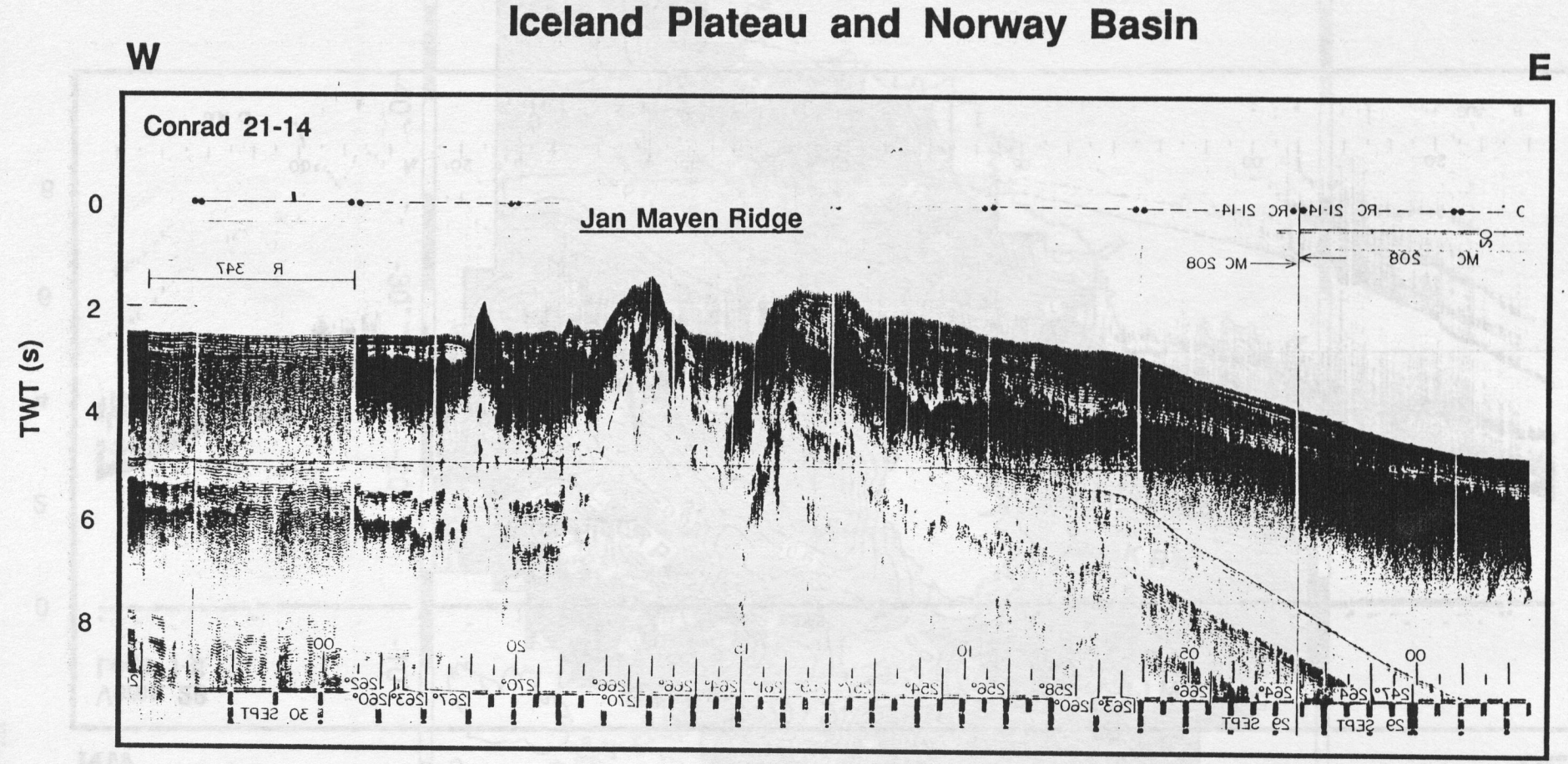
Iceland Plateau and Norway Basin
W
E
Conrad 21-14
Jan Mayen Ridge
TWT (s)
0
2
4
6
8

Figure 2.8

Norway Basin

NW SE

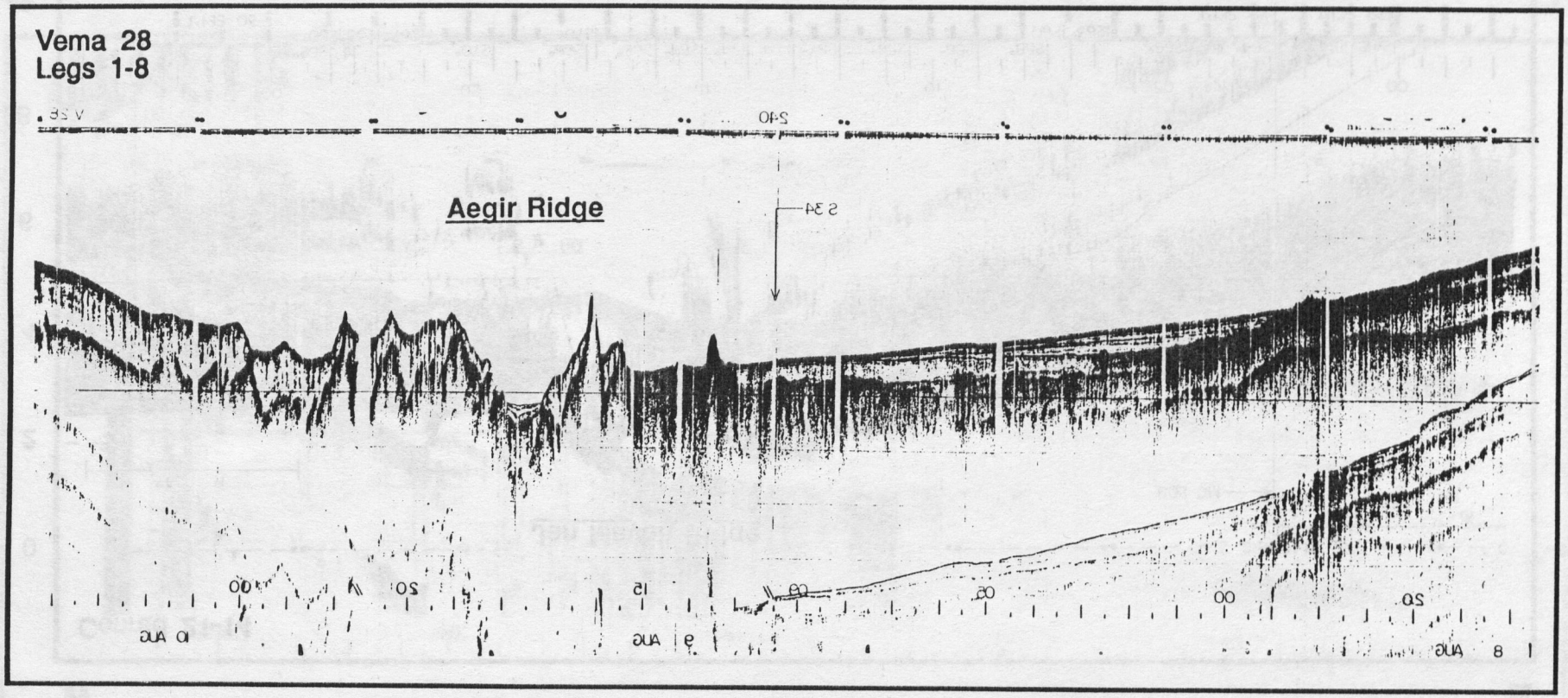

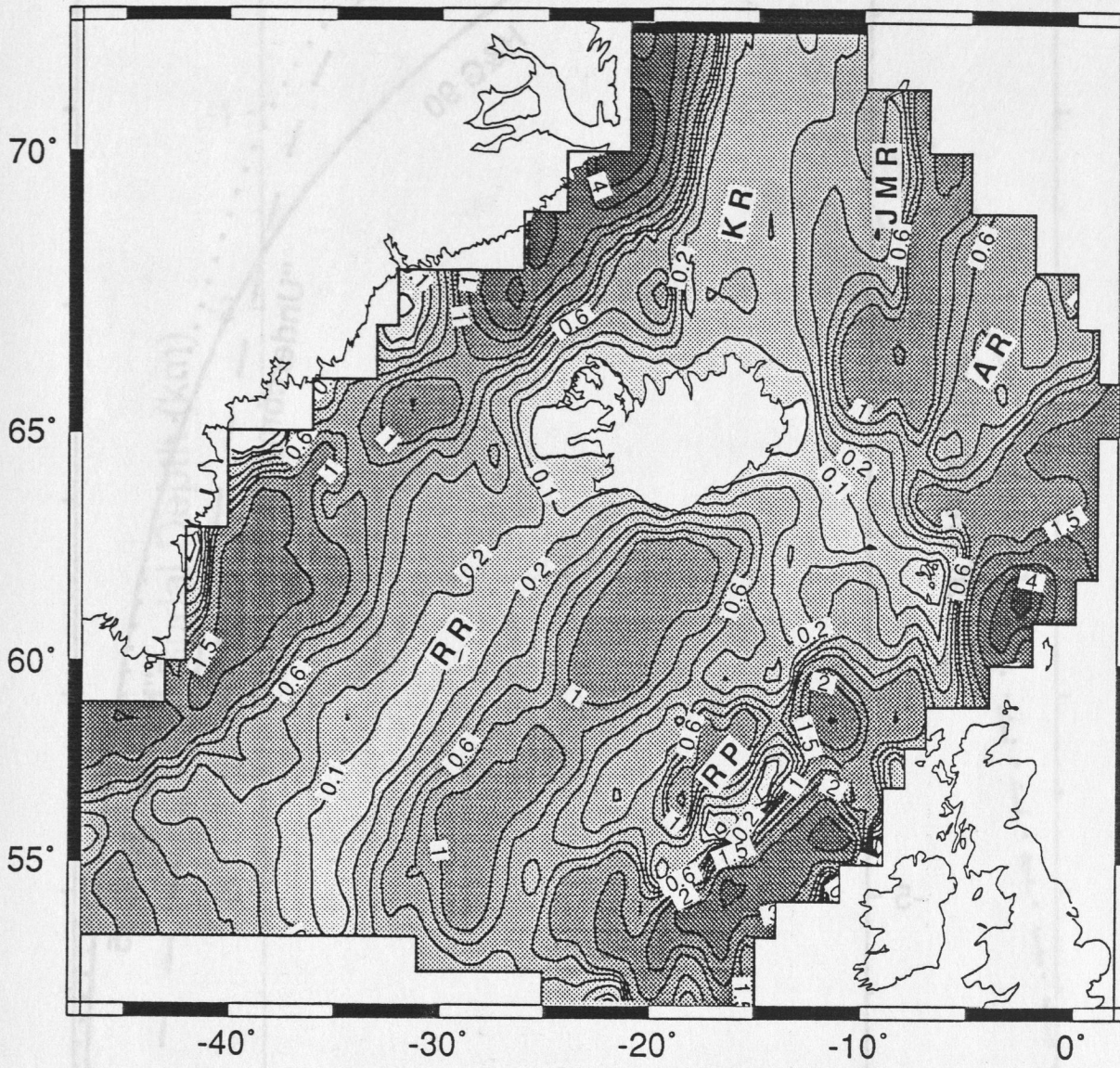

Figure 2.10

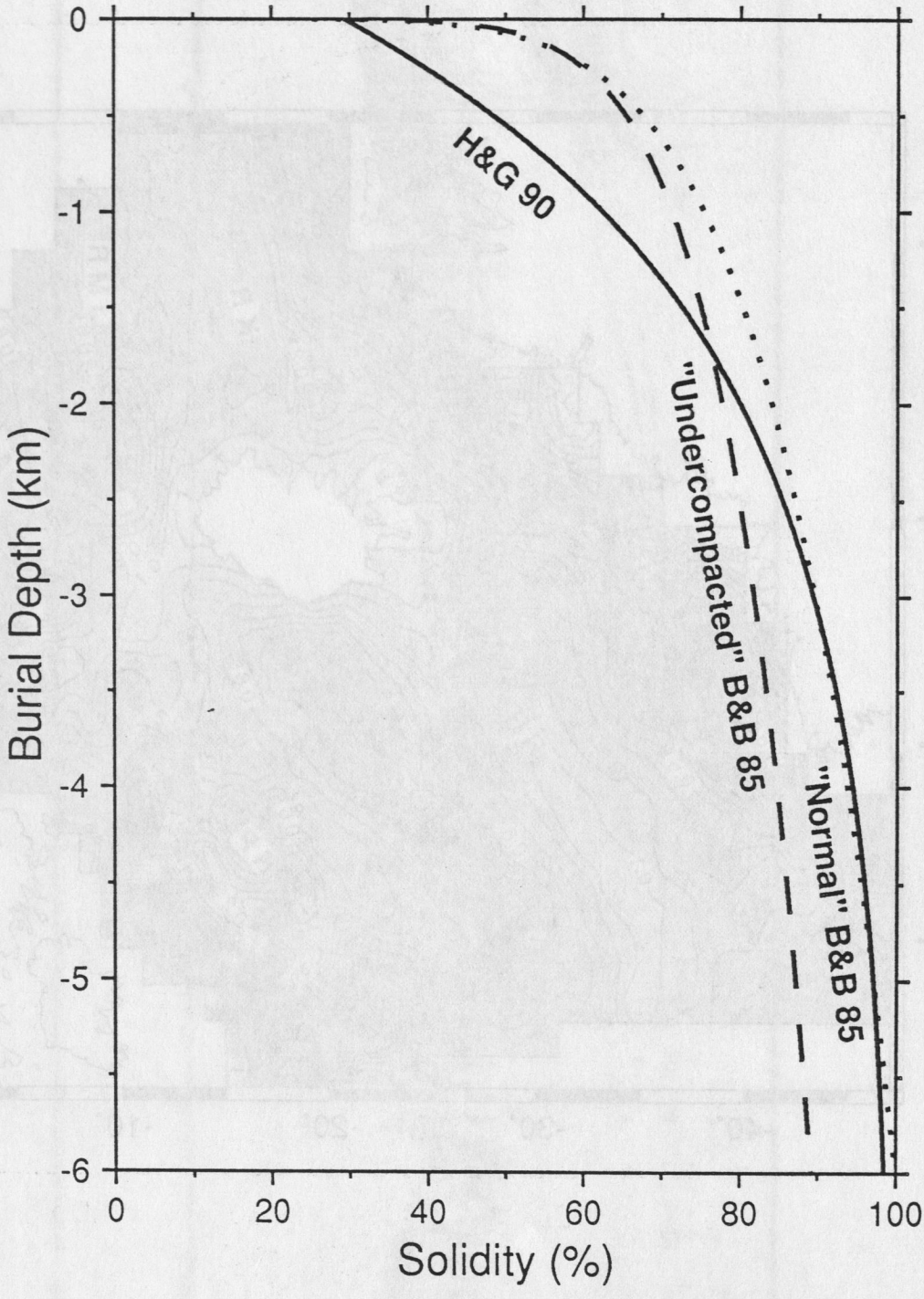
0
-1
-2
-3
-4
-5
-6
Burial Depth (km)
0
20
40
60
80
100
Solidity (%)
H&G 90
"Undercompacted" B&B 85
"Normal" B&B 85

Figure 2.11

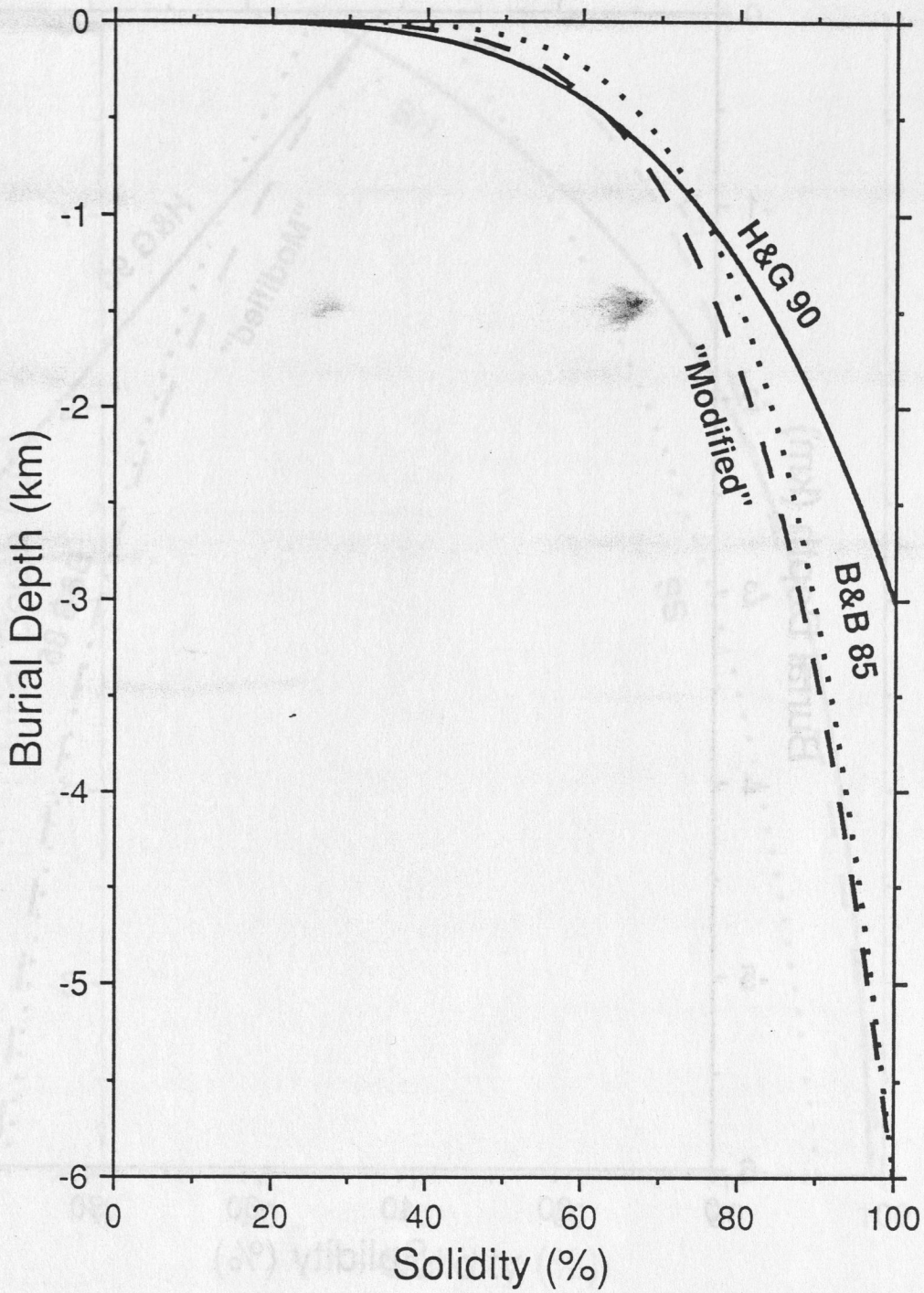
0
-1
-2
-3
-4
-5
-6
Burial Depth (km)
0
20
40
60
80
100
Solidity (%)
H&G 90
"Modified"
B&B 85

Figure 2.12

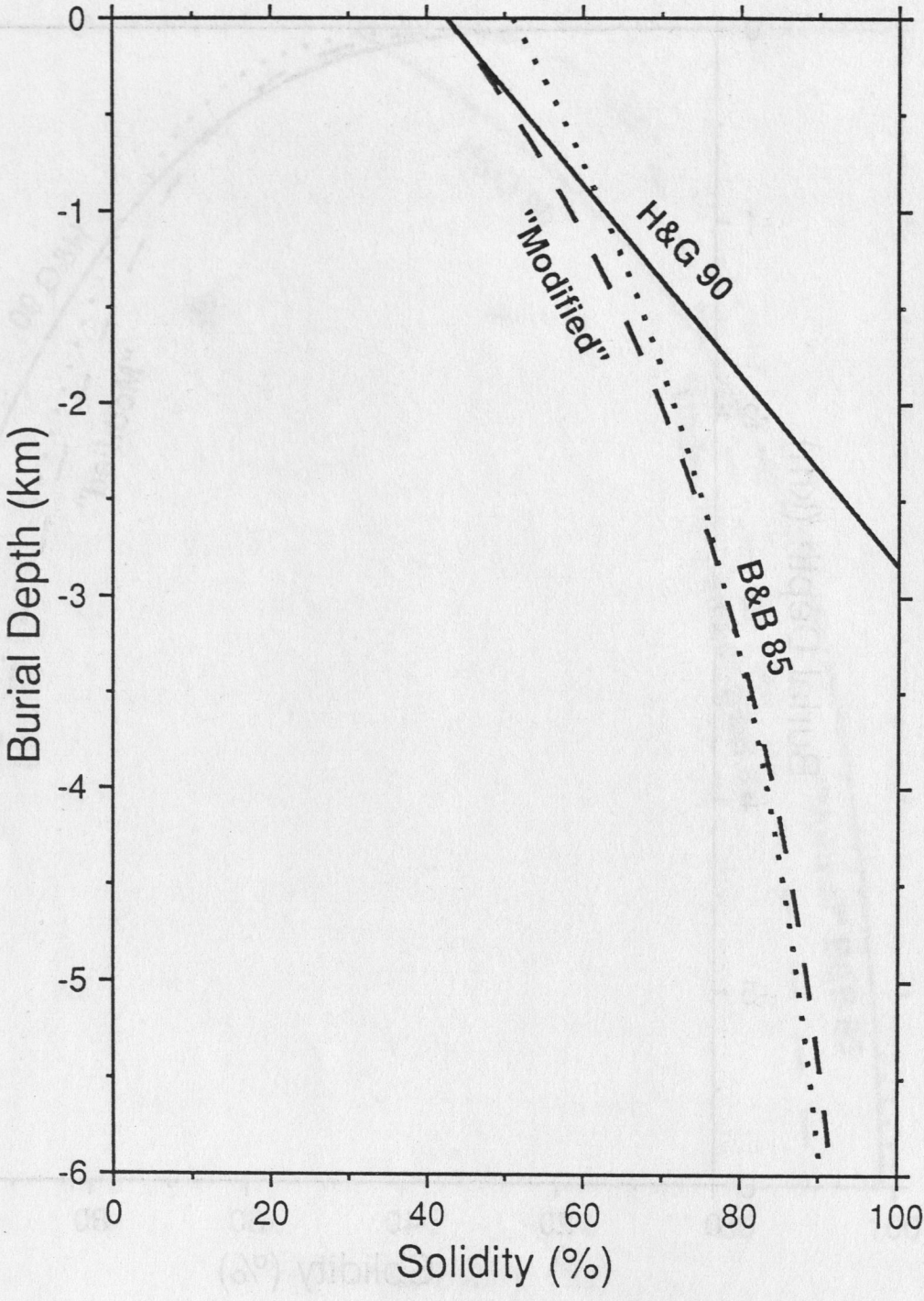
0
-1
-2
-3
-4
-5
-6
Burial Depth (km)
0
20
40
60
80
100
Solidity (%)
H&G 90
"Modified"
B&B 85

Figure 2.1

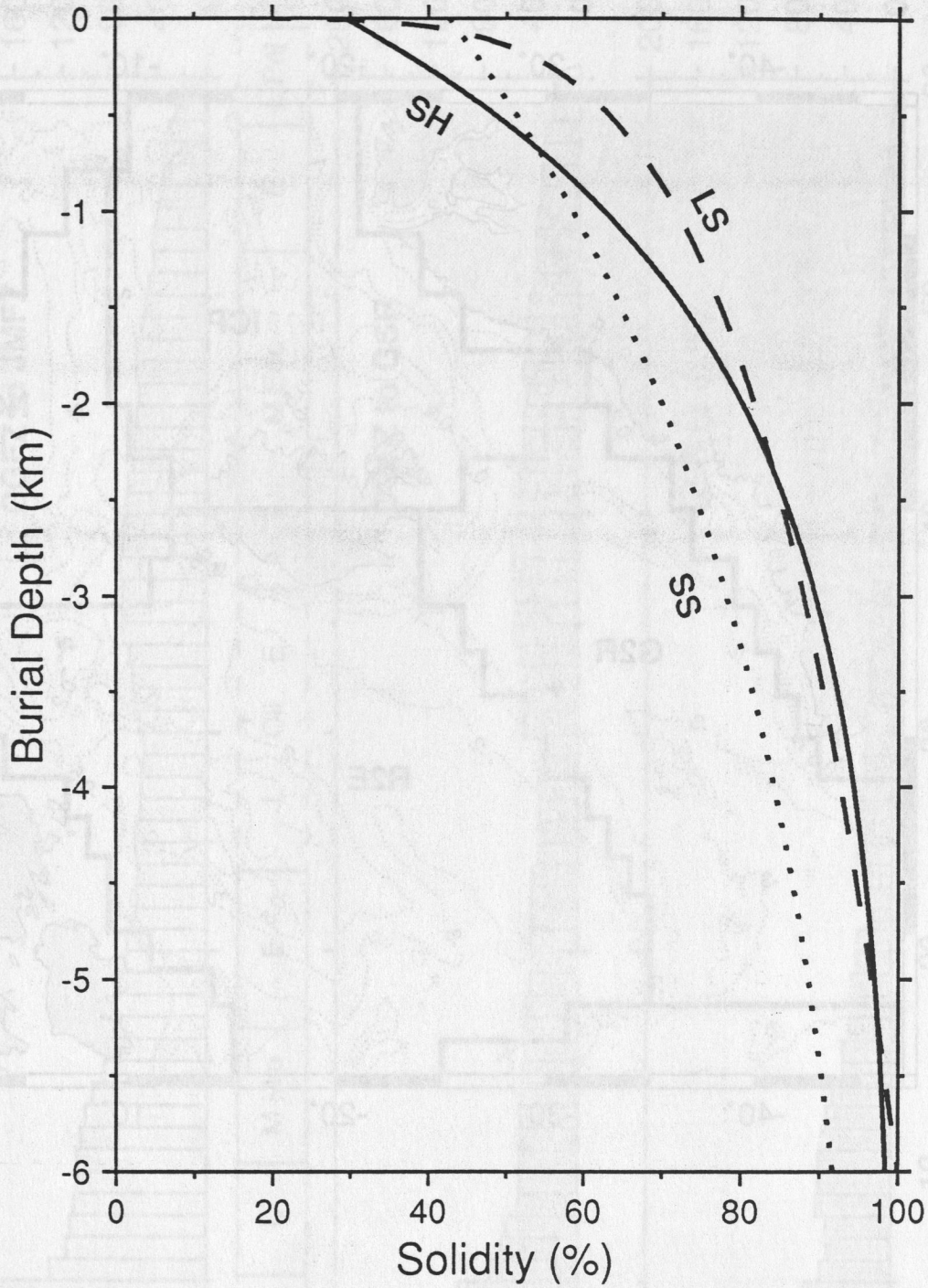

Figure 2.14

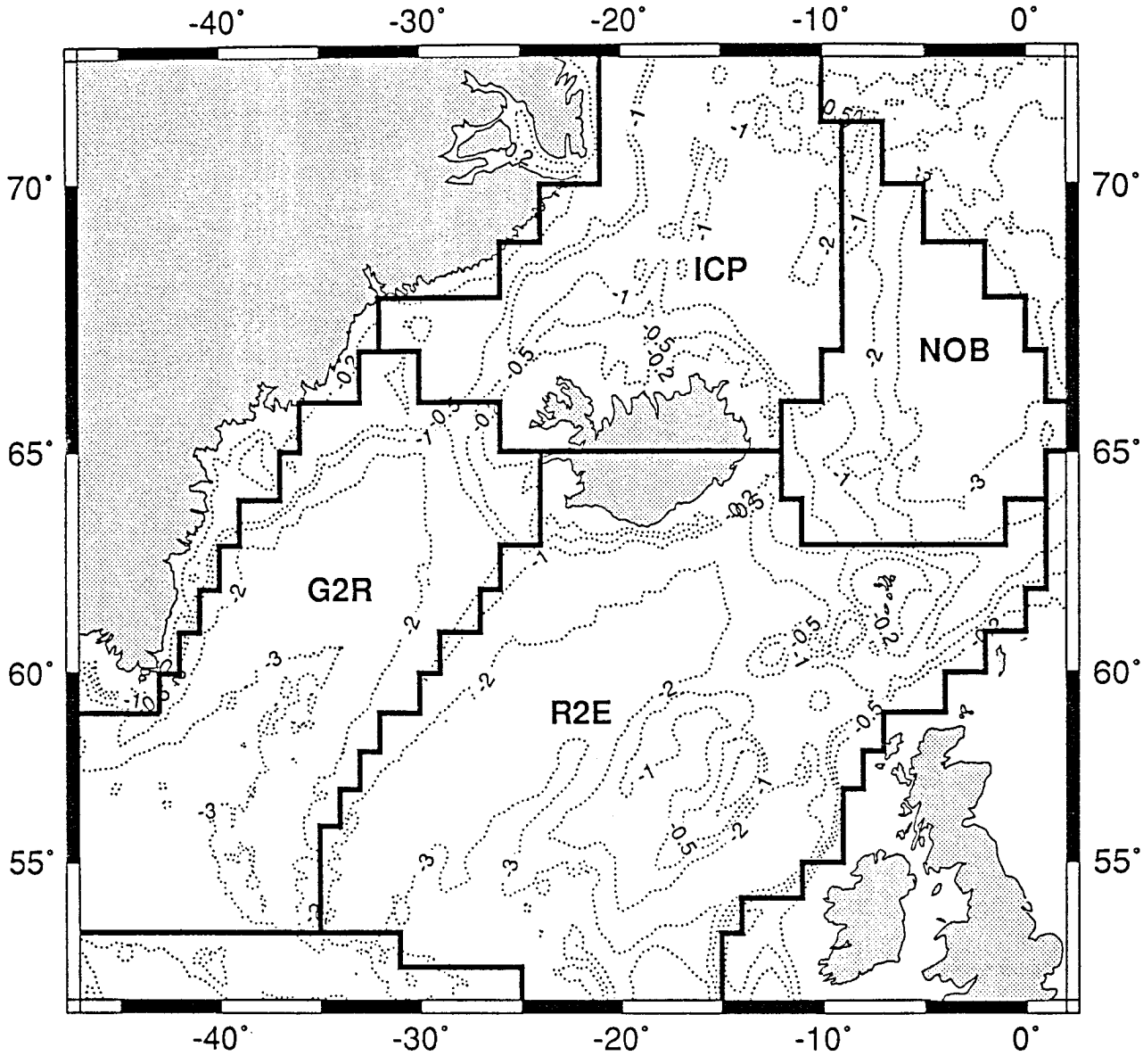

Figure 2.15

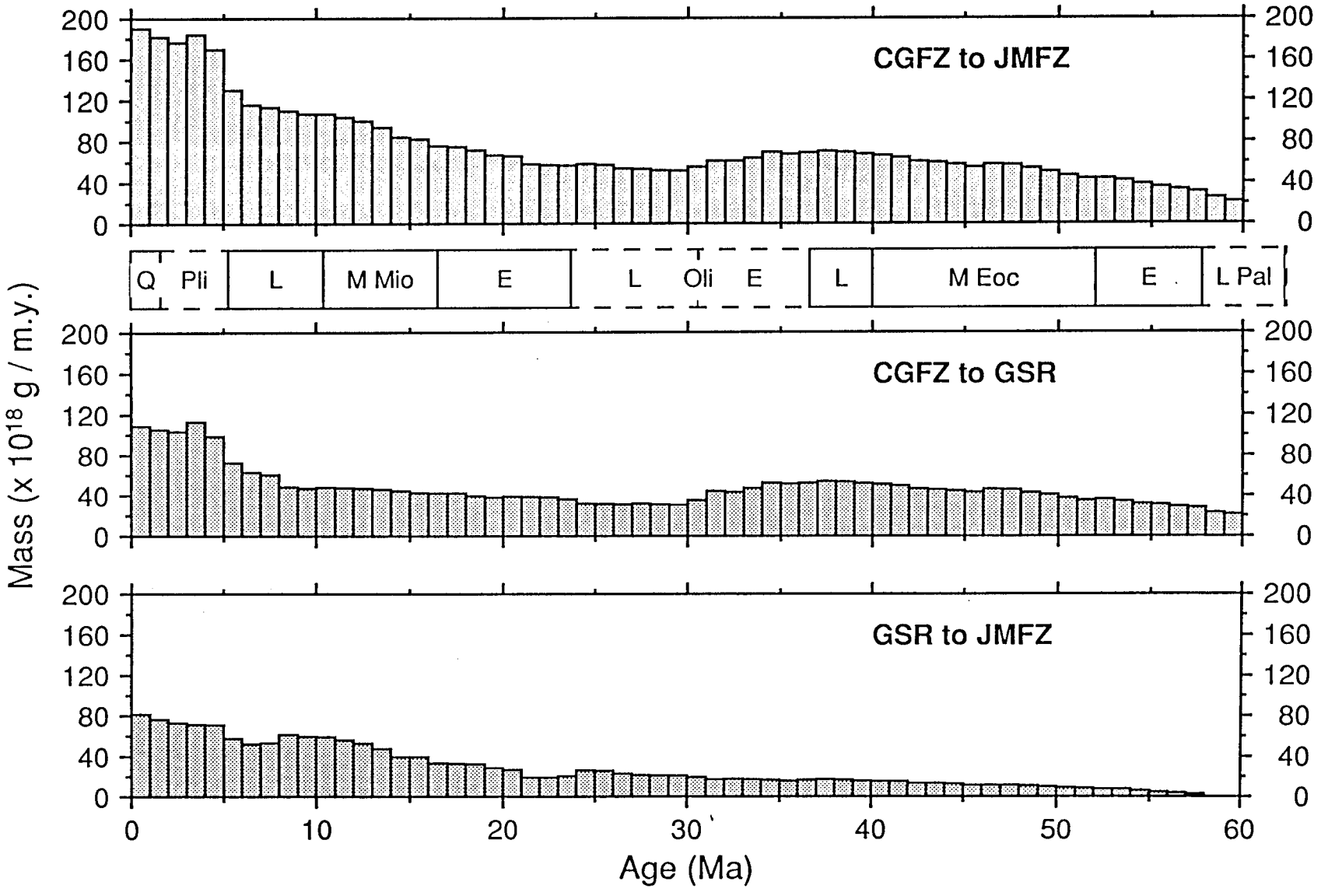
CGFZ to JMFZ
CGFZ to GSR
GSR to JMFZ
Mass (x 10^18 g / m.y.)
Age (Ma)
Q
Pli
L
M Mio
E
L
Oli
E
L
M Eoc
E
L Pal
0
10
20
30
40
50
60
0
40
80
120
160
200

Figure 2.16

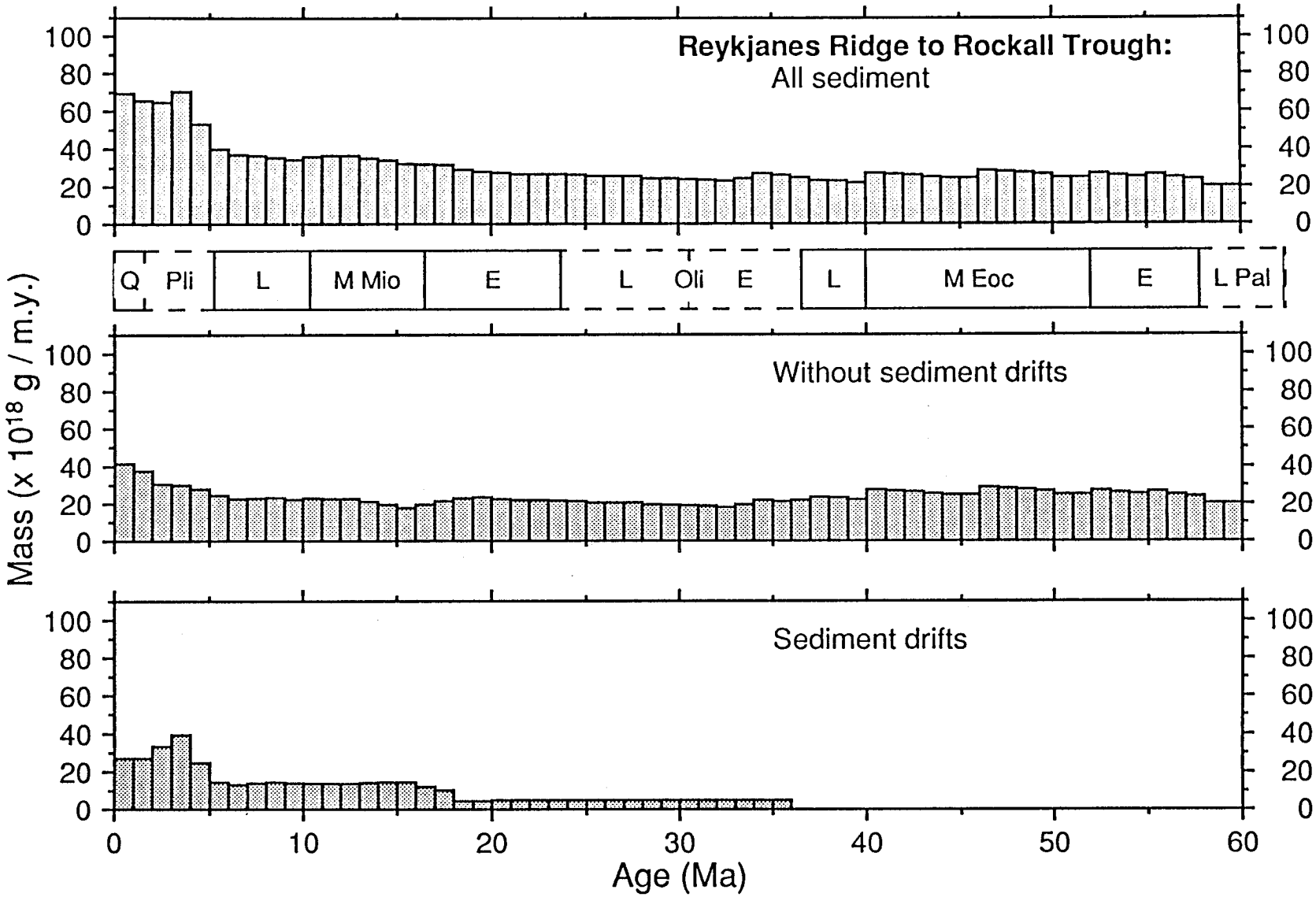
Reykjanes Ridge to Rockall Trough:
All sediment
Without sediment drifts
Sediment drifts
Mass (x 10^18 g / m.y.)
Age (Ma)
Q
Pli
L
M Mio
E
L
Oli
E
L
M Eoc
E
L Pal
0
10
20
30
40
50
60
0
20
40
60
80
100

Figure 2.17

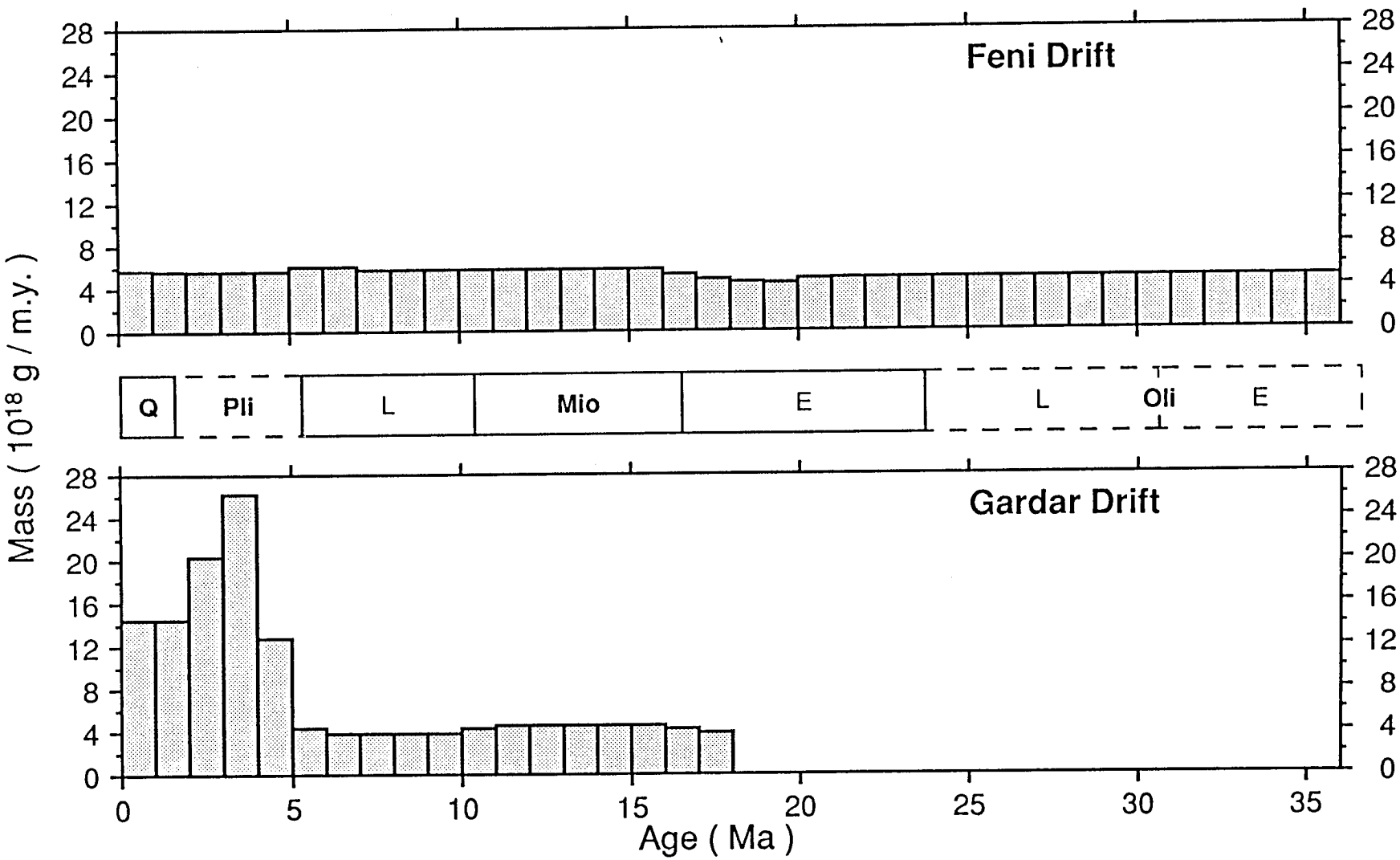
Feni Drift
Gardar Drift
Mass (10^18 g / m.y.)
Age (Ma)
Q
Pli
L
Mio
E
L
Oli
E
0
4
8
12
16
20
24
28
0
5
10
15
20
25
30
35

Figure 2.18

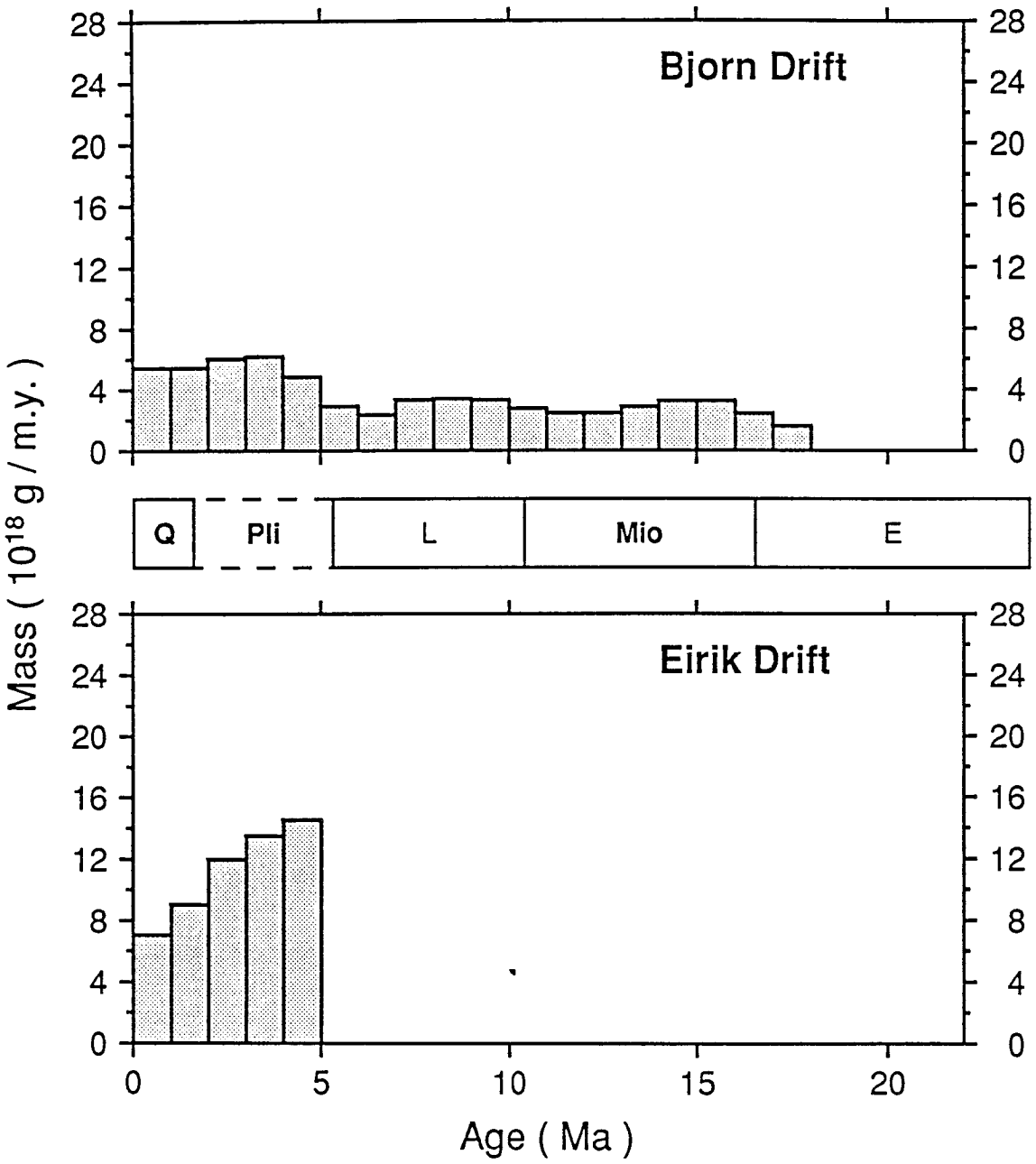
Bjorn Drift
Eirik Drift
Q
Pli
L
Mio
E
Mass (10^18 g / m.y.)
Age (Ma)
0
4
8
12
16
20
24
28
0
5
10
15
20

Figure 2.19

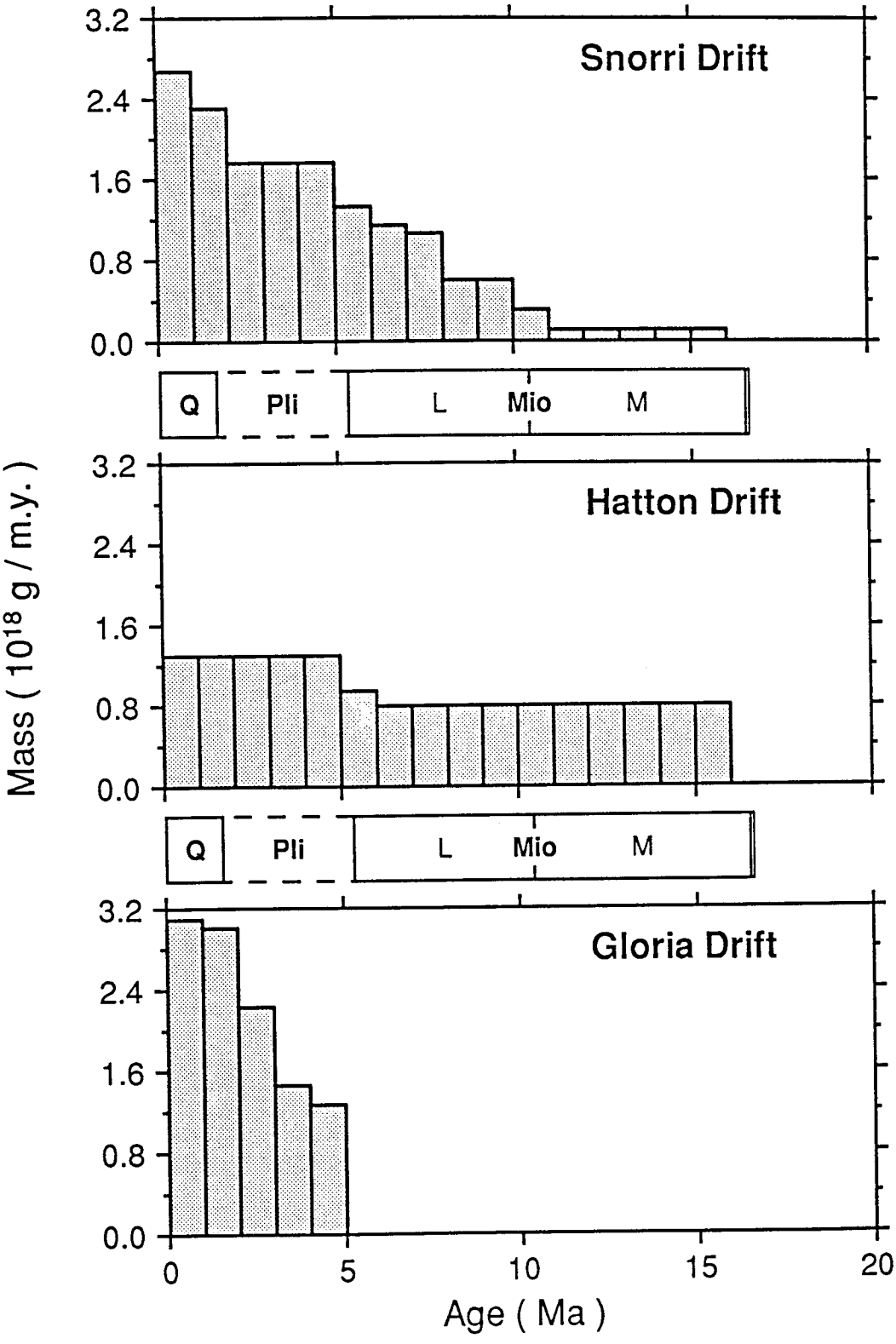
Snorri Drift
Hatton Drift
Gloria Drift
Mass (10^18 g / m.y.)
3.2
2.4
1.6
0.8
0.0
Q
Pli
L
Mio
M
0
5
10
15
20
Age (Ma)

Figure 2.20

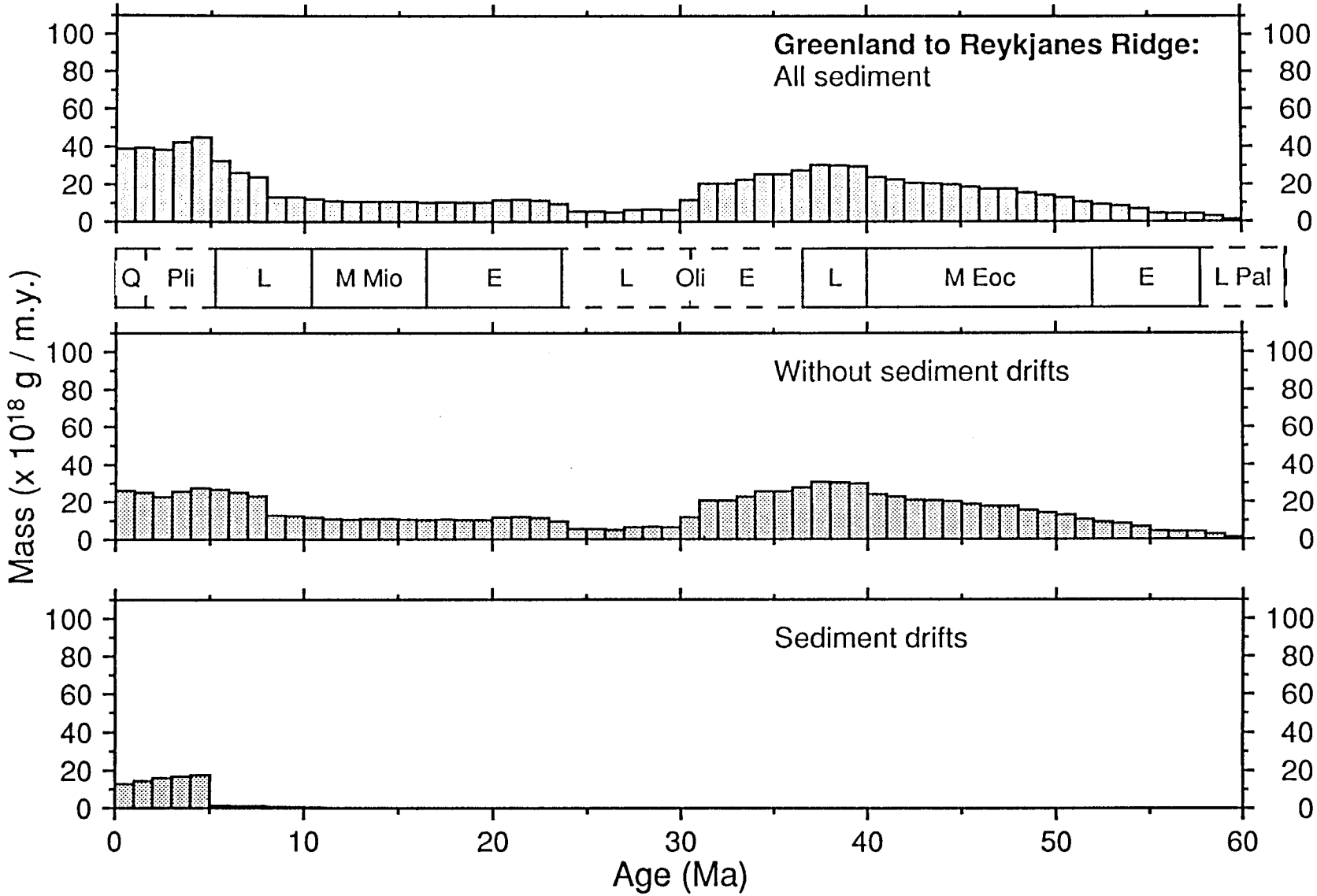
Greenland to Reykjanes Ridge:
All sediment
Without sediment drifts
Sediment drifts
Mass (x 10^18 g / m.y.)
Age (Ma)
Q
Pli
L
M Mio
E
L
Oli
E
L
M Eoc
E
L Pal
0
10
20
30
40
50
60
0
20
40
60
80
100

Figure 2.21

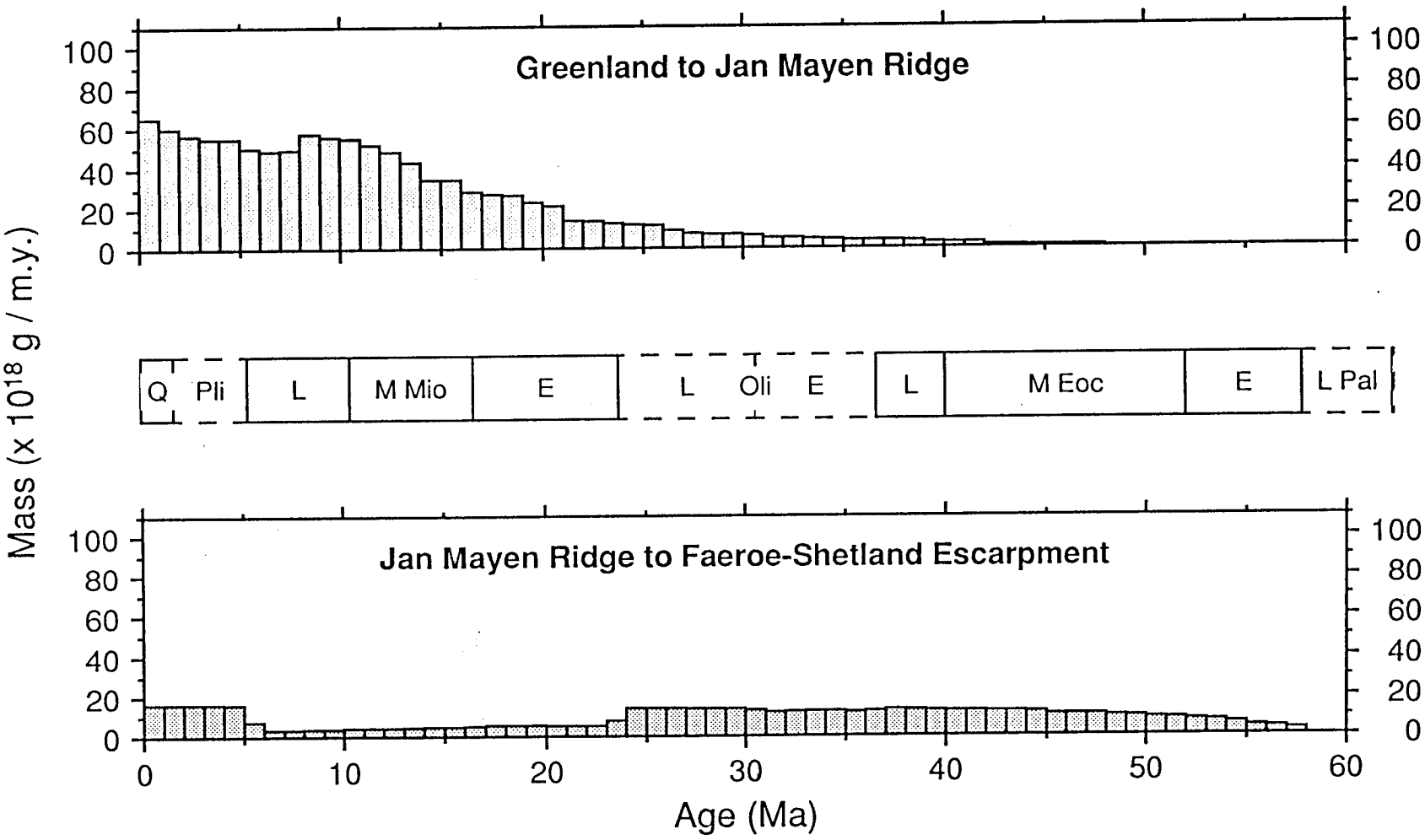
Greenland to Jan Mayen Ridge
Jan Mayen Ridge to Faeroe-Shetland Escarpment
Mass (x 10^18 g / m.y.)
Age (Ma)
Q
Pli
L
M Mio
E
L
Oli
E
L
M Eoc
E
L Pal
0
10
20
30
40
50
60
0
20
40
60
80
100

Figure 2.22

Rock Type	Grain Density ($g\ cm^{-3}$)	Compaction Code
Siliciclastics		
Breccia	2.65	Sandstone
Gravel	2.65	Sandstone
Conglomerate	2.65	Sandstone
Sand	2.65	Sandstone
Sandstone	2.65	Sandstone
Silt	2.65	Shale
Siltstone	2.65	Shale
Clay, Mud	2.65	Shale
Claystone, Mudstone	2.65	Shale
Shale	2.65	Shale
Tillite, Diamictite	2.65	Shale
Greywacke	2.65	Sandstone
Turbidite	2.65	Sandstone
Arkose	2.65	Sandstone
Tuff	2.65	Shale
Volcanic Agglomerate	2.65	Sandstone
Carbonates		
Limestone	2.71	Limestone
Dolomite	2.87	Limestone
Dolomitic limestone	2.79	Limestone
Chalk	2.71	Limestone
Calcareous ooze	2.71	Limestone
Mixed Siliciclastics-Carbonates		
Marl	2.68	Limestone
Marlstone	2.68	Limestone
Sandy limestone	2.68	Limestone
Evaporites		
Gypsum	2.31	No compaction
Anhydrite	2.96	No compaction
Salt in general	2.48	No compaction
Halite	2.16	No compaction
Micellaneous sediments		
Chert	2.27	No compaction
Glauconite	2.30	Sandstone
Siliceous Ooze	1.89	Limestone
Pelagic clay	2.65	Shale
Volcanic Rocks		
Basalt	3.03	No compaction

Table 2.1. Grain densities and BalPal compaction codes for selected rock types. Each of the different rock lithologies is compacted as shale, sandstone or limestone as indicated in the table.

Region	Area (10^6 km^2)	Volume (10^9 km^3)	Mass (10^{21} g)	Mass / Area
Reykjanes Ridge to Rockall Trough	1.77	1.68	2.75	1.55
Greenland to Reykjanes Ridge	1.09	0.73	1.00	0.92
Greenland to Jan Mayen Ridge	0.87	0.67	1.10	1.26
Jan Mayen Ridge to Norway	0.51	0.43	0.55	1.08
Charlie Gibbs F.Z. to Jan Mayen F.Z.	4.24	3.51	5.40	1.27

Table 2.2. The compiled area, volume and total mass of sediment in the four subregions (Fig. 2.15) of the study area.

CHAPTER 3. Paleobathymetric Reconstruction on a Gridded Database

3.1 Introduction

Because some of the basins in the pilot study area have formed and grown during the Cenozoic, paleobathymetric reconstruction requires combining the techniques of backstripping and plate tectonic reconstruction.

As discussed in Chapter 2 and shown in Figure 2.1, the study area extends from the Charlie Gibbs Fracture Zone to Jan Mayen Fracture Zone and from the eastern margin of Greenland to the edge of the European continental shelf. Also, as mentioned in Chapter 2, I follow the terminology of Coachman and Aagaard (1974), in referring to the region between Greenland, Jan Mayen and Spitsbergen as the Greenland Sea, the region between Greenland, Jan Mayen and Iceland as the Iceland Sea, and the remainder as the Norwegian Sea; the entire ocean area between Greenland-Scotland Ridge and the Fram Strait is referred to as the Greenland-Iceland-Norwegian (GIN) Sea.

Backstripping involves the removal of layers of sediment that are younger than the age of the reconstruction from a stratigraphic column, restoration of the underlying sediment to its unloaded condition (decompaction), incorporation of the sea level at that time, removal of the effects of thermal subsidence, and isostatic adjustment. Plate tectonic reconstruction involves movement of different parts of the area with respect to each other using rotations on the surface of a sphere.

The paleobathymetric reconstruction program (BalPal) requires that certain data be input as boundary conditions to run the model: 1) stratigraphic-lithologic sections; 2) thermal age of the lithosphere; 3) a eustatic sea level curve; 4) definition of continent-ocean and plate boundaries; and 5) rotation parameters for plate tectonic reconstructions. The program works with gridded data. A 1 x 1° latitude-longitude grid was chosen for the study area. The area contains a total of 668 grid cells, shown in Figure 2.2.

To reconstruct paleobathymetry the program (BalPal) makes a series of operations on each grid cell: 1) young sediments are removed from the top of grid cell columns; 2) the remaining sediment thickness is unloaded (decompacted) based on empirical equations for the

porosity vs. depth relationship of different sediment lithologies; 3) the effects of thermal subsidence are removed by changing the mantle density based on lithosphere subsidence curves; 4) the thickness of the overlying water column is changed according to the eustatic sea level curve; and finally, 5) the elevation of each grid cell is adjusted assuming Airy-type isostatic compensation.

3.2 Boundary Conditions

3.2.1 Stratigraphic-Lithologic Sections

As described in Chapter 2, the stratigraphy and lithology of the sedimentary rocks in each grid cell was derived from Reports of the Deep Sea Drilling Project (DSDP) and Ocean Drilling Project (ODP), from other literature sources, and from single-channel reflection seismic profiles distributed by the Marine Geophysics Section of the NOAA (U.S. National Oceanographic and Atmospheric Administration) National Geophysical Data Center (Boulder, Colorado). The locations of DSDP and ODP Sites and of the reflection seismic profiles used in the compilation are shown in Figure 2.4.

3.2.2 Thermal Age of the Lithosphere

The term "thermal age" refers to the time when the lithosphere was heated. The hypothesis is that on being heated the lithosphere expands, becoming less dense and causing and the surface of the land or seafloor to rise. Starting from the time of maximum heating, the "thermal age", the lithosphere contracts by cooling, becoming progressively more dense resulting in subsidence. The thermal ages of the lithosphere in the grid cells were calculated from plate tectonic modelling using gridded plates at 1 m.y. time increments. The crustal age for each grid cell of ocean crust was determined from the age of seafloor magnetic anomalies and the time when grid cells on adjacent plates overlapped (see discussion below). The thermal ages of continental crust are taken to be the time of rifting or thermal uplift indicated by other geologic evidence. The seafloor magnetic anomalies and continent-ocean boundaries used for establishing thermal age are shown in Figure 3.1

3.2.3 Eustatic Sea Level Curve

The eustatic sea level curve of Haq et al. (1987) serves as the basis for determining relative sea level at times in the past. Hay et al. (1989) argued that although the timing and relative magnitude of the sea level fluctuations may be correct, the absolute magnitudes of sea level change given by Haq et al. (1987) for the Cenozoic are too large. Hay et al. (1989) suggested that the correct magnitude is probably on the order of 1/2 that given by Haq et al. (1987). For the model results presented here I follow Hay et al. (1989) and use 1/2 of the amplitude of the Haq et al. (1987) sea level curve. The full-amplitude and half-amplitude sea level curves after Haq et al. (1987) averaged over 1 m.y. intervals are shown in Figure 3.2.

3.2.4 Definition of Continent-Ocean and Plate Boundaries

3.2.4.1 The Continent-Ocean Boundary

The least well-defined aspect of plate tectonic models for the North Atlantic is the position of the continent-ocean boundary (COB). Fracture zones and seafloor magnetic anomalies constrain the seafloor spreading history of lithospheric plates (Pitman and Talwani, 1972), but the plate configuration at the initiation of seafloor spreading depends on the fit of conjugate COB's.

Along the margin of the Bay of Biscay the COB is well defined in reflection seismic sections (Montadert et al., 1979). However, the COB is not always a clearly defined boundary but can occur as a transition zone between continental and ocean crust (eg. Roberts et al., 1984).

Another method used to locate the continent-ocean transition is from magnetic surveys (Kristoffersen, 1978). Continental crust (granodorite) is characterized by irregular or weak magnetic patterns whereas oceanic crust is characterized by magnetic lineations and generally stronger magnetization. From interpretation of aeromagnetic data off the northeast Newfoundland margin and off Goban Spur Srivastava et al. (1988a) concluded that a large amplitude magnetic anomaly between continental and oceanic crust corresponds closely to the location of the COB.

Differential stretching during the formation of a passive margin may make definition of the COB difficult. As suggested by Vink (1982) and modelled by Courtillot (1982), a rift propagating through a continent may result in differential stretching. The idea that the rift propagated from the south to north between Greenland and Eurasia is supported by the decreasing distance between the COB and anomaly 24 towards the north. This was apparently also the case between Flemish Cap and Charlie Gibbs Fracture Zone where the COB decreases in distance to anomaly 34 from south to north on both sides of the Atlantic (Scrutton, 1985; Srivastava et al., 1988b).

Prior to and during the initiation of seafloor spreading in the northern North Atlantic Ocean and GIN Sea there was much volcanic activity. This activity is documented by the widespread occurrence of seaward-dipping reflectors (Hinz, 1981; Mutter et al., 1982), now known to be subaerial tholeiitic flood basalts within a region known as the Tertiary Igneous Province (White, 1992). The volcanic rocks were emplaced approximately 57 Ma within a timespan of about 3 m.y. (Eldholm, 1991). They cover a region almost 3000 km in diameter that was centered over the Iceland Hotspot (White, 1992) at that time. Lava flows and sills of the Tertiary Igneous Province can be found on Disco Island (Davis Strait, western Greenland margin), on the eastern Greenland margin from the southern tip of Greenland to the Jan Mayen Fracture Zone, and along the continental margin of Europe from Hatton Bank to the Vøring Plateau. The flood basalt volcanism was succeeded by a phase of pyroclastic volcanism that resulted in widespread ash deposits recognizable throughout the NE Atlantic region (Roberts et al., 1984).

There have been two main hypotheses for the emplacement of seaward-dipping reflectors. Hinz (1981) recognized seaward-dipping reflectors in seismic reflection profiles from a number of passive margins around the world and suggested that they are emplaced during the late rifting stages on thinned continental lithosphere. However, Mutter et al. (1982) proposed that seaward-dipping reflectors are emplaced during the early stages of seafloor spreading on oceanic lithosphere. Both models assume that the layered basalt sequences were deposited either subaerially or in shallow water as has been confirmed by drilling on DSDP Leg 38 (Talwani, Udintsev et al., 1976) and ODP Leg 104 (Eldholm, Thiede, Taylor et al., 1987) on the outer Vøring Plateau.

Independant of the model for emplacement of seaward-dipping reflectors, their location is closely associated with the transition from continental to oceanic crust. Skogseid and Eldholm (1987) interpreted the COB off the Vøring Plateau Escarpment to lie near the seaward edge of the base of the seaward-dipping reflector sequence. North of the Faeroe Islands, Smythe (1983) interpreted the COB to be located near the landward end of the oldest seaward-dipping reflectors off the Faeroe-Shetland Escarpment. On the western margin of Rockall Plateau (western margin of Hatton Bank) the emplacement of the seaward-dipping reflector sequences occurred within the interval between Anomalies 25 to 24B (Roberts et al., 1984). Along the western margin of Rockall Plateau the COB is more difficult to locate and may occur as a transition zone beneath the seaward-dipping reflectors (Roberts et al., 1984). It has also been interpreted to lie near the 2000 m bathymetric contour including Edoras Bank (Roberts et al., 1981; Srivastava and Tapscott, 1986; Morgan et al., 1989). The location of the COB on the southwest margin of Rockall Bank is from Roberts et al. (1981); it is assumed to terminate to the south at the Charlie Gibbs Fracture Zone. The exact location of the COB along the southeastern Greenland margin is not well known and there have been several proposed locations (Featherstone et al., 1977; Surlyk et al., 1981; Larsen, 1984, 1990). The COB chosen by Larsen (1984, 1990) lies closer to Greenland than those previously proposed. It was chosen as approximating the fit between Greenland and Europe just prior to the initiation of seafloor spreading. Along the eastern Greenland margin seaward-dipping reflectors were emplaced on extended continental crust (Roberts et al., 1984).

3.2.4.2 Iceland and the Greenland-Scotland Ridge

The Greenland-Scotland Ridge began to form as a result of excessive volcanism from the Iceland Hotspot at the same time that seafloor spreading started between Greenland and the Faeroe Islands. The Faeroe Islands are assumed to be underlain by continental crust (Bott et al., 1976); the continent-ocean boundary occurs to the west between the Faeroe Block and the oceanic Iceland-Faeroe Ridge and also north of the Faeroes. Bott (1983, 1985) used a model for the thermal subsidence of seafloor (Parsons and Sclater, 1977) and Thiede and Eldholm (1983) used a thermal subsidence model for aseismic ridges (Detrick et al., 1977) to reconstruct the subsidence history of the Greenland-Scotland Ridge. Weber (1990) used an Airy-type isostatic model to reconstruct the elevation of the Greenland-Scotland Ridge. All

of these authors concluded that the Greenland-Scotland Ridge was formed more than 1000 m above sea level and that parts of the Greenland-Scotland Ridge began to subside below sea level in the Eocene. Thiede (1980) and Thiede and Eldholm (1983) argued that the Iceland-Faeroe Ridge was emergent until the Middle Miocene.

The subsidence of the Greenland-Scotland Ridge has played an important role in the paleoceanography of the Atlantic, controlling the exchange of water between the North Atlantic Ocean and GIN Sea. It has generally been assumed that as the Greenland-Scotland Ridge subsided below sea level dense water from the GIN Sea spilled over the Greenland-Scotland Ridge and formed abyssal currents flowing south. These bottom currents eroded sediment and initiated the accumulation of sediment drifts.

The present spreading center in eastern Iceland has only been active for the last 3-4 m.y. (Saemundsson, 1974; Palmason, 1974). Prior to that time spreading occurred along the western rift axis (Talwani and Eldholm, 1977). In their reconstruction of the North Atlantic, Talwani and Eldholm (1977) modelled the formation of Iceland between Anomaly 7 and Anomaly 5 (25.5 to 10 Ma) citing estimates of the maximum age of Icelandic rocks as 20 Ma (Dagley et al., 1967; Moorbath et al., 1968). Vogt et al. (1980) interpreted basement steps (paleo-shelf edge) on the southeast (Kristjansson, 1976) and southwest (Egloff and Johnson, 1979) margins of Iceland as reflecting abrupt increases in mantle plume discharge and basalt magmatism. They concluded that the insular platform of Iceland began to form ca. 25 Ma ago (Anomaly 7).

3.2.4.3 Extension along the European Continental Margin

There have been differing opinions whether the crust underlying the Rockall Trough is oceanic (Roberts, 1975; Roberts et al., 1983) or continental (Talwani and Eldholm, 1977). Roberts et al. (1988) interpreted seismic refraction and wide-angle reflection profiles to indicate that the crust is continental and has been stretched to 1/5 of its initial thickness. Extension in the Rockall Trough probably began in the late Early Cretaceous (Montadert et al., 1979; Roberts et al., 1981) and was complete by the late Cretaceous (Roberts, 1975; Roberts et al., 1981, 1984).

Stretching in the Rockall Trough propagated from the south towards the north with the youngest stretching the Møre Basin (Hanisch, 1984). Kristoffersen (1978) assumed that Rockall Trough was formed by seafloor spreading during the Cretaceous Normal Quiet interval (approx. 118-84 Ma) and that spreading ended near the end of the interval around Anomaly 34 time. Hanisch (1984) modelled the Cretaceous opening of the Northeast Atlantic as a continuous rift extending from Rockall Trough through the Faeroe-Shetland Channel to end in the Møre Basin. Roberts et al. (1981) concluded that spreading in Rockall Trough could have occurred later, between the Aptian and Maastrichtian (124 to 65 Ma). Hanisch (1984) concluded that rifting was Aptian or younger and ended between Anomaly 32 to 31 (72 to 69 Ma). Crustal extension in the Hatton-Rockall Basin may have occurred between Anomalies 32 and 31 (Hanisch, 1984) and was probably complete prior to the initiation of seafloor spreading west of Hatton Bank.

3.2.5 Rotation Parameters for Plate Tectonic Reconstructions

3.2.5.1 Previous Plate Tectonic Reconstructions of the North Atlantic

Bullard et al. (1965) presented a quantitative method for rotating digitized outlines of continents together to find the best pre-rift fit, using the Atlantic as an illustration. Pitman and Talwani (1972) showed that seafloor magnetic anomalies could be used to reconstruct the positions of lithospheric plates with respect to one another in the past. Talwani and Eldholm (1977) provided a detailed spreading history for the GIN Sea based on the then newly identified magnetic anomalies, fracture zones and the fit of the conjugate continent-ocean boundaries (COB). They concluded that the initiation of seafloor spreading occurred between Anomalies 25 and 24. Le Pichon et al. (1977) reconstructed the pre-rift fit of the continents around the North Atlantic using 3000 m isobaths along the older margins (Africa-North America) and the 2000 m isobaths between younger conjugate margins (Greenland-Eurasia). They noted that the pre-rift fit of conjugate continental margins could be further constrained by taking preexisting lineaments into account (Ramsay, 1969; Arthaud and Matte, 1975). The reconstruction of Sclater et al. (1977) differed from that of Le Pichon et al. (1977) in that Iberia was fit closer to the Grand Banks of Newfoundland, thus reducing the gap between the continental margins. Kristoffersen (1978) and Srivastava (1978) treated Rockall Plateau as part

of Greenland during the early rifting (Cretaceous) of the North Atlantic to explain the opening of Rockall Trough.

Most plate tectonic reconstructions of the northern North Atlantic Ocean and GIN Sea have used a three-plate model consisting of Greenland, Eurasia and the Jan Mayen microplate (Talwani and Eldholm, 1977; Unternehr, 1982; Nunns, 1982, 1983; and Bott, 1985). The Jan Mayen plate was originally added to the basic two-plate configuration of Greenland and Eurasia to account for the fan-shaped seafloor magnetic anomalies around the extinct Aegir Ridge in the Norway Basin.

The Jan Mayen plate adds significant complexity to the development of this region. Unternehr (1982) showed detailed reconstructions of the position of Jan Mayen Ridge based on seafloor spreading about Kolbeinsey and Aegir Ridges. These reconstructions were modified by Nunns (1983) who assumed that spreading along the Greenland-Scotland Ridge was analogous to the spreading history along the Reykjanes Ridge. Nunns (1983) outlined the spreading history between the Greenland-Scotland Ridge and Jan Mayen Fracture Zone. He believed that there were initially two spreading centers, one along the Reykjanes and the other along the Aegir Ridge, separated by a transform fault north of the Greenland-Scotland Ridge. At about Anomaly 20 time, Jan Mayen began to separate from Greenland and there was spreading to both the west and east of Jan Mayen Ridge. Then at Anomaly 7 time spreading stopped along Aegir Ridge and shifted entirely to the Kolbeinsey Ridge where it continues today. The width of the rift valley of the Aegir Ridge is greater than those of active slow spreading centers, this may reflect ultra-slow spreading along the Aegir ridge just before it became extinct (Vogt, 1986). Bott (1985) followed the same chronology of events in the spreading history north of the Greenland-Scotland Ridge as outlined by Nunns (1983), but modified the rotation of Jan Mayen with respect to Greenland based on the magnetic anomaly map of Nunns et al. (1983).

The Cretaceous history of the North Atlantic south of Charlie Gibbs Fracture Zone was equally complex. Srivastava et al. (1988b) revised the earlier reconstruction parameters of Srivastava and Tapscott (1986) for Anomaly 34. They also identified Anomaly K in the Cretaceous Quiet Zone south of Flemish Cap and north and south of the Bay of Biscay and showed that it represents a triple junction that existed during the separation of the Grand Banks, Europe and Iberia. They gave rotation parameters for Anomalies K and M-0 for Eurasia relative to North America, showing the development of the Porcupine Plate from the

triple junction. Roest and Srivastava (1989) published reconstruction parameters for magnetic anomalies 25 and older based on newly acquired geophysical data. Their rotation parameters resulted in a fit of Greenland to North America 100 km further south than the reconstruction of Srivastava and Tapscott (1986). Müller and Roest (1992) used Geosat/Seasat altimetry data to identify new fracture zones and extend old ones closer to continental margins in the North Atlantic.

Verhoef et al. (1989, 1990) described a method of gridded plate tectonic reconstruction illustrating the technique with the NE Atlantic. The boundaries of the plates along a mid-ocean rift were defined by seafloor magnetic anomalies and the plates rotated together so that the conjugate boundaries coincided. They used this method to display present bathymetry on a palinspastically corrected database.

3.2.5.2 Rotations for the New Plate Tectonic Reconstruction of the Northern North Atlantic

In order to find the best fit between magnetic anomalies and the along-strike position of the plates with respect to one another I compared different published rotation models with newly digitized information. I used rotations from the literature when they provided the best fits, otherwise I calculated new rotations to fit conjugate anomalies. The Charlie Gibbs Fracture Zone and Jan Mayen Fracture Zone, and the Hudson, Snorri, Minna and Leif Fracture Zones constrain the reconstructions. The magnetic anomalies, fracture zones and ridges were digitized from Cande et al. (1989), Nunns et al. (1983) and Bott (1985). The ages of the anomalies are from the timescale of Kent and Gradstein (1986) and are given in table 3.1 along with the rotation parameters. The rotations given in table 3.1 were recalculated so that all are expressed as total reconstruction poles. A total reconstruction pole is a single rotation starting at the present and going backward in time to reconstruct the position of a plate at some specific time in the past (Cox and Hart, 1986). The reference frame for the reconstructions presented here is based on paleomagnetic data for the North American plate. The paleolatitude total reconstruction poles for North America (Table 3.2) have been derived from the polar wander curve calculated from paleomagnetic poles by Harrison and Lindh (1982).

The best fits between Greenland and Eurasia for Anomalies 5, 13 and 24 use the total reconstruction poles and rotations of Srivastava (1985) and Srivastava and Tapscott (1986). The fit between Greenland and Eurasia for Anomaly 7 is from Bott (1985). The fit of Greenland to Europe uses the closure rotation from Talwani and Eldholm (1977). The published rotations used in the literature to fit Anomalies 6, 20 and 21 between Greenland and Eurasia (Talwani and Eldholm, 1977; Nunns, 1983; Bott, 1985; Srivastava, 1985; Srivastava and Tapscott, 1986; and Rowley and Lottes, 1988) were not satisfactory. The new total reconstruction poles and rotation angles for these anomalies are presented in Table 3.1.

The youngest seafloor magnetic anomaly in the southern Labrador Sea is Anomaly 20 (Cande et al., 1989) which formed approximately 45 Ma (according to the timescale of Kent and Gradstein, 1986). The age of the extinct spreading center in the southern Labrador Sea is not exactly known but seafloor spreading is thought to have continued until approximately 35 Ma (Vogt and Avery, 1974; Emery and Uchupi, 1984; Srivastava and Tapscott, 1986; Srivastava and Arthur, 1989). The fit of Anomalies 25 and 31 in the southern Labrador Sea are from Roest and Srivastava (1989). The best fits for Anomalies 20, 21 and 24 were determined from digitization of the Cande et al. (1989) map and are presented in Table 3.1.

Nunns (1983) reconstructed the position of the Jan Mayen Microplate with respect to Eurasia and Greenland since the time of initial seafloor spreading. A good fit of Anomaly 20 on the Jan Mayen and Eurasian plates was not achieved with the Nunns (1983) rotation, but Anomaly 13 did fit satisfactorily using his rotation. The age of initial rifting between Jan Mayen and Eurasia is the same as that in the rest of the northern North Atlantic (just prior to Anomaly 24B). Based on the fit of conjugate anomalies about the Aegir and Reykjanes Ridges, Jan Mayen is modelled here as having begun to separate from Greenland at Anomaly 20 time with contemporaneous spreading to the west and east of Jan Mayen Ridge.

Seafloor spreading between Rockall Plateau and southeast Greenland began prior to Anomaly 24 (Roberts et al., 1979, Srivastava and Tapscott, 1986). The plate tectonic reconstructions presented here begin just after initiation of seafloor spreading between Rockall and Greenland (50 Ma).

3.3 Reconstructing the Paleobathymetry

3.3.1 Previous Paleobathymetric Reconstructions

Sclater et al. (1977) reconstructed the sediment-free bathymetry of the North Atlantic. They calculated depth along magnetic anomalies at times in the past using the thermal subsidence curves of Parsons and Sclater (1977) without correction for sediment loading. They also assumed symmetric spreading about the mid-ocean ridges.

Sclater et al. (1985) reconstructed Neogene paleobathymetry for the global ocean basins at DSDP sites. Using the equations of Parsons and Sclater (1977) they calculated the sediment-free water depths of the sites (T_{w1}). They referred to the present water depths (with sediment cover) with the term, T_{w2}. To calculate the sediment-free water depth they developed an isostatic model assuming a compensation depth at the base of the lithosphere. They described the mass equivalent relationship between the sedimented and sediment-free water depths as

$$T_{w1}\rho_w + T_L\rho_L + y\rho_m = T_{w2}\rho_w + T_L\rho_L + T_s\rho_s \qquad (3.1)$$

where ρ_w is the density of sea water, T_L is the thickness of lithosphere, ρ_L is the density of lithosphere, y is the thickness of asthenosphere that accounts for isostatic equilibrium and ρ_m is the density of the mantle. The sediment thickness (T_s) and sediment density (ρ_s) were taken from DSDP drill site reports. They described the depth equivalent relationship between the two columns as

$$T_{w1} + T_L + y = T_{w2} + T_s + T_L \qquad (3.2)$$

Solving Eqns. (3.1) and (3.2) for T_{w1} they derived

$$T_{w1} = T_{w2} + T_s\,[(\rho_s - \rho_m) / (\rho_w - \rho_m)] \qquad (3.3)$$

Here, T_{w1} is independent of lithosphere thickness and can be used to calculate the depth of the ocean crust with or without a sediment load. From equation (3.3) they calculated the sediment-free water depths (T_{w1}) and the difference between the depth predicted by the Parsons and Sclater (1977) curve and that predicted by their isostatic model. They referred to the difference between these two values as the offset (depth anomaly). This was assumed to be a constant value for calculation of paleobathymetry. Sclater et al. (1985) chose sites that they thought lie on ocean crust that had subsided without being influenced by thermal swells (hot spots). They reconstructed the paleobathymetry for those sites at 8, 16 and 22 Ma. They

used age-depth information from the drill sites to estimate total sediment thickness at times in the past. They did not decompact the older sediment to restore it to its thickness before loading by younger sediment. Their method also did not include estimates of changes in the water depth due to sea level change. Their reconstructed paleobathymetric maps however, were calculated for sediment-free ocean crust.

Tucholke and McCoy (1986) published paleogeographic maps of the North Atlantic showing coastlines, major sediment lithologies, major plate boundaries, paleobathymetry and paleocirculation patterns. They used an age-depth equation for the Atlantic based on DSDP drill sites (Tucholke and Vogt, 1979) and showed paleobathymetry for sediment-free oceanic lithosphere.

Shaw (1989) used the methods described by Hay et al. (1989) to backstrip sediment from the Gulf of Mexico and eastern U.S. margin. His model included sediment decompaction and no palinspastic correction was needed because seafloor spreading occurred earlier than his reconstruction ages.

3.3.2 Subsidence of Oceanic Lithosphere

Young oceanic lithosphere is elevated along mid-ocean ridges and subsides to greater depths with increasing age and distance from the ridge. Menard (1969) noted the correlation between the depth and age of oceanic lithosphere. Sclater and Francheteau (1970) and Sclater et al. (1971) described the empirical relationship between the depth of ocean crust and its age, where increasing depth is proportional to the square root of age. Davis and Lister (1974) analyzed the data of Sclater et al. (1971) and found a linear relationship between increasing depth and the square root of age ($t^{1/2}$) for ocean crust from 0 to 80 Ma. The equations expressing this relationship have the form

$$d(t) = a + b\, t^{1/2}$$

where d(t) is the depth of the ocean crust at time t (in millions of years), a is the initial depth of the ocean crust at the ridge crest in meters, and b is a constant describing the time-dependent subsidence rate.

Parsons and Sclater (1977) calculated two equations for the depth of oceanic lithosphere as a function of age for the northwest Pacific and western North Atlantic. For sediment-free lithosphere less than 70 Ma depth was given as

$$d(t) = 2500 + 350\ t^{1/2} \quad (3.4)$$

where the ridge depth at t = 0 is assumed to be 2500 m. For lithosphere older than 20 Ma, they calculated

$$d(t) = 6400 - 3200\ e^{(-t/62.8)} \quad (3.5)$$

where 6400 m was assumed to be the maximum depth to which sediment-free ocean crust could subside.

Heestand and Crough (1981) concluded that the data Parsons and Sclater (1977) had used to calculate the age-depth relationship was affected by hot spots. Hotspots are thought to represent plumes of hotter mantle material that rise from the lower mantle to the base of the lithosphere. The surface expression of a hotspot is a broad region of elevated topography about 1 km high at its center and covering a radius of about 500 km (Heestand and Crough, 1981) from the center of the hotspot. Reheating of lithosphere by hotspots could account for the flattening of the Parsons and Sclater (1977) curve (Eqn. 3.5). Heestand and Crough (1981) modelled age-depth for oceanic lithosphere they thought to be unaffected by hotspots and calculated depth as

$$d(t) = 2700 + 295\ t^{1/2} \quad (3.6)$$

for seafloor between the ages of 0 and 80 Ma, where the ridge depth at t = 0 is assumed to be 2700 m. Hotspots have either remained fixed (Morgan, 1983) or move slowly with respect to the mantle (eg. Jurdy and Stefanick, 1991). Lithospheric plates move more rapidly, so that as a plate moves over a hotspot a linear feature is produced. This feature may be elevated topography, a volcanic ridge or a seamount chain.

Schroeder (1984) calculated the age-depth relationship for lithosphere in the Pacific Ocean basin for regions greater than 800 km from known hotspots and their tracks. He found the following relationship to be true for lithosphere within the 0 to 80 Ma age range

$$d(t) = 2846 + 298\ t^{1/2}. \quad (3.7)$$

Lithosphere in the Pacific Ocean basin that is older than 80 Ma has been reheated by hotspots (Schroeder, 1984) and was found to be shallower than the depth predicted by Eqn. (3.4). Like Parsons and Sclater (1977), Schroeder (1984) found the age-depth relationship for the older lithosphere to be best modelled by an exponential decay curve

$$d(t) = 6400 - 3116\ e^{(-t/54.9)}. \quad (3.8)$$

The $t^{1/2}$ age-depth relationship for young oceanic lithosphere was also found to be true in a major back-arc basin where Park et al. (1990) analyzed age and bathymetric data for the

Philippine Basin. There the age of the lithosphere ranges from 0 to 60 Ma and the sediment-free depth is approximated as

$$d(t) = 3222 + 366\ t^{1/2}. \qquad (3.9)$$

The similarity of the coefficients, 350 and 366, in Eqns. (3.4) and (3.9) for the western North Atlantic, northwest Pacific and Philippine Sea back-arc basin indicate that subsidence curves for these regions have approximately the same shape. However, the depth to basement in the Philippine Basin about 800 m greater than in major ocean basins. The data used to calculate the coefficients for young lithosphere unaffected by hotspots (Eqns. 3.6 and 3.7) come from the Pacific Ocean basin, which is characterized by higher spreading rates than the Atlantic. The coefficients, 295 and 298, in Eqns. (3.6) and (3.7) are less than the 350 of Parsons and Sclater (1977) indicating that oceanic lithosphere in the Pacific subsides less rapidly than Atlantic ocean lithosphere.

Detrick et al. (1977) studied results from DSDP drill sites to model the subsidence of aseismic ridges. Aseismic ridges occur throughout the world ocean basins and are defined as linear volcanic ridges free of earth quake activity (Laughton et al., 1970). Detrick et al. (1977) found that the Ninetyeast Ridge and southeast Mascarene Plateau (Indian Ocean), Rio Grande Rise and Walvis Ridge (South Atlantic Ocean) and the Chagos-Laccadive Ridge (eastern Central Pacific Ocean) all formed close to sea level and subsided at rates comparable to normal ocean crust. From analysis of DSDP Site 336 (Talwani, Udintsev et al., 1976) however, Detrick et al. (1977) found it to be anomalously shallow for its age and suggested that the Iceland-Faeroe Ridge was above sea level near Site 336 for the first 15 m.y. after its formation. They used empirical curves from Sclater et al. (1971) for depth versus age of oceanic lithosphere in the East Pacific to model the subsidence of the aseismic ridges.

3.3.3 Gridded Plate Tectonic Reconstructions: Modelling the Age of Oceanic Lithosphere

The main objective of using a gridded plate tectonic model for reconstructing paleobathymetry is to be able to calculate lithospheric ages and rotation parameters that are consistent with one another. The primary sources of information for determining the age of oceanic lithosphere are interpreted seafloor magnetic anomalies. These were digitized from maps published by Cande et al. (1989), Nunns et al. (1983) and Bott (1985), and are shown

in Figure 3.1. Although it is conceivable that the lithospheric ages for the grid cells could be calculated from interpolation using a gridding algorithm, this would only be a first approximation. When the plates were rotated together there would invariably be gross overlaps and gaps.

Verhoef et al. (1989, 1990) described a method of gridded plate tectonic reconstruction in the NE Atlantic. The boundaries of the plates along a mid-ocean rift were defined by seafloor magnetic anomalies and the plates rotated together so that the conjugate boundaries coincided. In their method, Verhoef et al. (1990) defined the plate boundaries along a given anomaly and applied rectangular grids to the plates in their present positions. One plate was kept fixed and the polygon representing the other plate is rotated to the fixed plate. After rotation only the grid on the fixed plate remained rectangular. The rotated grids were distorted, so they then applied a new grid to data on the rotated plates. They used an interpolation algorithm to transfer the digitized data from the initial grid to the new one.

There are two important differences between the method used by Verhoef et al. (1989, 1990) and the new method described here. First, the new method palinspastically reconstructs plate positions continuously along spreading centers. Positions can be interpolated to any time within the interval defined by the rotation model; it is not restricted to the specific times represented by the magnetic anomalies. Second, the new method does not use a rectangular grid in Cartesian Coordinates, but a spherical grid that remains fixed on each plate.

To set up the initial conditions for the model, the region that is to be reconstructed is first divided into a grid. The most readily available grid on a sphere is the present grid of latitude and longitude. On a spherical grid each cell should have the same dimensions, and a 1 x 1° grid was chosen for this study. Although equidimensional in terms of angular measure, the 1 x 1° grid "squares" are not equidimensional in terms of linear measure. At the latitude of the northern North Atlantic and southern GIN Sea they are trapezoids that are about half as wide in the E-W direction as they are high in the N-S direction. The area of a 1 x 1° grid "square" decreases from 7718 km^2 at the southern side of the study area (Lat. 51.5° N) to 3949 km^2 at the northern side (Lat. 71.5° N).

The boundaries of oceanic lithosphere for each plate are defined at different times by present and extinct spreading centers, transform faults, plate convergence zones and the continent-ocean boundary. The boundaries are located along the present latitude-longitude grid and magnetic lineations are digitized to assign initial ages to the grid cells. Magnetic

lineations that are discontinuous are interpolated from existing data. The last step in setting up the initial conditions is to find the Euler poles and rotation angles (Cox and Hart, 1986) that can be used to fit conjugate magnetic lineations. During seafloor-spreading the lateral position of the plates relative to one another is constrained such that any transform motion can only occur along fracture zones.

The changing plate boundaries along spreading centers are reconstructed from: 1) age of magnetic lineations; 2) age of adjacent grid cells that lie along the current vector of plate motion; and 3) the amount of overlap with grid cells on the adjacent plate. The age of a grid cell formed by seafloor spreading is calculated starting with the present plate configuration and working backwards in time. The plate boundaries are redefined along spreading centers with each timestep.

Figure 3.3 illustrates the method for determining the age of the lithosphere on a spherical grid. The present (t = 0) plate configuration from 60 to 63° N latitude along a section of the Reykjanes Ridge is shown in Figure 3.3A. The ridge is shown as a heavy solid line in the center of the diagram and magnetic lineations are thin lines parallel to the ridge. The ages of the magnetic lineations, given in millions of years B.P., increase symmetrically away from the Reykjanes Ridge and the ridge is the youngest tectonic feature on the map. There are also two lithospheric plates shown as 1 x 1° grids in Figure 3.3A. The boundary between the plates is defined by the Reykjanes Ridge. The Greenland plate is on the left (solid grid) and the Eurasian plate is on the right (dashed grid). Figure 3.3B shows the grid of the Eurasian plate rotated to its position at 2 Ma relative to a fixed Greenland plate. Three pairs of grid cells overlap along the spreading center, but only 3 cells can be removed from the grids to make a palinspastic reconstruction of the gridded Greenland and Eurasian plates. The cells that must be removed depend on the age of the magnetic lineations that pass through them. Comparing the age of magnetic lineations in pairs of adjacent grid cells of the two plates, it is apparent (Figure 3.3A) that the cells containing the largest proportion of young seafloor are the Eurasian grid cell from 60 to 61° N, the Greenland grid cell from 61 to 62° N and the Eurasian grid cell from 62 to 63° N latitude. The age of these three grid cells is then 2 Ma, i.e. at the resolution of the grid these cells were formed by seafloor spreading 2 Ma, as shown in Figure 3.3C. In the 2 Ma reconstruction the grid cell along the spreading center between 62 and 63° N is part of the Greenland plate and those between 60

and 62° N would be part of the Eurasian plate as shown in Figure 3.3D. This procedure, which cannot be automated readily, must be performed for all plate boundaries every million years.

The gridded plate tectonic model was used to estimate the age of ocean crust younger than 60 Ma (Fig. 3.4). Regions landwards of the 60 Ma isochron are underlain by continental crust except in the Labrador Sea. The age isochrons in the Rockall-Faeroe region represent a model for the timing of Cretaceous rifting in the Rockall Trough, Faeroe-Shetland Channel and Hatton-Rockall Basin.

3.3.4 Backstripping Layers of Sediment

The term "backstripping" was introduced by Steckler and Watts (1978) to describe the process whereby layers are progressively removed from a column of sedimentary rock and the new water depths to the top of the remaining sedimentary rock or to basement are calculated. This technique was developed to study different styles of subsidence on passive margins and to separate the effect of thermal subsidence due to upwelling of hot asthenospheric material during rifting from that due to sediment and water loading. Backstripping consists of the following steps: 1) removal of sediment younger than the age of the reconstruction; 2) restoration of the remaining sediment column to its thickness prior to loading and compaction ("decompaction"); 3) removal of the effect of thermal subsidence; 4) change of sea level to its position at the time relative to present sea level; and 5) bringing the entire area into isostatic equilibrium.

3.3.4.1 Removal of Sediment Younger than the Age of the Reconstruction

The minimum thickness of sediment that existed at times in the past is estimated by removing sediment younger than the reconstruction age and restoring the older sediment layers to their condition prior to loading. This process is called "decompaction" and is based on estimates of the increasing solidity of sediment layers with depth of burial. In the NE Atlantic there are both regional unconformities and significant sediment drifts. The drifts are current-controlled accumulations of sediment indicating erosion and redistribution of sediment within the basin. A more realistic model would include estimates of the thickness of sediment

eroded where unconformities are observed today, but this is beyond the scope of the present study.

3.3.4.2 Decompaction of the Remaining Sediment Column

Decompaction requires knowledge of how the porosity and its reciprocal, the solidity, of the sediment vary with burial depth and lithology. The solidity of a layer of sediment at any given depth can be estimated with one of the three equations (2.7, 2.10 or 2.14) depending on lithology. The increase of solidity with increasing burial depth for shale, limestone and sandstone has been shown in Figure 2.4. The pore space in sediment below sea level is assumed to be filled with seawater (ρ_W = 1027 kg/m^3). The average solidity of a sediment layer is assumed to be equal to the solidity calculated for the depth (D) at the midpoint of that layer.

When younger layers of sediment are removed from the top of the column, D will decrease because of the isostatic response to unloading and the solidity (S) will also decrease. The result is a new sediment surface at a level intermediate between the original surface and the original depth of base of the younger sediment that was removed. Prior to unloading a given sediment layer has thickness, T and solidity S. After unloading the new solidity (S') of the layer is calculated from the solidity/depth relation and the decompacted thickness (T') of the layer is

$$T' = T\,(S / S'). \qquad (3.10)$$

Eqn. (3.10) is used to calculate the decompacted thickness of each remaining sediment layer after stripping off the younger layers of sediment. Decompacted thicknesses are estimated from the top of the column towards the bottom. This is because the thickness of each layer increases after decompaction, requiring that the depth to the middle of the next layer be increased by the amount the intervening sediment was decompacted. After decompaction the total sediment thickness is the sum of all the decompacted layer thicknesses.

3.3.4.3 Removal of the Effect of Thermal Subsidence

Hay et al. (1989) suggested using the isostatic balance of a column of rock and water above a horizontal isobaric surface to compensate for the effects of thermal subsidence. In

the model described here this isobaric surface will be called the compensation depth and is taken to be 100 km below present sea level. Isostatic equilibrium across a region is maintained by requiring that the total mass (M) of each column be equal at the compensation depth.

Columns contain a layer of mantle and crust, they may also have layers of sediment and a layer of water. A "layer" is a three-dimensional entity, and can either be mantle, crust, sediment or water. The height of a column (H_l) varies and is equal to the sum of the thickness of mantle (T_M), crust (T_C), sediment (T_S) and water layer on the top of the column (T_W) above the compensation depth

$$H_l = T_M + T_C + T_S + T_W. \qquad (3.11)$$

For any given column the total mass of all the layers is equal to a constant value, M:

$$M = T_M\rho_M + T_C\rho_C + T_S\rho_S + T_W\rho_W \qquad (3.12)$$

where the thickness of each layer can be considered numerically equivalent to volume for a column with unit area of 1 m^2. Any column that is in isostatic equilibrium has a mass equal to M regardless of whether the column is above or below sea level. M is calculated using values from Hay et al. (1989) assuming that a 6.5 km thick layer of sediment-free 200 Ma ocean crust (ρ_C = 2750 kg/m^3) lies at a depth of 6268 m beneath the ocean surface (ρ_W = 1027 kg/m^3). The thickness of the water layer (T_W) is calculated from Eqn. (3.5) for 200 Ma ocean crust (Fig. 3.5) with no sediment (T_S = 0) and the mantle density (ρ_M) is assumed to be 3300 kg/m^3, then

$$M = (87232\ m^3 \times 3300\ kg/m^3) + (6500\ m^3 \times 2750\ kg/m^3) + (6268\ m^3 \times 1027\ kg/m^3)$$

$$M = 3.1218 \times 10^7\ kg.$$

To simplify the calculations and eliminate the problem of uncertainty whether crust at a particular site is oceanic or continental, the same density (ρ_C = 2750 kg/m^3) is assumed for both. This is reasonable because young ocean crust includes many cracks and spaces that reduce its density below that of basalt, and old ocean crust contains much light altered material as a result of submarine weathering.

The subsidence of lithosphere due to cooling with increasing age (thermal subsidence) is modelled here by changing the density of the upper mantle. Both the thickness of the crust and its density are assumed to remain constant through time. This is an obvious oversimplification, but adding the complexities of increasing crustal thickness and changing

its density with age would not appreciably affect the paleobathymetric reconstructions. The depth from present sea level to the top of the crust is calculated using Eqns. (3.4) and (3.5) for a sediment-free ocean crust with a thickness of 6500 m and density of 2750 kg/m^3. As discussed above, Sclater et al. (1985) suggested that Eqn. (3.4) be used for crust younger than 70 Ma and Eqn. (3.5) for older crust. However, the depth vs. age curves predicted by these two equations intersect at 26.4 Ma (Fig. 3.5). Switching from Eqn. (3.4) to Eqn. (3.5) at 70 Ma would result in a sudden decrease in depth from the older crust. Because depth must increase smoothly with age I use Eqn. (3.4) for crust less than or equal to 26.4 Ma and Eqn. (3.5) for all older crust.

The equation to calculate mantle density was derived from Eqns. (3.11) and (3.12) where the unknown terms were ρ_M and T_M

$$\rho_M = (M - T_C\rho_C - T_W\rho_W) / (H_I - T_C - T_W). \qquad (3.14)$$

The water depth (T_W) was calculated as described above and the average thickness of ocean crust (T_C = 6500 m) was used. Mantle density is thus modelled only as a function of age, i.e. all columns with the same age crust have the same mantle density.

Isostatic equilibrium is achieved assuming Airy-type isostatic compensation and is implemented by calculating the present thickness of the crust in each column. This thickness is kept constant through time. When the stratigraphic column is compiled for each grid cell, the following values are either known or have been estimated: M, H_I, T_W, ρ_W, T_S, ρ_S, ρ_C, ρ_M, leaving T_M and T_C unknown. Because there are two equations (Eqns. 3.11 and 3.12) and two unknowns, we can solve for either of the unknown values. From Eqns. (3.11) and (3.12) the thickness of the crust is

$$T_C = [M - \rho_M (H_I - T_S - T_W) - T_S\rho_S - T_W\rho_W] / (\rho_C - \rho_M). \qquad (3.13)$$

Before any backstripping can be performed the thickness of the crust in each column must be calculated.

The present thickness of the crust (Fig. 3.6) was estimated using Eqn. (3.13). The model presented here predicts anomalously thick crust over the entire study area from the Charlie Gibbs to Jan Mayen Fracture Zones. Normal ocean crustal thicknesses (6-8 km) only occur in the southeast corner of the study area in the Porcupine Abyssal Plain. Crustal thicknesses in Figure (3.6) agree well with published estimates along the Iceland-Scotland Ridge and in the Rockall-Faeroe region. From gravity-density modelling, Bott and Gunnarsson (1980) estimated up to 30 km of anomalously thick crust in center of the Iceland-Faeroe

Ridge with the crust thickening to approximately 35 km under the Faeroe Block. The thickness of the crust predicted by Eqn. (3.13) at the center of the Iceland-Faeroe Ridge is slightly less (26 km). Assuming a two-layer crust Weber (1990) also used a gravity-density model to estimate the crustal thickness across the Iceland-Faeroe Ridge. His estimate was approximately the same as that of Bott and Gunnarsson (1980). Crustal thicknesses estimated with Eqn. (3.13) show a local maximum under the Faeroe Block of more than 30 km.

Based on wide-angle ocean bottom seismometer and multichannel seismic refraction profiles Morgan et al. (1989) constructed a velocity model across the western margin of Hatton Bank. Their maximum estimated crustal thickness was 24 km and that estimated from Eqn. (3.13) in Fig. (3.6) is 22 km. In the northern Rockall Trough Roberts et al. (1988) used ocean bottom seismometers and wide-angle seismic reflection measurements to model seismic velocities. They indicated that the crust under Rockall Bank was approximately 30 km thick and 20 km thick in the northern Rockall Trough. This agrees well with the estimated crustal thicknesses in Fig. (3.6) where the maximum thickness under Rockall Bank is 30 km and thicknesses in the North Rockall Trough are approximately 18 km.

3.3.4.4 Change of Sea Level to its Position at the Time of the Reconstruction

If a column is below sea level and covered by seawater, then a change in sea level is taken into account by changing the height of the column (H_1). If the top of a column was initially above sea level and the change of sea level does not submerge it, the height of the column is not affected. A sea level curve averaged for 1 m.y. intervals relative to present eustatic sea level is one of the parameters input to the model (Fig. 3.2). The age scale of the Haq et al. (1987) eustatic curve was adjusted to conform to the Berggren et al. (1985) timescale that was used to assign ages to sediments compiled for paleobathymetric reconstructions. The eustatic curve was then averaged along 1 m.y. time intervals. Hay et al. (1989) suggested that the Haq et al. (1987) sea level curve is too high in the Paleogene. The problem of overestimation of the magnitude of sea level changes has been recognized by Haq (1989), who suggested that it may be the result of failing to take isostatic effects into account. Accordingly, I reduced the amplitude of the Haq et al. (1987) sea level curve by a factor of 1/2 (after Hay et al., 1989) to approximate a more realistic estimate of the relative sea level in the past.

3.3.4.5 Bringing the Area into Isostatic Equilibrium

The last step to complete the backstripping process and reconstruct the paleobathymetry of a single column is to balance the column isostatically assuming Airy-type equilibrium. After removing the younger sediment and decompacting what remained, a new total sediment thickness (T_S) and sediment density (ρ_S) were calculated for the column. An age-dependant mantle density (ρ_M) was calculated from modelling the thermal subsidence. The thickness and density of the crust (T_C and ρ_C) are assumed to remain constant. The present thickness of the crust has been calculated from the observed sediment thickness and elevation of its surface. The total mass of the column (M) is also a constant value (3.1218 x 10^7 kg) and the height of the column (H_I) has been adjusted to account for relative sea level change. An isostatically-balanced elevation is now calculated from Eqns. (3.11) and (3.12). The unknown parameters are T_W and T_M. We can solve Eqns. (3.11) and (3.12) for T_W and the result of the calculation will tell us if the column was above or below sea level after isostatic balance and what the reconstructed water depth or elevation was.

$$T_W = [M - \rho_M (H_I - T_C - T_S) - T_C\rho_C - T_S\rho_S] / (\rho_W - \rho_M) \qquad (3.15)$$

The technique for backstripping developed here is based on the assumption that the thermal history of a region is better known than the paleobathymetric history. The thermal history is derived using Eqns. (3.4) and (3.5) from Parsons and Sclater (1977) solved in conjunction with Eqns. (3.11) and (3.12) to calculate the age-dependant mantle density. The fundamental equations for backstripping (Eqns. 3.11 and 3.12) are robust and can be solved to calculate mantle density, crustal thickness or elevation. The model could also be used to calculate the thermal history under the assumption that paleobathymetry is known. This would be useful for predicting past heat flow based on paleobathymetry.

3.4 A Test of Sensitivity of the Paleobathymetric Reconstruction Model (BalPal) to Variations in the Thermal Age of the Lithosphere

Thermal subsidence curves (Fig. 3.5) predict the most rapid subsidence of oceanic lithosphere during the first 50 m.y. after its formation at a mid-ocean ridge. BalPal reconstructs paleobathymetry based on an input thermal history for each grid cell. In the simplest case thermal history is calculated from lithospheric age or the time of the last major

reheating event. The age of oceanic lithosphere formed since the end of the Paleocene can be calculated from seafloor magnetic lineations and plate tectonic modelling. The thermal age of thinned or reheated continental lithosphere along the passive margins in the NE Atlantic is more difficult to determine.

The first model uses an older thermal age for the lithosphere in the Rockall-Faeroe region, assuming that rifting or extension in the Rockall Trough, Faeroe-Shetland Channel and Hatton-Rockall Basin occurred during the Cretaceous (Hanisch, 1984). This is referred to as the "Cretaceous rifting" model and assumes that the thermal history of this area dates from the time when rifting occurred between Greenland-Rockall and Western Europe (Fig. 3.4). The youngest lithosphere is centered in the Rockall Trough, Faeroe-Shetland Channel and Hatton-Rockall Basin with the oldest or coolest lithosphere along the European shelf, Hatton Bank and from Rockall Bank to the Faeroe Islands (Fig. 3.4).

The second model assumes that the entire region was reheated during an episode of early Tertiary volcanism that lasted approximately 3 m.y. near the Paleocene-Eocene boundary (Eldholm, 1991). In the second model, referred to as the "Paleocene reheating" model, the thermal age of each grid cell in the Rockall-Faeroe region was set to 60 Ma. The Paleocene reheating model is preferred by several investigators because it takes into account the evidence for widespread volcanism and thermal rejuvenation during the Paleocene-Eocene continental breakup. At this time large quantities of lava were erupted along the conjugate margins of Greenland and Europe and in the Rockall-Faeroe region (White et al., 1987; Dickin, 1988; White, 1988).

Both models were backstripped as described previously using the Haq et al. (1987) eustatic curve with 1/2 of its original amplitude. The difference in reconstructed paleobathymetry is shown in Figs. 3.9 through 3.13. The model assuming Paleocene reheating of the lithosphere (Figs. 3.9A through 3.13A) shows significantly shallower bathymetry than the normal rifting model (Figs. 3.9B through 3.13B). It is apparent from the reconstructions (Figs. 3.9 through 3.13) that the reconstructions are highly sensitive to the thermal age of the lithosphere. All of the reconstructions are reasonable in terms of paleogeographic configuration. In the absence of other evidence it would be difficult to determine which of these reconstructions is more likely to be correct.

3.5 Paleobathymetric Reconstructions of the Northern North Atlantic and Southern GIN Sea

There are two sets of reconstructions of the northern North Atlantic and southern GIN Sea (Figs. 3.9A-3.13A and 3.9B-3.13B). The first set assuming the "normal" thermal history or "Cretaceous rifting" model, and the second set assuming the "Paleocene reheating" thermal history model. The reconstructions are shown on a gridded database corrected for seafloor-spreading. Paleolatitude (Table 3.2) was calculated relative to a North American reference frame using the apparent polar wander curve of Harrison and Lindh (1982). Both sets of reconstructions will be described starting from the present and going back to 50 Ma.

As was discussed in Chapter 2, the general bathymetric features of the region are seen in the 1 x 1° grid (Fig. 3.8) but features smaller than the resolution of the 1 x 1° grid (Fig. 3.7) are not resolved in Figure 3.8. The 1 x 1° resolution was chosen to conform to the density of seismic lines in this region, and, as outlined in Chapter 2, the stratigraphic data used in this study were compiled on the 1 x 1° grid.

At 1 x 1° grid resolution (Fig. 3.8) the depth of the Faeroe-Shetland Channel is about 500 m and the Faeroe Islands appear to be about 100 m below sea level. Rockall Bank is below sea level with a minimum depth of about 200 m. Hatton Bank is deeper with a depth less than 1000 m. Rockall and Hatton Banks are separated from Lousy Bank by shallow ridge to the north of Rockall Bank that is about 1200 m deep. The maximum depth of Rockall Trough is approximately 2800 m and the bathymetry drops off sharply south of Rockall Trough to depths greater than 4000 m. The South Iceland Basin is about 3000 m deep and the Iceland-Faeroe Ridge has a sill depth of 500 m. The shallow platform around Iceland is delineated by the 250 m bathymetric contour and is oriented along the axis of the Greenland-Scotland Ridge. Reykjanes Ridge presently has an average depth of about 1500 m. The Irminger Basin has approximately the same depth as the South Iceland Basin with an average depth of about 3000 m. There is a broad shelf along East Greenland and bathymetric contours drop off sharply into the Irminger Basin. The shelf break along East Greenland is deep and lies more than 500 m below sea level. On the 1 x 1° average bathymetric map (Fig. 3.8) the Denmark Strait also has a sill depth of approximately 500 m. The Iceland Plateau is generally shallow with an average depth of about 1200 m. The southwest-northeast trending Kolbeinsey Ridge separates the Iceland Plateau into two basins to the west and east of it. The basin

between Greenland and Kolbeinsey Ridge is about 1500 m deep and the basin between Kolbeinsey and Jan Mayen Ridge is close to 2000 m deep. The Jan Mayen Ridge is apparent in Figure 3.8 as a north-south linear feature separating the Iceland Plateau from the Norway Basin. The Norway Basin including the extinct Aegir Ridge is the deepest basin in the study region with an average depth of about 3200 m.

The general morphology of the region in the early Late Miocene assuming the Cretaceous rifting model (10 Ma; Fig. 3.9A) was similar to present. The Faeroe-Shetland Channel was slightly shallower than at Present with an average depth less than 500 m. The Faeroe Islands appear to be about 100 m below sea level. The depth of Rockall and Hatton Banks was approximately the same as at Present but the connection between Rockall and Lousy Bank was shallower with a depth of about 900 m. The bathymetry in Rockall Trough was symmetrical and slightly shallower than at present, with a maximum depth of about 2600 m. The abyssal plain to the south of Rockall Trough was still relatively deep reaching about 4000 m. The South Iceland Basin was slightly shallower that at present and was 2700 m deep. The Iceland-Faeroe Ridge was also shallower with a sill depth less than 500 m. The shallow platform around Iceland was oriented more along the axis of Reykjanes Ridge. Reykjanes Ridge was deeper than at present with an average depth of about 1700 m. The Irminger Basin and South Iceland Basin were still approximately the same depth (2700 m). There was still a broad shelf along East Greenland but the shelf break appeared slightly shallower at 500 m below sea level. In the 10 Ma reconstruction (Fig. 3.9A), the Denmark Strait was approximately as deep as it is at Present and was thus the deepest connection between the eastern North Atlantic and the GIN Sea at that time. The Iceland Plateau was much reduced in area due to rapid seafloor-spreading the interval from 10 Ma to Present. The shallow basin seen in Fig. 3.8 north of Scoresby Sund between Greenland and Kolbeinsey Ridge at Present had not yet been formed in the 10 Ma reconstruction (Fig. 3.9A). At 10 Ma a basin south of Scoresby Sund between Greenland and the Kolbeinsey Ridge that is not well defined in present bathymetric maps is seen in Fig. 3.9A. Thus Iceland Plateau appears to have two different basins between Greenland and Kolbeinsey Ridge, the younger basin to the north and the older basin to the south of Scoresby Sund. The Kolbeinsey Ridge is visible in the 10 Ma reconstruction (Fig 3.9A) as a bathymetric high at approximately 20° W longitude. The linear trend of Jan Mayen Ridge was more pronounced at 10 Ma as it formed a boundary between

the Iceland Plateau and Norway Basin. The Norway Basin was still the deepest basin in the study region with an average depth of about 3000 m.

Differences between the Cretaceous rifting model (Fig. 3.9A) and Paleocene reheating model (3.9B) for paleobathymetry in the early Late Miocene (10 Ma) occur only in the Rockall-Faeroe region. The general morphology is similar to the Cretaceous rifting model (Fig. 3.9A) with the following exceptions: The Faeroe-Shetland Channel is slightly shallower and narrower with the northwest Scottish coastline further seaward. The Faeroe Islands still appear to be about 100 m below sea level. Rockall Bank is shallower and Hatton Bank is less well defined bathymetrically. Rockall, Hatton and Lousy Banks now appear to form a single platform with a depth of about 900 m. Rockall Trough is also shallower with a maximum depth of about 2500 m.

The paleobathymetry reconstructed with the Cretaceous rifting model in the Early Miocene (20 Ma; Fig. 3.10A) is similar to the early Late Miocene reconstruction (10 Ma). The Faeroe-Shetland Channel was shallower than at 10 Ma with an average depth of approximately 350 m. The Faeroe Islands were apparently below sea level. The depth of Rockall and Hatton Banks was approximately the same as at 10 Ma and the Hatton-Rockall Basin was shallower. The shape of Rockall Trough was approximately the same as at 10 Ma and the maximum depth was the same (2600 m). The abyssal plain to the south of Rockall Trough was as deep as it was 10 Ma (Fig. 3.9A). The South Iceland Basin was shallower 20 Ma (2500 m) than at 10 Ma. The Iceland-Faeroe Ridge was shallower with a sill depth of 250 m. The subareal platform around Iceland was narrower and still oriented southwest-northeast along the axis of Reykjanes Ridge. Reykjanes Ridge was deeper than at 10 Ma with an average depth of about 2000 m. The vertical relief between Reykjanes Ridge and the Irminger and South Iceland Basins to it's northwest and southeast respectively was steadily decreasing from Present to 20 Ma. The Irminger and South Iceland Basins were both shallower with approximately the same depth (2600 m). The shelf break off East Greenland was much shallower in the 20 Ma reconstruction (Fig. 3.10A) at approximately 300 m water depth. When the Irminger Basin was younger (20 Ma), the Denmark Strait was narrower but may actually have been deeper 20 Ma than it was 10 Ma where the sill depth has increased from 500 to approximately 600 m. The basin south of Scoresby Sund and west of Kolbeinsey Ridge is depicted as two smaller basins in the 20 Ma reconstruction (Fig. 3.10A). Kolbeinsey Ridge extended to the northwest from Iceland 20 Ma and may have been stationary adjacent

to the continental margin of East Greenland as Jan Mayen Ridge was separating from Greenland. Sediment input from Greenland to the basin between Kolbeinsey Ridge and Jan Mayen Ridge may have spilled over into the much deeper Norway Basin. It was still the deepest basin in the study region with an average depth of about 3000 m.

Paleobathymetric features of the Paleocene reheating model (Fig. 3.10B) that are different from the Cretaceous rifting model (Fig. 3.10A) for the Early Miocene (20 Ma) are as follows: The Faeroe-Shetland Channel was significantly narrower and shallower with a sill depth of about 250 m. The region around the Faeroe Islands was above sea level (Fig. 3.10B). Rockall Bank was also subaerially exposed and Hatton Bank was about 700 m below sea level. Rockall Trough was shallower in the Paleocene reheating model with a maximum depth of less than 2500 m.

Paleobathymetry reconstructed with the Cretaceous rifting model for the middle Oligocene (30 Ma; Fig. 3.11A) looks very different from younger reconstructions. The Faeroe-Shetland Channel was almost non-existent and appeared as a shallow bank with an average depth less than 250 m. The Faeroe Islands were above sea level on the eastern end of a subaerial ridge extending over the central portion of the Greenland-Scotland Ridge. Rockall and Hatton Banks were both shallower with an average depth of about 500 m. The shape of Rockall Trough was similar to younger reconstructions, but it was slightly shallower (2500 m). The abyssal plain to the south of Rockall Trough remained deep at about 4000 m below sea level. The South Iceland Basin was shallower than at 20 Ma and was about 2200 m deep. Iceland was an indistinct feature because it was part of the subaerial ridge extending along the Greenland-Scotland Ridge from the eastern margin of the Denmark Strait to the Faeroe Islands. Reykjanes Ridge was approximately as deep as in the 20 Ma reconstruction (Fig 3.10A) with an average depth of about 2000 m. The vertical relief between Reykjanes Ridge and the Irminger and South Iceland Basins was only about 500 m. The Irminger Basin was shallower with a depth of approximately 2200 m. The shelf break along the East Greenland margin was very shallow in the 30 Ma reconstruction (Fig. 3.11A) and was coincident with the eastern Greenland paleoshoreline. The Denmark Strait was more constricted than in younger reconstructions and as shallow as the Faeroe-Shetland Channel (200 m). Kolbeinsey Ridge was oriented approximately north-south at 24° W longitude. There was subaerial seafloor spreading along most of the Kolbeinsey Ridge 30 Ma and two distinct basins to the west and east of it. Jan Mayen Ridge was also a north-south bathymetric rise

located at 20° W (Fig. 3.11A). The Norway Basin was shallower in the middle Oligocene with a depth of approximately 2700 m.

In the middle Oligocene (30 Ma; Fig. 3.11B) the thermal model based on Paleocene reheating has started to have a large impact on paleobathymetric reconstructions. Features observed on the paleobathymetric reconstruction assuming the Paleocene reheating model (Fig. 3.11B) that are not seen on paleobathymetry assuming the Cretaceous rifting model (Fig. 3.11A) are as follows: The Faeroe-Shetland Channel did not exist 30 Ma, but was part of a subaerial ridge extending from the eastern margin of the Denmark Strait to Scotland. Rockall Bank had significant subaerial exposure in the middle Oligocene (Fig. 3.11B) and could have been a local source of detrital sediment deposited in Rockall Trough. Hatton Bank was shallower (Fig. 3.11B) and was about 500 m below sea level. Rockall Trough was shallower in the Paleocene reheating model (Fig. 3.11B) with a maximum depth of approximately 2200 m.

The Faeroe-Shetland Channel was at or above sea level on the eastern end of the subaerial Greenland-Scotland Ridge in the Late Eocene (40 Ma; Fig. 3.12A) based on paleobathymetry reconstructed with the Cretaceous rifting model. The narrow width of the ridge across the site of the future Faeroe-Shetland Channel does not rule out the possibility of a shallow surface water connection in the Late Eocene. Rockall Bank was shallower with a depth less than 250 m below sea level. Hatton Bank was about 500 m below sea level. Rockall Trough was also slightly shallower with a depth of about 2200 m. The abyssal plain to the south of Rockall Trough was slightly shallower with a depth of approximately 3700 m. The South Iceland and Irminger Basins and Reykjanes Ridge were almost indistinguishable from one another as bathymetric features in the Late Eocene. The ocean basin between Rockall Plateau and Greenland was approximately 1800 m deep with only about 250 m difference in elevation between the central spreading center and adjacent ocean basins. The shelf break along the East Greenland margin was probably coincident with the paleoshoreline along eastern Greenland. The Denmark Strait did not exist in the Late Eocene (Fig. 3.12A) and was almost certainly above sea level. The proto-Kolbeinsey Ridge was a slight bulge on the northern margin of the Greenland-Scotland Ridge at 23° W longitude. The basin to the west of Kolbeinsey Ridge was a shallow platform in the Late Eocene that would have allowed fine-grained sediment to be transported across this basin and into the Norway Basin. In the

Late Eocene Jan Mayen Ridge was rifting from Greenland. The Norway Basin was slightly shallower in the Late Eocene with a depth of approximately 2400 m.

Paleobathymetry reconstructed for the Late Eocene (40 Ma; Fig. 3.12B) using the Paleocene reheating model indicates that the Greenland-Scotland Ridge was more than 200 km wide along its entire length and was above sea level along its entire length. Rockall Bank was well above sea level and must have supplied more sediment into the Rockall Trough and the South Iceland Basin than in younger times. Hatton Bank was shallower in the Late Eocene with a water depth of about 250 m and Rockall Trough was also shallower with a maximum depth of approximately 2000 m.

The site of the future Faeroe-Shetland Channel was probably above sea level on the eastern end of the Greenland-Scotland Ridge in the early Middle Eocene (50 Ma; Fig. 3.13A) assuming the validity of the Cretaceous rifting model for reconstructed paleobathymetry. Surface water connections between the Norwegian Sea and North Atlantic across this ridge were unlikely in the early Middle Eocene. Rockall, Hatton and Lousy Banks were at or slightly above sea level in the early Middle Eocene (Fig. 3.13A). Rockall Trough was also shallower with a depth of about 2100 m. The abyssal plain to the south of Rockall Trough was slightly shallower with a depth of approximately 3500 m. The Reykjanes Ridge was not a distinct bathymetric feature at the 1 x 1° resolution of the early Middle Eocene reconstruction (Fig. 3.13A). The young ocean basin that existed between the Rockall Plateau and Greenland was only about 1600 m deep in the early Middle Eocene. Rifting between Jan Mayen Ridge and Greenland had not yet started in the early Middle Eocene and the Kolbeinsey Ridge did not yet exist. The Norway Basin appears in the reconstruction to have been isolated and relatively shallow in the early Middle Eocene with a depth of approximately 2000 m.

The Greenland-Scotland Ridge was a broad topographic feature in the early Middle Eocene (50 Ma; Fig. 3.13B) that may have had elevations of more than 1000 m assuming that the Paleocene reheating model for reconstructed paleobathymetry is correct. The Paleocene reheating model also indicates that Rockall Bank was a significant topographic feature connected to the Greenland-Scotland Ridge by a land bridge. Hatton Bank may have been above sea level and separated from Rockall Bank by a shallow basin. Rockall Trough was also shallower with a maximum depth of approximately 1700 m. If the Paleocene reheating model is correct then Rockall Trough and the South Iceland Basin would have received more

sediment from erosion of the surrounding land areas than at any time since the early Middle Eocene.

3.6 Paleobathymetry of the Greenland-Scotland Ridge

Reconstructed profiles along the length of Greenland-Scotland Ridge for the Cretaceous rifting and Paleocene reheating models are based on data compiled on the 1 x 1° grid (Figs. 3.14A-3.19A and 3.14B-3.19B). For the Present, the sill depths through the Denmark Strait and over the Iceland-Faeroes segment of the ridge are correctly shown. However, because it is so narrow, the Faeroe-Shetland Channel is shown as 100 meters shallower than it actually is. The reconstructed profiles are plotted against the time-varying sea level (1/2 of Haq et al., 1987) used for the maps.

At present the significant overflows occur only where the passages are 400 m deep or more. Because overflow water forms in the Norwegian Sea above the pycnocline with an average depth between 300 and 350 m (Dietrich, 1969; Johannessen, 1986) we can assume that a dense deep water flow from the GIN Sea would require a sill depth of at least 300 meters. Based on this assumption we can establish the times when the models predict deep water might flow from the GIN Sea into the North Atlantic. It must be recalled that because the Faeroe Bank Channel and Wyville-Thompson Ridge are so narrow, they are not resolved at the 1 x 1° resolution of the grid. Nevertheless, as discussed in Chapter 2, we know that Faeroe Bank Channel is at least 350 m deeper than its grid cell appears to be, and the Wyville-Thompson Ridge is at least 150 m deeper than its grid cell appears to be.

Both models show that the Denmark Strait, presently about 500 m deep, has been shallowing since 15 Ma when it was almost 1000 m deep. As it is traced back in time it shallows, reaching the 300 m threshold about 28 Ma. At 35 Ma it was very narrow and had a depth of less than 100 m. In the Cretaceous rifting model the Iceland-Faeroe segment is shown with sill depth of 500 m at present. Traced back, it reached its greatest depth in the Late Pliocene, about 3 Ma. Traced further back, it progressively shallows, crossing the 300 m threshold at about 21 Ma. It becomes very narrow and shallow at 30 Ma and remains in that state to 35 Ma. The Faeroe-Shetland Channel appears to be 600 m deep at present on the profile, due to the inability of the coarse data base to adequately resolve this narrow feature. It becomes shallower back through the Cenozoic, reaching the 300 m threshold at 24 Ma.

Adding 350 m to approximate the real depth of the Faeroe Bank Channel and 150 m to approximate the real depth of the Wyville-Thompson Ridge, they would have been 650 m and 450 m deep respectively. They continue to become shallower in the Early Oligocene, but at 35 Ma the grid cells still have a depth of about 200 m, suggesting that Faeroe Bank Channel might have been 550 and the Wyville-Thompson Ridge 350 m deep.

The Paleocene reheating model presents a different picture for the area that underwent reheating, the Iceland-Faeroe segment and the Faeroe-Shetland Channel. Again, the Iceland-Faeroe Ridge is shown as having its maximum depth during the Late Pliocene, at 3 Ma. Then it progressively shallows, reaching 300 m at 19 Ma and rising above sea level at 30 Ma. The grid cells including the Faeroe Bank Channel and Wyville-Thompson Ridge reach 300 m at 22 Ma, and are barely awash from 30 to 35 Ma. This implies that the Faeroe Bank Channel might have been 350 m deep and the Wyville-Thompson Ridge 150 m deep, both probably too shallow to allow appreciable deep water from the Norwegian Basin.

The stratigraphic resolution that can be obtained from DSDP and ODP Sites in this region is probably not adequate to resolve the 2 million year differences in subsidence of the Faeroe-Shetland and Iceland-Faeroe region.

It is important to note that both models suggest that the Denmark Strait has always been the major connection between the North Atlantic and GIN Sea.

3.7 Discussion

The two sets of maps show very different paleogeographies but there are no direct geologic data that can be used to verify one or the other of the models. The reconstructions are not intended to model paleogeography for any time prior to the early Middle Eocene (50 Ma). Paleobathymetric reconstructions of the Paleocene and older times will require additional modelling techniques not discussed here. The reconstructed bathymetry is dependant primarily on the initial boundary conditions of the model: present elevation, present sediment thickness and the assumed thermal age of the lithosphere. The most important factor for modelling the pre-Eocene paleogeography of the region is the effect of reheating and crustal intrusion and underplating that resulted from the late Paleocene-early Eocene volcanism centered around the Iceland Hotspot.

The Paleocene reheating model conforms to the most generally accepted view of the thermal evolution of the area. The assumption of a thermal reheating event, where the thermal age of the lithosphere was essentially reset to zero 60 Ma, is not unreasonable considering that a region almost 3000 km in diameter was heated by the mantle plume forming the Iceland Hotspot in the early Tertiary (White et al., 1987; White, 1988; Parson et al., 1988; White, 1989; Eldholm, 1991; White, 1992) that was centered only hundreds of kilometers to the west of the Faeroe-Shetland Channel at that time. According to this model, the Faeroe-Shetland Channel was rifted in the Cretaceous (Hanisch, 1984) and uplifted by reheating in the Late Paleocene. The Paleocene was also the time of emplacement of seamounts in Rockall Trough (eg. Anton Dohrn) and around Rockall Bank.

The paleobathymetric reconstructions (Figs. 3.9B through 3.13B) and reconstructed profiles along the Greenland-Scotland Ridge (Figs. 3.14B through 3.19B) based on the Paleocene reheating model indicate that the Iceland-Scotland Ridge was at or above sea level until between 30 and 25 Ma. If one were to assume that there was no reheating event approximately 60 Ma, then the Faeroe-Shetland Channel would have begun to subside below sea level prior to the Denmark Strait approximately 35 Ma.

The paleobathymetric reconstruction based on the Paleocene reheating model for the Early Oligocene (Fig. 3.11B) indicates subareal to shallow water conditions along the entire Iceland-Scotland Ridge. It would then be unlikely that the Norwegian Sea could have been a source of bottom water in the northern North Atlantic prior to the Early Oligocene. However the Cretaceous rifting model reconstruction (Fig. 3.11A), indicates that it would have been possible for overflow from the Norwegian Sea to pass through the Faeroe-Shetland Channel. Sill depths along the Iceland-Scotland Ridge were too shallow until late Oligocene-early Miocene time (Figs. 3.11, 3.12 and 3.18) to allow overflow of Norwegian Sea Overflow Water (NSOW). DSDP Sites 352 and 336 (Talwani, Udintsev et al., 1976) on the southwest and northeast sides of the Iceland-Faeroe Ridge respectively, indicate that erosive bottom currents could not have flowed over the Iceland-Faeroe Ridge prior to the Late Oligocene (Shor and Poore, 1979). This agrees with both reconstruction models (Figs. 3.17A and 3.17B) where the sill depth along the Iceland-Faeroe Ridge increased in the Early Miocene. Information from DSDP sites drilled during Leg 48 (Montadert, Roberts et al., 1979) on Hatton Drift indicate initiation of significant bottom-water activity along the eastern margin of the South Iceland Basin during the Early to Middle Miocene when Hatton Drift began to

accumulate (Shor and Poore, 1979; Stow and Holbrook, 1984). Based on results from Sites 336 and 352, Shor and Poore (1979) concluded that NSOW did not enter the eastern North Atlantic until after the mid-Oligocene. Further they suggested that the Iceland-Faeroe Ridge was emergent 30 Ma and that bottom water could not have flowed over the Iceland-Faeroe Ridge earlier than the Late Oligocene (25 Ma).

If present deep-water circulation patterns (Worthington, 1976; Warren, 1981) in the northern North Atlantic can be extrapolated to the past, then the reconstruction of the Greenland-Scotland Ridge paleobathymetry is a key factor for understanding the timing of deep-water flow from the Norwegian Sea into the northern North Atlantic. Sediment drifts are the primary source of information available concerning pre-Pleistocene overflow of the Greenland-Scotland Ridge (Shor and Poore, 1979) and bottom water circulation patterns in the North Atlantic.

The formation of sediment drifts requires a sediment source and a strong bottom current. The sediment supply could be from either erosion on land or in shallow water areas, or from erosion by bottom currents in the deep sea. The bottom currents require a source of dense water. To form a bottom current, the dense water must form in volumes large enough and be dense enough to reach the deep sea floor after dilution by entrainment of less dense waters at mid-depths (Peterson, 1979). Water can become unusually dense by being cooled, by becoming more saline due ice building or increased evaporation or by having a high load of suspended particles.

Today, the dense water overflowing the Greenland-Scotland Ridge towards the south is both cold and saline. It owes its origin to the high salinity of North Atlantic waters flowing into the Norwegian Sea across the Iceland-Scotland segment of the Greenland-Scotland Ridge, and to the cold climate of the GIN Sea. There the water can be chilled and can form sea ice, further increasing its salinity. These conditions have not existed throughout the history of the GIN Sea, but are a result of the increase in the Earth's meridional temperature gradient during the later Cenozoic (Barron, 1985).

Ridd (1983) presented information from a commercial well on the eastern side of the Faeroe-Shetland Channel containing gray shales with Late Cretaceous dolomitic limestone beds and foraminifera. He concluded that the Faeroe-Shetland Channel was a deep-water marine environment in the Late Cretaceous. Based on the assumption that the Rockall Trough and Faeroe-Shetland Channel formed a continuous seaway from the mid-Cretaceous through

Paleocene, Roberts et al. (1983) concluded from dredging of Maastrichtian foraminifera at the Anton Dohrn Seamount (Fig. 2.1) that the Rockall Trough and Faeroe-Shetland Channel were approximately 1000 m deep in the Cretaceous. However, neither Ridd (1983) or Roberts et al. (1983) stated whether the foraminifera were planktic or benthic, thus making their interpretation of a deep seaway more ambiguous. This continuous seaway was divided when the volcanic Wyville-Thompson Ridge was emplaced in the Late Paleocene (Roberts et al., 1983) as part of the late Paleocene-early Eocene volcanic event. As indicated in the reconstructions presented here, the Wyville-Thompson Ridge probably formed a land bridge between the Faeroes and the emergent Scotland shelf (Roberts et al., 1983) before subsiding below sea level in the early Oligocene. Nilsen (1978; 1983) has noted the presence of early Tertiary lateritic soils on the Iceland-Faeroe Ridge and on the Faeroe Islands, in Scotland and Northern Ireland where bauxites also occur. These suggest warm, seasonally humid conditions promoting deep weathering. Schweitzer (1980) suggested from land floras on Spitsbergen that the mean annual temperatures there were 15 to 18° C during the Paleocene and Eocene. Berggren and Schnitker (1983) cite a variety of evidence suggesting that the land and shallow seas of Europe were very warm, with near-shore water temperatures up to 27° C. Arid conditions were characteristic of the Paris Basin in the Late Eocene, leading to the deposition of anhydrite and gypsum of the Ludian (Cavelier et al., 1980).

The GIN Sea was relatively warm during the Eocene (Müller, 1976; Schrader et al., 1976; Berggren and Schnitker, 1983; Henrich et al., 1989; Goll, 1989; Thiede et al., 1989). During this time the regional temperatures, the expected excess of precipitation over evaporation at its paleolatitude (60-65° N), and the fresh water input from the surrounding land areas would have precluded the GIN Sea from having become a deep water source. It must have been a positive fresh-water balance sea with inflow at depths and outflow at the surface.

Although the data are generally of a poor quality and the faunas are often endemic, there is evidence from sediments and plankton faunas and floras that the Norwegian Sea was indirectly connected to the North Atlantic in the Eocene (Schrader et al, 1976). The paleobathymetric reconstructions shown here (Figs. 3.12A, 3.12B, 3.13A, 3.13B) depict it as isolated from the North Atlantic by an emergent Greenland-Scotland Ridge. Ziegler (1982) indicated that during the early Cenozoic the connection from the Atlantic to the North Sea and thence to the Norwegian Sea was via shallow seas across western Europe. Ziegler (1982)

believed that the Greenland-Scotland Ridge was emergent in the Paleocene-Eocene but did not publish any evidence to support this hypothesis. Ziegler (1988) showed the Greenland-Scotland Ridge as "plateau basalts" on his Paleocene paleogeographic-paleotectonic map, but offered no indication whether they were deposited above or below sea level. In the text he stated that during the mid-Paleocene sea level lowstand deltaic systems prograded over the flanks of the Faeroe-Shetland Trough and widespread clastic deep-water fans accumulated in its axis. It is not clear from the discussion whether he believed there was a marine connection from Rockall Trough into the Norway Basin during the Paleocene and Eocene. The Wyville-Thompson Ridge was interpreted to be emergent in the Late Paleocene paleogeographic map of Murray (1992). However, he also drew a marine connection from the South Iceland Basin across the emergent Iceland-Faeroe Ridge into the Norway Basin in the Late Paleocene. His Eocene maps did not depict the Greenland-Scotland Ridge area. The Oligocene history of the study area is not much better known than that of the Paleocene and Eocene (Müller, 1976; Schrader et al., 1976; Berggren and Schnitker, 1983; Henrich et al., 1989; Thiede et al, 1989). Ziegler (1982) showed the Wyville-Thompson Ridge emergent on his Oligocene paleogeographic map. Ziegler (1988) displayed the Wyville Thompson Ridge and Denmark Strait emergent and the Iceland-Faeroe shelf submerged on his Late Oligocene paleogeographic-paleotectonic map. He also showed a "deltaic-shallow marine" connection from the English Channel through Germany into the North Sea. Murray (1992) showed a narrow submerged connection between Rockall Trough and the Norway Basin across Wyville-Thompson Ridge. Müller (1976) suggested that the occurrence of abundant calcareous nannoplankton in Oligocene GIN Sea sediments suggested that there was a surface inflow from the North Atlantic. This implies a reversal of the deep circulation from estuarine in the Eocene to lagoonal in the Oligocene, and is consistent with the idea of a northern deep or intermediate water source.

Feni Drift had its origin at the end of the Eocene (Masson and Kidd, 1987). There would have been adequate sediment sources on the surrounding shelves, but what could the dense water source for the bottom current have been? Miller and Tucholke (1983) suggested that there was a deep water source in the Arctic that fed cold, dense water into the GIN Sea. Their model would suggest that Arctic water overflowed the Greenland-Scotland Ridge to initiate the formation of Feni Drift. However, the plate tectonic reconstructions of Lawver et al. (1990) indicate that there was no deep water connection between the Arctic Ocean and the

GIN Sea until 5 Ma. A connection of intermediate depth and sufficient width would be required to allow enough Arctic Basin deep water to flow into the GIN Sea basins. A second problem in attributing the early development of Feni Drift to waters overflowing the Faeroes-Shetland segment of the Greenland-Scotland Ridge is the configuration of the passages. At present the Faeroe-Shetland Channel leading from the Norway Basin merges with the Faeroe Bank Channel leading to the South Iceland Basin (Fig. 4.10). The sill depth along this route is 850 m. The direct passage into Rockall Trough is blocked by the Wyville-Thompson Ridge (Fig. 4.10); its lowest crestal elevations are about 650 m. To accept the overflow hypothesis we must assume that Faeroe Bank Channel is a younger feature and did not exist or at least was shallower than Wyville-Thompson Ridge in the Oligocene. Faeroe Bank Channel is subparallel to fracture zones to the north and south, and may perhaps have been formed by tension as sea-floor spreading continued during the Cenozoic. Alternatively, it is possible that Feni Drift reflects early production of Antarctic Bottom Water coincident with the sudden cooling at the Eocene-Oligocene boundary recorded by oxygen isotopes across the Eocene-Oligocene boundary (Kennett and Shackleton, 1976; Keigwin, 1980; Matthews and Poore, 1980; Corliss and Keigwin, 1986). However, it is difficult to imagine that bottom water production at a site so far away should have had such a specific effect as to initiate formation of a single sediment drift at the other end of the Atlantic. Another possibility is that there could have been an Oligocene dense water source in the last remnant of the Tethys as there was in the Early and Middle Miocene (Woodruff and Savin, 1989), but again this is far from the site of Feni Drift.

A final possibility is that there was a local dense water source. A local source could not have been cold, but it could have been saline if enough of Rockall Plateau had been shallow. A shallow Rockall Plateau could be the source of dense water formed through increase of salinity from high rates of evaporation at the sea surface. The paleobathymetric reconstructions for middle Oligocene, 30 Ma (Figs. 3.11A and 3.11B) can shed some light on these alternatives. The Cretaceous rifting model shows shallow passages across the Wyville-Thompson Ridge and Denmark Strait. The Paleocene reheating model shows only a shallow connection through the Denmark Strait. It must be recalled that the Faeroe-Shetland Channel is too narrow to be resolved by the model and is presently about 300 m deeper than the average elevation of the 1 x 1° grid cell in which it lies. The sections along the Greenland-Scotland Ridge for the Early Oligocene, 35 Ma (Figs. 3.19A, 3.19B), are also

informative. For the Cretaceous rifting model, the Faeroe-Shetland Channel is shown as significantly deeper than the Denmark Strait. For the Paleocene reheating model, the Faeroe-Shetland Channel was emergent or shallow. If we assume that a deep or intermediate water passage between the Arctic Basin and the GIN Sea basins existed during the Oligocene, and that Arctic Deep Water flowed south, then the Cretaceous rifting model predicts that it would overflow the Greenland-Scotland Ridge through the Faeroe-Shetland Channel. If it were able to cross Wyville-Thompson Ridge, it could then flow down into Rockall Trough to form Feni Drift. The alternative, that Feni Drift was initiated by warm saline dense waters flowing off Rockall Plateau is supported by the Paleocene reheating model, which shows Rockall Plateau as having large shallow areas, but seems less likely to be correct. Climatologically, it is known that extreme aridity occurred in the Rhine Graben in the Oligocene but this could have been a local effect due to the continental rift environment, culminating in the deposition of potassium salts (Pflug, 1982), but it is believed that a general cooling took place in mid and high latitudes (Berggren and Schnitker, 1983).

During the Early Miocene and Middle Miocene (21.7 - 13.4 Ma) biogenic silica was deposited in the Norwegian Sea. Henrich et al. (1989) suggest that this was the result of nutrient and silica input from weathering of the adjacent land areas under a warm climate.

Hatton, Gardar, Bjorn and Snorri Drifts are all thought to have had their origin in the early Middle Miocene, about 15-18 Ma, but timing cannot be determined exactly because of the inadequacy of the stratigraphic records. Nevertheless, these suggested times of origin are close to the time cited by Henrich et al. (1989) as the time when the transition from a warm to cool regime occurred in the Norwegian Sea. The transition is recognized as one from biogenic silica deposition to carbonate deposition. Spiegler and Jansen (1989) noted that this is the time when planktonic foraminifera become abundant. Locker and Martini (1989) described this as a time when silicoflagellate assemblages changed from "warm" to "cool". Henrich et al. (1989) also regarded this interval as the time when a major reorganization of the circulation in the Norwegian Sea took place, tracing the origin of the Norwegian Current to this time interval. Hatton (and Feni) Drifts would respond to dense water flow from the Faeroe-Shetland Channel across Wyville-Thompson Ridge. Gardar, Bjorn, and Snorri Drifts would form in response to dense water flow from Iceland-Faeroe Ridge. The coincidence suggests that the flows occurred over both of these eastern segments of the Greenland-Scotland Ridge, but drifts apparently did not form along the margin of the Irminger Basin

downstream of the Denmark Strait. The bottom currents flowing through the Denmark Strait must have had a higher velocity than those that flowed south from the Iceland-Faeroe Ridge, thus resulting in erosion along the eastern Greenland margin and transporting sediment to south of the Charlie Gibbs Fracture Zone.

The change from siliceous to carbonate pelagic sedimentation on Vøring Plateau at 13.4 Ma probably marks the time where several events conspired to make it possible for the GIN Sea to change from a positive fresh-water balance sea to a negative fresh-water balance sea with inflow at the surface and outflow at depth. The oxygen isotope record does not show a major change at this time, so that it is unlikely that the switch from estuarine to lagoonal circulation in the GIN Sea was the result of a sudden global cooling that increased the meridional temperature gradient. It is more likely that the shift from one regime to the other occurred in response to changes in the fresh-water balance of the GIN Sea. The width and depth of the passages over the Iceland-Shetland segment of the Greenland-Scotland Ridge are critical to allowing entry of enough saline water to balance the large fresh-water balance from precipitation and river influx. The paleobathymetric models both suggest that these passages were open by 20 Ma. In examining the profiles along the length of the Greenland-Scotland Ridge (Figs. 3.14-3.19) it is evident that the passages change their shape only gradually from 22 Ma to Present. However, the Paleocene reheating model suggests that these passages underwent a rapid increase in cross-sectional area between 20 and 12 Ma. This may mean that the volumes of saline water entering the Norwegian Sea increased rapidly at that time.

Most investigators (Jones et al, 1970; Schrader et al., 1976; Miller and Tucholke, 1983; Henrich et al., 1989) have assumed that the sediment drifts of the northern North Atlantic formed in response to waters overflowing the Greenland-Scotland Ridge. In the Middle and Late Miocene flows from the passages between Iceland and the Shetlands initiated and maintained sediment drift formation while there was no corresponding effect south of the Denmark Strait. Both reconstructions indicate that the Denmark Strait was the deepest and broadest passage during the Miocene and most of the Pliocene. On the southern margin of the Norway Basin, Miocene unconformities suggest that bottom currents transported sediment to the north, away from the Greenland-Scotland Ridge.

As an alternative to the overflow hypothesis, I suggest that the dense waters that flowed into Rockall Trough and the South Iceland Basin may have formed in the shallow waters of the Iceland-Faeroe Ridge segment. The Paleocene reheating model suggests that

during the Miocene large areas of this part of the Greenland-Scotland Ridge were shallow. As Killworth (1983) has discussed, ocean deep waters form in either marginal settings, such as shelf seas, or in cyclonic gyres in the open ocean. In high latitudes shelf seas provide sites where sea-ice formation can take place more readily than in the open ocean. It seems plausible that during the Middle and Late Miocene the extensive shallow shelves between Iceland and the Shetlands may have served as a site of dense water formation as the shelf northwest of Iceland does today. This would explain why drift formation started in the South Iceland Basin and on western Reykjanes Ridge but not on the western side of Irminger Basin in the Miocene. The water that flows through the bottom of the Denmark Strait today is thought to form in the shallow sea northwest of Iceland (Swift et al., 1980). The paleobathymetric reconstructions show that this feature is very young geologically. It must have formed about 5 Ma, strongly suggesting that its existence is linked to the origin of Eirik and Gloria Drifts.

The apparent constant sedimentation on Feni Drift is an unsolved problem. The most likely source for bottom water to form Feni Drift in the late Eocene-early Oligocene was water flowing through the Faeroe-Shetland Channel and across Wyville-Thompson Ridge down into Rockall Trough. The shift in the late Early Miocene to a more proximal bottom-water source from the shelf around Wyville-Thompson Ridge would have caused a change in the sedimentation regime, yet there is no stratigraphic record of it. However, the stratigraphy I used to compile the mass/age distribution for Feni Drift (Fig. 2.20) followed the interpretation of Masson and Kidd (1987). They had concluded that the upper Lower Miocene seismic reflector R2 (their green reflector) represented a conformable sequence recording an oceanographic event. Miller and Tucholke (1983) however have suggested that R2 represents an erosional unconformity. This would seem plausible if there was a switch from one bottom-water source to another in the Early Miocene.

3.8 Summary and Conclusions

The reconstructions presented here are the first that combine a backstripping model including decompaction of sediment with a gridded plate tectonic model. Paleobathymetry or elevation of a stratigraphic column is calculated based on the age of the lithosphere or last major reheating event. The fundamental equations for backstripping (Eqns. 3.11 and 3.12) are

robust and can be solved to calculate mantle density, crustal thickness or elevation. The model could also be used to determine the thermal history if the paleobathymetry were known. This would be useful for predicting past heat flow based on paleobathymetry.

The model for Paleocene reheating of the lithosphere indicates significantly shallower bathymetry than the Cretaceous rifting model. In the middle Oligocene (30 Ma) reconstructions based on the Paleocene reheating model the Greenland-Scotland Ridge is above sea level except through a shallow Denmark Strait. Rockall Bank is also shown above sea level. The Cretaceous rifting model however, indicates that these regions were approximately 200 m below sea level at that time. It is apparent from the reconstructions (Figs. 3.9 through 3.19) that the model is sensitive to the input thermal age of the lithosphere. This has important implications for the reconstruction of paleobathymetry and for the paleoceanography of the region.

Although many geologists accept the concept of extensive reheating of the Rockall-Faeroes region during the Paleocene, evidence from sediment drift formation favors the Cretaceous rifting model. The initiation of Feni Drift at the beginning of the Oligocene could have been in response to Arctic deep or intermediate waters flowing through Faeroe-Shetland Channel, across Wyville-Thompson Ridge, and into Rockall Trough. However, as discussed above, a deep marine connection between the GIN and Arctic Seas did not exist until 5 Ma. It may be that the dense water formed on shallow shelves north of Rockall Trough in the region around the Faeroe-Shetland Channel and did not originate in the Arctic Ocean. A less likely possibility is that Feni Drift was initiated by dense warm saline flow off Rockall Plateau. Extensive shallow areas on Rockall Plateau shown in the Paleocene reheating model would make this area a possible dense water source if the climate were sufficiently arid. At present the Faeroe Bank Channel diverts approximately 80 percent of water flowing through the Faeroe-Shetland Channel into the South Iceland Basin. Because Feni Drift has not been accumulating sediment due to contour currents since 2.4 Ma (Kidd and Hill, 1987) the currents that formed it in the early Oligocene must have been significantly more vigorous than at present. A larger influx of dense water from the Faeroe-Shetland Channel into Rockall Trough could be acheived by a larger volume and/or higher velocity of bottom water. An interesting alternative is that the Faeore Bank Channel is a relatively young feature formed after the early Oligocene. Intraplate stresses in the Eurasian plate parallel to existing fracture

zones could have opened the Faeroe Bank Channel when sea-floor spreading north of the Greenland-Scotland Ridge became localized about the Kolbeinsey Axis in the late Oligocene.

The expansion of drift formation to the South Iceland Basin (Hatton, Gardar and Bjorn Drifts) and west side of Reykjanes Ridge (Snorri Drift) in the early Middle Miocene may be the result of a shift in the site of deep water formation to include the shallow areas of the Iceland-Faeroe Ridge. Waters formed on the ridge between Iceland and the Faeroes could flow into both the South Iceland and Norway Basins. The cross-sectional area of the water connection over the Iceland-Faeroe Ridge increases rapidly from 20 to 12 Ma based on the Paleocene reheating model. This may have made it possible for enough saline water to enter the GIN Sea from the south to overcome its large fresh-water balance resulting in outflow of dense water at depth rather than on the surface over the Iceland-Faeroe Ridge.

During the Miocene bottom water flow from the Denmark Strait may have been too strong to accumulate sediment on Eirik Drift and prohibited accumulation of Gloria Drift. Bottom water currents eroded sediment along the eastern Greenland margin transporting material to the South Labrador Sea and further south. In the late Miocene and early Pliocene the strength of bottom water currents on southeast Greenland decreased enough to begin accumulation of Eirik Drift. The decreased intensity of bottom water flow along East Greenland allowed deep water currents to flow west from the Reykjanes Ridge to begin accumulating Gloria Drift in the early Pliocene.

3.9 Figure Captions

Figure 3.1. Present tectonic features digitized for plate tectonic modelling of the southern Labrador Sea, northern North Atlantic and southern GIN Sea. The seafloor magnetic anomalies are shown as thin solid lines, fracture zones are heavy solid lines, ridges are dashed and Present COB's are shown at 1° resolution. Longitude is negative towards the west and latitude is positive towards the north. Tectonic features are labelled in the diagram: JMFZ = Jan Mayen Fracture Zone, AR = extinct Aegir Ridge, KR = Kolbeinsey Ridge, COB = continent-ocean boundary, RR = Reykjanes Ridge, CGFZ = Charlie Gibbs Fracture Zone, LS = Labrador Sea extinct spreading center, and L = the Leif, M = Minna, S = Snorri and H = Hudson Fracture Zones in the Labrador Sea.

Figure 3.2. Sea level curve digitized from that published by Haq et al. (1987). The age of the curve was converted to the Berggren et al. (1985) Cenozoic timescale. The curves shown in this diagram were averaged to 1 m.y. intervals and plotted at the midpoint of each interval. The dotted curve is the full amplitude of the averaged eustatic curve and the solid curve is half of the full amplitude. The timescale (Berggren et al., 1985) is shown on the bottom of the diagram and present sea level is marked by the horizontal dashed line.

Figure 3.3. Illustration of the gridded plate tectonic method for determining the age of the lithosphere on a spherical grid. Part A shows the present (t = 0) plate configuration from 60 to 63° N latitude along a section of the Reykjanes Ridge, the ridge is shown as a heavy solid line in the center of the diagram and magnetic lineations are thin lines parallel to the ridge. The ages of the magnetic lineations are given in Ma. The Greenland plate is on the left (solid grid) and the Eurasian plate is on the right (dashed grid). Part B shows the present grid of the Eurasian plate rotated to its position at 2 Ma relative to a fixed Greenland plate. Part C shows the three grid cells that were removed from the 2 Ma reconstruction. At the resolution of the grid the oceanic lithosphere in these three grid cells is 2 million years old. Part D shows the palinspastically reconstructed plate configuration at 2 Ma.

Figure 3.4. Age of the ocean crust (less than 60 Ma) calculated using the gridded plate tectonic method outlined in Section 3.3.3 and in Fig. (3.3). The contour interval from 0 to 60 Ma is 5 m.y. and from 60 to 140 Ma the contour interval is 20 m.y. Except for the South Labrador Sea, the regions in this figure that are older than 60 Ma are assumed to be underlain by continental crust. The age isochrons in the Rockall-Faeroe region were estimated assuming that extension in the Rockall Trough, Faeroe-Shetland Channel and Hatton-Rockall Basin occurred during the Cretaceous (Hanisch, 1984). This is referred to as the "Cretaceous rift" model and approximates the time when the main phase of continental extension probably occurred.

Figure 3.5. Thermal subsidence curves for oceanic lithosphere plotted using Eqns. (3.4) and (3.5) shown on the diagram. The subsidence equations are from Parsons and Sclater (1977). Depth is given in meters below a constant sea level.

Figure 3.6. Present thickness of crust in the study area estimated from Eqn. (3.13). The region is assumed to be in isostatic equilibrium, the mantle density was calculated from the age of the crust and the thickness of the crust was calculated from the mantle density, total thickness and mass of sediment and the present water thickness or elevation above sea level.

Figure 3.7. Present bathymetry of the northern North Atlantic and southern GIN Sea plotted from ETOPO5 (1986) elevations averaged to a 10 x 10' latitude-longitude grid.

Figure 3.8. Present bathymetry of the northern North Atlantic and southern GIN Sea plotted from ETOPO5 (1986) elevations averaged to a 1 x 1° latitude-longitude grid. The location of the profiles shown in Figs. 3.14-3.19 is shown here by the line of black dots along the Greenland-Scotland Ridge.

Figure 3.9A. Cretaceous rifting model for reconstructed early Late Miocene (10 Ma) paleobathymetry. The boundary of the reconstructed region is marked by the edge of the gray-shading and contour lines. Contours at the edges of the reconstructed region do not reflect true bathymetry but are an artifact of the contouring algrithm. The present coastlines of Greenland and the U.K. are shown for reference and depths are given in kilometers below sea level. White areas within the reconstructed region are modelled to be at or above sea level at that time. Sea level is 8 m lower than at present (Fig 3.2).

Figure 3.9B. Paleocene reheating model for reconstructed early Late Miocene (10 Ma) paleobathymetry. The boundary of the reconstructed region is marked by the edge of the gray-shading and contour lines. The present coastlines of Greenland and the U.K. are shown for reference and depths are given in kilometers below sea level. White areas within the reconstructed region are modelled to be at or above sea level at that time. Sea level is 8 m lower than at present (Fig 3.2).

Figure 3.10A. Cretaceous rifting model for reconstructed Early Miocene (20 Ma) paleobathymetry. The boundary of the reconstructed region is marked by the edge of the gray-shading and contour lines. The present coastlines of Greenland and the U.K. are shown for reference and depths are given in kilometers below sea level. White areas within the reconstructed region are modelled to be at or above sea level at that time. Sea level is 42 m higher than at present (Fig. 3.2).

Figure 3.10B. Paleocene reheating model for reconstructed Early Miocene (20 Ma) paleobathymetry. The boundary of the reconstructed region is marked by the edge of the gray-shading and contour lines. The present coastlines of Greenland and the U.K. are shown for reference and depths are given in kilometers below sea level. White areas within the reconstructed region are modelled to be at or above sea level at that time. Sea level is 42 m higher than at present (Fig. 3.2).

Figure 3.11A. Cretaceous rifting model for reconstructed mid-Oligocene (30 Ma) paleobathymetry. The boundary of the reconstructed region is marked by the edge of the gray-shading and contour lines. The present coastlines of Greenland and the U.K. are shown for reference and depths are given in kilometers below sea level. White areas within the reconstructed region are modelled to be at or above sea level at that time. Sea level is 14 m higher than at present (Fig. 3.2).

Figure 3.11B. Paleocene reheating model for reconstructed mid-Oligocene (30 Ma) paleobathymetry. The boundary of the reconstructed region is marked by the edge of the gray-shading and contour lines. The present coastlines of Greenland and the U.K. are shown for reference and depths are given in kilometers below sea level. White areas within the reconstructed region are modelled to be at or above sea level at that time. Sea level is 14 m higher than at present (Fig. 3.2).

Figure 3.12A. Cretaceous rifting model for reconstructed early Late Eocene (40 Ma) paleobathymetry. The boundary of the reconstructed region is marked by the edge of the gray-shading and contour lines. The present coastlines of Greenland and the U.K. are shown for reference and depths are given in kilometers below sea level. White areas within the reconstructed region are modelled to be at or above sea level at that time. Sea level is 56 m higher than at present (Fig. 3.2).

Figure 3.12B. Paleocene reheating model for reconstructed early Late Eocene (40 Ma) paleobathymetry. The boundary of the reconstructed region is marked by the edge of the gray-shading and contour lines. The present coastlines of Greenland and the U.K. are shown for reference and depths are given in kilometers below sea level. White areas within the reconstructed region are modelled to be at or above sea level at that time. Sea level is 56 m higher than at present (Fig. 3.2).

Figure 3.13A. Cretaceous rifting model for reconstructed early Middle Eocene (50 Ma) paleobathymetry. The boundary of the reconstructed region is marked by the edge of the gray-shading and contour lines. The present coastlines of Greenland and the U.K. are shown for reference and depths are given in kilometers below sea level. White areas within the reconstructed region are modelled to be at or above sea level at that time. Sea level is 106 m higher than at present (Fig. 3.2).

Figure 3.13B. Paleocene reheating model for reconstructed early Middle Eocene (50 Ma) paleobathymetry. The boundary of the reconstructed region is marked by the edge of the gray-shading and contour lines. The present coastlines of Greenland and the U.K. are shown for reference and depths are given in kilometers below sea level. White areas within the reconstructed region are modelled to be at or above sea level at that time. Sea level is 106 m higher than at present (Fig. 3.2).

Figure 3.14A. Cretaceous rifting model for reconstructed paleobathymetry along the Greenland-Scotland Ridge from NW (Greenland) to SE (Scotland). Paleobathymetry was reconstructed as described in the text and paleotopography is approximated along profiles from Present to 5 Ma. Sea level at the time of the reconstruction (from Fig. 3.2) is shown as a dashed horizontal line. The location of the profile is given in Figure 3.8. The Denmark Strait extends from 0 to 500 km on the profiles, Iceland is above sea level from 500 to 1000 km, the Iceland-Faeroe Ridge is below sea level from 1000 to 1700 km, the Faeroe Shelf extends from 1700 to 1900 km and the Faeroe-Shetland Channel is below sea level from 1900 to 2100 km.

Figure 3.14B. Paleocene reheating model for reconstructed paleobathymetry along the Greenland-Scotland Ridge from NW (Greenland) to SE (Scotland). Paleobathymetry was reconstructed as described in the text and paleotopography is approximated along profiles from Present to 5 Ma. The Denmark Strait extends from 0 to 500 km on the profiles, Iceland is above sea level from 500 to 1000 km, the Iceland-Faeroe Ridge is below sea level from 1000 to 1700 km, the Faeroe Shelf extends from 1700 to 1900 km and the Faeroe-Shetland Channel is below sea level from 1900 to 2100 km.

Figure 3.15A. Cretaceous rifting model for reconstructed paleobathymetry along the Greenland-Scotland Ridge from NW (Greenland) to SE (Scotland). Paleobathymetry was reconstructed as described in the text and paleotopography is approximated along profiles from 6 to 11 Ma. Sea level at the time of the reconstruction (from Fig. 3.2) is shown as a dashed horizontal line. The location of the profile is given in Figure 3.8. The Denmark Strait extends from 0 to 500 km on the profiles, Iceland is above sea level from 500 to 1000 km, the Iceland-Faeroe Ridge is below sea level from 1000 to 1700 km, the Faeroe Shelf extends from 1700 to 1900 km and the Faeroe-Shetland Channel is below sea level from 1900 to 2100 km.

Figure 3.15B. Paleocene reheating model for reconstructed paleobathymetry along the Greenland-Scotland Ridge from NW (Greenland) to SE (Scotland). Paleobathymetry was reconstructed as described in the text and paleotopography is approximated along profiles from 6 to 11 Ma. The Denmark Strait extends from 0 to 500 km on the profiles, Iceland is above sea level from 500 to 1000 km, the Iceland-Faeroe Ridge is below sea level from 1000 to 1700 km, the Faeroe Shelf extends from 1700 to 1900 km and is just at sea level and the Faeroe-Shetland Channel is below sea level from 1900 to 2100 km.

Figure 3.16A. Cretaceous rifting model for reconstructed paleobathymetry along the Greenland-Scotland Ridge from NW (Greenland) to SE (Scotland). Paleobathymetry was reconstructed as described in the text and paleotopography is approximated along profiles from 12 to 17 Ma. Sea level at the time of the reconstruction (from Fig. 3.2) is shown as a dashed horizontal line. The location of the profile is given in Figure 3.8. The Denmark Strait extends from 0 to 500 km on the profiles, Iceland is above sea level from 500 to 1000 km, the Iceland-Faeroe Ridge is below sea level from 1000 to 1500 km, the Faeroe Shelf extends from 1500 to 1700 km and is just below sea level the Faeroe-Shetland Channel is below sea level from 1700 to 2000 km.

Figure 3.16B. Paleocene reheating model for reconstructed paleobathymetry along the Greenland-Scotland Ridge from NW (Greenland) to SE (Scotland). Paleobathymetry was reconstructed as described in the text and paleotopography is approximated along profiles from 12 to 17 Ma. The Denmark Strait extends from 0 to 500 km on the profiles, Iceland is above sea level from 500 to 1000 km, the Iceland-Faeroe Ridge is below sea level from 1000 to 1400 km, the Faeroe Shelf is above sea level and extends from 1400 to 1700 km and the Faeroe-Shetland Channel is below sea level from 1700 to 1900 km.

Figure 3.17A. Cretaceous rifting model for reconstructed paleobathymetry along the Greenland-Scotland Ridge from NW (Greenland) to SE (Scotland). Paleobathymetry was reconstructed as described in the text and paleotopography is approximated along profiles from 18 to 23 Ma. Sea level at the time of the reconstruction (from Fig. 3.2) is shown as a dashed horizontal line. The location of the profile is given in Figure 3.8. The Denmark Strait extends from 50 to 500 km on the profiles, Iceland is above sea level from 500 to 1000 km, the Iceland-Faeroe Ridge is below sea level from 1000 to 1400 km, the Faeroe Shelf extends from 1400 to 1600 km and is just below sea level the Faeroe-Shetland Channel is below sea level from 1600 to 1900 km.

Figure 3.17B. Paleocene reheating model for reconstructed paleobathymetry along the Greenland-Scotland Ridge from NW (Greenland) to SE (Scotland). Paleobathymetry was reconstructed as described in the text and paleotopography is approximated along profiles from 18 to 23 Ma. The Denmark Strait extends from 50 to 500 km on the profiles, Iceland is above sea level from 500 to 1000 km, the Iceland-Faeroe Ridge is below sea level from 1000 to 1400 km, the Faeroe Shelf is above sea level and extends from 1400 to 1600 km and the Faeroe-Shetland Channel is below sea level from 1600 to 1800 km.

Figure 3.18A. Cretaceous rifting model for reconstructed paleobathymetry along the Greenland-Scotland Ridge from NW (Greenland) to SE (Scotland). Paleobathymetry was reconstructed as described in the text and paleotopography is approximated along profiles from 24 to 29 Ma. Sea level at the time of the reconstruction (from Fig. 3.2) is shown as a dashed horizontal line. The location of the profile is given in Figure 3.8. The Denmark Strait extends from 150 to 450 km on the profiles, the Iceland-Faeroe Ridge is above sea level from 450 to 1350 km and the Faeroe-Shetland Channel is below sea level from 1350 to 1600 km.

Figure 3.18B. Paleocene reheating model for reconstructed paleobathymetry along the Greenland-Scotland Ridge from NW (Greenland) to SE (Scotland). Paleobathymetry was reconstructed as described in the text and paleotopography is approximated along profiles from 24 to 29 Ma. The Denmark Strait extends from 150 to 450 km on the profiles, the Iceland-Faeroe Ridge is above sea level from 450 to 1400 km and the Faeroe-Shetland Channel is below sea level from 1400 to 1500 km.

Figure 3.19A. Cretaceous rifting model for reconstructed paleobathymetry along the Greenland-Scotland Ridge from NW (Greenland) to SE (Scotland). Paleobathymetry was reconstructed as described in the text and paleotopography is approximated along profiles from 30 to 35 Ma. Sea level at the time of the reconstruction (from Fig. 3.2) is shown as a dashed horizontal line. The location of the profile is given in Figure 3.8. The Denmark Strait is just below sea level and extends from 200 to 400 km on the profiles, the Iceland-Faeroe Ridge is above sea level from 400 to 1300 km and the Faeroe-Shetland Channel is just below sea level from 1300 to 1500 km.

Figure 3.19B. Paleocene reheating model for reconstructed paleobathymetry along the Greenland-Scotland Ridge from NW (Greenland) to SE (Scotland). Paleobathymetry was reconstructed as described in the text and paleotopography is approximated along profiles from 30 to 35 Ma. The Denmark Strait is just below sea level and extends from 150 to 450 km on the profiles, the Iceland-Faeroe Ridge is above sea level from 450 to 1500 km and the Faeroe-Shetland Channel is at or above sea level.

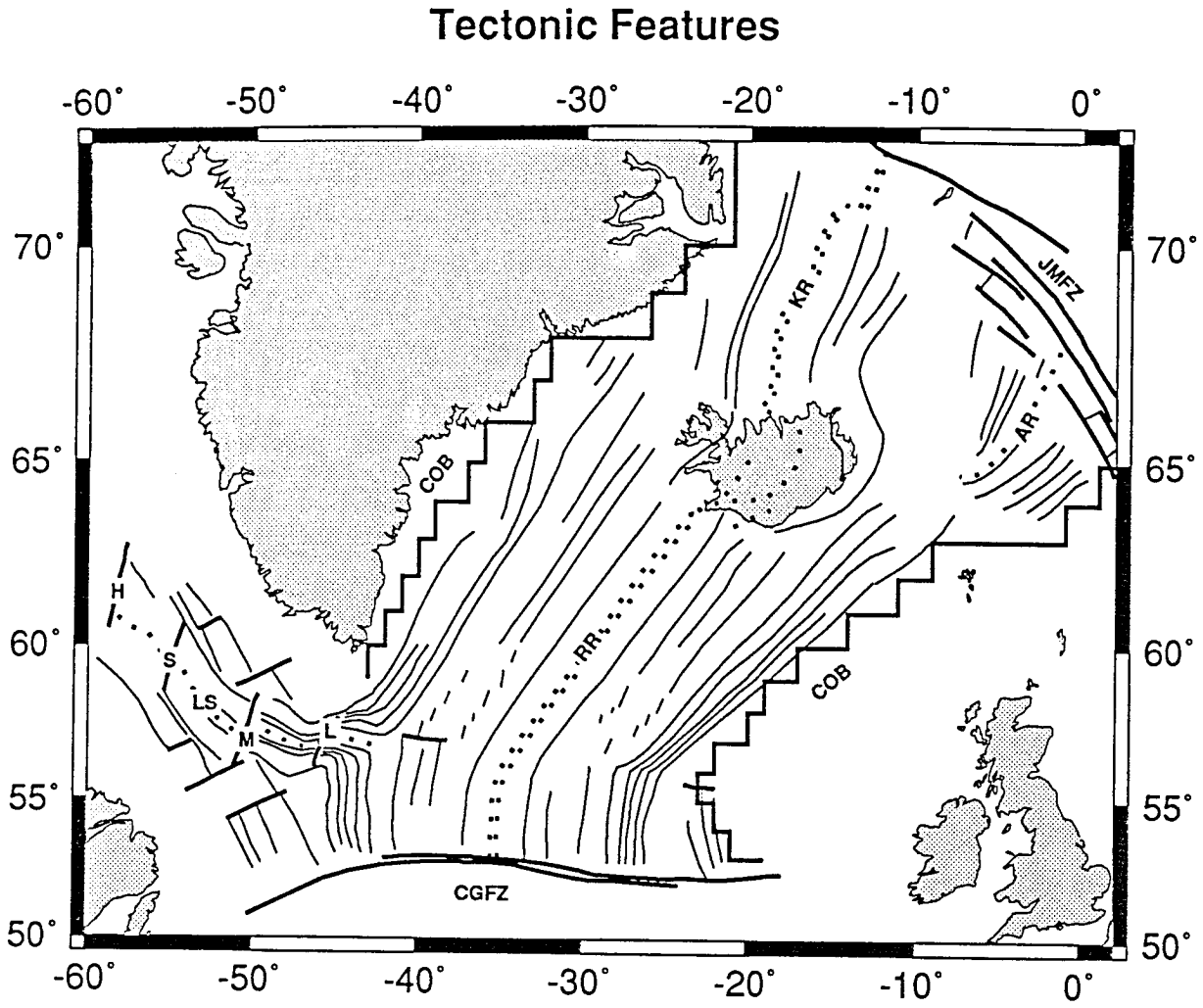
Tectonic Features
-60°
-50°
-40°
-30°
-20°
-10°
0°
70°
65°
60°
55°
50°
COB
KR
JMFZ
AR
RR
CGFZ
H
S
LS
M
L

Figure 3.1

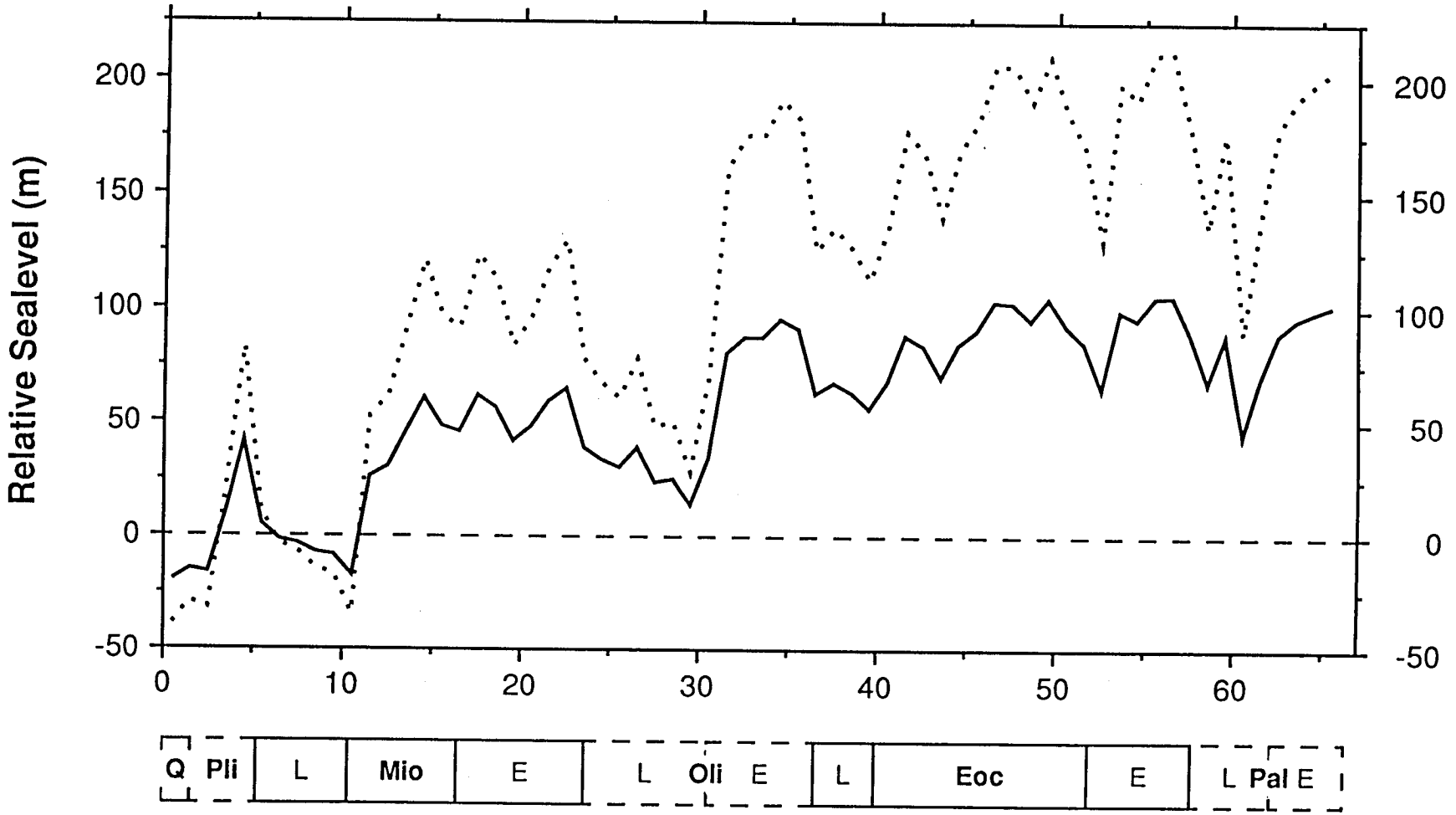
Relative Sealevel (m)
200
150
100
50
0
-50
0
10
20
30
40
50
60
Q
Pli
L
Mio
E
L
Oli
E
L
Eoc
E
L
Pal
E

Figure 3.2

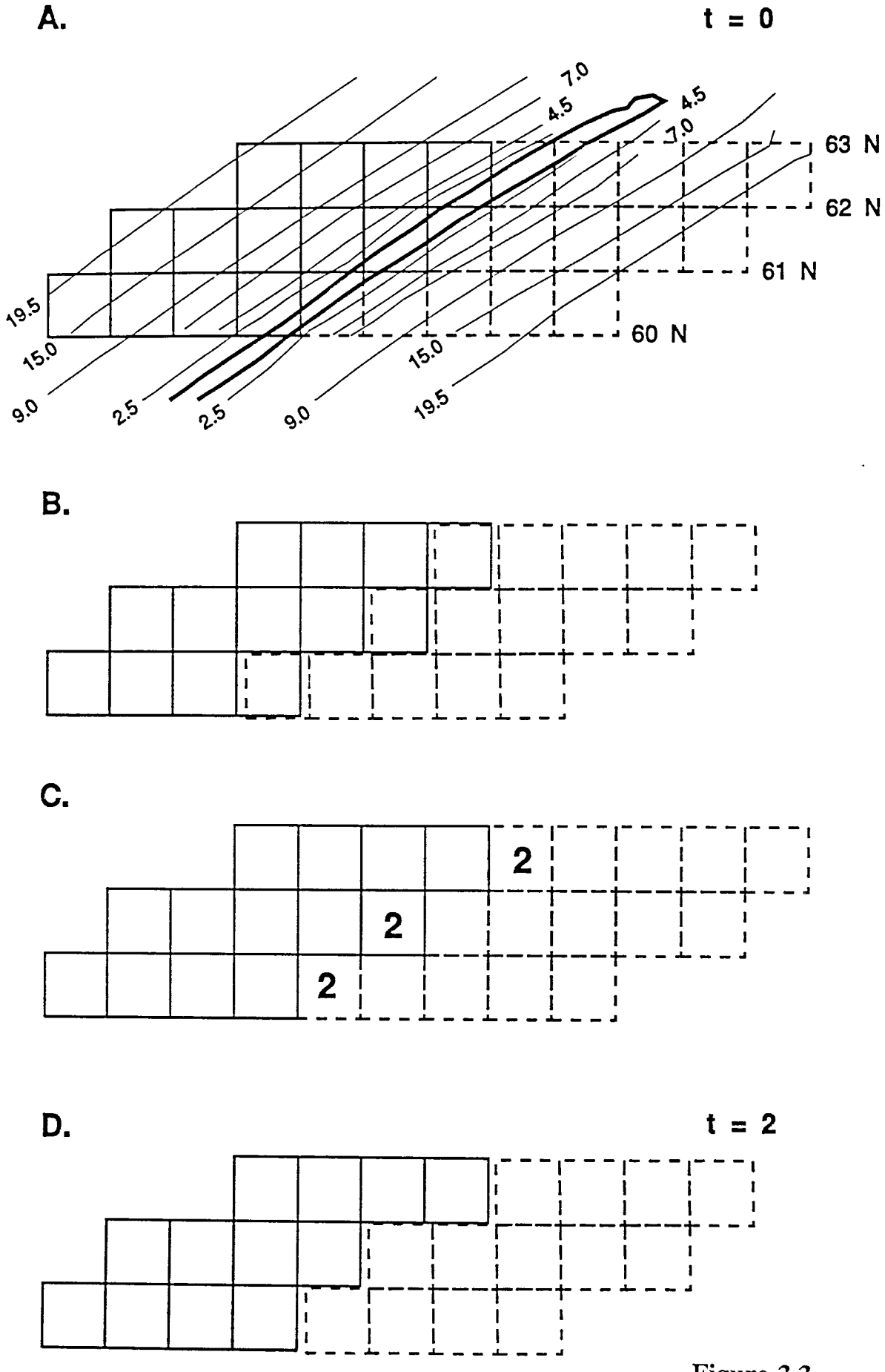
A.
t = 0
7.0
4.5
4.5
7.0
63 N
62 N
61 N
60 N
19.5
15.0
9.0
2.5
2.5
9.0
15.0
19.5
B.
C.
2
2
2
D.
t = 2

Figure 3.3

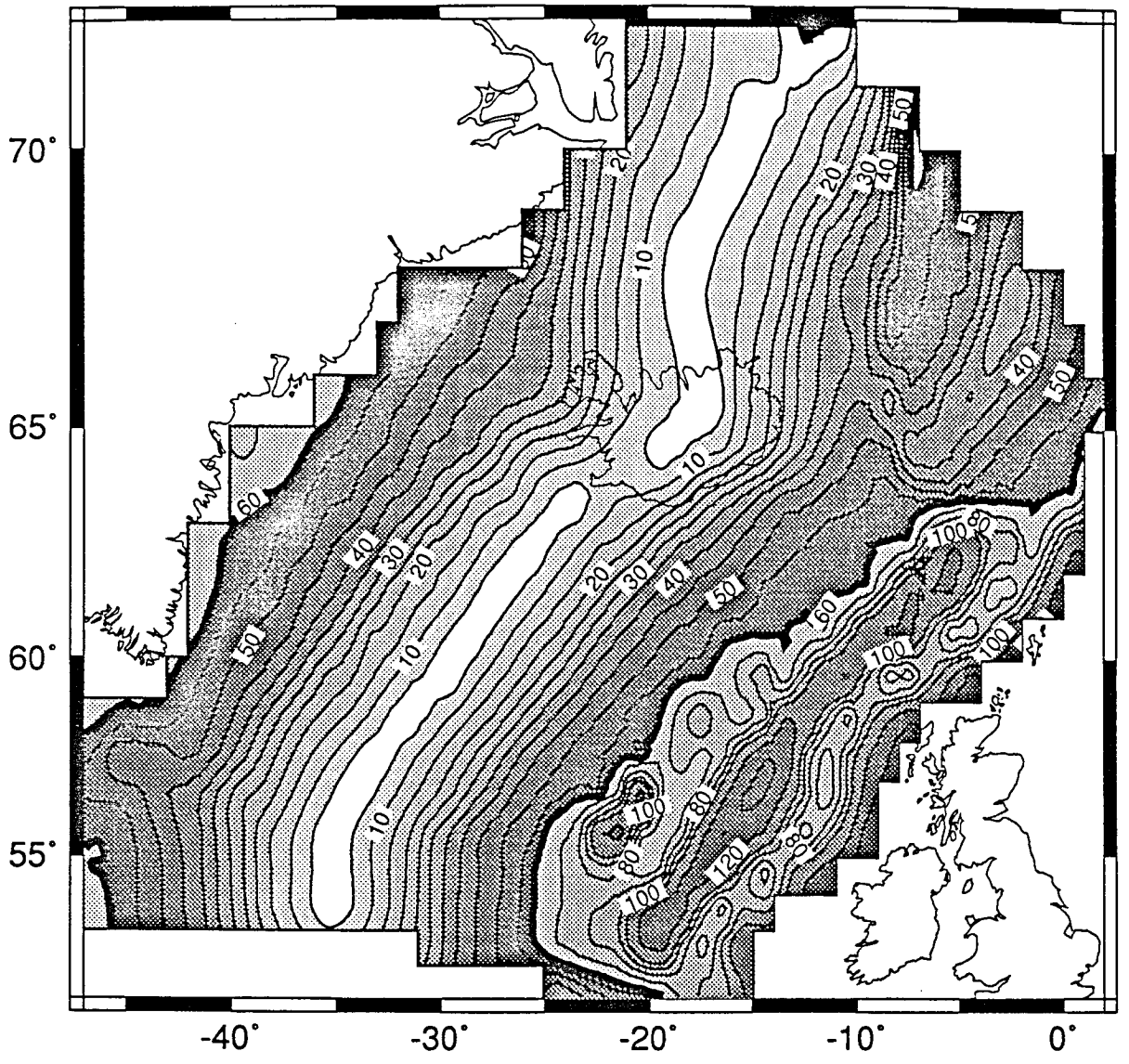

Figure 3.4

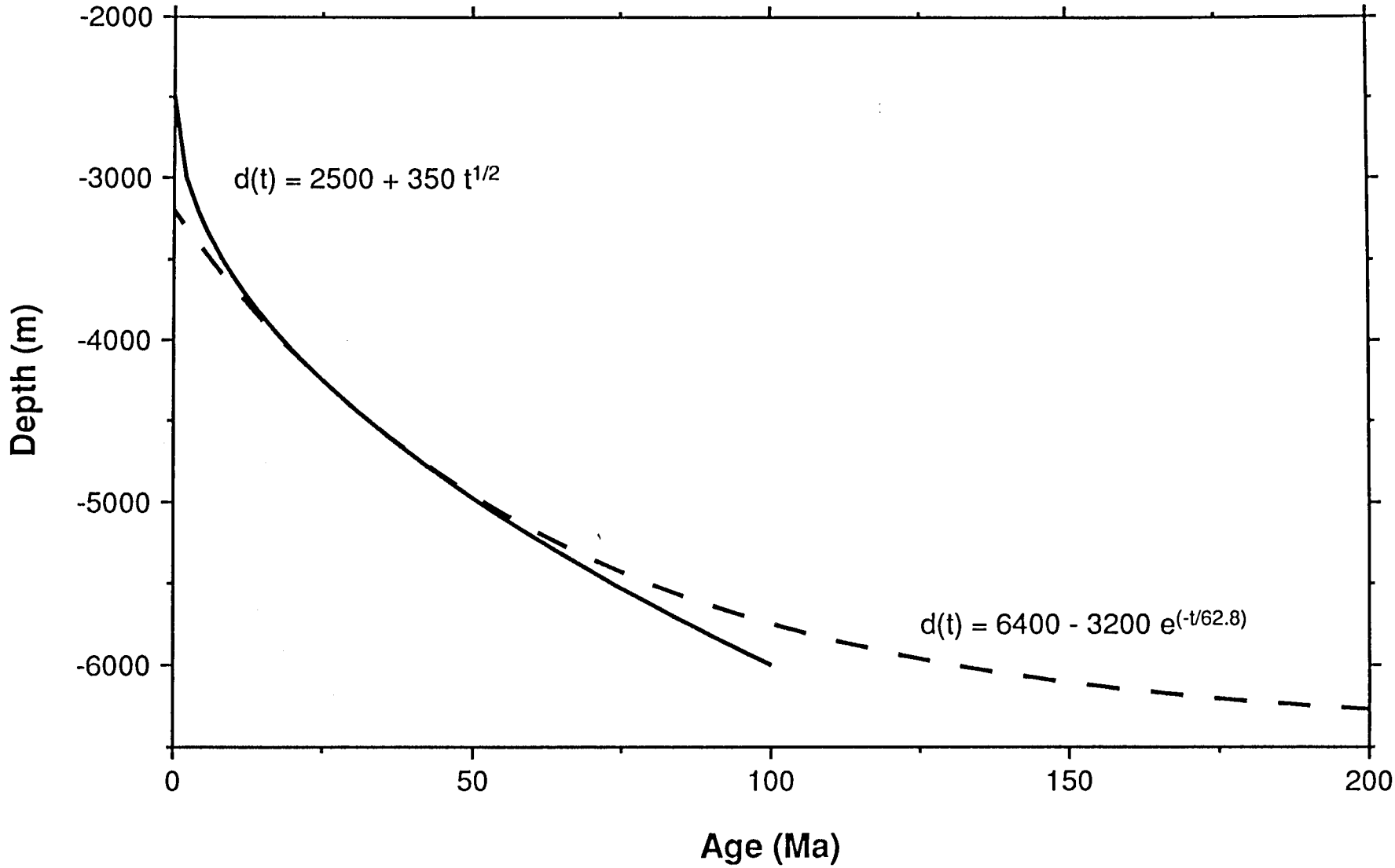
-2000
-3000
-4000
-5000
-6000
Depth (m)
d(t) = 2500 + 350 t^1/2
d(t) = 6400 - 3200 e^(-t/62.8)
0
50
100
150
200
Age (Ma)

Figure 3.5

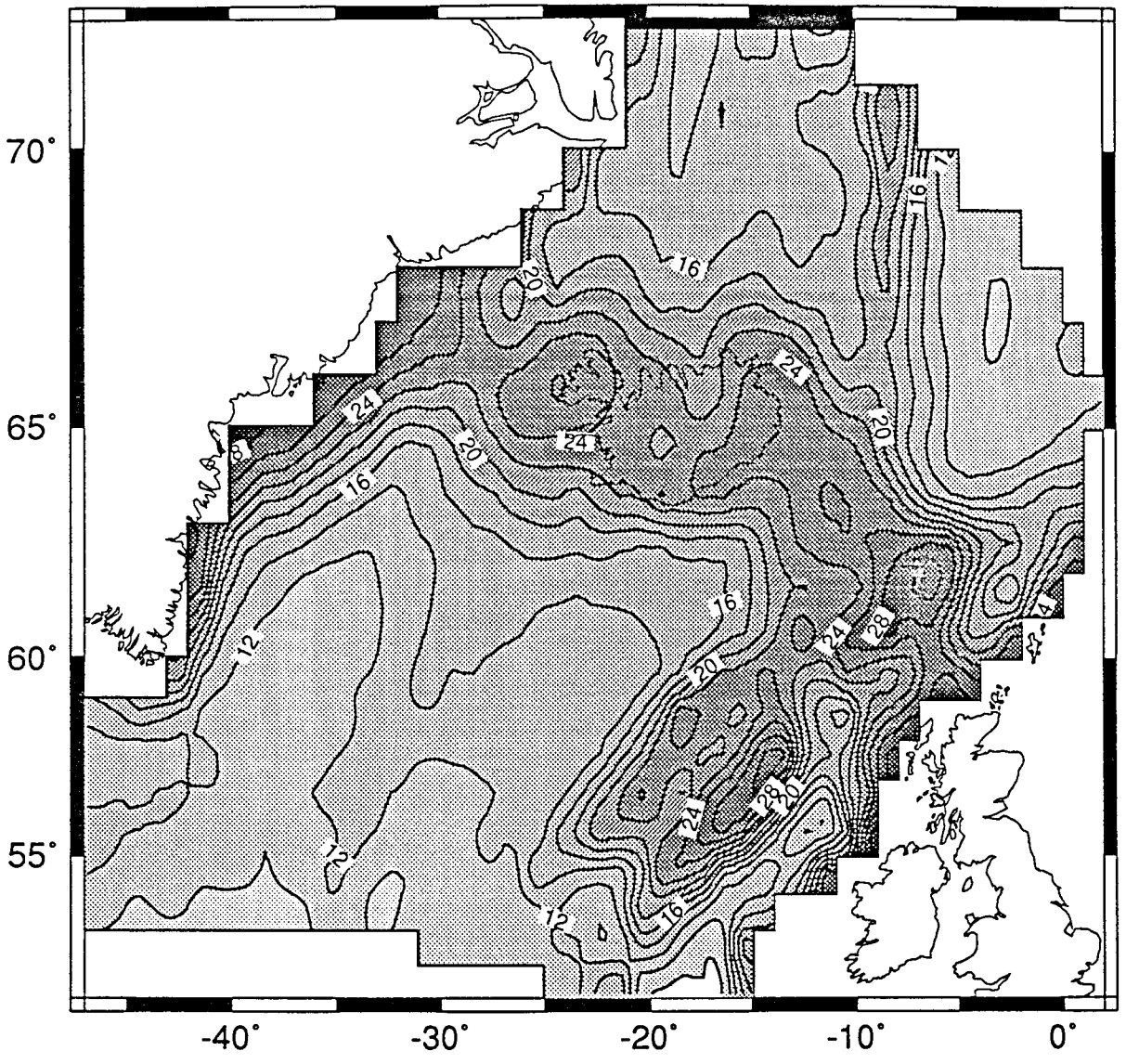

Figure 3.6

Present Bathymetry

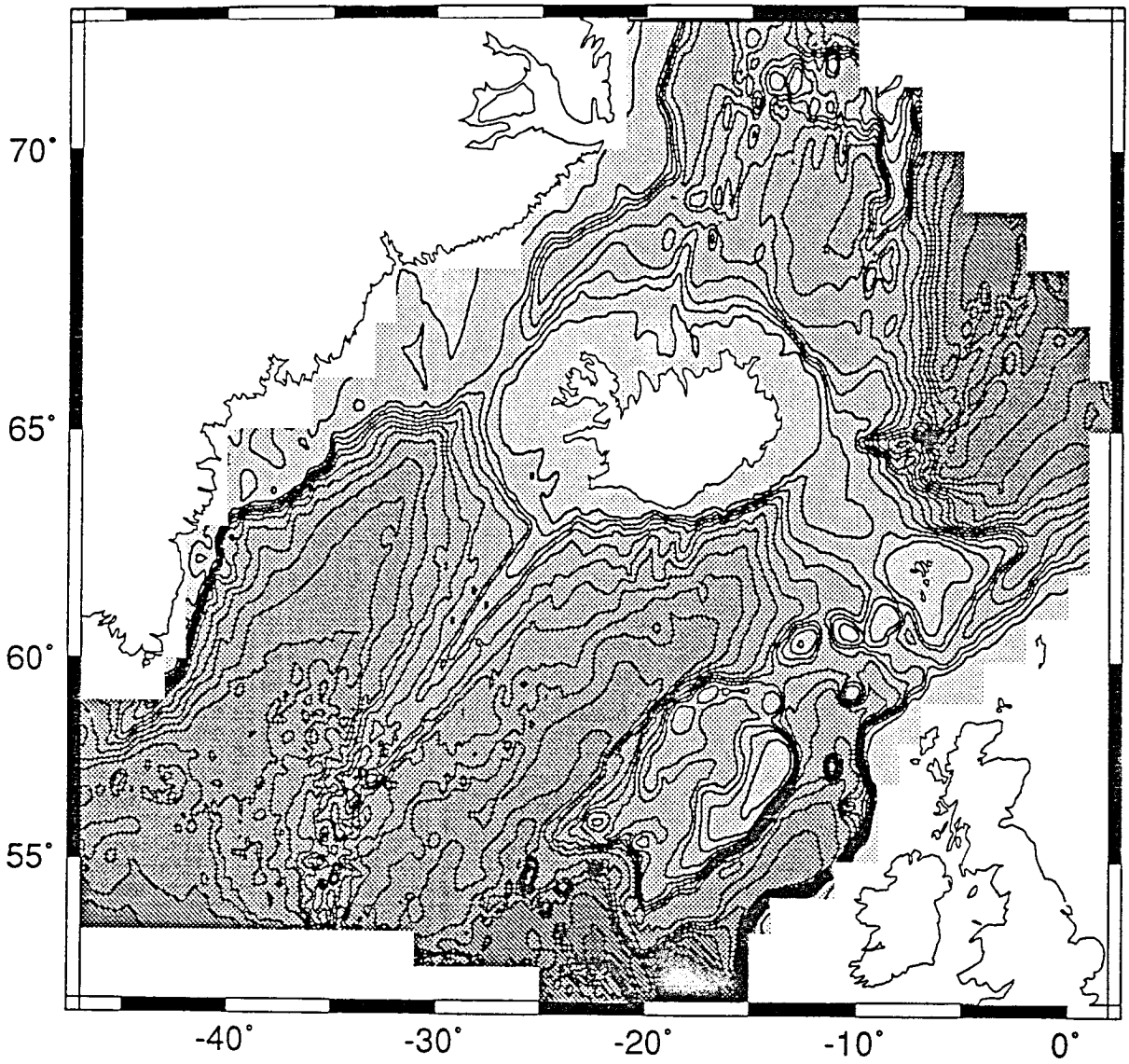

Figure 3.7

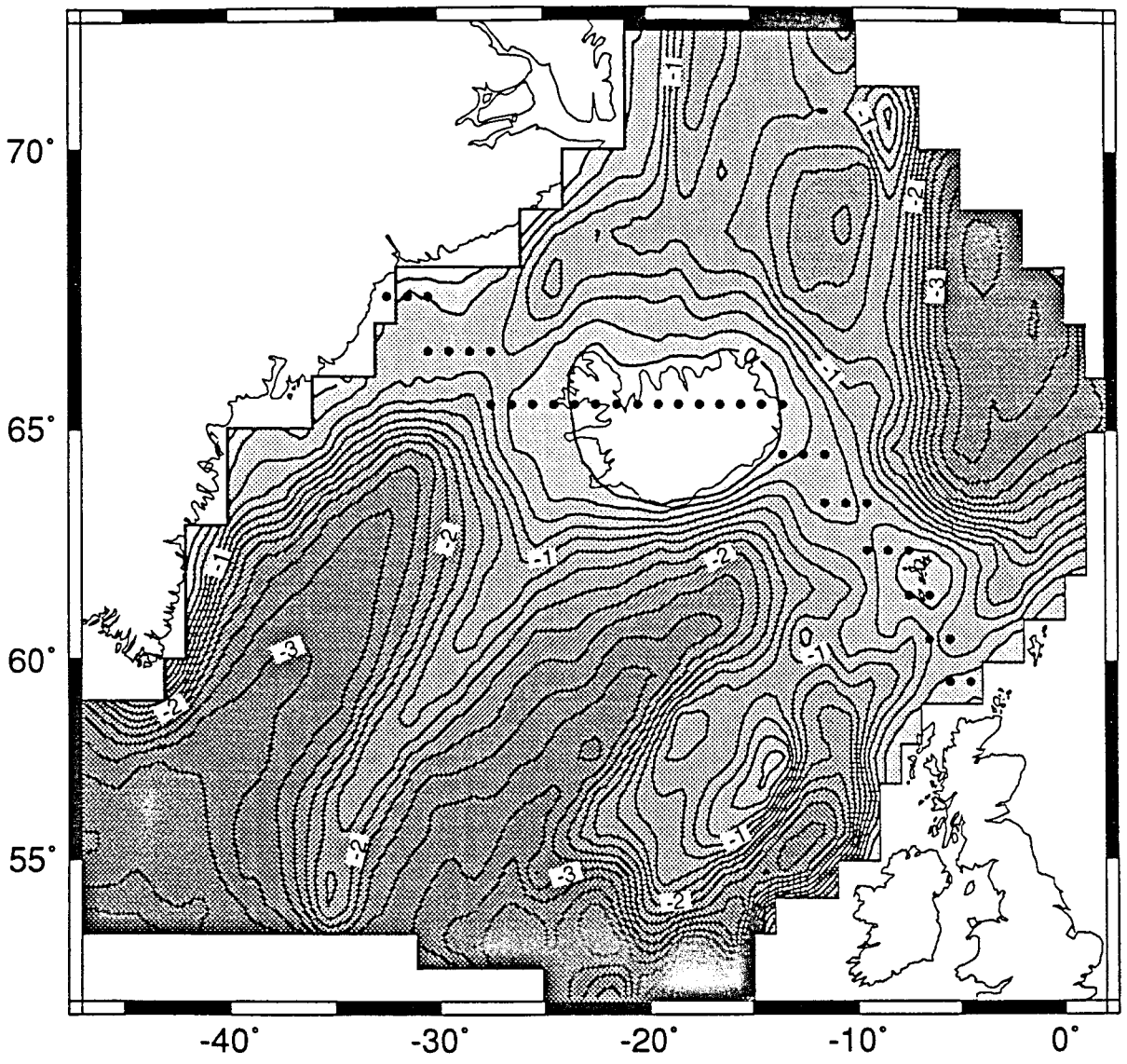

Figure 3.8

10 Ma - Reconstructed Paleobathymetry

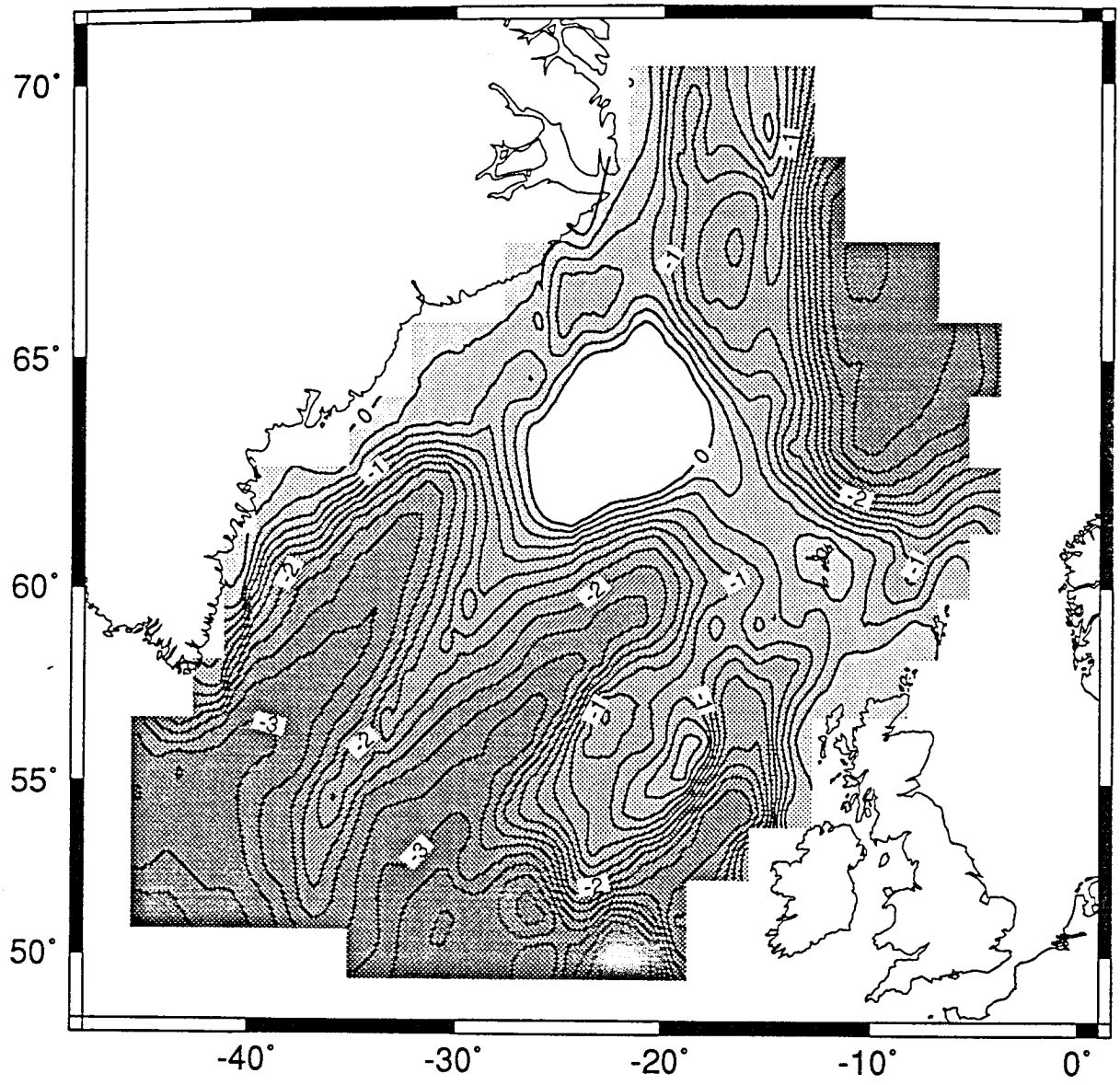

Figure 3.9A

10 Ma - Reconstructed Paleobathymetry

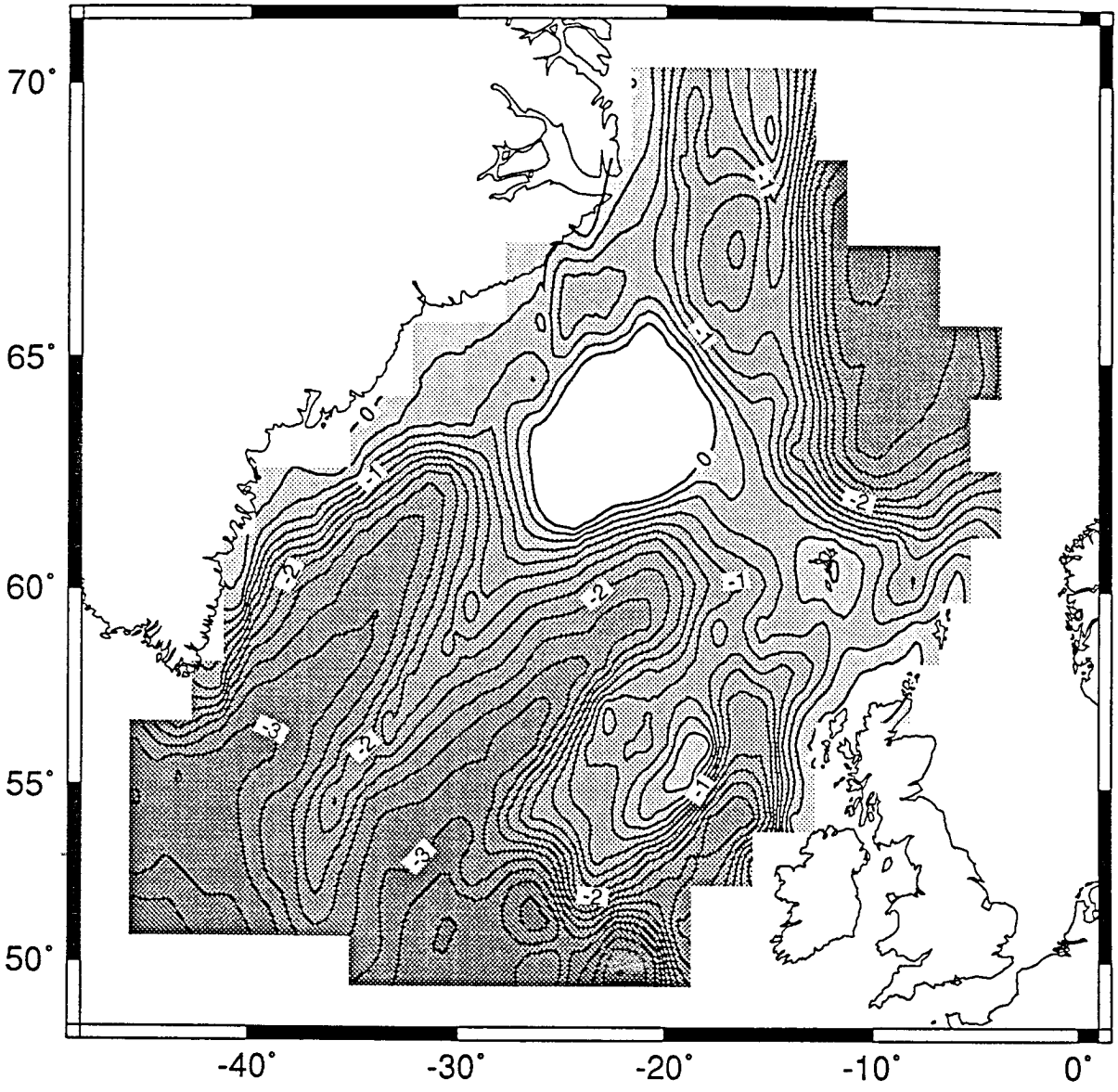

Figure 3.9B

20 Ma - Reconstructed Paleobathymetry

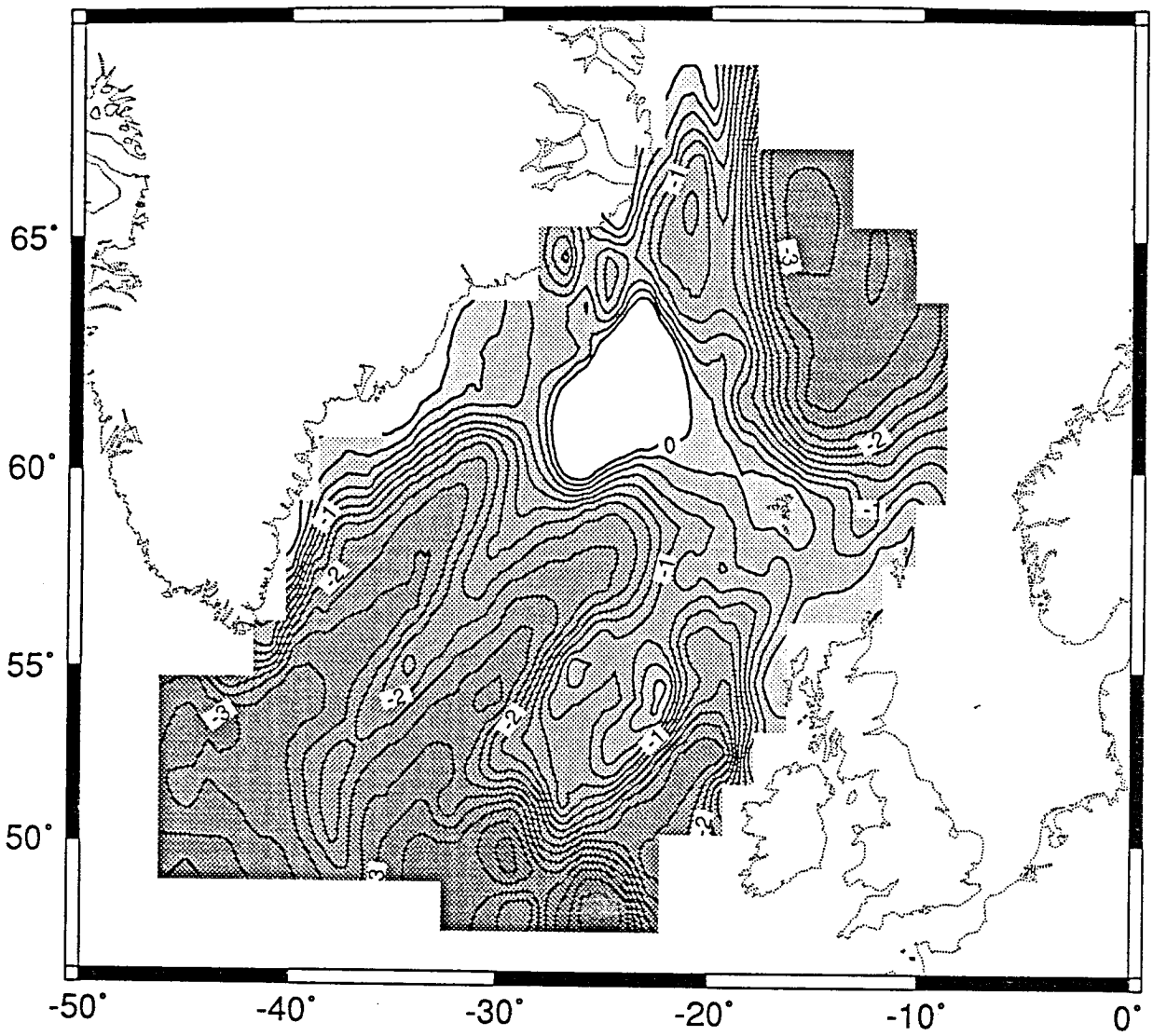

Figure 3.10A

20 Ma - Reconstructed Paleobathymetry

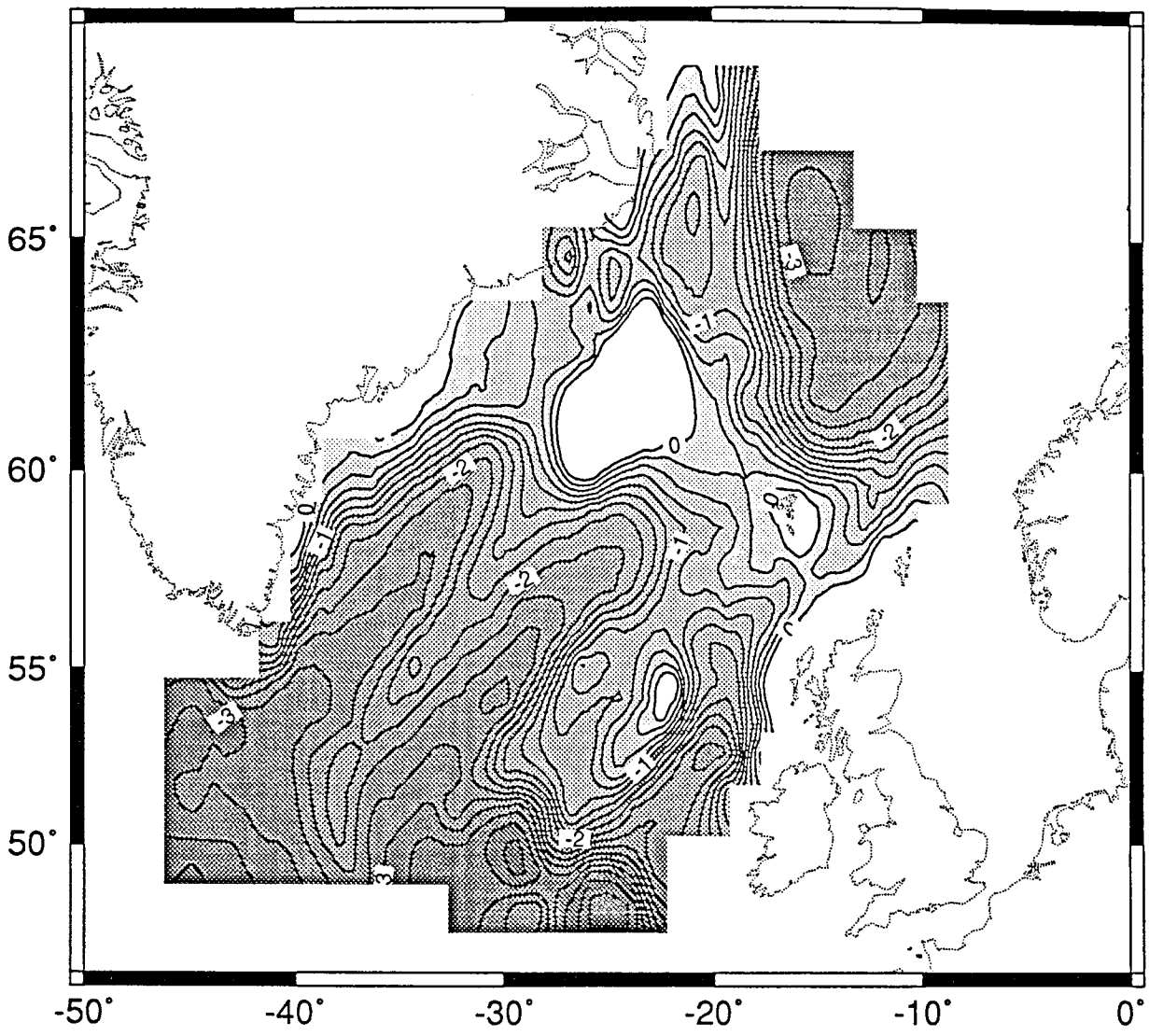

Figure 3.10B

30 Ma - Reconstructed Paleobathymetry

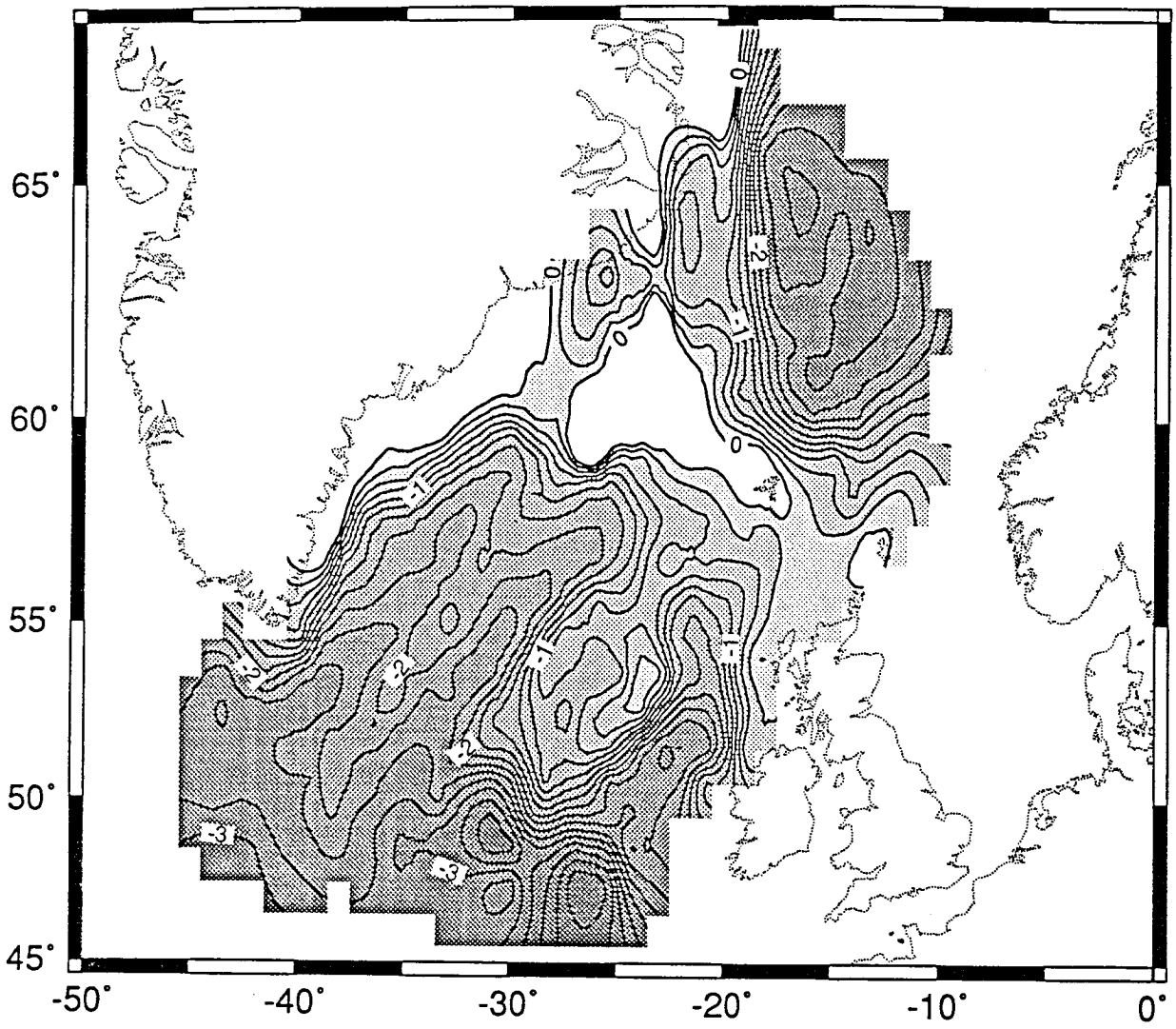

Figure 3.11A

30 Ma - Reconstructed Paleobathymetry

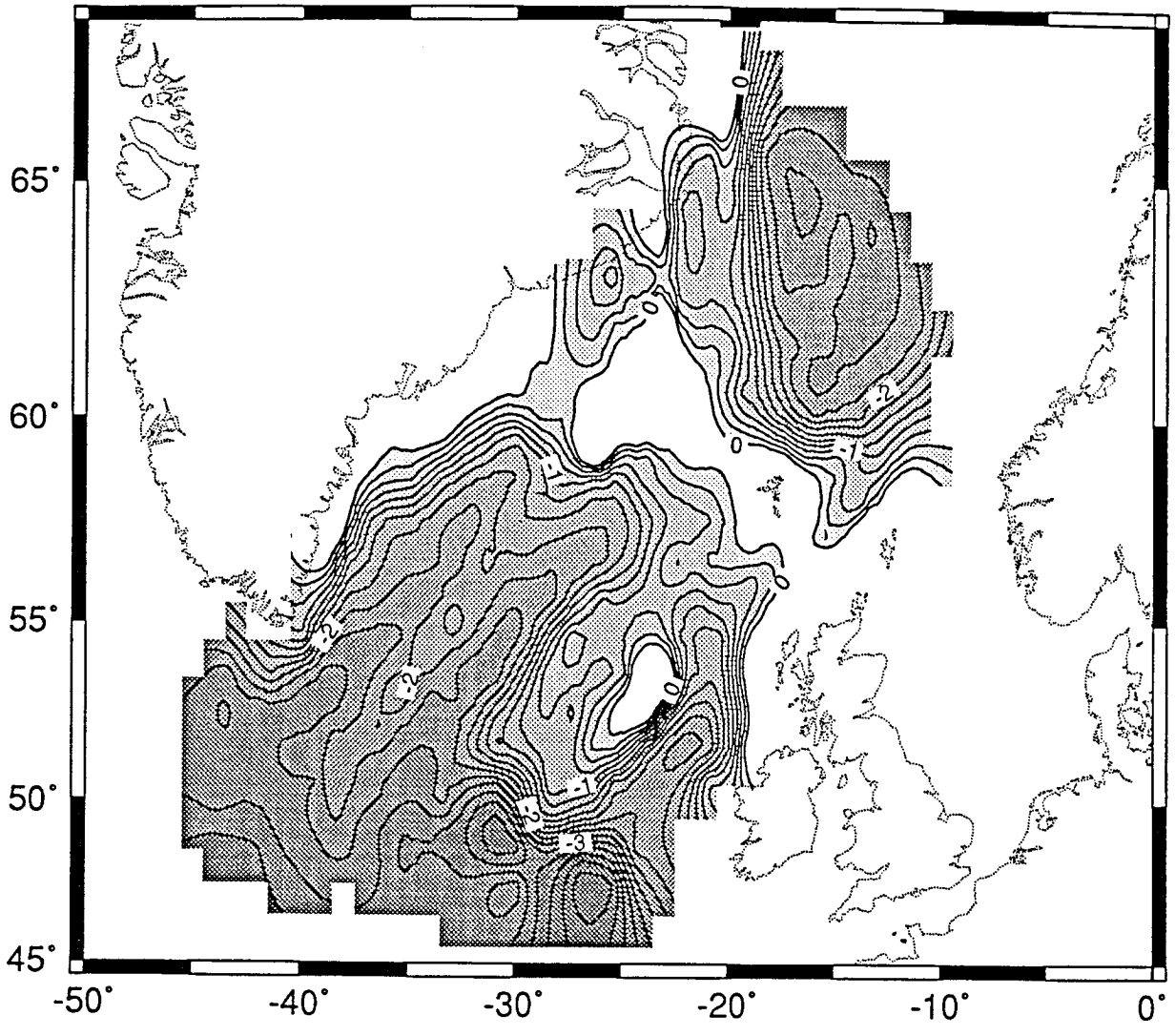

Figure 3.11B

40 Ma - Reconstructed Paleobathymetry

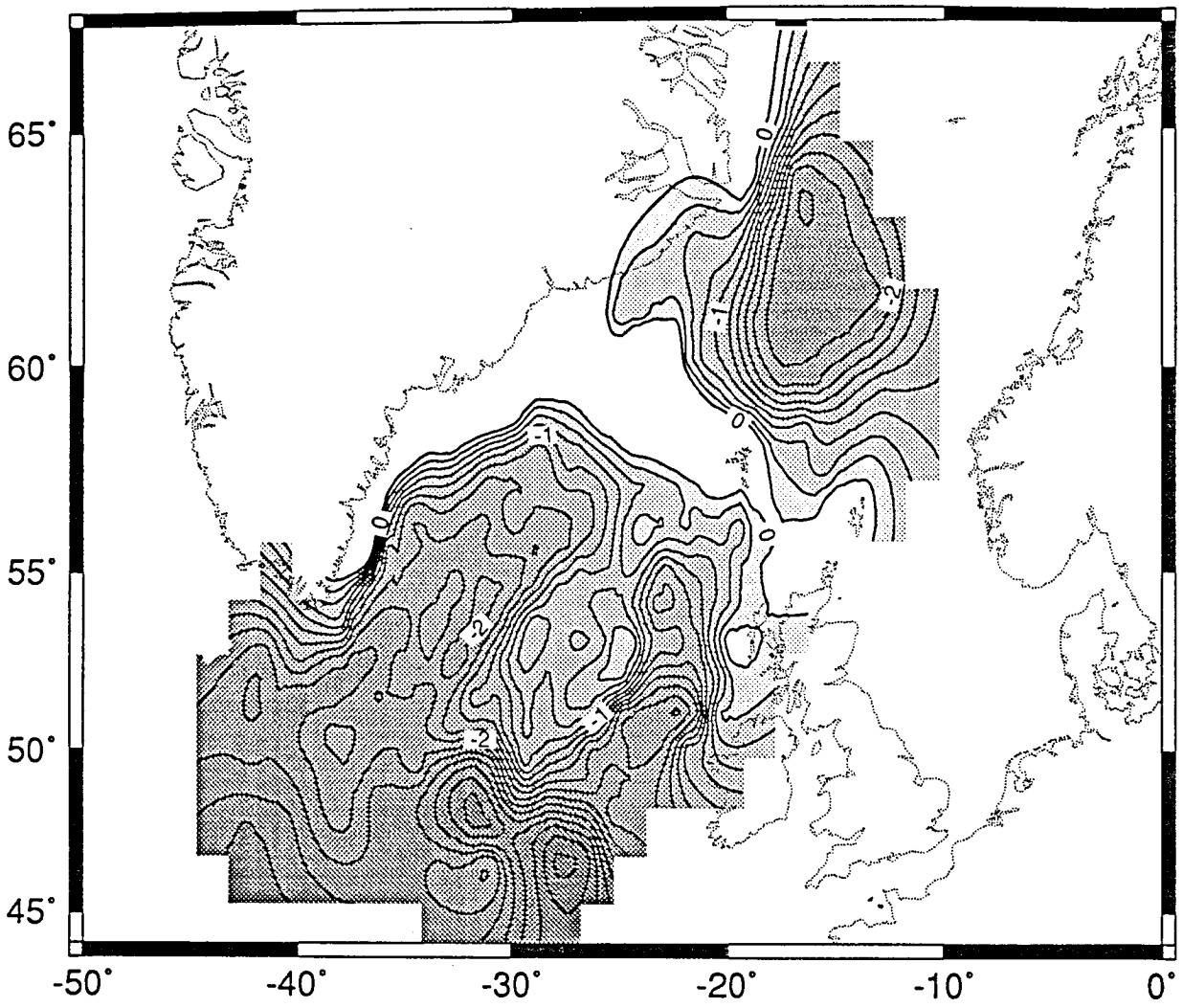

Figure 3.12A

40 Ma - Reconstructed Paleobathymetry

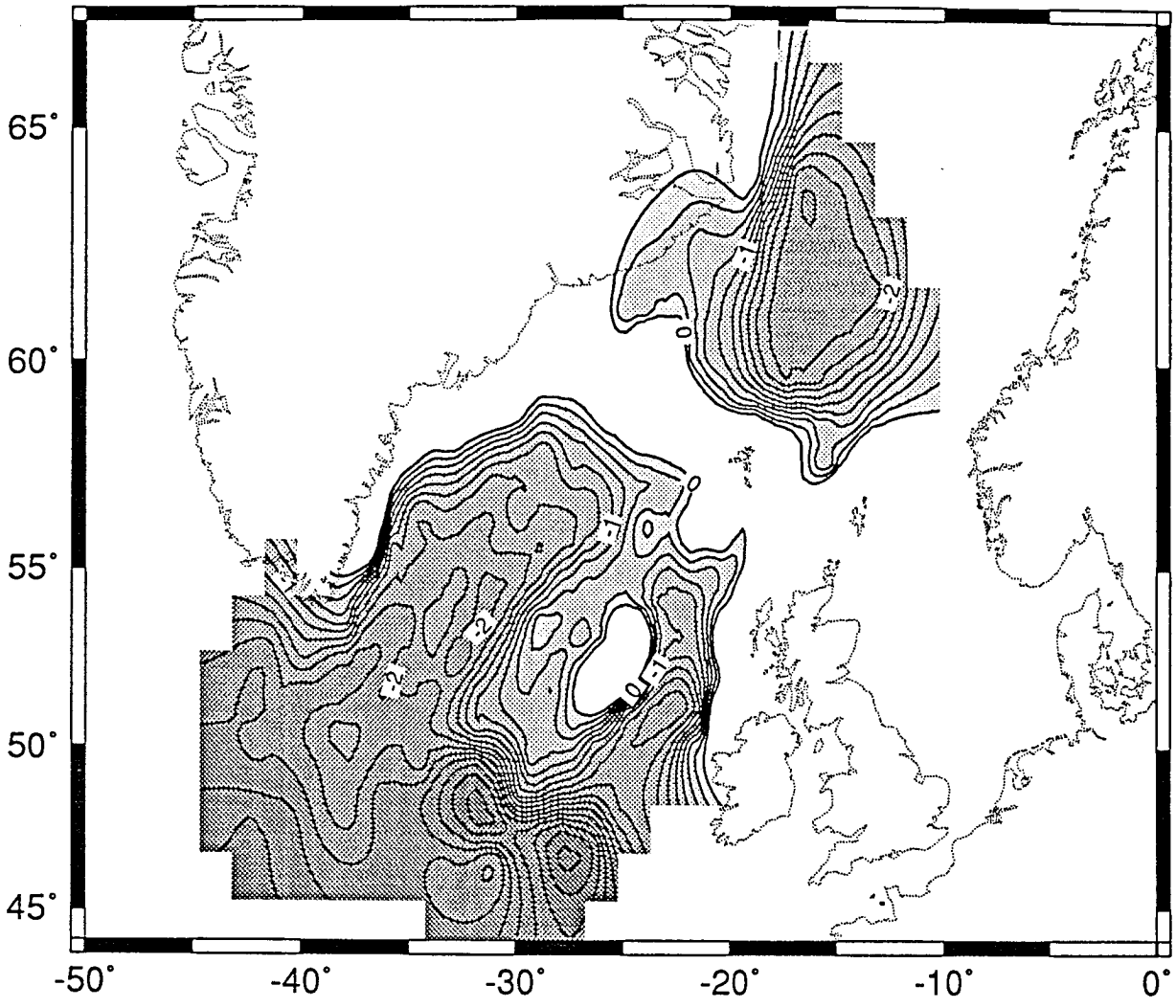

Figure 3.12B

50 Ma - Reconstructed Paleobathymetry

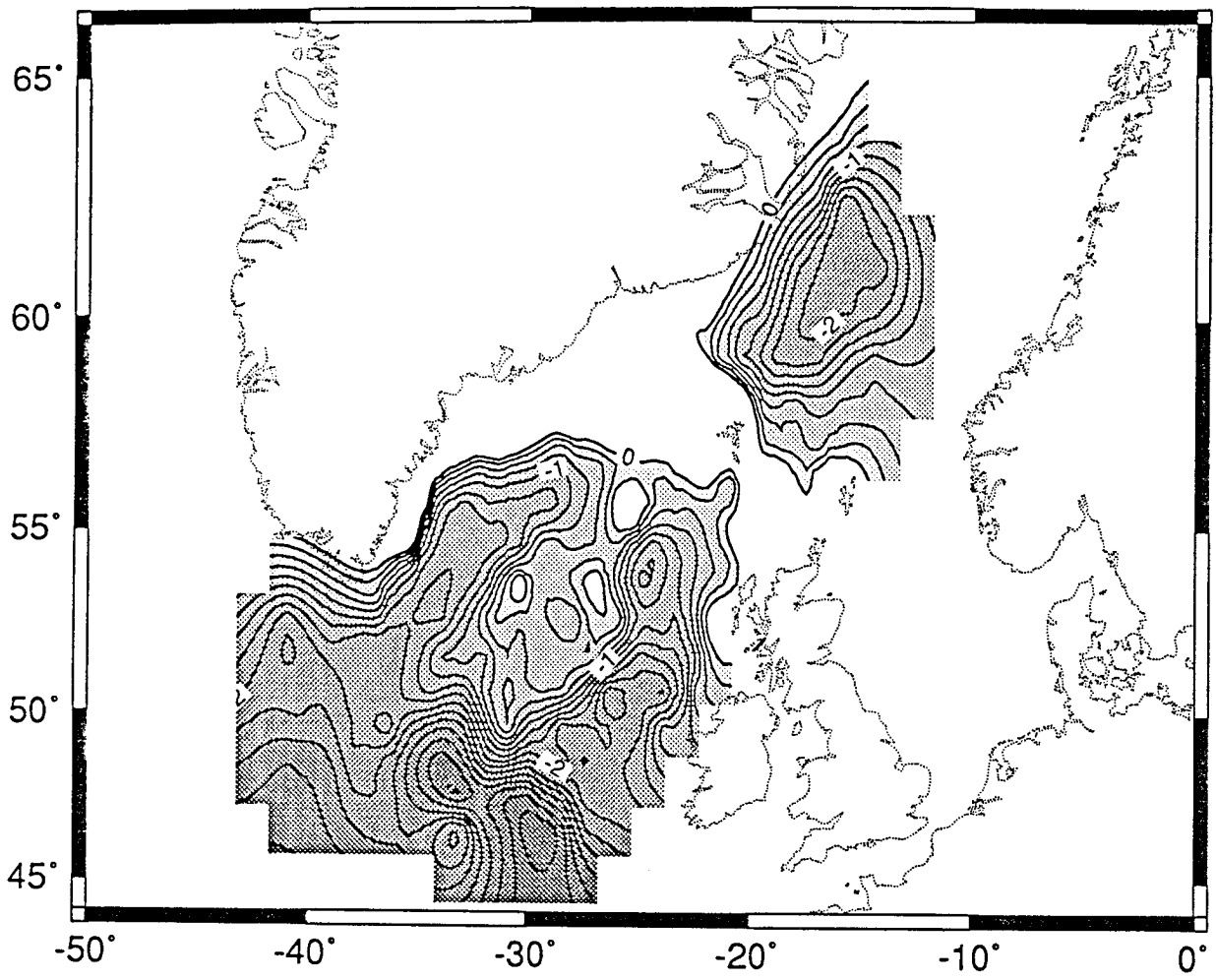

Figure 3.13A

50 Ma - Reconstructed Paleobathymetry

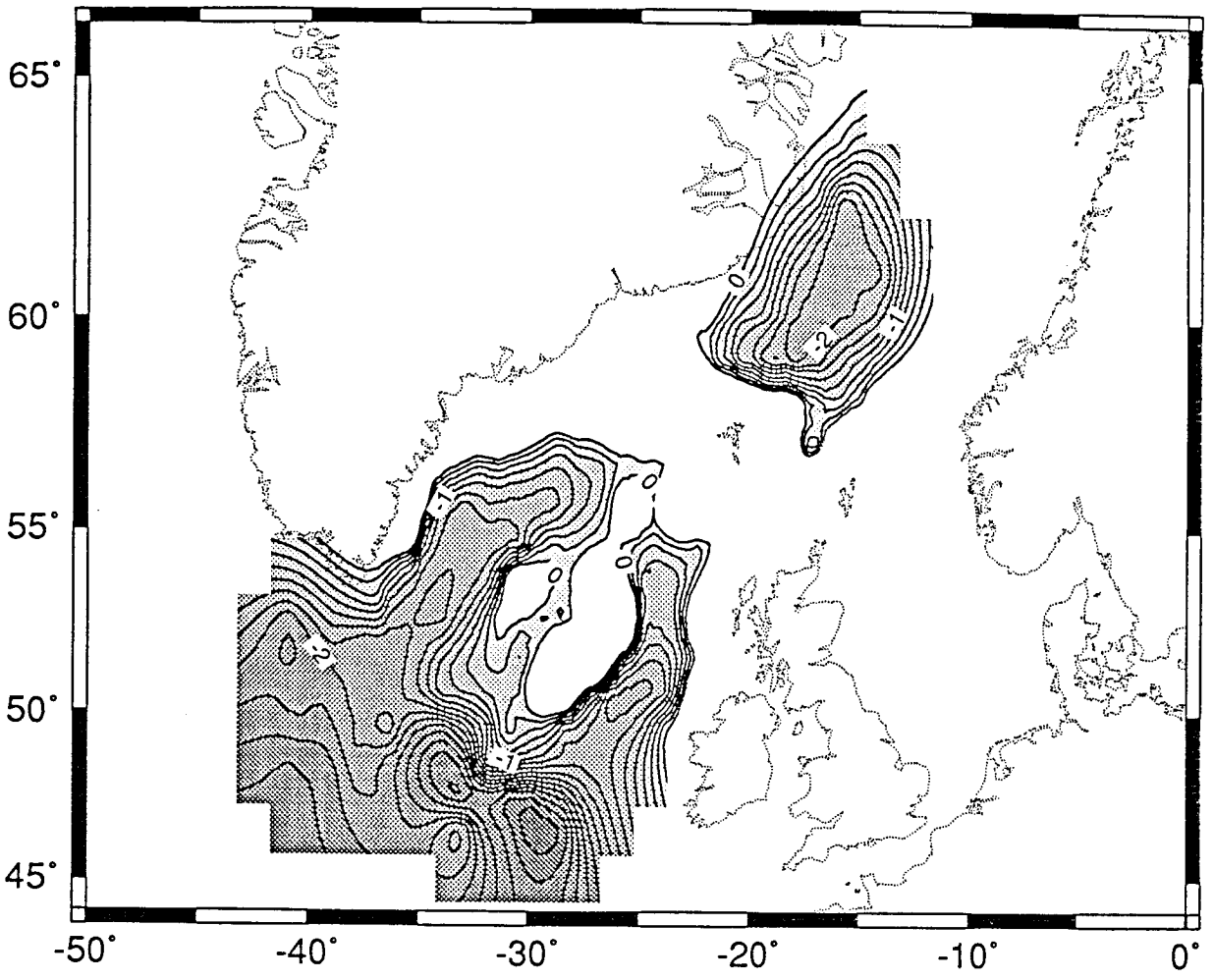

Figure 3.13B

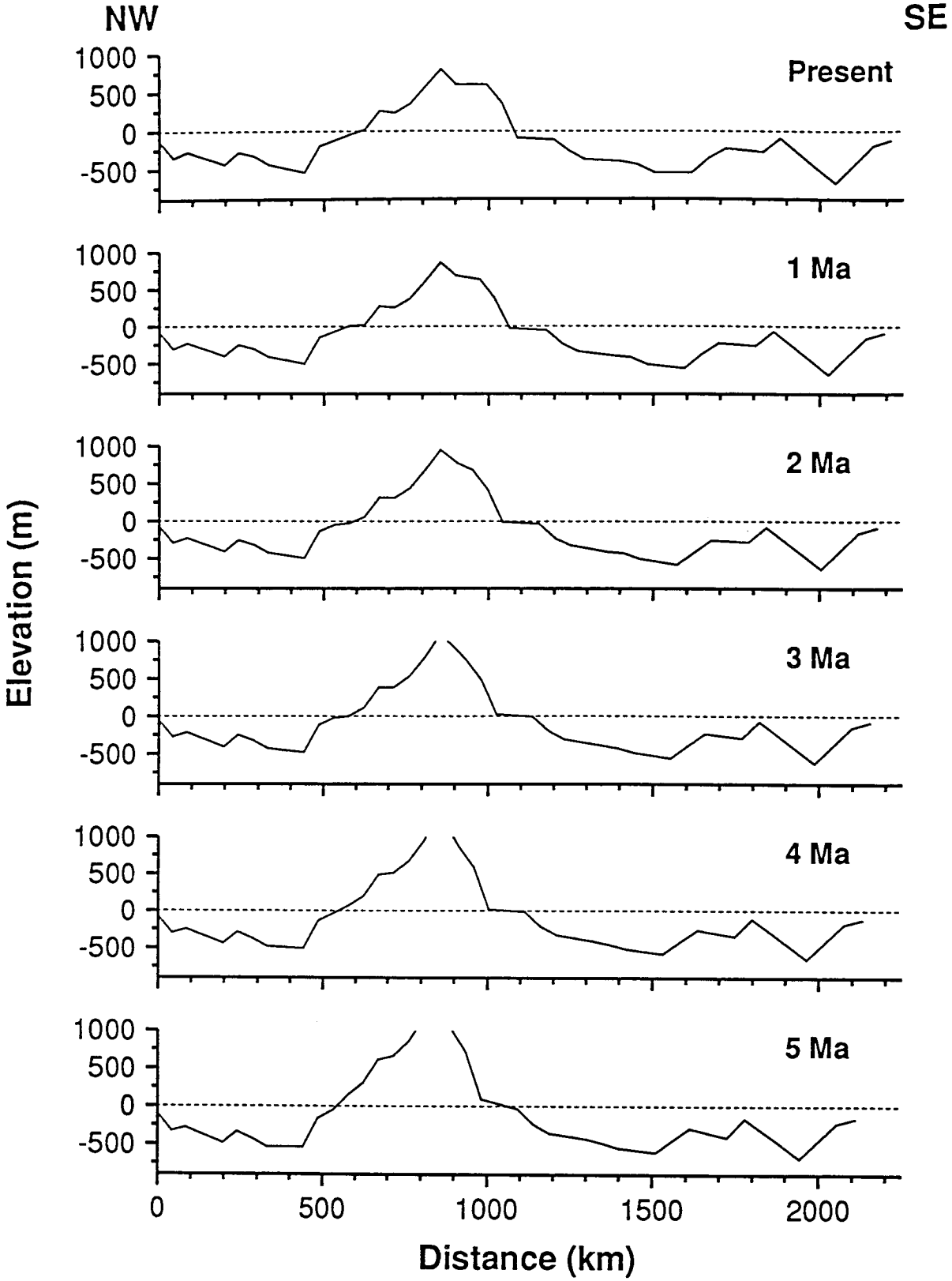
NW
SE
Present
1 Ma
2 Ma
3 Ma
4 Ma
5 Ma
1000
500
0
-500
Elevation (m)
0
500
1000
1500
2000
Distance (km)

Figure 3.14A

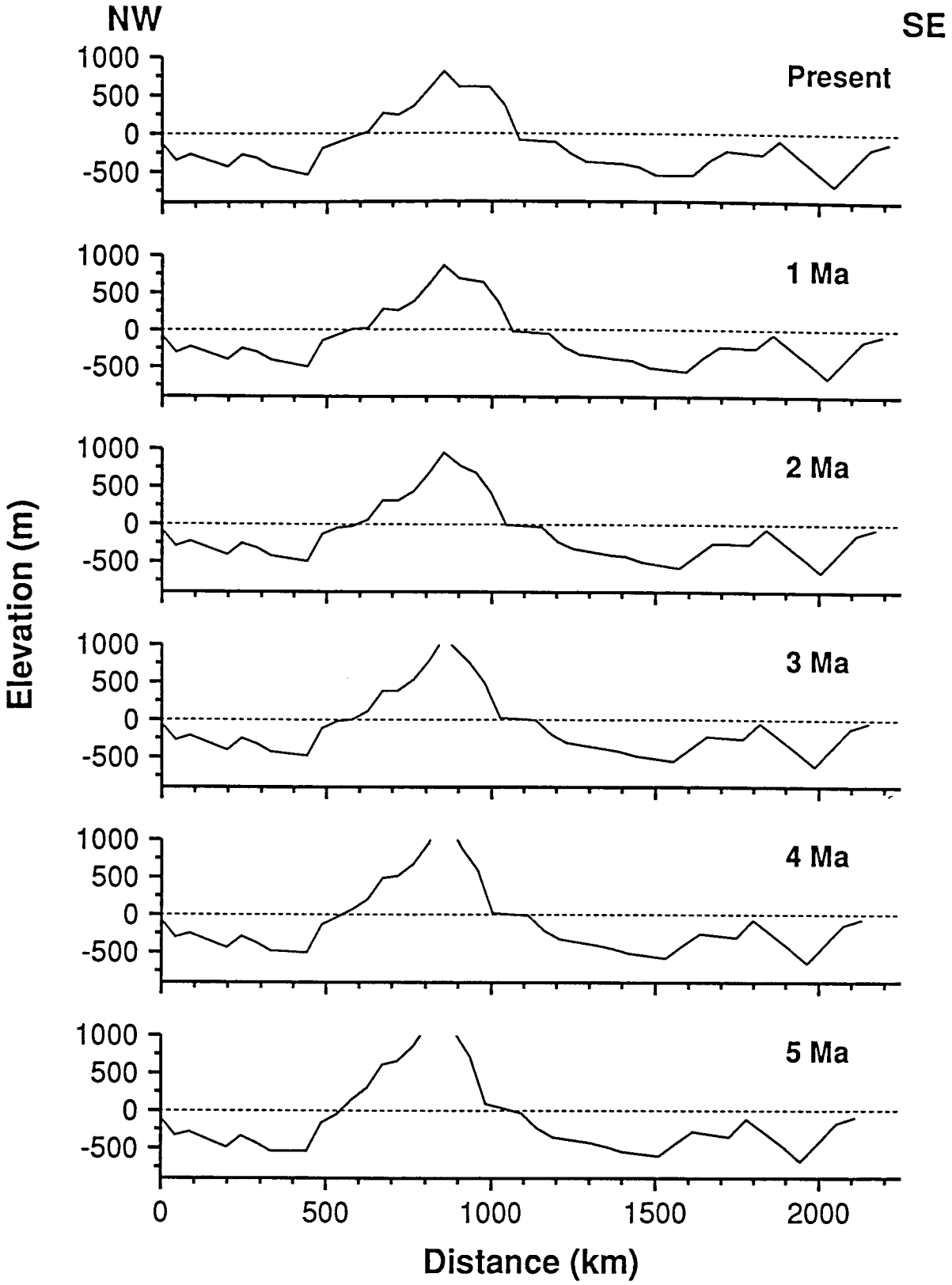
NW
SE
Present
1 Ma
2 Ma
3 Ma
4 Ma
5 Ma
1000
500
0
-500
Elevation (m)
0
500
1000
1500
2000
Distance (km)

Figure 3.14B

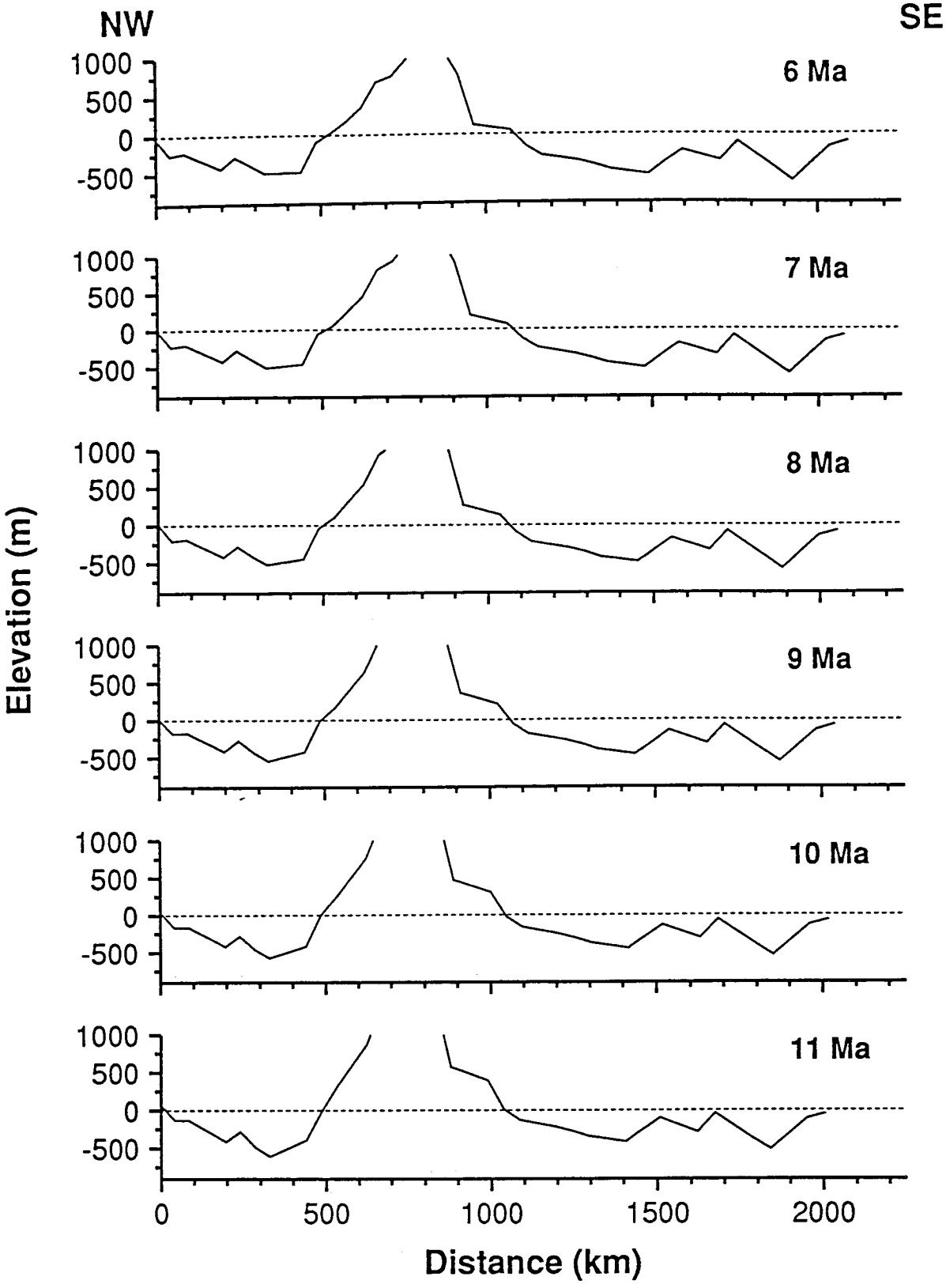
NW
SE
6 Ma
7 Ma
8 Ma
9 Ma
10 Ma
11 Ma
1000
500
0
-500
Elevation (m)
0
500
1000
1500
2000
Distance (km)

Figure 3.15A

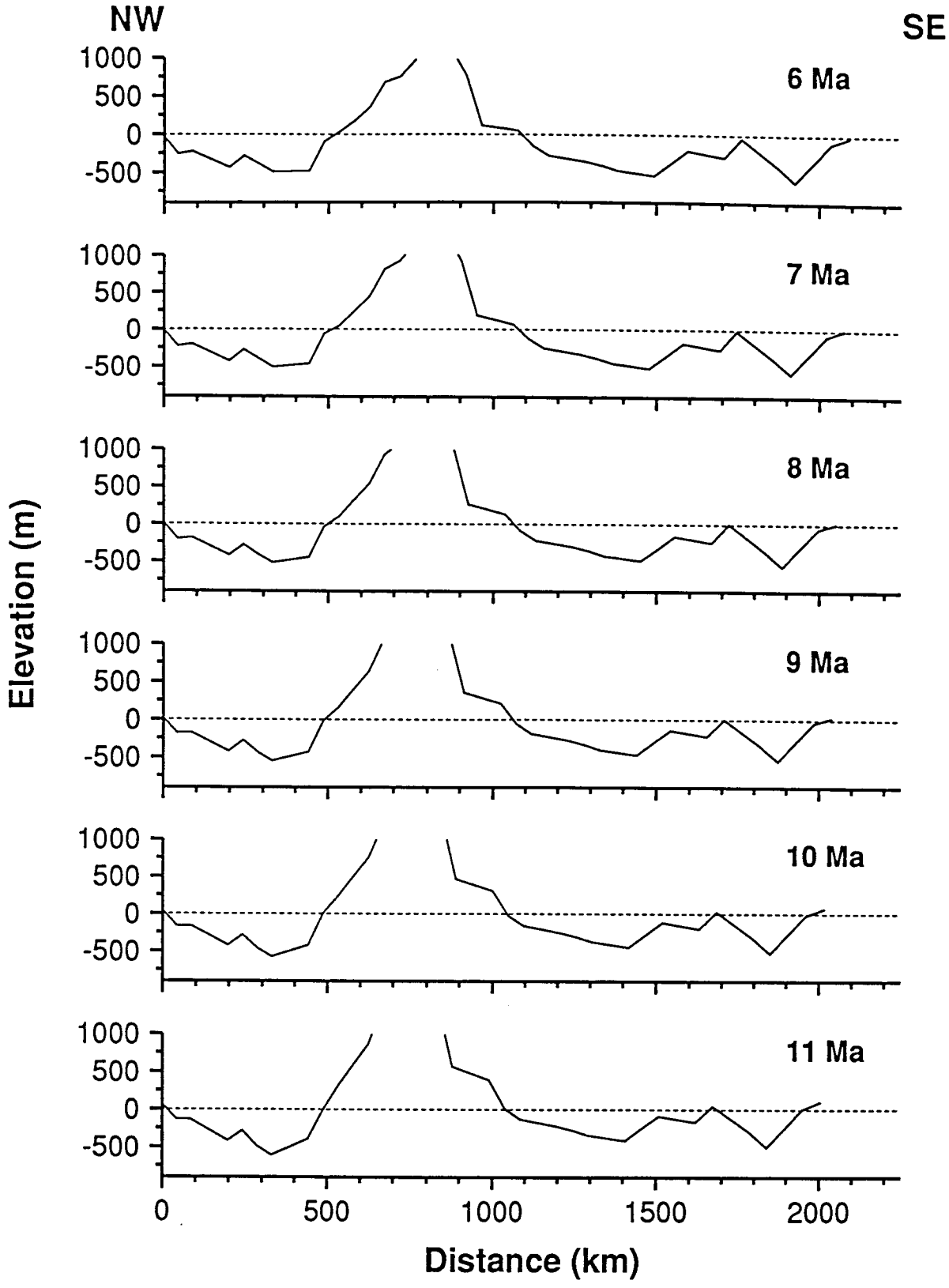
NW
SE
6 Ma
7 Ma
8 Ma
9 Ma
10 Ma
11 Ma
1000
500
0
-500
Elevation (m)
0
500
1000
1500
2000
Distance (km)

Figure 3.15B

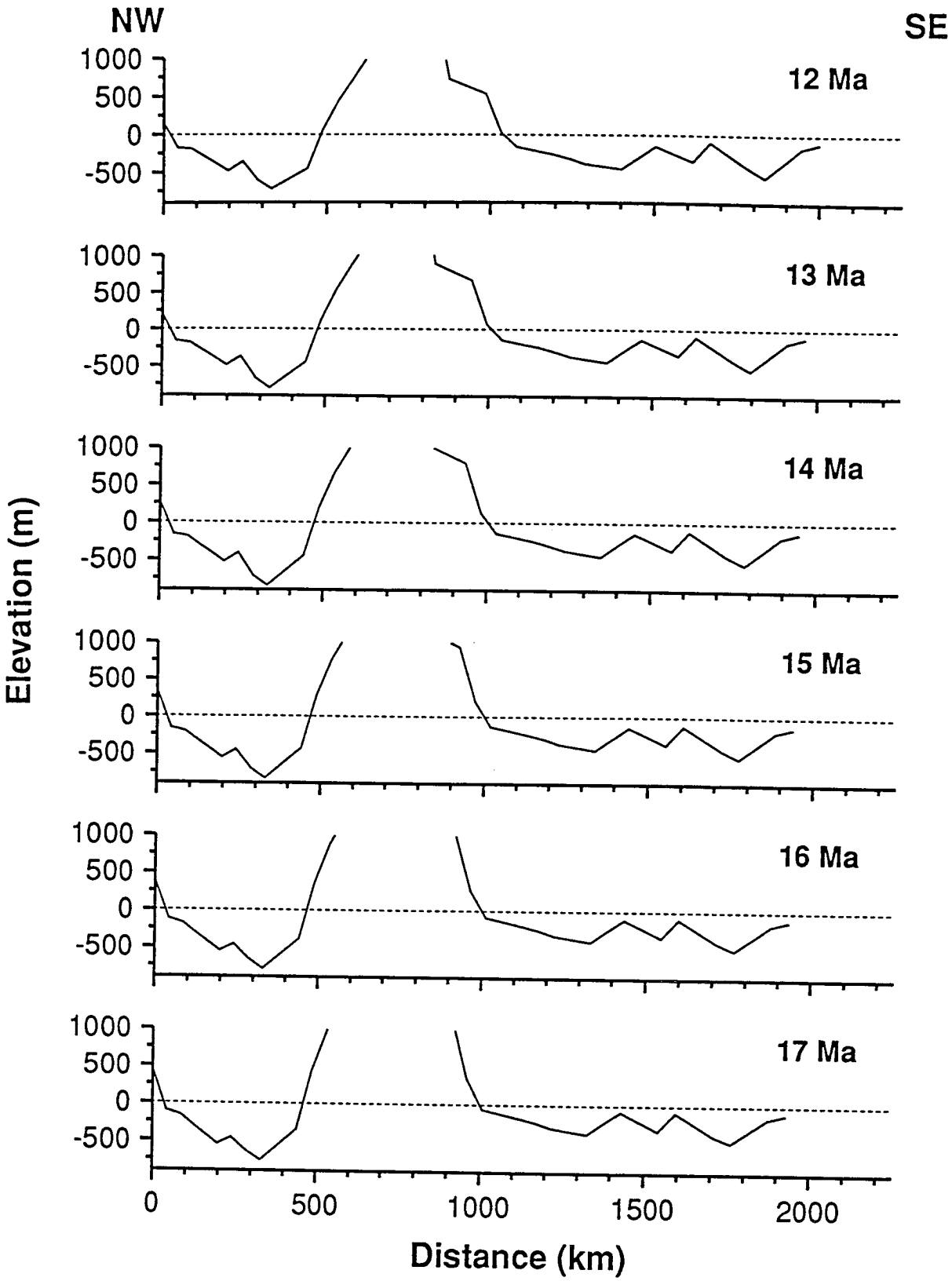
NW
SE
12 Ma
13 Ma
14 Ma
15 Ma
16 Ma
17 Ma
1000
500
0
-500
Elevation (m)
0
500
1000
1500
2000
Distance (km)

Figure 3.16A

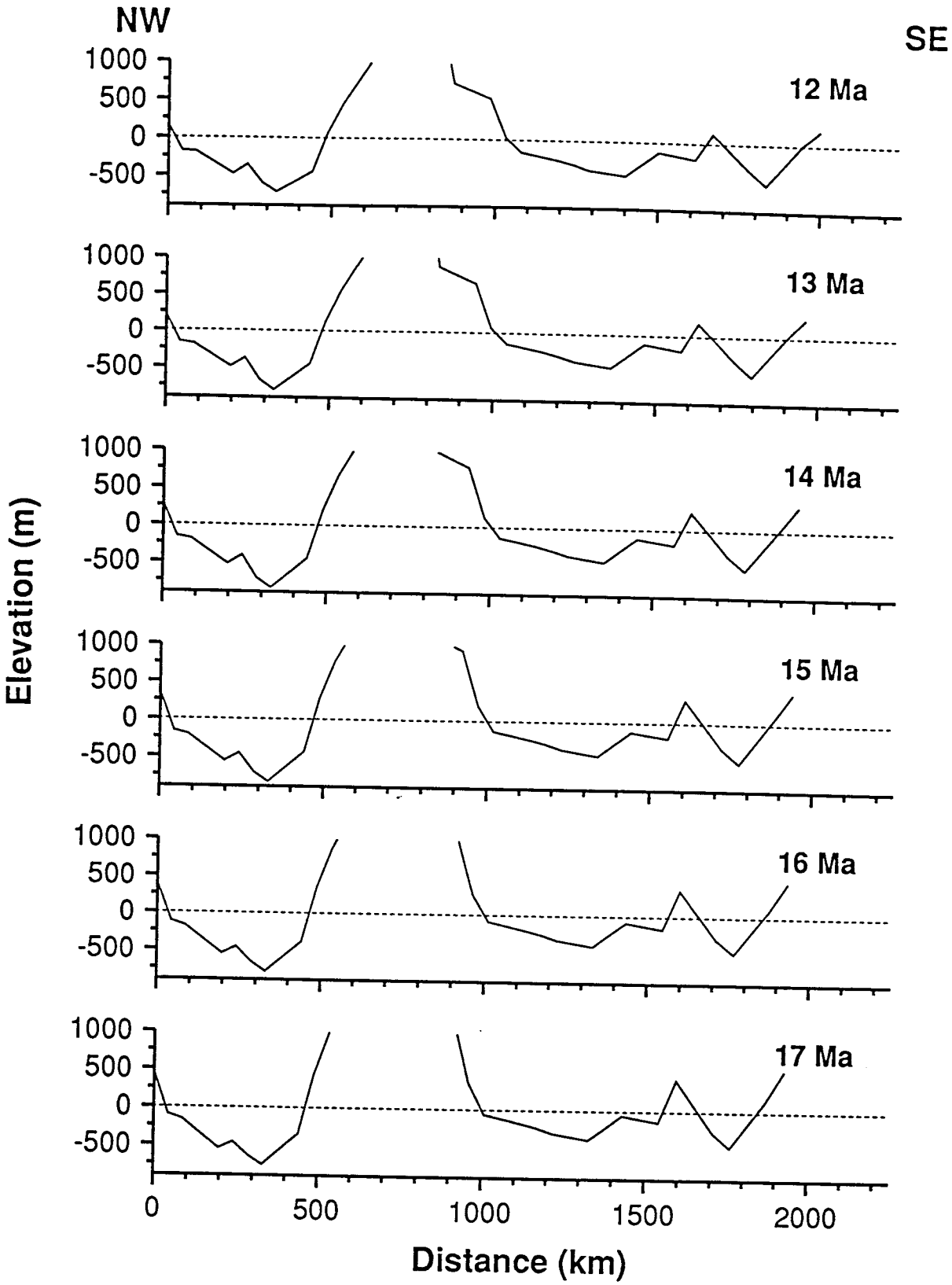
NW
SE
1000
500
0
-500
12 Ma
13 Ma
14 Ma
15 Ma
16 Ma
17 Ma
Elevation (m)
0
500
1000
1500
2000
Distance (km)

Figure 3.16B

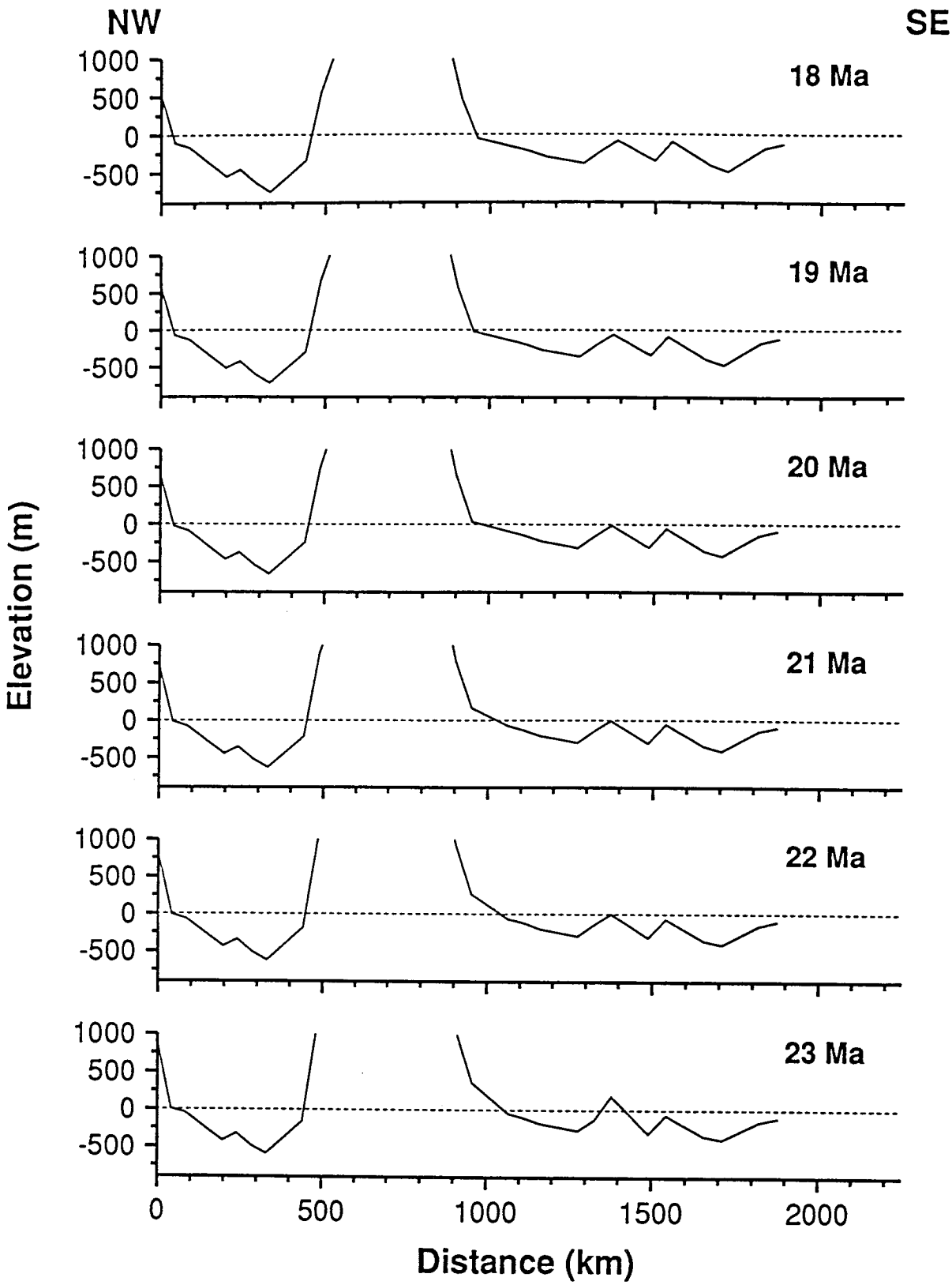
NW
SE
18 Ma
19 Ma
20 Ma
21 Ma
22 Ma
23 Ma
1000
500
0
-500
Elevation (m)
0
500
1000
1500
2000
Distance (km)

Figure 3.17A

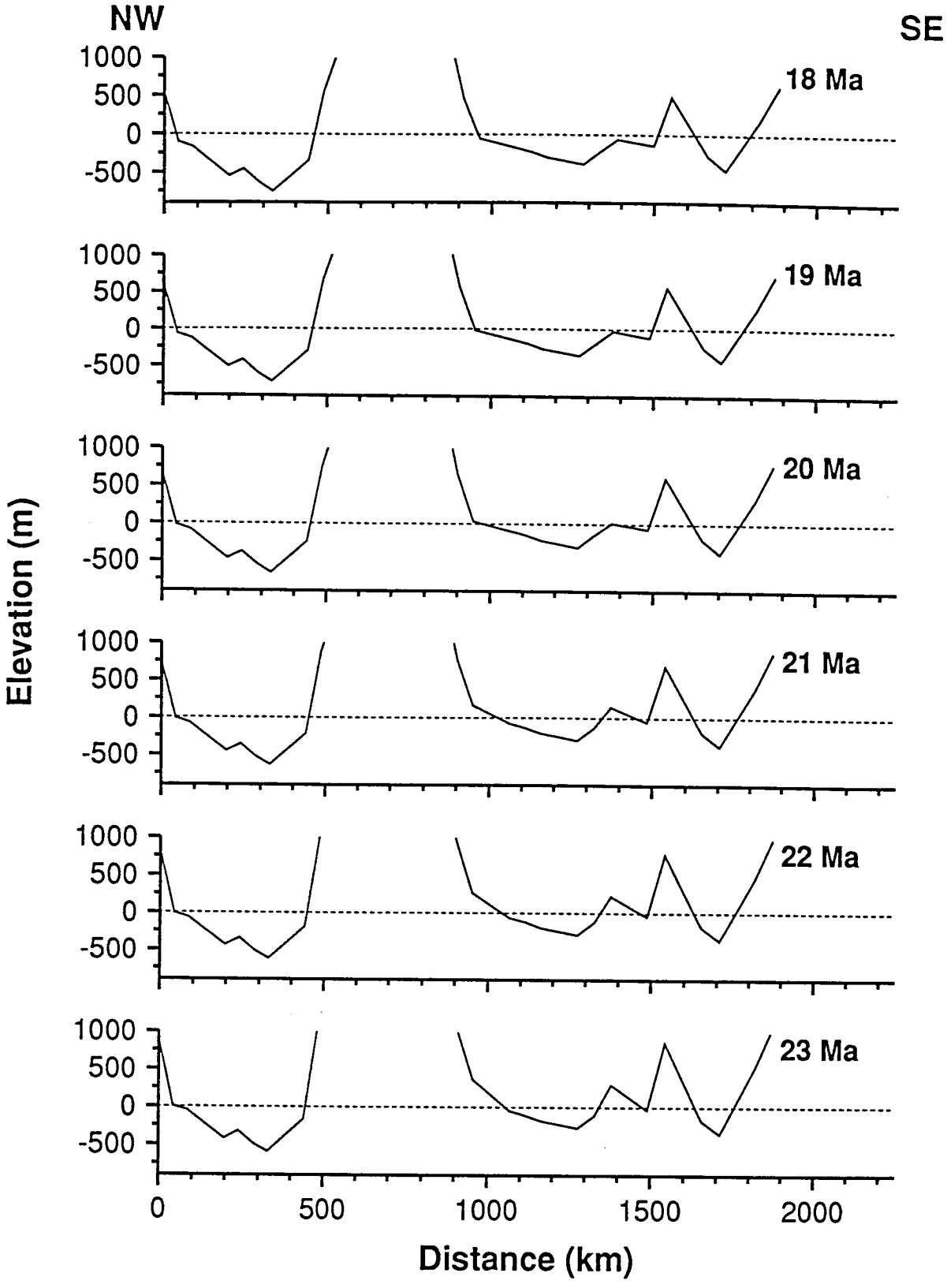
NW
SE
1000
500
0
-500
18 Ma
19 Ma
20 Ma
21 Ma
22 Ma
23 Ma
Elevation (m)
0
500
1000
1500
2000
Distance (km)

Figure 3.17B

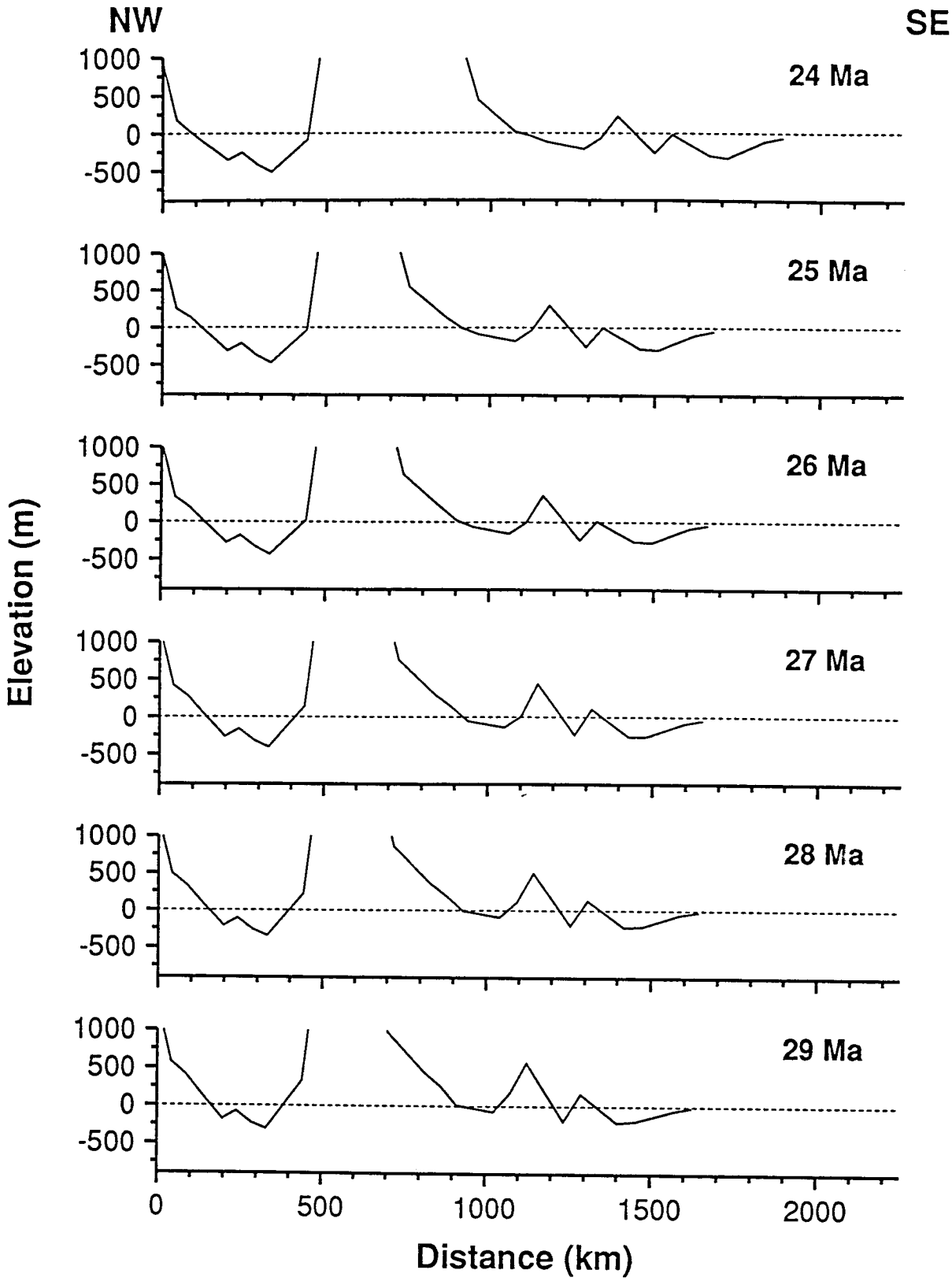
NW
SE
24 Ma
25 Ma
26 Ma
27 Ma
28 Ma
29 Ma
1000
500
0
-500
Elevation (m)
0
500
1000
1500
2000
Distance (km)

Figure 3.18A

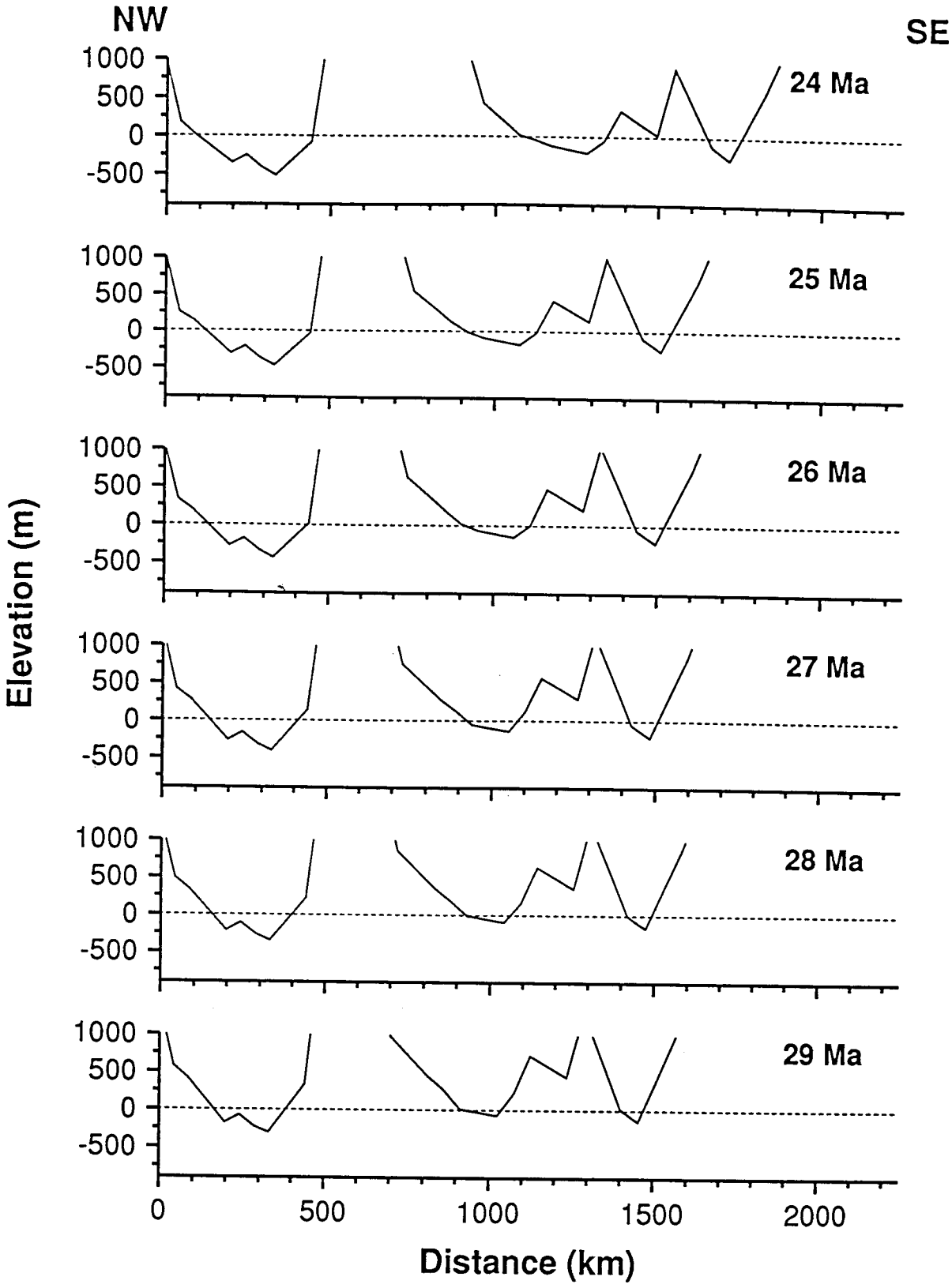
NW
SE
1000
500
0
-500
24 Ma
25 Ma
26 Ma
27 Ma
28 Ma
29 Ma
Elevation (m)
0
500
1000
1500
2000
Distance (km)

Figure 3.18B

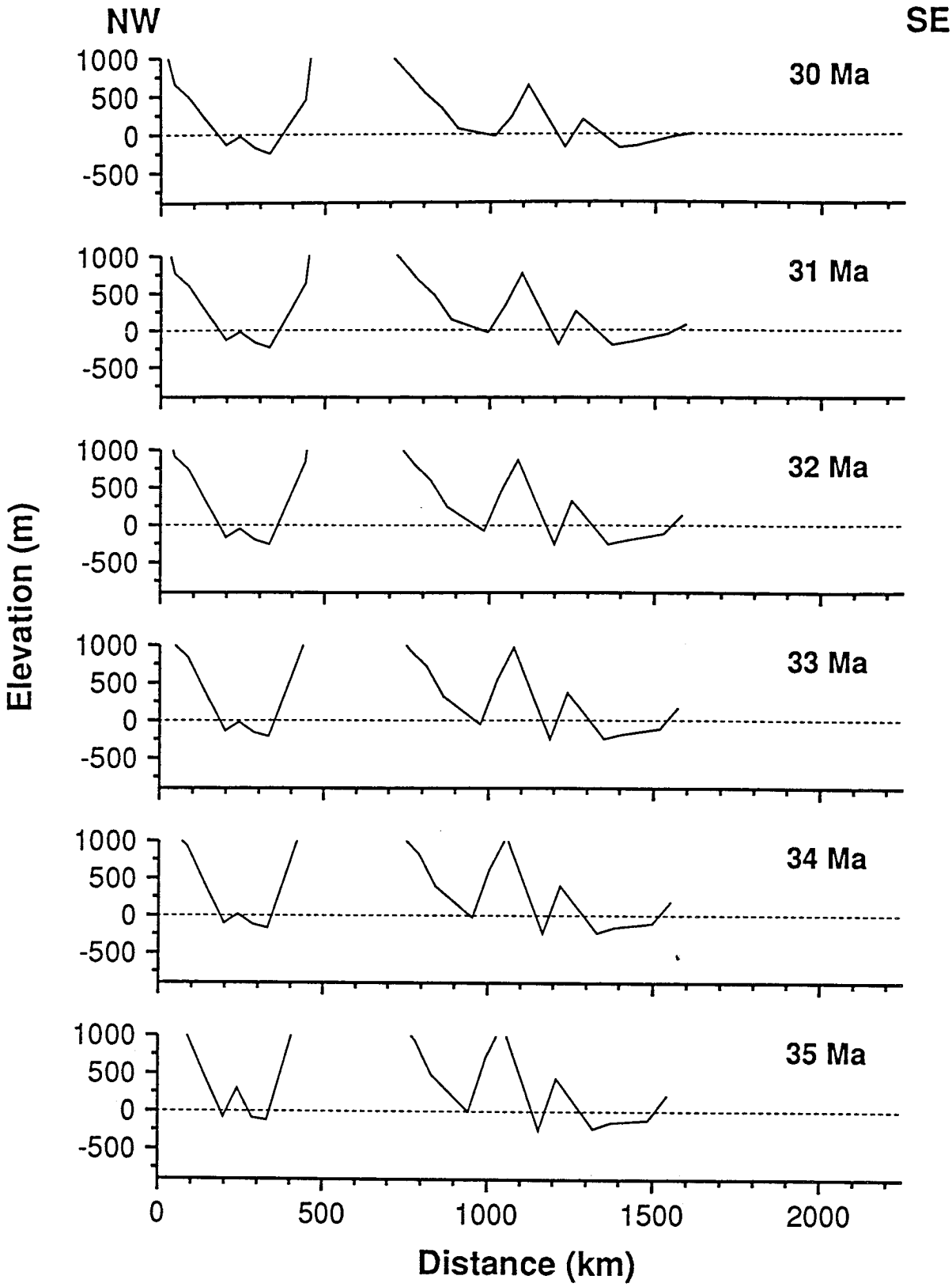
NW
SE
30 Ma
31 Ma
32 Ma
33 Ma
34 Ma
35 Ma
1000
500
0
-500
Elevation (m)
0
500
1000
1500
2000
Distance (km)

Figure 3.19A

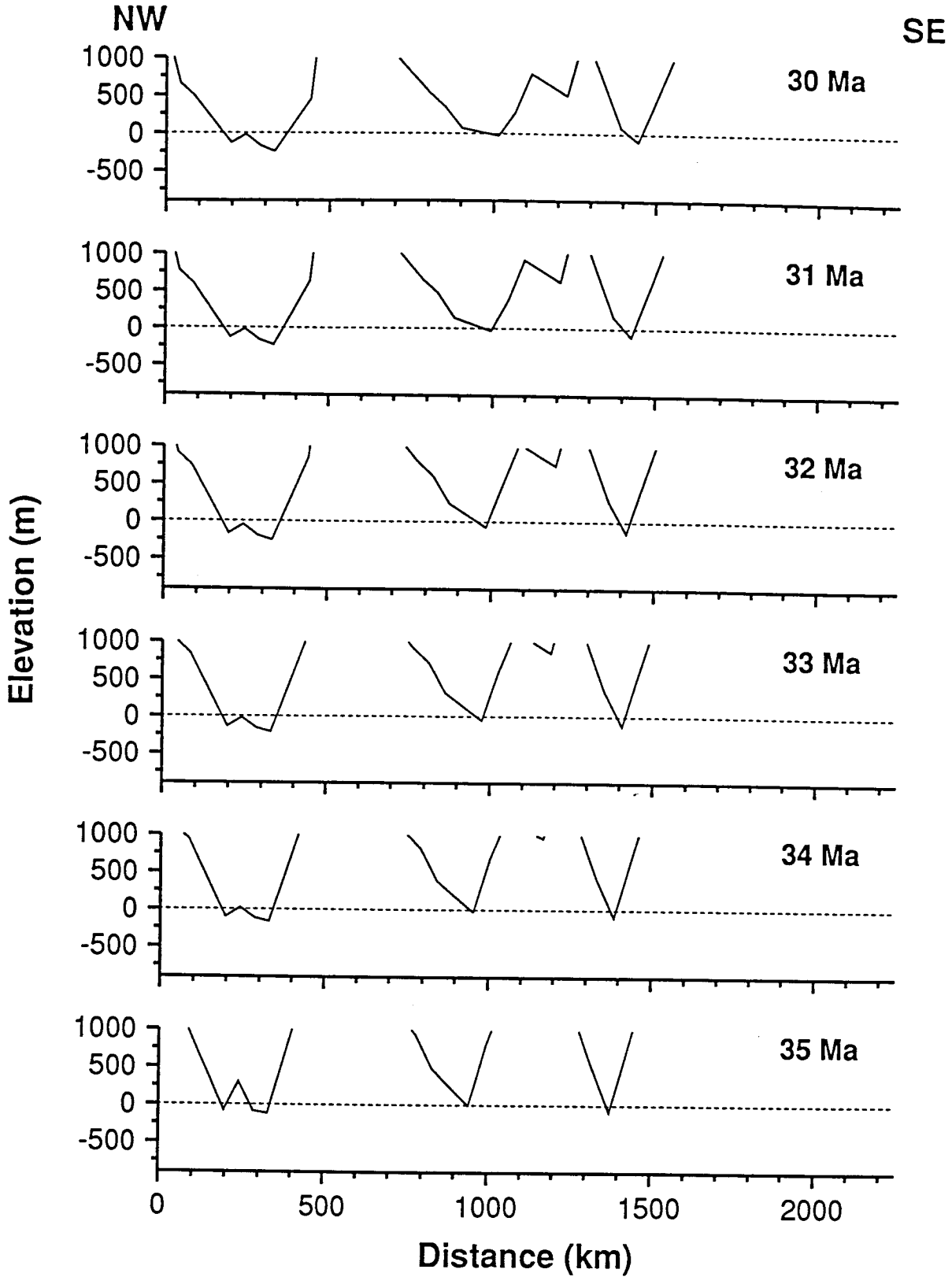
NW
SE
1000
500
0
-500
30 Ma
31 Ma
32 Ma
33 Ma
34 Ma
35 Ma
Elevation (m)
0
500
1000
1500
2000
Distance (km)

Figure 3.19B

Chron	Age, Ma	Lat.	Long.	Angle	Source
		Greenland Relative to North America			
	35.00	-	-	-	7,8,4,9
20	44.66	-62.10	119.37	3.19	1
21	48.75	-61.71	110.51	4.42	1
24	55.14	-5.36	18.33	2.03	1
25	58.64	-24.48	42.75	3.12	2
31	69.00	-43.94	34.69	4.92	2
		Jan Mayen Relative to Eurasia			
7	25.50	-	-	-	3
13	35.29	64.9	-12.3	-8.0	3
		Jan Mayen Relative to Greenland			
20	44.66	77.61	-3.3	-32.82	1
		Eurasia Relative to Greenland			
5	8.92	68.00	137.00	-2.50	4
6	19.35	68.94	135.30	-5.09	1
7	25.50	67.05	128.95	-5.85	5
13	35.29	68.00	129.90	-7.78	4
20	44.66	48.92	134.88	-8.10	1
21	48.75	69.44	137.86	-11.15	1
24	55.14	46.78	126.85	-10.50	4
fit	57.50	41.70	124.50	-10.15	6

Table 3.1. Total reconstruction poles for Greenland, Europe and Jan Mayen. Data sources: [1]Wold, this work; [2]Roest and Srivastava (1991); [3]Nunns (1983); [4]Srivastava and Tapscott (1986); [5]Bott (1985); [6]Talwani and Eldholm (1977); [7]Vogt and Avery (1974); [8]Emery and Uchupi (9184); [9]Srivastava and Arthur (1989).

North American Paleolatitude

Age, Ma	Lat.	Long.	Angle
20	0	61.1	4.1
30	0	67.7	5.3
40	0	75.4	6.6
50	0	88.2	6.9
60	0	93.8	10.0

Table 3.2. Total reconstructions poles for North America paleolatitude. These values were derived from the Harrison and Lindh (1982) apparent polar wander curve for North America.

Chapter 4: Cenozoic Sediment Accumulations

4.1 Introduction

Having reconstructed the paleobathymetry and used the information from mass/age distributions to develop hypotheses concerning the geologic history of the region, the distribution of the sediments can be plotted and further analyzed to test the tentative conclusions reached in Chapter 3. The region with sediment drifts between the Charlie Gibbs Fracture Zone and the Greenland-Scotland Ridge should contain most of the evidence for deep water circulation. As described in Chapter 2, the area has been divided into 1 x 1° grid cells. The stratigraphy and lithology of the sedimentary rocks in each grid cell was derived from Reports of the Deep Sea Drilling Project (DSDP) and Ocean Drilling Project (ODP), from other literature sources, and from single-channel seismic reflection profiles (Fig. 4.1) distributed by the Marine Geophysics Section of the NOAA (U.S. National Oceanographic and Atmospheric Administration) National Geophysical Data Center (Boulder, Colorado).

4.2 Deep-Water Sediment of the Northern North Atlantic

Deep-water fine-grained sediments can be divided into three main facies groups: fine-grained turbidites, pelagites and hemipelagites, and muddy contourites (Stow and Piper, 1984). Turbidites and contourites, as the terrigenous components of deep sea sediments, make up about half of the total sediment mass in the ocean basins (Hay et al., 1988).

Deposition of sediment drifts is driven by intense thermohaline circulation and the location of sediment drifts is controlled by pre-existing topography and sediment supply. Terrigenous sediment input to ocean basins along continental margins is an important source of material for drift accumulation. At present sediment drifts occur mostly along continental margins on the western sides of the ocean basins. They result from the intensification of the equatorially directed thermohaline circulation in response to the Coriolis Force. The equatorward-flowing currents hug the margin and flow along the slope as contour currents. These currents can erode and transport material and deposit the sediment as drifts.

Large sediment drifts occur along the eastern flanks of the present active spreading center in the North Atlantic, the Reykjanes Ridge (Bjorn and Gardar Drifts), and on the eastern flank of the continental fragment, Rockall-Hatton Bank (Feni Drift). For Gardar Drift the main sediment source since the Late Miocene has been eroded and redeposited pelagic sediment (Kidd and Hill, 1987). As evidenced from DSDP Site 114 (Laughton, Berggren et al., 1972) Bjorn Drift is composed of terrigenous silt probably derived from erosion of Iceland basalts (McCave and Tucholke, 1986). The deposition of Gardar and Bjorn Drifts is controlled by southward flowing Norwegian Sea Overflow Water (NSOW) and North Atlantic Deep Water (NADW) held against the slope by the Coriolis Force (Fig. 4.2). Early Miocene to recent sediment in Feni Drift is mostly pelagic (Kidd and Hill, 1987). This sediment was probably eroded from the northern Rockall Trough and Faeroe-Shetland Channel by southward flowing Wyville-Thompson Ridge Overflow Water (WTROW), a component of the Norwegian Sea Overflow.

Two moderately large sediment drifts have formed off the south ends of two continental blocks, Rockall-Hatton Bank (South Feni Drift), and Greenland (Eirik Drift). These have formed where sediment is deposited when the Coriolis Force causes the southward flowing current on the eastern margin of these features to turn back northward to flow along their western margins (Fig. 4.2). The thick accumulation of sediment in Eirik Drift is derived from sediment eroded from the Denmark Strait and eastern Greenland margin suspended in Denmark Strait Overflow Water. This combines with North Atlantic Deep Water to flow south along the eastern Greenland margin (Fig. 4.2).

Small sediment drifts occur on the western side of Rockall-Hatton Bank (Hatton Drift) and Reykjanes Ridge (Snorri Drift). The currents depositing them are the northward flowing continuation of the flows that have rounded the southern ends of Rockall-Hatton Bank and Reykjanes Ridge respectively (Fig. 4.2). The combined effect of the Coriolis Force and topography directs the current to the right and causes the initial southward flows to turn northward along the western sides of the rises.

A small, isolated feature south of Greenland, Gloria Drift, appears to derive its sediment from a small portion of NADW that continues to flow west instead of north after crossing the Mid-Atlantic Ridge through the Charlie Gibbs Fracture Zone.

The gross morphology of sediment drifts (Fig. 4.3) was described by McCave and Tucholke (1986) who suggested a classification as: 1) double drifts with subparallel crests,

one located higher and the other lower on a slope and presumably generated by a contour current flowing between them (eg. Bjorn and Gardar Drifts); 2) plastered drifts that are elongate, lens-shaped and lie along depth contours on rises, presumably generated by upslope transport of sediment by a bottom current flowing along the base of the slope (Hatton and North Feni Drift); 3) detached drifts that extend from a rise out into an ocean basin marking the place where the Coriolis Force causes a bottom-water current to reverse its course (Eirik, South Feni, Isengard and the southern end of Gardar Drifts); and 4) separated drifts where an abyssal current is concentrated in a narrow channel between a platform and the crest of the drift (Caicos Drift north of Puerto Rico, no drifts of this type have been identified in the region discussed here).

4.3 Sediment Drifts between the Charlie Gibbs Fracture Zone and Greenland-Scotland Ridge

The most prominent sedimentary features between the Charlie Gibbs Fracture Zone and Greenland-Scotland Ridge are the sediment drifts. As noted by McCave and Tucholke (1986), they are most easily recognized in single-channel seismic profiles by mud waves on their surfaces (eg. Feni, Gardar and Gloria Drifts) and by their multiple high-amplitude parallel to subparallel seismic reflectors (eg. Eirik Drift). The present areal extent of sediment drifts between Charlie Gibbs Fracture Zone and Greenland-Scotland Ridge has been interpreted from single-channel seismic reflection profiles (Fig. 4.9). The area, volume, mass and age of each of the drifts in this region has been calculated (Table 4.1).

Feni Drift (Johnson and Schneider, 1969; Jones et al., 1970) is located on the western margin of Rockall Trough. It was drilled at DSDP Site 610 (Ruddiman, Kidd, Thomas et al., 1987) and the upper Lower Miocene "green reflector" of Masson and Kidd (1987) was just penetrated. The average sedimentation rate for Lower Miocene through Quaternary sediment in Feni Drift is 4.6 to 5.1 cm $k.y.^{-1}$. The sediments are mainly pelagic and consist of pelagic ooze and calcareous mud (Kidd and Hill, 1986). Masson and Kidd (1987) correlated their "green reflector" with reflector "R2" of Miller and Tucholke (1983). They found it to mark an opal layer in the sediment, suggesting that it may have been caused by an episode of increased production of biogenic silica. From multichannel seismic data Kidd and Hill (1987) interpreted the onset of sedimentation on Feni Drift to correspond to their "brown reflector"

which they believed to be as old as late Eocene to early Oligocene. The "brown reflector" may correlate with Miller and Tucholke's (1983) "R4" reflector, thought to mark a Upper Eocene to Lower Oligocene unconformity along the margins of northern North Atlantic ocean basins (Miller and Tucholke, 1983). There are two sediment ridges on the southern portion of South Feni Drift (Fig. 4.5). The eastern ridge crest is smaller than the main crest to the west. The eastern ridge crest is only developed on Feni Drift in the southern part of Rockall Trough. Further north the eastern ridge crest disappears and there is only a single ridge crest on Feni Drift. In North Feni Drift the western ridge crest disappears and Feni Drift becomes plastered against the eastern margin of Rockall Bank.

From the differential rates of accumulation and varying thicknesses of sediment layers in Hatton Drift (Ruddiman, 1972) on the western margin of Hatton Bank, Stow and Holbrook (1984) concluded that deposition has been influenced by abyssal circulation since the Early Eocene, but that until the mid-Miocene the currents were too strong to allow the drift to accumulate. The age of initiation of Hatton Drift is thus assumed to be early Middle Miocene. The present bottom-water that flows north along Hatton Drift is mainly NSOW that overflowed the Iceland-Scotland Ridge but includes a component of Antarctic Bottom Water (AABW) (McCave et al., 1980). Hatton Drift is a plastered drift (McCave and Tucholke, 1986) on the relatively steep western margin of Rockall Plateau west of Hatton Bank (Fig. 4.6). The drift extends along the entire western margin of Rockall Plateau (Fig. 4.4), is narrow compared to its length and is lens-shaped in cross-section (Fig. 4.6).

Bjorn and Gardar Drifts lie along the eastern flank of Reykjanes Ridge. Bjorn Drift (Laughton, Berggren et al., 1972) occupies a position high on the ridge, at an average depth of about 1800 m. Gardar Drift (Johnson and Schneider, 1969) lies further down the flank of Reykjanes Ridge at a depth of about 2800 m and extends into the South Iceland Basin. The crests of these two drifts merge south of 57° N latitude (Figure 8 of Kidd and Hill, 1987). Considered together they comprise the largest drift complex between the Charlie Gibbs Fracture Zone and Greenland-Scotland Ridge. Bjorn Drift was drilled on DSDP Leg 12 at Site 114 (Laughton, Berggren et al., 1972) and the southern tip of Gardar Drift was drilled during DSDP Leg 94 at Site 611 (Ruddiman, Kidd, Thomas et al., 1987). At Site 114 the stratigraphic section through Bjorn Drift consists of Pleistocene and Pliocene terrigenous clayey silts, and the average sedimentation rate is 12 cm $k.y.^{-1}$ (Laughton, Berggren et al., 1972). At Site 611 on Gardar Drift the section consists of Pleistocene to Late Pliocene

calcareous muds with some ice-rafted material and lower Pliocene to Miocene oozes and chalks; the average sedimentation rate is 5.8 cm k.y.$^{-1}$ (Ruddiman, Kidd, Thomas et al., 1987). Site 611 did not reach basement but provides evidence of continuous deposition of Gardar Drift since the Late Miocene. The location of the southern portion of Gardar Drift is most clearly defined in single-channel seismic reflection profiles by sediment waves on its surface (Fig. 4.7). High amplitude seismic reflectors within the drift also help to a lesser degree to delineate it. Further to the north sediment waves are not visible on the surface of Gardar Drift (Fig. 4.6). In this region the location of the drift can be interpreted from single-channel seismic reflection profiles by the location of the crest of the drift and from sediment thickness profiles that are unrelated to basement topography (Fig 4.6). It is possible that Gardar and Bjorn Drifts are deposited directly on basement (Kidd and Hill, 1986) and have been accumulating sediment continuously since the Late Eocene. However, McCave et al. (1980) indicate in a cross-sectional sketch of Gardar Drift that it lies on older pre-drift sediment. From interpretation of single-channel seismic profiles it appears that Gardar Drift began to accumulate above the late Early Miocene "IR" seismic reflector of Ruddiman (1972) which corresponds to the R2 reflector of Miller and Tucholke (1983).

Sediment waves on the surface of Gloria Drift (Egloff and Johnson, 1975) are apparent in seismic reflection profiles (Figs. 4.8 and 4.9) and serve as the primary means to distinguish this drift from the surrounding sediments. The internal reflectors in Gloria Drift have a smaller amplitude than those in Eirik Drift and are more difficult to recognize (Fig. 4.8). In cross-section (Fig. 4.9) Gloria Drift appears to be very thin and its surface topography generally parallels the basement. The bottom current responsible for the deposition of Gloria Drift is North West Atlantic Deep Water (NWADW) that flows from the northeastern North Atlantic through the Charlie Gibbs Fracture Zone and continues to the west over Gloria Drift (McCave and Tucholke, 1986). Drilling at DSDP Site 647 (Srivastava, Arthur, Clement et al., 1987) and evidence from seismic stratigraphy (Arthur et al., 1989) conclude that Gloria Drift began to accumulate in the Pliocene. Beneath the drift are Lower Oligocene to Lower Eocene sediments having an apparent sedimentation rate of 3.6 cm k.y.$^{-1}$. The Pliocene and Quaternary sediments of Gloria Drift are dominantly terrigenous, with ice-rafted debris. The average sedimentation rate of the drift sediments is 4.6 cm k.y.$^{-1}$.

The areal extent of Snorri Drift (Egloff and Johnson, 1979) on the western flank of Reykjanes Ridge in the Irminger Basin was difficult to determine from seismic profiles because of poor areal coverage of the profiles and because the drift does not have the well defined morphology typical of larger drifts. The indistinct morphology of Snorri Drift could be due to a low sediment supply. The contour current on the west side of the South Iceland Basin flows south along the eastern side of Reykjanes Ridge until the ridge crest is deep enough for the current to cross the ridge and turn north to flow along the western side of Reykjanes Ridge, over Snorri Drift (Fig. 4.2). It is this flow of NWADW that originated from Iceland-Scotland Overflow Water and NADW east of Reykjanes Ridge that transports sediment to Snorri Drift.

Eirik Drift (Johnson and Schneider, 1969) off the southern tip of Greenland is distinguished from the surrounding sediment in single channel seismic profiles by the reflection characteristics of its seismic sequences and from the pronounced increase in sediment thickness compared to the surrounding region (Fig. 4.8). Sediment waves on the surface of Eirik Drift are not apparent in seismic reflection profiles (Fig. 4.8), but parallel to subparallel internal reflectors are numerous (Arthur et al., 1989). Drilling at ODP site 646 on the northwestern flank of Eirik Drift revealed that accumulation did not begin until the Early Pliocene and that the most rapid accumulation occurred during the Pliocene (Srivastava, Arthur, Clement et al., 1987). The sediments of the drift are dominantly terrigenous clay and silt. The average Pliocene-Pleistocene sedimentation rate is 8.8 cm k.y.$^{-1}$, almost double the average Late Miocene sedimentation rate of 4.9 cm k.y.$^{-1}$. According to Arthur et al. (1989) initiation of drift accumulation occurred in the Late Miocene and is marked by seismic reflector R2 of Miller and Tucholke (1983). In the eastern North Atlantic R2 is a upper Lower Miocene reflector that marks the base of sediment accumulation in Bjorn and Gardar Drifts. In the western North Atlantic and southern Labrador Sea, however, R2 appears to be of Late Miocene age (Arthur et al., 1989). The reflector does not mark an erosional unconformity, but may represent an increase in carbonate preservation (Arthur et al., 1989). The sediment of the Upper Pliocene to Pleistocene seismic sequence can be traced to ODP Site 647 on the western side of Gloria Drift (Arthur et al., 1989) and consists of terrigenous clays and silts.

There is a boundary condition that can be applied to constrain the maximum age of sediment drifts deposited along the flanks of an active spreading center. The maximum age of the sediment drifts that accumulated along the flanks of Reykjanes Ridge (Bjorn, Gardar

and Snorri) cannot be older than the age of the oceanic basement. This constrains their interpreted areal extent along the path of contour-following bottom currents on the ridge flank and not on the ridge crest. The base of Bjorn and Gardar Drifts is defined by the upper Lower Miocene seismic reflector R2 (Miller and Tucholke, 1983), but Snorri Drift appears to lie directly on the basement. The age of the ocean crust was thus used to constrain the age of Snorri Drift as well as portions of Bjorn and Gardar Drifts that lie on ocean crust younger than R2.

4.4 Present Bottom Water Circulation

At present the dense waters flowing over the Greenland-Scotland Ridge and out of the Labrador and Mediterranean Seas mix to form North Atlantic Deep Water (NADW). Although NADW is a mixture of water from several sources, the flows over the Greenland-Scotland Ridge are, through entrainment of surrounding waters, its most important component (Meincke, 1983). The volume flux of NADW should be approximated by the net amount of deep water exported from the North Atlantic to the Southern hemisphere, but the amount is not exactly known. Philander and Pacanowski (1986) suggest that about 8.5 Sverdrup (Sv; 1 Sv = 1 x 10^6 m^3 s^{-1}) of equatorial water surface is diverted into the North Atlantic. This must be balanced by export of water to the Pacific and Indian Oceans through net evaporation of 0.2 Sv in the North Atlantic (Baumgartner and Reichel, 1975), and the net return flow to the South Atlantic as NADW, which must then be about 8.3 Sv.

Contour-following bottom currents have been the primary mechanism responsible for erosion of pre-existing sediment and deposition of sediment drifts south of the Greenland-Scotland Ridge. These currents presently derive mostly from dense waters formed in the Greenland-Iceland-Norwegian (GIN) Seas overflowing the Greenland-Scotland Ridge. The general term for waters overflowing the Greenland-Scotland Ridge is Norwegian Sea Overflow Water (NSOW), but in reality, the overflows at different points on the Greenland-Scotland Ridge have different temperature-salinity characteristics. The densest water and the largest volume flux flows through the Denmark Strait between Greenland and Iceland. The other major contributions are from the Norwegian Sea flowing through passages between Iceland and the Faeroes and between the Faeroes and Shetlands. The Norwegian Sea outflow is less dense than that from the Greenland Sea. All of these flows are forced against the right-

hand slopes of the basins by the Coriolis force. Peterson and Rooth (1976) noted that none of the water flowing into the North Atlantic across the Greenland-Scotland Ridge is deep water, but all are shallow intermediate waters formed above the main pycnocline. Swift et al. (1980) have shown that the overflow through the Denmark Strait is low salinity Arctic Intermediate Water (AIW) formed in the sea north of Iceland. The overflow waters are denser than the NADW that occupies intermediate levels in the North Atlantic and flow down the slopes into the basins beneath the NADW. Estimates of the magnitude of the different flows varies because of the methods used to calculate them and the lack of direct measurements. Coachman and Aagaard (1974) reported that 2.5 Sv of NSOW overflow the Iceland-Scotland Ridge.

The major flows have been illustrated by McCave and Tucholke (1986, Fig. 4.2). The "upstream" overflows are over the east end of the Greenland-Scotland Ridge. The paths of the most easterly overflows are complex, following narrow bathymetric features (Fig. 4.10). From east to west the overflows are:

4.4.1 Norwegian Sea to Rockall Trough over the Wyville-Thompson Ridge

Some dense Norwegian Sea water flows south through the Faeroe-Shetland Channel and overflows the Wyville-Thompson Ridge (Fig. 4.10), with a sill depth of about 650 m, to descend into Rockall Trough (Wyville-Thompson Ridge Overflow = WTRO of McCave and Tucholke, 1986). The amount that enters Rockall Trough is small compared with the other overflows (Ellett and Martin, 1973; Roberts, 1975). Meincke (1983) estimated its flow rate at 0.3 Sv. From Gorshkov (1977) I estimate that this water has a salinity of 35.1 and a potential temperature of 6° C, and its density (σ_t; sigma-t) estimated using the International Equation of State of Sea Water - 1980 (Millero and Poisson, 1981) is 27.632. Although this is the flow considered responsible for formation of Feni Drift, it should be noted that sediment waves on the surface of Feni Drift are relict features and that present sedimentation on Feni Drift is pelagic and not due to contour-following bottom water currents (Kidd and Hill, 1987). Sedimentation of southern Feni Drift near DSDP Site 611 (Ruddiman, Kidd, Thomas et al., 1987) has been pelagic since about 2.4 Ma preserving sediment waves formed prior to 2.4 Ma (Kidd and Hill, 1987).

4.4.2 Norwegian Sea to the South Iceland Basin via Faeroe Bank Channel

Most of the dense Norwegian Sea water flowing southward through the Faeroe-Shetland Channel continues through the Faeroe Bank Channel between the Faeroe Shelf and Faeroe Bank to descend into the South Iceland Basin (Fig. 4.10). This is presently the deepest of the passages across the Greenland-Scotland Ridge with a sill depth of about 850 m. From Gorshkov (1977) I estimate that this water has a salinity of 35.1, a potential temperature of 3° C and σ_t = 27.965. Warren, (1981) gave the amount of water passing through the Faeroe Bank Channel as about 1 Sv. Meincke estimated the flow to be 1.1 Sv. As it flows down into the South Iceland Basin it entrains another 4 Sv of water to become North-East Atlantic Deep Water (NEADW).

4.4.3 Norwegian Sea to the South Iceland Basin across the Iceland-Faeroe Ridge

Dense Norwegian Sea water also flows over the ridge between Iceland and the Faeroe Islands (Fig. 4.2; Iceland-Scotland Overflow Water = ISOW of McCave and Tucholke, 1986). From Gorshkov (1977) I estimate that this water has the same salinity as Faeroe Bank Overflow Water and WTRO (35.1), a potential temperature of 5° C and σ_t = 27.775. The sill depth over this segment of the Greenland-Scotland Ridge is about 400 m. The volume flux was estimated to be 1 Sv by both Warren (1981) and Meincke (1983).

4.4.4 Iceland Sea to the Irminger Basin via the Denmark Strait

Dense water flows through the Denmark Strait between Greenland and Iceland and descends into the Irminger Basin (Denmark Strait Overflow Water = DSOW of McCave and Tucholke, 1986). This is the densest water flowing over the Greenland-Scotland Ridge and comes from the Iceland Sea. It has a potential temperature of 1° to 2° and a salinity of 34.9. and σ_t is estimated to be 28.025. Peterson and Rooth (1976) observed that it is not Greenland Sea Deep Water that flows over the sill, which presently has a depth just over 600 m, but intermediate water. Swift et al. (1980) noted that the densest water above the sill is Norwegian Sea Deep Water (T< 0° C, S =34.9, σ_t = 28.026) but that this contributes only 10% of the outflow. The major outflow is an intermediate water "of Arctic origin" (Arctic

Intermediate Water) formed at least in part north of Iceland during the winter. The volume flux of bottom water through the Denmark Strait has been estimated at 4 Sv by Warren (1981) and at 2.5 Sv by Meincke (1983). It flows down the slope and along the eastern margin of south Greenland, where, according to Warren (1981) it entrains another 1 Sv of Atlantic water to form North-West Atlantic Bottom Water.

4.4.5 Bottom Currents in the Northern North Atlantic

The Coriolis Force causes each of these bottom currents to flow along contours on the slope to its right. This combines with the unique bathymetric features of the region to produce a complex bottom current system. The flow of WTRO into Rockall Trough hugs the west side of the basin along the margin of Rockall Bank flowing over Feni Drift. On reaching the southern end of Rockall Bank, the current turns to the right, leaving South Feni and Isengard Drifts (Figs. 2.1 and 4.9) as an extension to the south. As it turns west it is joined by a flow of Antarctic Bottom Water (AABW) that enters the eastern basins of the North Atlantic through the equatorial fracture zones and is directed onto the margin of Iberia and Europe. A tongue of AABW is thought to underlie the WTRO and to circulate cyclonically in the deeper part of Rockall Trough (Lonsdale and Hollister, 1979). Both of these water masses flow south over Feni Drift (McCave and Tucholke, 1986). The double ridge observed on South Feni Drift (Fig. 4.3) is probably the result of northward flow of AABW and the combined southward flow of WTRO and AABW. Interaction of NSOW (WTRO) with AABW and NADW have had a combined effect on sedimentation patterns (Kidd and Hill, 1987). The combined currents flow northward along the eastern side of the South Iceland Basin west of Hatton Bank, and over Hatton Drift. At the north end of the Iceland Basin, they are joined by the overflow descending the Faeroe Bank Channel, and the combined flows turn west along the lower slope of the Greenland-Scotland Ridge. As they flow along the Greenland-Scotland Ridge they are joined by overflow between Iceland and the Faeroes. The combined NSOW flows west along the southern side of the Iceland-Faeroe Ridge and entrains another 3 Sv of overlying North Atlantic Water (Warren, 1981) to form North East Atlantic Deep Water (NEADW). The combined flows then turn south along the west side of the South Iceland Basin, the Reykjanes Ridge (Steele et al., 1962; Worthington and Volkmann, 1965), flowing over Bjorn and Gardar Drifts (Worthington and Volkmann, 1965). The crest of the

Reykjanes Ridge descends from Iceland to the Charlie Gibbs Fracture Zone. The combined deep water flows, having acquired a considerable thickness, turn across the Reykjanes Ridge over a broad area near 52° N, with the deepest westward flow passing through the Charlie Gibbs Fracture Zone into the western basin. Some of the deeper water that flows through Charlie Gibbs Fracture Zone continues to flow to the west and may be responsible for the accumulation of sediment in Gloria Drift (McCave and Tucholke, 1986).

After crossing Reykjanes Ridge the combined currents are referred to as Western North Atlantic Deep Water (WNADW). Upon entering the Irminger Basin, the upper part of the flow, with a flux of 5 Sv (Worthington, 1976), turns north along the west side of the Reykjanes Ridge, passing over Snorri Drift. At the north end of the Irminger Basin the waters turn west along the Greenland-Scotland Ridge where they override and mix with the water from the Denmark Strait. South of the Denmark Strait, the DSOW entrains 5 Sv of NWADW (Warren, 1981) to produce a current with a flow rate of 10 Sv (Worthington, 1976; Warren, 1981). The admixture of dense DSOW rejuvenates the current which scours the East Greenland margin at the base of the slope. At the southern tip of Greenland, the Coriolis Force causes the current to reverse its direction to flow north into the Labrador Sea along the west Greenland margin. The loss of velocity associated with the reversal of current direction results in deposition of suspended sediment and the formation of Eirik Drift (McCave and Tucholke, 1986). The NWADW continues into the southern Labrador Sea where it entrains Labrador Sea Deep Water and then flows south along North American margin as the Western Boundary Undercurrent.

Some of the combined flow of 10 Sv from the Irminger Basin around the southern tip of Greenland mixes with waters in the Labrador Sea to form Lower NADW. Deep water formed by ocean convection in the Labrador Sea flows out into the Western North Atlantic Basin, overriding the Greenland-Scotland Ridge overflow waters as middle NADW. Outflow of saline water from the Mediterranean spreads in the Central and North Atlantic at depths of 1000 to 1500 m, and is termed Mediterranean Water or Upper NADW (Kellogg, 1987).

4.5 Paleoceanographic Controls on Drift Sedimentation

The sediment drifts between the Charlie Gibbs Fracture Zone and Greenland-Scotland Ridge presently lie between 1000 and 3000 m water depth along the path of the Greenland-Scotland Ridge overflows. They are deposited along the western margin of Rockall Trough and on both sides of the Irminger and South Iceland Basins. The largest drifts are on the western sides of basins and the smallest on the eastern margins. This is directly related to sediment supply and inputs of overflow waters at different sites along the Greenland-Scotland Ridge.

It has been proposed that dense water began to overflow the Greenland-Scotland Ridge near the time of the Eocene/Oligocene boundary (Nilsen, 1983; Kidd and Hill, 1987) or earlier (Vogt, 1972; Berggren and Hollister, 1977; Miller and Tucholke, 1983). Kidd and Hill (1986; 1987) have suggested that this led to the initiation of accumulation in Feni and Gardar Drifts. Miller and Tucholke (1983) thought that deposition started later (late Early Miocene) after bottom water circulation patterns became more coherent. Other authors have proposed that pre-Oligocene paleocirculation was dominated by the circulation of proto-AABW (Schnitker, 1980; Scrutton and Stow, 1984; Stow and Holbrook, 1984). Scrutton and Stow (1984) interpreted sediment drifts in the eastern end of the Charlie Gibbs Fracture Zone of Eocene and perhaps Paleocene age from seismic data. They believed that the position of these drifts, plastered along the northern side of the fracture zone, indicates west to east flow through the Charlie Gibbs Fracture Zone during the Eocene and in the Paleocene. They attributed this Paleocene-Eocene thermohaline circulation to proto-AABW or to a deep-water gyre system associated with a proto-Gulf Stream.

Thiede and Eldholm (1983) suggested that there has been surface water exchange across the Greenland-Scotland Ridge since Eocene-Oligocene time but that most of the Greenland-Iceland-Faeroe Ridge did not subside below sealevel until the middle Miocene. They reconstructed the paleobathymetry of the Denmark Strait and Faeroe-Shetland Channel assuming that the Denmark Strait began subsiding 50 Ma and the Faeroe-Shetland Channel 70 Ma. Thiede and Eldholm (1983) used the sealevel curve of Vail et al. (1977) and subsidence model for aseismic ridges from Detrick et al. (1977) to reconstruct the paleobathymetry of the Greenland-Scotland Ridge. They estimated initial subsidence of the

Denmark Strait below sealevel between 15 and 18 Ma and subsidence of the Faeroe-Shetland Channel below sealevel between 40 and 50 Ma.

A late Eocene-early Oligocene initiation of dense water flow over the Greenland-Scotland Ridge has also been held responsible for a regional unconformity of late Eocene-early Oligocene age in the North Atlantic Basin (Miller and Tucholke, 1983). This unconformity is a prominent seismic reflector. It was originally called "R" by Jones et al. (1970) and "R4" by Roberts (1975) and Roberts et al. (1981).

Along the margins of the South Iceland Basin the lower Oligocene-upper Eocene unconformity interpreted from seismic profiles is thought to be marked by reflector "R4" of Miller and Tucholke (1983) who correlate it with reflector R of Jones et al. (1970) and Ruddiman (1972). The upper Lower Miocene reflector R2 (Miller and Tucholke, 1983) overlies R4 and is interpreted here from the existing data to mark the beginning of Gardar and Bjorn Drift accumulation.

In the Rockall Trough R4 was called the "Challenger reflector" by Dingle et al. (1982) and is the "green reflector" of Masson and Kidd (1987). In the southern Rockall Trough around Feni Drift, R4 was reinterpreted from drilling at DSDP Site 610 (Ruddiman, Kidd, Thomas et al., 1987) to be a late Early Miocene oceanographic event (Masson and Kidd, 1987) and not an unconformity as was believed previously. This corresponds to reflector R2 of Miller and Tucholke (1983) which is of regional extent south of the Greenland-Scotland Ridge.

4.6 Paleobathymetric Controls on Drift Sedimentation

As described in Chapter 3, the paleobathymetry of the region was reconstructed from early Middle Eocene (50 Ma) to Present. Two models were used, one assuming Cretaceous rifting to produce Rockall Trough and uninterrupted thermal subsidence since then, and the other model assuming that the Rockall-Faeroe region was reheated during the Paleocene and that its subsidence history dates from that time. As noted in Section 3.7 above, the history of Feni drift appears to favor the Cretaceous rifting model. There is a paleobathymetric problem that lies below the resolution of the models and cannot be investigated: the paths from the Faeroe-Shetland Channel into Rockall Trough and the South Iceland Basin. At present the deepest exit from the Faeroe-Shetland Channel is through Faeroe Bank Channel into the South

Iceland Basin (Fig. 4.10), but in the Early Eocene drift sedimentation was initiated in Rockall Trough and not in the South Iceland Basin. Furthermore, it is inferred from non-migration of sediment waves on Feni Drift (Kidd and Hill, 1987), that it has not been accumulating sediment due to contour-currents for the past 2.4 m.y. The most obvious solution to these problems would be to assume that Faeroe Bank Channel had its origin in the Middle Miocene, when drift sedimentation began in the South Iceland Basin, and that the Faeroe Bank Channel deepened in the Pliocene, diverting most of the deep water flow into the South Iceland Basin and terminating drift sedimentation in Rockall Trough. There is presently no direct evidence for the timing or nature of the origin of Faeroe Bank Channel. The Faeroe Bank Channel is roughly parallel to the fracture zones in this region, and it seems possible that its origin may be related to transtensional motions resulting from changes in spreading direction.

The Cretaceous rifting model (Chapter 3) was used to reconstruct the paleobathymetry of the region between Charlie Gibbs Fracture Zone and the Greenland-Scotland Ridge from the present to late Eocene-early Oligocene (Figs. 4.11-4.17) and to display the areal extent of sediment drifts through time. This does not however, imply that the Cretaceous rifting model represents the most realistic thermal history of the Rockall-Faeroe region.

The early Pliocene distribution of sediment drifts (5 Ma; Fig. 4.11) between Charlie Gibbs Fracture Zone and the Greenland-Scotland Ridge was similar to that at present. In the early Late Miocene (10 Ma; Fig. 4.12) Eirik and Gloria Drifts did not exist and Snorri and Bjorn Drifts had a much smaller areal extent than in the early Pliocene. By the early Middle Miocene (15 Ma; Fig. 4.13) it is questionable whether Snorri Drift existed. Bjorn-Gardar Drift was a narrow linear feature along the western margin of the South Iceland Basin. The areal extent of Hatton and Feni Drifts is assumed to have remained approximately constant from the early Middle Miocene (Fig. 4.13) to present.

It is likely that only Feni Drift was accumulating sediment in the region between Charlie Gibbs Fracture Zone and the Greenland-Scotland Ridge in the Early Miocene (20 Ma; Fig. 4.14). This could be explained by increased elevation of the Iceland-Faeroe Ridge at 20 Ma that did not allow significant overflow of ISOW into the South Iceland Basin. The Faeroe-Shetland Channel however, appears significantly deeper in the paleobathymetric reconstruction (Figs. 3.10A and 4.14) which could explain sediment accumulation of Feni Drift if bottom water was flowing into Rockall Trough from the Faeroe-Shetland Channel.

Due to an insufficient seismic control of Feni Drift over its present extent, its areal distribution was assumed to be constant from the early Oligocene to present. In the Late Oligocene (25 Ma; Fig. 4.15) the Faeroe-Shetland Channel was at least 250 m deep and may have allowed sufficient bottom water to flow into Rockall Trough to deposit sediment on Feni Drift. By mid-Oligocene (30 Ma; Fig. 4.16) the Faeroe-Shetland Channel was not shallower than 200 m and was probably deeper if Feni Drift is indeed as old as early Oligocene-late Eocene. In the Early Oligocene (35 Ma; Fig. 4.17) the Faeroe-Shetland Channel was not significantly shallower than in the mid-Oligocene and it is possible that Feni Drift began to form at this time (Masson and Kidd, 1987).

4.7 Sediment Mass/Age Distributions

Sediment mass/age distributions are spatially averaged summaries of regional geologic history (see Chapter 2). Peaks in the mass/age distribution often correlate with times of tectonic uplift and the resulting increased rates of erosion in sediment source areas (Hay et al., 1989). Smaller observed sediment masses can indicate times of tectonic quiescence, decreased rates of sediment input or periods of increased erosion in basins. The compilation of sediment mass/age distributions was described in Chapter 2.

4.7.1 Correcting Mass/Age Distributions for the Effects of Sea-Floor Spreading

A mass/age distribution for sediment typically has the form of a slow exponential decay. In most areas the apparent exponential decay is the result of erosion of older sediment and its redeposition as young sediment ("cannibalization" of the older sediment to make new sediment). On ocean crust formed by sea-floor spreading the rate of exponential decay is amplified by the increasing space available for sediment accumulation (Fig. 4.18). This effect is especially pronounced when the sedimentation is exclusively pelagic. Neglecting the effects of erosion by bottom currents and dissolution, a constant rain of pelagic sediment over an opening ocean would result in a mass/age distribution that reproduces the rate of increase of sea-floor area (Fig. 4.18). The bias introduced by growth of an ocean basin can be eliminated by taking the increase in area of sea-floor into account, using regional cumulative area/age distributions for the ocean floor. By dividing the mass of sediment of a given age by the area

of sea-floor in existence at that time, we obtain an "apparent accumulation rate" expressed in mass per unit area per unit time (g cm^{-2} $k.y.^{-1}$). It is an "apparent" rather than "true" accumulation rate because this correction does not eliminate the effect of erosion subsequent to sediment deposition. The cumulative area of ocean crust decreases approximately linearly with increasing age in the region between the Charlie Gibbs Fracture Zone and the Greenland-Scotland Ridge (Fig. 4.19).

The global rain rates for pelagic sediment for 5 million year intervals through the Cenozoic have been calculated from the data presented by Hay et al. (1988) and are given in Table 4.2. The northern North Atlantic is not a highly productive area, so that the background pelagic sedimentation rate for the Pliocene and Quaternary is probably in the order of 1.5 g cm^{-2} $k.y.^{-1}$, declining to 1.0 g cm^{-2} $k.y.^{-1}$ by the Middle Miocene.

There are several major differences between apparent accumulation rate/age diagrams for the region between the Charlie Gibbs Fracture Zone and the Greenland-Scotland Ridge, the Irminger Basin, and the South Iceland Basin-Rockall Plateau-Rockall Trough (Figs. 4.20-4.22) and the mass/age distributions for these regions presented in Chapter 2 (Figs. 2.16-2.18). Most significant is the large apparent increase in Eocene-Early Oligocene sedimentation in the Irminger Basin, (Fig. 4.22). As discussed in Chapter 2, this is most likely a delayed response to the separation of Greenland from Rockall Plateau, caused by reversal of drainage as the Greenland margin subsided. It is important to note that the expected apparent increase in young sediment accumulation that would result from pelagic sedimentation on an opening ocean basin is not obvious. This demonstrates that the bulk of the sediment in the northern North Atlantic is not of pelagic origin, but has been introduced by bottom transport processes. In the basins south of the Greenland-Scotland Ridge apparent sediment accumulation rates exceed the expected pelagic rain rate by a factor of two or more except for the Late Oligocene of the Irminger Basin.

The apparent accumulation rate/age diagrams for sediment drifts (Figs. 4.23-4.25) have essentially the same appearance as their mass/age distributions (Figs. 2.20-2.22). Apparent accumulation rates on all of the larger drifts (Feni, Bjorn, Gardar and Eirik) on the western sides of the basins are several-fold the expected rain rate of pelagic sediment. The apparent accumulation rates on the small drifts (Hatton, Snorri, Gloria) are only slightly higher than the expected pelagic rain rate. The similarity of the apparent accumulation rate/age and mass/age diagrams for Feni, Hatton, Gloria and Eirik Drifts is explained by the fact that these

drifts are all deposited on older sediment. Bjorn and Gardar Drifts are interpreted here to have begun accumulating on the upper Lower Miocene reflector R2 (Miller and Tucholke, 1983), however the western margins of these drifts lie on ocean crust that is younger than R2. Snorri Drift is interpreted from seismic reflection profiles to lie entirely on basement along the western flank of Reykjanes Ridge. The apparent accumulation rate for Snorri is less than the expected rain rate of pelagic sediment in its early history, suggesting that the older part of the drift may have been reworked into younger sediment. The areal distribution of these drifts (Figs. 4.11-4.13) was constrained by spreading along the Reykjanes Ridge.

4.7.2 Comparing the Study Area with the Global Ocean

The data assembled by Hay et al. (1988) was used to determine the apparent rain rates of the major components of pelagic sediment (Table 4.2). The total apparent accumulation rates of pelagic sediments vary from a maximum of 1.33 g cm^{-2} $k.y.^{-1}$ for the last 5 m.y. to a minimum of 0.37 g cm^{-2} $k.y.^{-1}$ in the Paleocene.

The data of Hay et al. (1988) for the mass/age distribution of the total sediment in the world's ocean basins, both pelagic and terrigenous, can be compared with the total sediment accumulation in the study area. From their mass/age distribution I have calculated the global apparent accumulation rate for sediment in the ocean basins, and compare it with the results for the study area in Figure 4.26. The apparent accumulation rates in the study area between the Charlie Gibbs and Jan Mayen Fracture Zones are essentially the same as the average for the world ocean for the Quaternary, Pliocene and Miocene, but are significantly higher for the Oligocene and Eocene. The Paleogene excess is caused by sediment derived from Greenland and deposited in the Irminger Basin.

4.8 Areal Distribution of Apparent Accumulation Rates

Apparent accumulation rate maps show the accumulation rate obtained by dividing the existing mass of sediment of a given time interval by the length of the interval. They are not "true" sediment accumulation rate maps, because no correction has been made for erosion of sediment subsequent to its deposition. The global average apparent accumulation rates for pelagic sediments during the Cenozoic (Table 4.2) range from 0.37 to 1.33 g cm^{-2} $k.y.^{-1}$. The

apparent accumulation rates are shown with the paleobathymetry reconstructed according to the Cretaceous Rifting model (see Chapter 3). The time intervals represented by the apparent accumulation rate maps were chosen from examination of average accumulation rates for the study region in Figure 4.20. Apparent accumulation rate maps were reconstructed for the time interval from 0-1 Ma, representing the Late Quaternary, 3-4 Ma, representing the middle Pliocene time of maximum apparent accumulation rates, 9-10 Ma, representing the early Late Miocene time of low apparent accumulation rates, 19-20 Ma, representing the Early Miocene low apparent accumulation rates, 29-30 Ma, representing the middle Oligocene time of minimal apparent accumulation, 39-40 Ma representing the Late Eocene apparent accumulation maximum, and 49-50, representing the early Middle Eocene time of moderate apparent accumulation. The apparent accumulation rate maps (Figs. 4.27-4.33) are based on the compiled stratigraphic columns (see Chapter 2) and a different interpretation of the regional stratigraphy would lead to a different descriptive history of the regional sedimentation.

During the last million years the apparent global pelagic sediment rain rate (Table 4.2) was 1.33 g cm^{-2} $k.y.^{-1}$. During this time, there has been a maximum in apparent accumulation rates on the eastern edge of Rockall Trough (Fig. 4.27). This represents input from the continental margin off northern Ireland. Apparent accumulation rates in Rockall Trough are offset with respect to the bathymetric contours, with the greater rates being on the western side of the trough over Feni Drift and north of Porcupine Bank. Apparent accumulation rates in Rockall-Hatton Basin on top of the Rockall-Hatton Bank are half those in Rockall Trough. Rockall Bank is probably a site of erosion. High apparent accumulation rates occurred in the north end of the South Iceland Sea adjacent to the Greenland-Scotland Ridge. Very high sedimentation rates (greater than 12 g cm^{-2} $k.y.^{-1}$) occurred on the lower part of the east flank of the Reykjanes Ridge on the southern part of Gardar Drift. There has also been an area of very high apparent accumulation rates around the southern tip of Greenland over Eirik and Gloria Drifts. A broad area of the Greenland-Scotland Ridge near Iceland has had no apparent sediment accumulation and may be an area of active erosion. In the Iceland Sea, apparent accumulation rates have been very high over a broad area of the Iceland Plateau, especially off Scoresby Sund. The thick sediments were derived from sources in Greenland and have been trapped by Kolbeinsey Ridge. In the Norway Basin sedimentation rates were low (1 to

2 g cm^{-2} $k.y.^{-1}$), approximating pelagic rain rates except locally off the Norwegian continental margin.

The largest masses of sediment in the northern North Atlantic are from the middle Pliocene, shown on the 3-4 Ma map (Fig. 4.28). At this time the apparent global pelagic rain rate was again about 1.33 g cm^{-2} $k.y.^{-1}$. During the middle Pliocene there was high input into eastern Rockall trough from the shelf off northern Ireland. The general pattern of sediment accumulation in Rockall Trough was more symmetrical than for the Late Quaternary. The area of high apparent accumulation at the north end of the South Iceland Basin did not yet exist in the middle Pliocene. Apparent accumulation rates over the southern part of the eastern flank of Reykjanes Ridge (Gardar Drift) were even higher than during the Late Quaternary, up to 18 g cm^{-2} $k.y.^{-1}$. Apparent accumulation rates in the northwestern Irminger Basin along the Greenland margin exceeded 6 g cm^{-2} $k.y.^{-1}$. Very high sedimentation rates had just begun off the southern tip of Greenland, over Eirik Drift. There was an extensive area of erosion on the Greenland-Scotland Ridge. The highest apparent accumulation rates (greater than 40 g cm^{-2} $k.y.^{-1}$) were on the Iceland Plateau off Scoresby Sund. Apparent accumulation rates in the Norway Basin were as low as they were in the Quaternary except along the Norwegian margin.

In the early Late Miocene, 9-10 Ma map (Fig. 4.29), the apparent global pelagic sediment rain rates were about 1 g cm^{-2} $k.y.^{-1}$. Input into eastern Rockall trough from the shelf off northern Ireland was high. The general pattern of sediment accumulation in Rockall Trough was symmetrical as it was later in the Pliocene (Fig 4.28). There was an area of no apparent accumulation in the northern South Iceland Basin in the early Late Miocene, reflecting erosion of sediment. Apparent accumulation rates over the flanks of Reykjanes Ridge were low. The reconstruction (Fig. 4.29) indicates that there was no area of unusual apparent accumulation on Gardar Drift in the early Late Miocene. Apparent accumulation rates in the center of the northern Irminger Basin may have reached 4 g cm^{-2} $k.y.^{-1}$ but in the southern part of Irminger Basin there was probably erosion. There were no high sediment accumulation rates off the southern tip of Greenland lending support to the hypothesis that Eirik and Gloria Drifts did not begin accumulating until later. There was an extensive area of erosion on the Greenland-Scotland Ridge that extended into the Norway Basin. The highest apparent accumulation rates (more than 60 g cm^{-2} $k.y.^{-1}$) were again on the Iceland Plateau off Scoresby Sund. Apparent accumulation rates in the Norway Basin were low except off the

Shetland margin. The locally high input off southern Norway did not exist in the early Late Miocene.

For the Early Miocene, 19-20 Ma map (Fig. 4.30), apparent global pelagic accumulation rates were lower than for younger sediment, 0.74 g cm^{-2} $k.y.^{-1}$. In the eastern Rockall trough apparent accumulation rates in the Early Miocene were considerably lower than in younger times (Figs. 4.27-4.29). There was a local unusually large apparent accumulation in western Rockall Trough just south of Rockall Bank (Feni Drift). Rockall Bank was again a site of erosion. There was an area of no apparent accumulation in the northern South Iceland Basin, probably reflecting erosion. Apparent accumulation rates over Reykjanes Ridge were higher than in the adjacent basins. Apparent accumulation rates were generally low in Irminger Basin and at its south end there was probably an area of erosion. There was an extensive area of non-deposition or erosion on the Greenland-Scotland Ridge and extending into the southern Norway Basin. The highest apparent accumulation rates (greater than 10 g cm^{-2} $k.y.^{-1}$) were on the Iceland Plateau off Scoresby Sund. The sediment eroded from Greenland was trapped very close to the margin by the young Kolbeinsey Ridge. Apparent accumulation rates in the Norway Basin were low everywhere.

In the Oligocene apparent global pelagic sediment accumulation rates continued to be low. For the middle of the Oligocene, the time represented by the 29-30 Ma map (Fig. 4.31) they were 0.77 g cm^{-2} $k.y.^{-1}$. Apparent sediment accumulation rates in western Rockall Trough over Feni Drift were relatively high compared to the rest of Rockall Trough in the middle Oligocene (Fig. 4.30). As in younger reconstructions Rockall Bank was a site of erosion. There was an area of no apparent accumulation in the southern South Iceland Basin, again probably reflecting erosion. Apparent accumulation rates over Reykjanes Ridge were higher than in the adjacent basins. Much of the central Irminger Basin was subsequently eroded. There were patches of erosion on the Greenland-Scotland Ridge. High apparent accumulation rates (greater than 10 g cm^{-2} $k.y.^{-1}$) occurred on the southern Iceland Plateau but off Scoresby Sund the sediment was able to cross over the incipient Kolbeinsey Ridge and southern Jan Mayen Ridge into the western Norway Basin. Apparent accumulation rates in the Norwegian Sea continued to be low.

Apparent global pelagic sediment accumulation rates decreased in the Late Eocene to 0.39 g cm^{-2} $k.y.^{-1}$. The interval is represented by the 39-40 Ma map (Fig. 4.32). Rockall Trough was not the site of large apparent accumulations in the Late Eocene but there was a

site of relatively high apparent accumulation rates south of Rockall Bank perhaps indicating sedimentation on Isengard Drift (Fig. 2.1). Most of Rockall-Hatton Bank was a probably a site of erosion. There was high apparent accumulation in the central South Iceland Basin, which at this time was adjacent to the East Greenland margin. There were patches of erosion along the Greenland-Scotland Ridge. Apparent accumulation rates off Greenland north of the Greenland-Scotland Ridge were low. Apparent accumulation rates in the Norway Basin were low except for locally high input from the Shetlands.

During the Middle Eocene, apparent global pelagic sediment accumulation rates increased to 0.49 g cm^{-2} $k.y.^{-1}$. The apparent accumulation rates in the early Middle Eocene, 49-50 Ma (Fig. 4.33), were very similar to those of the Late Eocene (Fig. 4.32). Apparent accumulation rates in Rockall Trough were not large and there appears to have been a site of higher accumulation south of Rockall Bank in Isengard Drift. Most of Rockall-Hatton Bank was a site of sediment erosion. High apparent accumulation again occurred in the central South Iceland Basin adjacent to the East Greenland margin. There were patches of erosion on the Greenland-Scotland Ridge. Apparent accumulation rates off Greenland north of the Greenland-Scotland Ridge were low. Apparent accumulation rates in the Norwegian Sea were low except for locally high input from the Shetlands.

4.9 Relative Apparent Sediment Accumulation Rates

Another way of analyzing apparent accumulation rates of sediment (Figs. 4.27-4.33) is to plot them relative to the average apparent accumulation rate for the region during a given reconstruction interval. Apparent accumulation rates for the region between the Charlie Gibbs Fracture Zone and Greenland-Scotland Ridge vary from a maximum of 4.01 g cm^{-2} $k.y.^{-1}$ during the interval from 3-4 Ma in the early Pliocene to a minimum of 1.57 g cm^{-2} $k.y.^{-1}$ during the interval from 27-28 Ma in the late Oligocene (Fig. 4.20). The apparent accumulation rates plotted in Figures (4.34-4.40) are relative to the average apparent accumulation rate for the study area during 1 m.y. intervals. The maps were derived by subtracting the regional average (Fig. 4.20) from the apparent accumulation rate within each grid cell during a 1 m.y. time interval. For example, if a grid cell has an apparent accumulation rate of 5 g cm^{-2} $k.y.^{-1}$ during the time interval from 9 to 10 Ma and the average apparent accumulation rate for the entire region (Fig. 4.20) for the same time interval is 1.73

g cm^{-2} $k.y.^{-1}$, then the apparent accumulation rate for the grid cell relative to the regional average is 3.27 g cm^{-2} $k.y.^{-1}$ during that time interval. For this set of maps the reconstructed paleobathymetry (dashed contour lines) is based on the Cretaceous rifting model (see Chapter 3). As in the previous section, the paleobathymetry is shown for location reference and not to suggest that the Cretaceous rifting model is the best thermal model for reconstructed paleobathymetry. The maps concentrate on the region south of the Greenland-Scotland Ridge (Figs. 4.34-4.40) in order to study the sedimentation history and specifically the development of sediment drifts and abyssal circulation.

During the last million years, the regional average accumulation rate was 3.71 g cm^{-2} $k.y.^{-1}$ (Fig. 4.34). In the southern Rockall Trough relative apparent accumulation rates were significantly higher than the regional average. The shape of the excess relative accumulation rates (Fig. 4.34) closely approximates the shape of Feni Drift to the east and south of Rockall Plateau (compare to Fig. 4.9). This is an interesting result because it is thought that Feni Drift has not been a site of active drift sedimentation for the past 2.4 m.y. (Kidd and Hill, 1987). Excess relative sediment accumulation north of Porcupine Bank reflects terrigenous input from the north Irish continental shelf. Relative apparent accumulation rates in Rockall-Hatton Basin were higher than the average during the last million years (Fig. 4.34) but not as great as those in Rockall Trough. The area around Wyville-Thompson Ridge, Lousy, Rockall and Hatton Banks were all sites of probable erosion. High relative apparent accumulation rates occurred in the north end of the South Iceland Sea adjacent to the Greenland-Scotland Ridge and perhaps along sections of the Iceland-Faeroe Ridge as well. Bjorn and Gardar Drifts are also delineated in the 0 to 1 Ma map (Fig. 4.34) by higher-than-average sediment accumulation rates. The Reykjanes Ridge was covered by generally lower-than-average amounts of sediment during this time interval. The relative rate of sediment accumulation was higher in the central portion of the Irminger Basin than along its margins except in the southwest. The excess sediment in the north of the Irminger Basin can be attributed to turbidity currents flowing down from Iceland in the north central part of the basin. Relative sediment deficits on the eastern side of the basin could be due to contour-following bottom currents flowing south along the eastern Greenland continental rise and then depositing eroded sediment south of Greenland in Eirik and perhaps Gloria Drifts where there is an excess in relative sediment accumulation.

The middle Pliocene regional average apparent accumulation rate was 4.01 g cm^{-2} $k.y.^{-1}$. The map (Fig. 4.35) indicates a broad region of erosion north of Rockall Plateau. The largest deficit in relative apparent sediment accumulation rates is found along the entire Greenland-Scotland Ridge including the northeast South Iceland Basin, the region around the Wyville-Thompson Ridge and Rockall and Hatton Banks. In the southern Rockall Trough relative apparent accumulation rates were again higher than the regional average. There was excess relative sediment accumulation north of Porcupine Bank reflecting terrigenous input from the north Irish continental shelf or perhaps sediment transport from the northern Rockall Trough towards the south. There was excess apparent accumulation rates in the central portion of the Rockall-Hatton Basin and southwest of Rockall Plateau. The greatest excess in relative apparent accumulation rates occurred over Gardar Drift in the middle Pliocene (Fig. 4.35). This region of excess sediment accumulation could partially account for deficits along the Iceland-Faeroe Ridge if there was an increased flow of erosive bottom water currents over the Iceland-Faeroe Ridge. These currents could have eroded sediment in the north and redeposited it in the south over Gardar Drift. Relative apparent accumulation rates over Reykjanes Ridge were lower in the middle Pliocene than in the Quaternary. Excess sediment accumulation was localized to the north-central and southern portions of the Irminger Basin with a deficit in the center around 60° N latitude. The excess sediment in the north of the Irminger Basin can again be attributed to turbidity currents flowing down from the shelf off Iceland although these appear to have had less ability to transport sediment as far as those in the Quaternary. Relative sediment deficits on the eastern side of the basin can again be attributed to contour-following bottom currents flowing south along the eastern Greenland continental rise and then depositing eroded sediment south of Greenland in Eirik Drift where there is an excess in relative sediment accumulation. In the region around Gloria Drift (55° N, 42° W) there is a deficit in the relative sediment accumulation rate.

In the early Late Miocene the regional average apparent accumulation rate was 1.73 g cm^{-2} $k.y.^{-1}$, much lower than for the Pliocene and Quaternary. Relative apparent sediment accumulation rates (Fig. 4.36) appear substantially different from those of the middle Pliocene. Sedimentation patterns appear to be far less influenced by contour-following bottom water currents than in the middle Pliocene and Quaternary. There was still a region of general sediment deficit along the Greenland-Scotland Ridge, northern South Iceland Basin, the region around the Wyville-Thompson Ridge and Rockall and Hatton Banks, but the deficit appears

less extreme than in the middle Pliocene. Relative apparent accumulation rates were higher than the regional average in both the northern and southern portions of Rockall Trough. The largest excess relative sediment accumulation occurred north of Porcupine Bank indicating input from the north Irish continental shelf. There was excess apparent accumulation rates over the entire Rockall-Hatton Basin and extending onto Hatton Bank. Only a small excess in relative apparent accumulation rates occurred over southern Gardar Drift. Excess sedimentation occurred over the entire southern half of the South Iceland Basin and sediment deficits across the northern half. Regions of excess and deficit in the relative apparent accumulation rates appear to parallel one another and trend northwest-southeast in the Irminger Basin and across the Reykjanes Ridge (Fig. 4.36).

The Early Miocene regional average apparent accumulation rate was 1.78 g cm^{-2} $k.y.^{-1}$. Like the regional average, Early Miocene relative apparent accumulation rates (Fig. 4.37) were similar to those of the early Late Miocene. In Rockall Trough the relative accumulation rates were generally high with the highest rates in the central part of the trough and north of Porcupine Bank. The area of excess apparent accumulation rates was smaller over Rockall-Hatton Basin than in the early Late Miocene. There was an excess in relative apparent accumulation rates over the central and eastern portions of Reykjanes Ridge. There was again a region of excess apparent accumulation rates across the center of the Irminger Basin that appears unrelated to contour-following bottom currents.

The average apparent accumulation rate in the middle Oligocene was the lowest during the Cenozoic, 1.58 g cm^{-2} $k.y.^{-1}$. Throughout Rockall Trough the relative accumulation rates were high in the middle Oligocene (Fig. 4.38) probably due to accumulation on Feni Drift. The other site of excess apparent accumulation rates was along the Reykjanes Ridge. Relative apparent accumulation rates were low in the western Irminger Basin and eastern South Iceland Basin.

During the Late Eocene, the regional average accumulation rate was higher than during the Oligocene or Miocene, 2.75 g cm^{-2} $k.y.^{-1}$. The largest excess in sediment accumulation relative to the average occurred along the southeast Greenland margin west of the young Reykjanes Ridge (Fig. 4.39). Excess accumulation rates occurred in the central Rockall Trough and south of the Rockall Plateau. There was a deficit of apparent accumulation over the entire Rockall Plateau.

The early Middle Eocene regional average apparent accumulation rate was 2.44 g cm^{-2} $k.y.^{-1}$, slightly less than during the Late Eocene. As shown in Figure 4.40, there was excess in sediment accumulation relative to the average in the young ocean basin west of Rockall Plateau in the early Middle Eocene. Excess accumulation rates occurred throughout Rockall Trough and south of Rockall Plateau. There was a deficit of apparent accumulation over Rockall Plateau to the Greenland-Scotland Ridge.

4.10 Discussion

South of the Greenland-Scotland Ridge sediments have been reworked and transported by abyssal currents.The current activity has resulted in regional unconformities and the deposition of sediment drifts. The sediment drifts, elongate bodies of fine-grained sediment deposited along bathymetric contours, range from 200 to 2000 m in thickness and may be over 1000 km in length. They make up a significant proportion of the total sediment between the Charlie Gibbs Fracture Zone and Greenland-Scotland Ridge. Apparent accumulation rate maps (Figs. 4.27-4.33) clearly show the concentration of sediment in the sediment drifts. Relative apparent accumulation rate maps (Figs. 4.34-4.40) show that the drifts have apparent accumulation rates that are up to several times those of the non-drift regions. The maps also show that the main phase of drift formation occurred during the Pliocene and Quaternary. Drift sedimentation during the Late and Middle Miocene was not nearly as extensive as during the Pliocene and Quaternary. Maps for earlier times show that except on the southeast margin of Rockall Plateau, where Feni Drift began to accumulate in the Oligocene, sedimentation throughout the region was dominated by high rates of accumulation of pelagic sediments on ocean ridges and plateaus, lower rates on the deeper flanks, and high rates of presumably terrigenous sedimentation in the basins bordering land areas.

Feni Drift has the largest mass (193 x 10^{18} g; Table 4.1) and is the oldest of the sediment drifts between the Charlie Gibbs Fracture Zone and Greenland-Scotland Ridge. The next largest drift in terms of mass is Gardar Drift (145 x 10^{18} g). Gardar Drift has a greater areal extent (180 x 10^3 km^2) than Feni Drift (117 x 10^3 km^2) but is thinner on average. The thicker sediments in Feni Drift have a higher estimated solidity than the sediment in Gardar Drift thus accounting for the greater total mass of Feni Drift. Bjorn Drift has the third largest total mass of sediment (64.8 x 10^{18} g). The division between Gardar and Bjorn Drifts is

artificial. Both have been deposited on the same flank of Reykjanes Ridge by the same current. The distinction between them is made because they have separate ridge crests north of 57° N. When considered together Gardar and Bjorn Drifts would be the largest sediment drift that has accumulated in the study area with a combined mass of 210 x 10^{18} g and area of 305 x 10^3 km^2. The sediment drift with the next largest mass is Eirik Drift off the southern tip of Greenland. It has a relatively small area (82.3 x 10^3 km^2) but is very thick and has a mass of 60.5 x 10^{18} g. Sediment drifts that lie on the western flanks of rises (Hatton and Snorri) are some of the smallest in the region, deriving their sediment from northward-flowing bottom currents. Snorri Drift on the western flank of the Reykjanes Ridge has a larger areal distribution (107 x 10^3 km^2) than Eirik Drift but it mass is four times smaller (16.0 x 10^{18} g) because it is so thin. The mass of Hatton Drift (15.9 x 10^{18} g) is essentially the same as Snorri Drift but it has a much smaller areal extent (62.1 x 10^3 km^2). The approximate mass equivalence between Snorri and Hatton Drifts can be attributed to the larger average thickness of Hatton Drift and thus higher values for the estimated solidity of the sediment. Gloria Drift has the smallest mass (11.4 x 10^{18} g) and is also the thinnest of the sediment drifts in the region. It was probably deposited from a sediment-depleted westward-flowing NWADW current.

4.11 Summary and Conclusions

Analysis of the sediment accumulations in the northern North Atlantic shows that the sediment drifts have a greater areal extent than has been indicated in the literature. Feni Drift, on the eastern and southern margins of Rockall Plateau, was the first to form and its areal extent has not appreciably increased in size since the early Oligocene. The current concept that sediment waves are no longer migrating on Feni Drift (Kidd and Hill, 1987) implies that it is not actively forming. This is in conflict with the higher than average sedimentation rates on it during the last 1 m.y. The double ridge on South Feni Drift indicates a more complicated bottom water circulation in Rockall Trough than simply a southward flow of WTRO along its western margin. Apparent accumulation rate/age and mass/age diagrams for Feni Drift show an increase in sediment accumulation per unit time when Hatton Drift began to form in the early Middle Miocene (16 Ma). Apparent accumulation rate/age diagrams are calculated by dividing the observed sediment mass by the total area of sea-floor in the study

area that existed at the time the sediment was deposited. These accumulation rates are "apparent" because they do not take into account the effect of subsequent erosion.

The formation of Gardar and Bjorn Drifts started in the late Early Miocene on seismic reflector R2 of Miller and Tucholke (1983). The area where they are accumulating has expanded gradually but continuously. Apparent accumulation rates of sediment in the early Pliocene (3-4 Ma) were much higher over Gardar Drift than the regional average. Sediment accumulation on Gardar Drift increased more than six-fold over Miocene rates in the Pliocene. However, apparent accumulation rates on Bjorn Drift only doubled in the Pliocene over earlier rates. The rate of sediment accumulation on both drifts has decreased from the Pliocene to Quaternary. The area of accumulation of Snorri Drift has increased steadily since the Middle Miocene. Both Eirik and Gloria Drifts appeared as drift sedimentation sites abruptly in the late Miocene-early Pliocene, but were deposited from different contour-following currents.

Sediment waves on the surface of drifts may develop from more dispersed, low-energy bottom water flowing over them than those drifts where sediment waves are absent. Sediment drifts that are covered by sediment waves include Gloria Drift, derived from a relatively weak westward-flowing NWADW, as well as southeastern Gardar Drift and South Feni Drift. The lack of sediment waves on the northern part of Gardar Drift and on Bjorn Drift may indicate a more intense bottom water flow than along the southeastern portion of Gardar Drift. The vigorous flow of approximately 10 Sv of bottom water over Eirik Drift off the southern tip of Greenland has resulted in a thick sediment accumulation but no sediment waves. This indicates a much stronger flow of bottom water over Eirik Drift than that responsible for the accumulation of Gloria Drift to the southeast.

Drift sedimentation has dominated the pattern of sediment accumulation between the Greenland-Scotland Ridge and the Charlie Gibbs Fracture Zone during the Quaternary and Pliocene. During the Late and Middle Miocene drift sedimentation was restricted to relatively small areas of the South Iceland Basin and to the western side of Rockall Trough. During the Early Miocene and Oligocene greater-than-average sediment accumulations were found mostly on the developing mid-ocean Reykjanes Ridge and on Rockall Plateau. In the Eocene the only areas that had above average apparent sediment accumulation rates were the basins, Rockall Trough, Porcupine Abyssal Plain, and Irminger Basin.

Maps of apparent sediment accumulation rates are a useful new tool for studying the spatial distribution of sedimentation through time. Apparent accumulation rate maps are calculated by dividing the existing mass of sediment in a grid cell of a given age by the area of the grid cell. Throughout the Cenozoic apparent accumulation rates in Rockall Trough were higher than the regional average. Apparent accumulation rates were always low along the Greenland-Scotland Ridge indicating its persistent environment of erosion. Apparent accumulation rates were highest over southern Gardar Drift in the Pliocene and Quaternary. Apparent accumulation rates were also high off southern Greenland in the Pliocene and Quaternary when Eirik Drift was deposited. During the Neogene apparent accumulation rates were highest off Scoresby Sund on the western Iceland Plateau. The apparent accumulation rate of sediment was consistently lower than the regional average in the Norway Basin during the Cenozoic. There was locally high rates of sediment input off the Faeroe-Shetland Escarpment during the Eocene and from the Late Miocene to present. Apparent accumulation rates were low in the Oligocene through Middle Miocene.

4.12 Figure Captions

Figure 4.1. The distribution of single-channel seismic reflection profiles and DSDP-ODP sites used to compile the stratigraphy south of the Greenland-Scotland Ridge. DSDP and ODP drill sites are shown as solid black circles and the seismic profiles are shown as solid lines. The coastlines and some bathymetric contours are shown for reference. Longitude is negative to the west and latitude is positive towards the north.

Figure 4.2. Direction of flow of present bottom currents (dashed arrows; after McCave and Tucholke, 1986) and approximate distribution of sediment drifts (dotted lines) between the Charlie Gibbs Fracture Zone and Greenland-Scotland Ridge. Greenland-Scotland Ridge overflow waters are labelled: Wyville-Thompson Ridge Overflow water (WTRO); Iceland Sea Overflow Water (ISOW) and Denmark Strait Overflow Water (DSOW). Other abbreviations include: Faeroe-Shetland Channel (); Wyville-Thompson Ridge (WTR); Faeroe Bank Channel (FBC); Feni Drift (FD); Hatton Drift (HAD); Bjorn Drift (BD); Gardar Drift (GD); Snorri Drift (SD); Eirik Drift (ED) and Gloria Drift (GLD).

Figure 4.3. Sediment drift morphologies (from McCave and Tucholke, 1986). The different types of sediment drifts are: A. Double Drifts; B. Plastered Drifts; C. Detached Drifts and D. Separated Drifts. The first three types of sediment drifts occur in the study area. Current flow towards the viewer (out of the page) is indicated by a dot inside a circle and current flow away from the viewer (into the page) is indicated by a cross inside a circle.

Figure 4.4. The present distribution of sediment drifts determined from single-channel seismic reflection profiles. Bathymetry was derived from a 1 x 1° grid, is shaded and contoured at 250 m intervals below sealevel. Sediment drifts are shown at the 1 x 1° resolution of the grid and are labelled: Feni Drift (FD); Hatton Drift (HAD); Bjorn Drift (BD); Gardar Drift (GD); Snorri Drift (SD); Eirik Drift (ED) and Gloria Drift (GLD).

Figure 4.5. Single-channel seismic reflection profile from west to east across South Feni Drift in Rockall Trough. Depth is given in seconds of two-way travel time. This profile was taken in 1966 from the Lamont-Doherty Geological Observatory (Columbia University, Palisades, N.Y.) ship R/V "Vema".

Figure 4.6. Single-channel seismic reflection profile from west to east across Gardar and Hatton Drifts near 60° N latitude in the South Iceland Basin. Depth is given in seconds of two-way travel time. This profile was taken in 1970 from the Lamont-Doherty Geological Observatory (Columbia University, Palisades, N.Y.) ship R/V "Vema".

Figure 4.7. Single-channel seismic reflection profile from west to east across the southern portion of Gardar Drift near 56° N latitude in the South Iceland Basin. Depth is given in seconds of two-way travel time. This profile was taken in 1969 from the Lamont-Doherty Geological Observatory (Columbia University, Palisades, N.Y.) ship R/V "Vema".

Figure 4.8. Single-channel seismic reflection profile from south to north across Gloria and Eirik Drifts near 46° W longitude in the South Labrador Sea and southern Irminger Basin. Depth is given in seconds of two-way travel time. This profile was taken in 1970 from the Lamont-Doherty Geological Observatory (Columbia University, Palisades, N.Y.) ship R/V "Vema".

Figure 4.9. Single-channel seismic reflection profile from northwest to southeast across Gloria Drift in the southern Irminger Basin. Depth is given in seconds of two-way travel time. This profile was taken in 1970 from the Lamont-Doherty Geological Observatory (Columbia University, Palisades, N.Y.) ship R/V "Vema".

Figure 4.10. Bathymetric features of the region around Wyville-Thompson Ridge that restrict the flow of bottom water. Bathymetry was derived from the ETOPO5 (1986) 5 x 5' elevation grid, is shaded and contoured at 250 m intervals below sealevel. Geographic features discussed in the text are labelled: Faeroe Islands (FI); Faeroe-Shetland Channel (); Wyville-Thompson Ridge (WTR); Faeroe Bank Channel (FBC); Faeroe Bank (FB); Bill Baileys Bank (BBB); Lousy Bank (LB); South Iceland Basin (SIB); Rosemary Bank (RB); George Bligh Bank (GBB) and Rockall Trough (RT).

Figure 4.11. Areal distribution of sediment drifts on early Pliocene (5 Ma) paleobathymetry reconstructed with the Cretaceous rifting model. Bathymetry is shaded and contoured at 0.25 km depth intervals and sediment drifts are represented by the white 1 x 1° grid cells. The sediment drifts that existed in this region in the early Pliocene include: Feni, Hatton, Bjorn, Gardar, Snorri, Eirik and Gloria.

Figure 4.12. Areal distribution of sediment drifts on early Late Miocene (10 Ma) paleobathymetry reconstructed with the Cretaceous rifting model. Bathymetry is shaded and contoured at 0.25 km depth intervals and sediment drifts are represented by the white 1 x 1° grid cells. The sediment drifts that existed in this region in the early Late Miocene include: Feni, Hatton, Bjorn, Gardar and Snorri.

Figure 4.13. Areal distribution of sediment drifts on early Middle Miocene (15 Ma) paleobathymetry reconstructed with the Cretaceous rifting model. Bathymetry is shaded and contoured at 0.25 km depth intervals and sediment drifts are represented by the white 1 x 1° grid cells. The sediment drifts that existed in this region in the early Middle Miocene include: Feni, Hatton, Bjorn, Gardar and Snorri.

Figure 4.14. Areal distribution of sediment drifts on Early Miocene (20 Ma) paleobathymetry reconstructed with the Cretaceous rifting model. Bathymetry is shaded and contoured at 0.25 km depth intervals and sediment drifts are represented by the white 1 x 1° grid cells. Only Feni Drift is assumed to have existed in this region in the Early Miocene.

Figure 4.15. Areal distribution of sediment drifts on Late Oligocene (25 Ma) paleobathymetry reconstructed with the Cretaceous rifting model. Bathymetry is shaded and contoured at 0.25 km depth intervals and sediment drifts are represented by the white 1 x 1° grid cells. Only Feni Drift is assumed to have existed in this region in the Late Oligocene.

Figure 4.16. Areal distribution of sediment drifts on mid-Oligocene (30 Ma) paleobathymetry reconstructed with the Cretaceous rifting model. Bathymetry is shaded and contoured at 0.25 km depth intervals and sediment drifts are represented by the white 1 x 1° grid cells. Only Feni Drift is assumed to have existed in this region in the mid-Oligocene.

Figure 4.17. Areal distribution of sediment drifts on Early Oligocene (35 Ma) paleobathymetry reconstructed with the Cretaceous rifting model. Bathymetry is shaded and contoured at 0.25 km depth intervals and sediment drifts are represented by the white 1 x 1° grid cells. Only Feni Drift is assumed to have existed in this region in the Early Oligocene.

Figure 4.18. Relationship between a sediment mass/age distribution and the areal distribution of pelagic sediment deposited at a constant rate over ocean crust. The mass/age distribution decreases exponentially with increasing age of the sediment (Part A.). In vertical cross-section perpendicular to the mid-ocean ridge, the age of the ocean crust increases from left to right and the sediment age increases downward. For an ocean basin whose area has been steadily increasing through time due to sea-floor spreading and where sedimentation has been at a constant rate, the area of the ocean floor continually increases allowing more room to deposit sediment and resulting in a mass/age distribution similar to that in part A.

Figure 4.19. Cumulative area versus age of ocean crust between the Charlie Gibbs Fracture Zone and Greenland-Scotland Ridge. The decrease of area with increasing age is approximately linear.

Figure 4.20. Apparent accumulation versus age for all Cenozoic sediment between the Charlie Gibbs Fracture Zone and Greenland-Scotland Ridge and from the continental margin of East Greenland to shelf-break west of the U.K. (upper diagram). In the lower diagram the apparent accumulation of sediment within sediment drifts has been subtracted from the accumulation versus age diagram.

Figure 4.21. Apparent accumulation versus age for all Cenozoic sediment between the Charlie Gibbs Fracture Zone and Greenland-Scotland Ridge and from the Reykjanes Ridge to continental shelf-break west of the U.K. (upper diagram). In the lower diagram the apparent accumulation of sediment within sediment drifts has been subtracted from the accumulation versus age diagram.

Figure 4.22. Apparent accumulation versus age for all Cenozoic sediment between the Charlie Gibbs Fracture Zone and Greenland-Scotland Ridge and from the continental margin of East Greenland to Reykjanes Ridge (upper diagram). In the lower diagram the apparent accumulation of sediment within sediment drifts has been subtracted from the accumulation versus age diagram.

Figure 4.23. Apparent accumulation versus age of sediment in Feni (upper diagram) and Gardar Drifts (lower diagram).

Figure 4.24. Apparent accumulation versus age of sediment in Bjorn (upper diagram) and Eirik Drifts (lower diagram).

Figure 4.25. Apparent accumulation versus age of sediment in Snorri (upper diagram), Hatton (middle diagram) and Gloria Drifts (lower diagram).

Figure 4.26. Apparent accumulation versus age of sediment between the Charlie Gibbs and Jan Mayen Fracture Zones and from the continental margin of East Greenland to the European margin averaged to 5 m.y. intervals (solid line) and the global apparent accumulation of sediment on the ocean floor (dashed line). The global values were calculated from Table 1 of Hay et al. (1988) by dividing the accumulation of sediment still in existence for 5 m.y. intervals by the cumulative area of ocean floor in existence at the midpoint of each interval.

Figure 4.27. Apparent accumulation rates for the interval from 0 to 1 Ma (Quaternary) between the Charlie Gibbs Fracture Zone and Greenland-Scotland Ridge and from the continental margin of East Greenland to shelf-break west of the U.K. Paleobathymetric contours reconstructed with the Cretaceous rifting model (Chapter 3) are shown (heavy lines) at 500 m contour intervals for reference.

Figure 4.28. Apparent accumulation rates for the interval from 3 to 4 Ma (Pliocene) between the Charlie Gibbs Fracture Zone and Greenland-Scotland Ridge and from the continental margin of East Greenland to shelf-break west of the U.K. Paleobathymetric contours reconstructed with the Cretaceous rifting model (Chapter 3) are shown (heavy lines) at 500 m contour intervals for reference.

Figure 4.29. Apparent accumulation rates for the interval from 9 to 10 Ma (early Late Miocene) between the Charlie Gibbs Fracture Zone and Greenland-Scotland Ridge and from the continental margin of East Greenland to shelf-break west of the U.K. Paleobathymetric contours reconstructed with the Cretaceous rifting model (Chapter 3) are shown (heavy lines) at 500 m contour intervals for reference.

Figure 4.30. Apparent accumulation rates for the interval from 19 to 20 Ma (Early Miocene) between the Charlie Gibbs Fracture Zone and Greenland-Scotland Ridge and from the continental margin of East Greenland to shelf-break west of the U.K. Paleobathymetric contours reconstructed with the Cretaceous rifting model (Chapter 3) are shown (heavy lines) at 500 m contour intervals for reference.

Figure 4.31. Apparent accumulation rates for the interval from 29 to 30 Ma (mid-Oligocene) between the Charlie Gibbs Fracture Zone and Greenland-Scotland Ridge and from the continental margin of East Greenland to shelf-break west of the U.K. Paleobathymetric contours reconstructed with the Cretaceous rifting model (Chapter 3) are shown (heavy lines) at 500 m contour intervals for reference.

Figure 4.32. Apparent accumulation rates for the interval from 39 to 40 Ma (early Late Eocene) between the Charlie Gibbs Fracture Zone and Greenland-Scotland Ridge and from the continental margin of East Greenland to shelf-break west of the U.K. Paleobathymetric contours reconstructed with the Cretaceous rifting model (Chapter 3) are shown (heavy lines) at 500 m contour intervals for reference.

Figure 4.33. Apparent accumulation rates for the interval from 49 to 50 Ma (early Middle Eocene) between the Charlie Gibbs Fracture Zone and Greenland-Scotland Ridge and from the continental margin of East Greenland to shelf-break west of the U.K. Paleobathymetric contours reconstructed with the Cretaceous rifting model (Chapter 3) are shown (heavy lines) at 500 m contour intervals for reference.

Figure 4.34. Relative apparent accumulation rates for the interval from 0 to 1 Ma (Quaternary) between the Charlie Gibbs Fracture Zone and Greenland-Scotland Ridge and from the continental margin of East Greenland to shelf-break west of the U.K. Paleobathymetric contours reconstructed with the Cretaceous rifting model (Chapter 3) are shown (heavy lines) at 500 m contour intervals for reference. The average apparent accumulation rate for the interval from 0 to 1 Ma is 3.71 g cm^{-2} $k.y.^{-1}$ (Fig. 4.20) and is indicated by the zero-contour line. Areas with apparent accumulation rates less than the average are shaded light gray to white and areas with apparent accumulation rates greater than the average are shaded dark gray to black.

Figure 4.35. Relative apparent accumulation rates for the interval from 3 to 4 Ma (Pliocene) between the Charlie Gibbs Fracture Zone and Greenland-Scotland Ridge and from the continental margin of East Greenland to shelf-break west of the U.K. Paleobathymetric contours reconstructed with the Cretaceous rifting model (Chapter 3) are shown (heavy lines) at 500 m contour intervals for reference. The average apparent accumulation rate for the interval from 3 to 4 Ma is 4.01 g cm^{-2} $k.y.^{-1}$ (Fig. 4.20) and is indicated by the zero-contour line. Areas with apparent accumulation rates less than the average are shaded light gray to white and areas with apparent accumulation rates greater than the average are shaded dark gray to black.

Figure 4.36. Relative apparent accumulation rates for the interval from 9 to 10 Ma (early Late Miocene) between the Charlie Gibbs Fracture Zone and Greenland-Scotland Ridge and from the continental margin of East Greenland to shelf-break west of the U.K. Paleobathymetric contours reconstructed with the Cretaceous rifting model (Chapter 3) are shown (heavy lines) at 500 m contour intervals for reference. The average apparent accumulation rate for the interval from 9 to 10 Ma is 1.73 g cm^{-2} $k.y.^{-1}$ (Fig. 4.20) and is indicated by the zero-contour line. Areas with apparent accumulation rates less than the average are shaded light gray to white and areas with apparent accumulation rates greater than the average are shaded dark gray to black.

Figure 4.37. Relative apparent accumulation rates for the interval from 19 to 20 Ma (Early Miocene) between the Charlie Gibbs Fracture Zone and Greenland-Scotland Ridge and from the continental margin of East Greenland to shelf-break west of the U.K. Paleobathymetric contours reconstructed with the Cretaceous rifting model (Chapter 3) are shown (heavy lines) at 500 m contour intervals for reference. The average apparent accumulation rate for the interval from 19 to 20 Ma is 1.79 g cm^{-2} $k.y.^{-1}$ (Fig. 4.20) and is indicated by the zero-contour line. Areas with apparent accumulation rates less than the average are shaded light gray to white and areas with apparent accumulation rates greater than the average are shaded dark gray to black.

Figure 4.38. Relative apparent accumulation rates for the interval from 29 to 30 Ma (mid-Oligocene) between the Charlie Gibbs Fracture Zone and Greenland-Scotland Ridge and from the continental margin of East Greenland to shelf-break west of the U.K. Paleobathymetric contours reconstructed with the Cretaceous rifting model (Chapter 3) are shown (heavy lines) at 500 m contour intervals for reference. The average apparent accumulation rate for the interval from 29 to 30 Ma is 1.58 g cm^{-2} $k.y.^{-1}$ (Fig. 4.20) and is indicated by the zero-contour line. Areas with apparent accumulation rates less than the average are shaded light gray to white and areas with apparent accumulation rates greater than the average are shaded dark gray to black.

Figure 4.39. Relative apparent accumulation rates for the interval from 39 to 40 Ma (early Late Oligocene) between the Charlie Gibbs Fracture Zone and Greenland-Scotland Ridge and from the continental margin of East Greenland to shelf-break west of the U.K. Paleobathymetric contours reconstructed with the Cretaceous rifting model (Chapter 3) are shown (heavy lines) at 500 m contour intervals for reference. The average apparent accumulation rate for the interval from 39 to 40 Ma is 2.76 g cm^{-2} $k.y.^{-1}$ (Fig. 4.20) and is indicated by the zero-contour line. Areas with apparent accumulation rates less than the average are shaded light gray to white and areas with apparent accumulation rates greater than the average are shaded dark gray to black.

Figure 4.40. Relative apparent accumulation rates for the interval from 49 to 50 Ma (early Middle Oligocene) between the Charlie Gibbs Fracture Zone and Greenland-Scotland Ridge and from the continental margin of East Greenland to shelf-break west of the U.K. Paleobathymetric contours reconstructed with the Cretaceous rifting model (Chapter 3) are shown (heavy lines) at 500 m contour intervals for reference. The average apparent accumulation rate for the interval from 49 to 50 Ma is 2.44 g cm^{-2} $k.y.^{-1}$ (Fig. 4.20) and is indicated by the zero-contour line. Areas with apparent accumulation rates less than the average are shaded light gray to white and areas with apparent accumulation rates greater than the average are shaded dark gray to black.

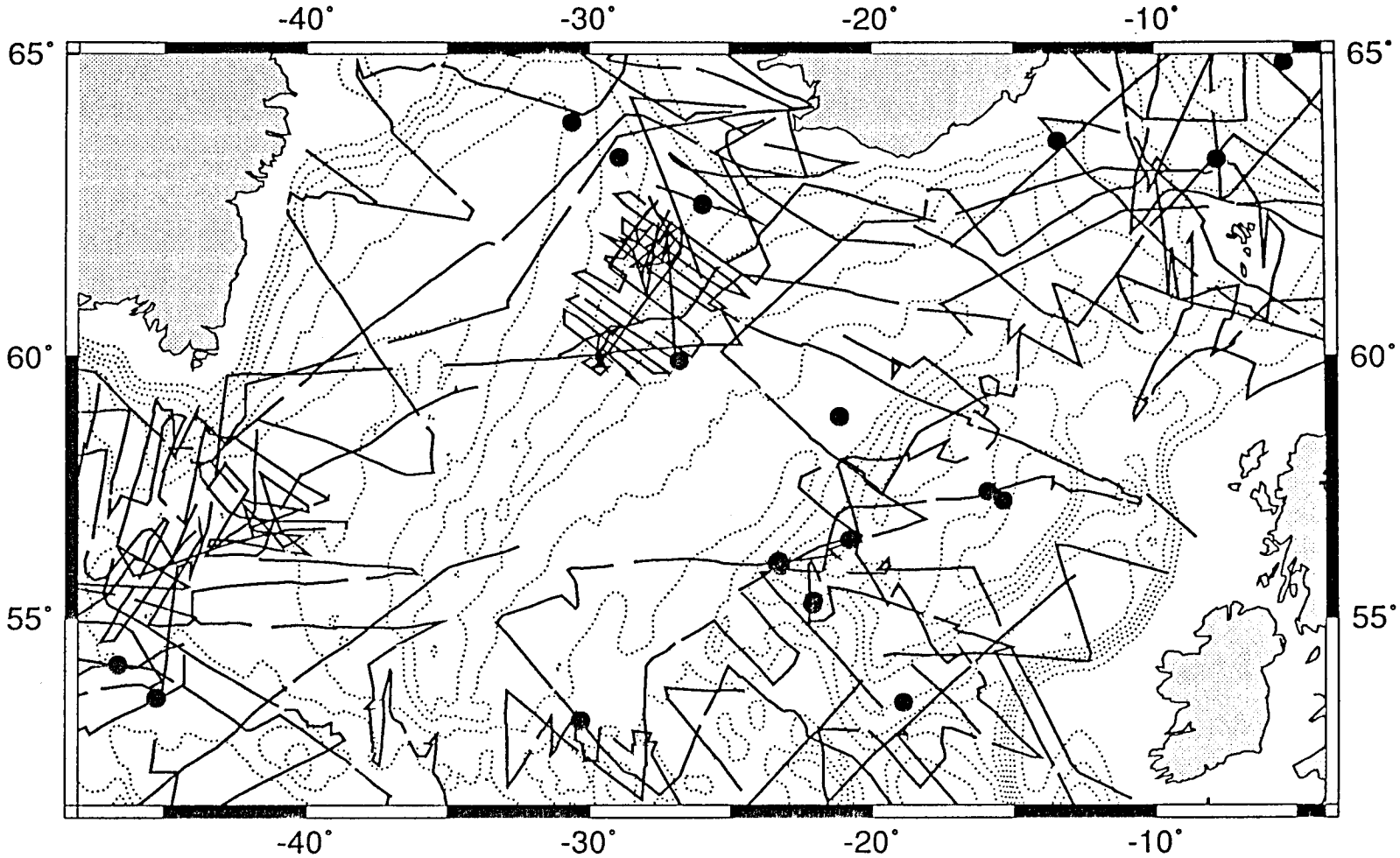

Figure 4.1

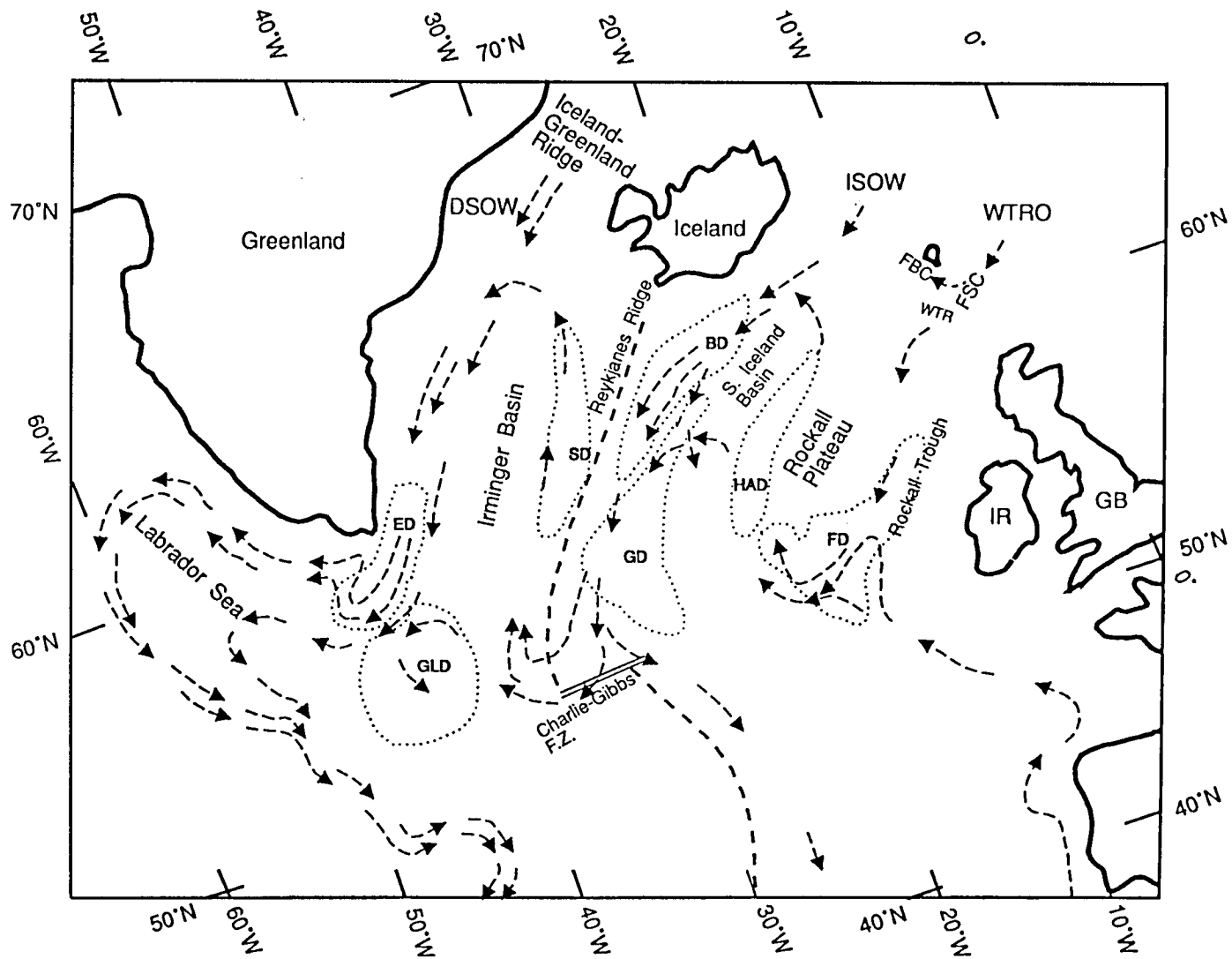
50°W
40°W
30°W
70°N
20°W
10°W
0°
Iceland-
Greenland
Ridge
ISOW
WTRO
DSOW
70°N
Greenland
Iceland
60°N
FBC
FSC
WTR
Reykjanes Ridge
BD
S. Iceland
Basin
60°W
Irminger Basin
SD
Rockall
Plateau
HAD
Rockall Trough
IR
GB
ED
FD
50°N
0°
Labrador Sea
GD
60°N
GLD
Charlie-Gibbs
F.Z.
40°N
50°N
60°W
50°W
40°W
30°W
40°N
20°W
10°W

Figure 4.2

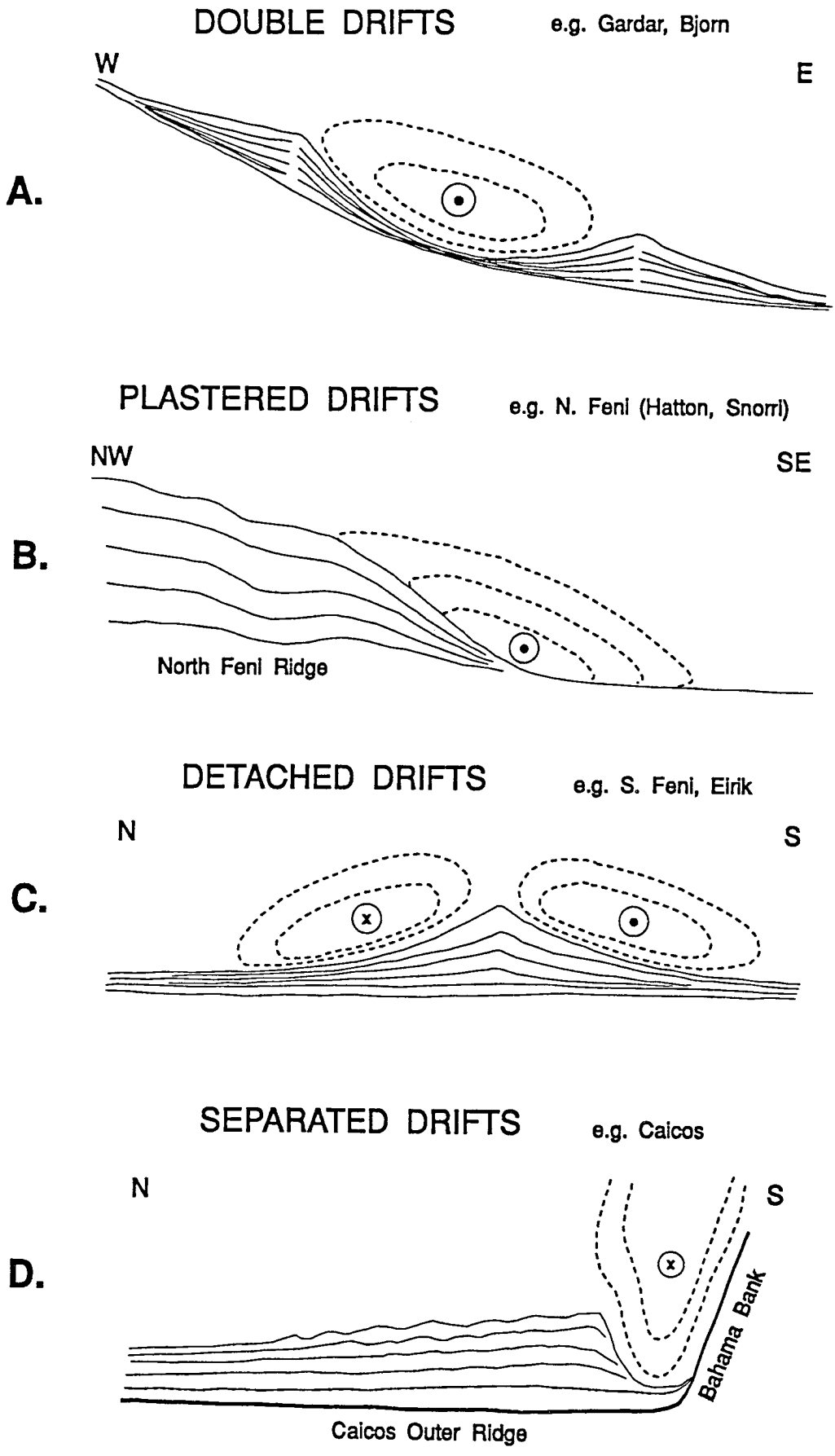
DOUBLE DRIFTS
e.g. Gardar, Bjorn
W
E
A.
PLASTERED DRIFTS
e.g. N. Feni (Hatton, Snorri)
NW
SE
B.
North Feni Ridge
DETACHED DRIFTS
e.g. S. Feni, Eirik
N
S
C.
SEPARATED DRIFTS
e.g. Caicos
N
S
D.
Bahama Bank
Caicos Outer Ridge

Figure 4.3

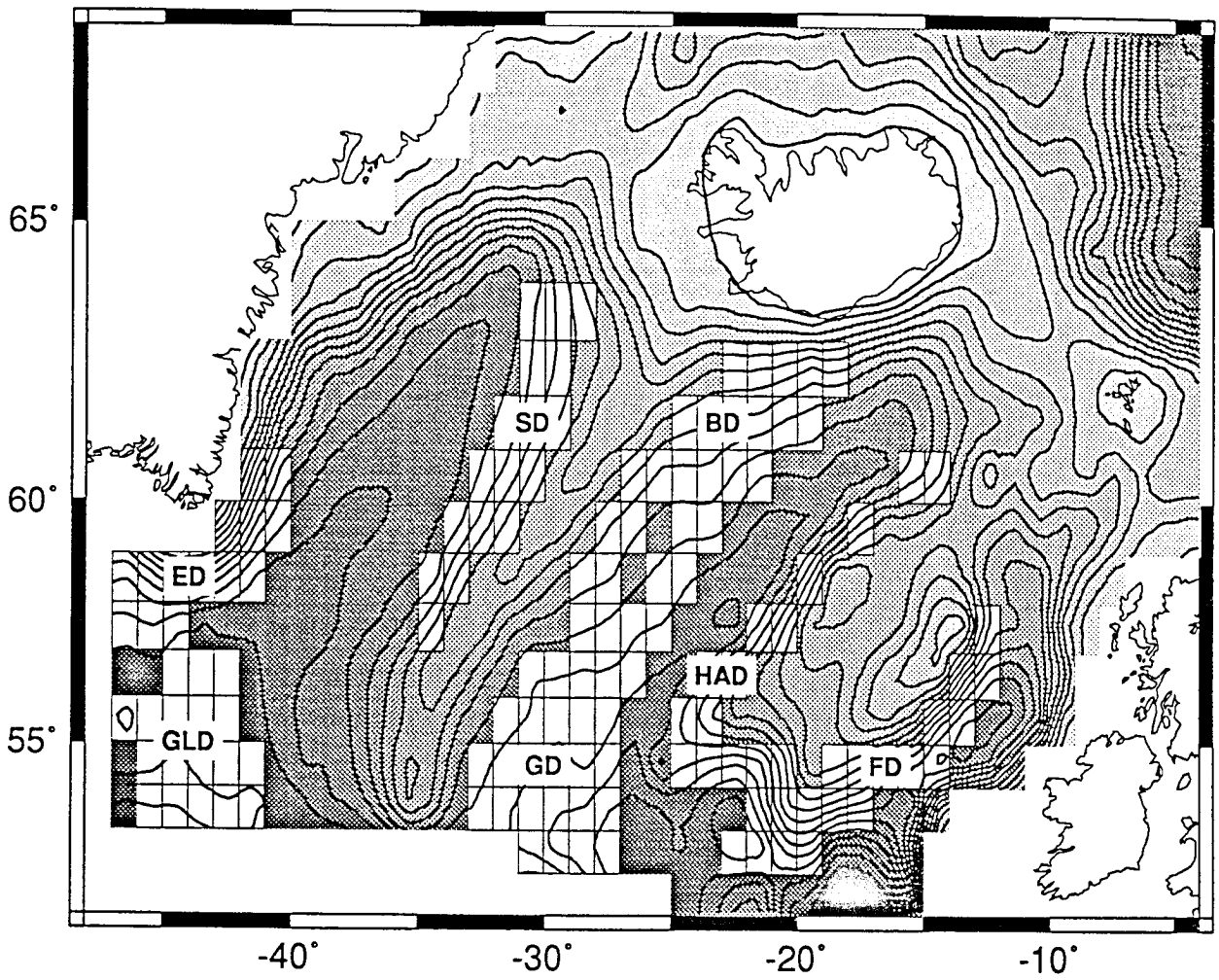

Figure 4.4

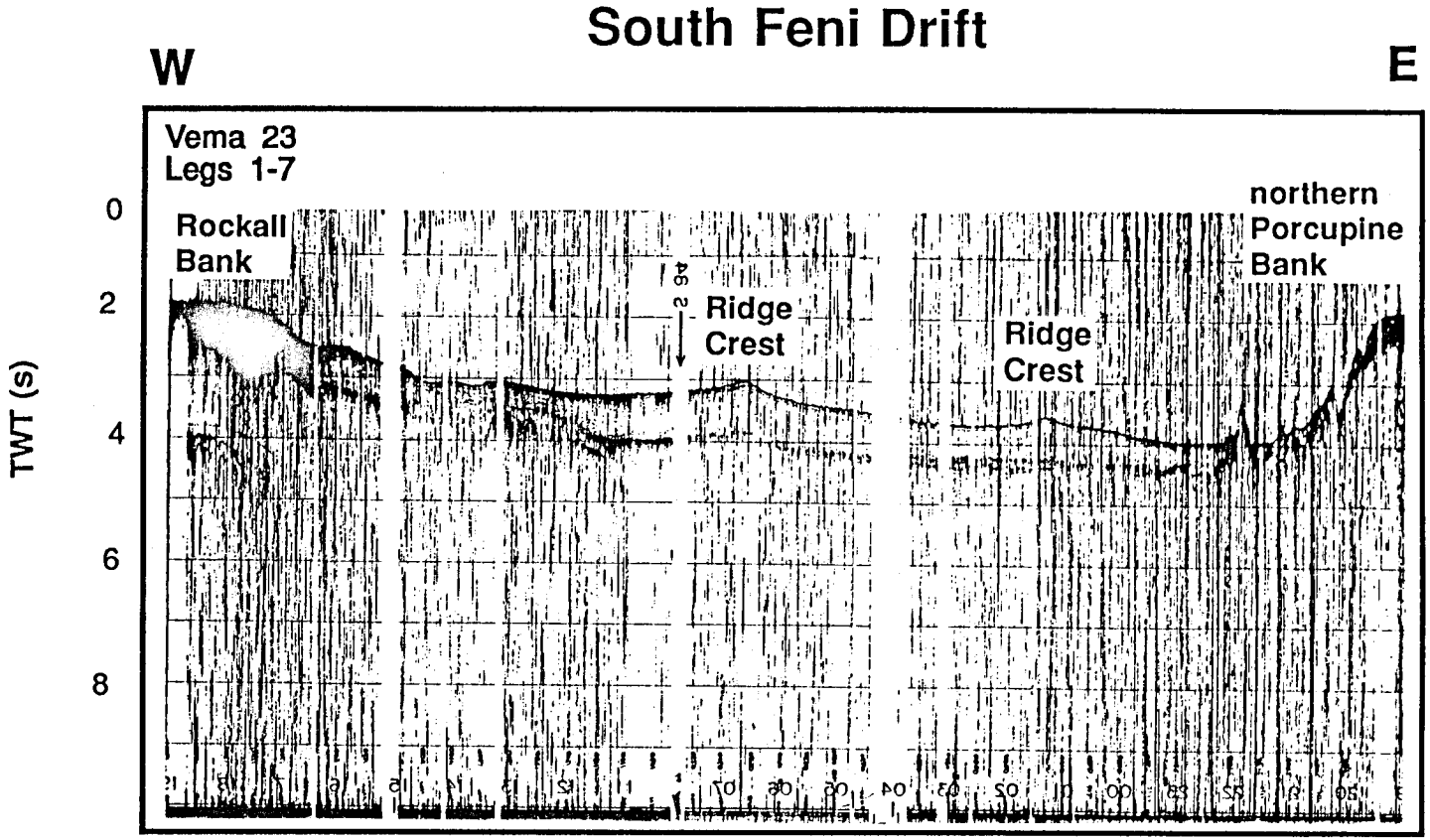
South Feni Drift
W
E
Vema 23
Legs 1-7
Rockall
Bank
Ridge
Crest
Ridge
Crest
northern
Porcupine
Bank
TWT (s)
0
2
4
6
8

Figure 4.5

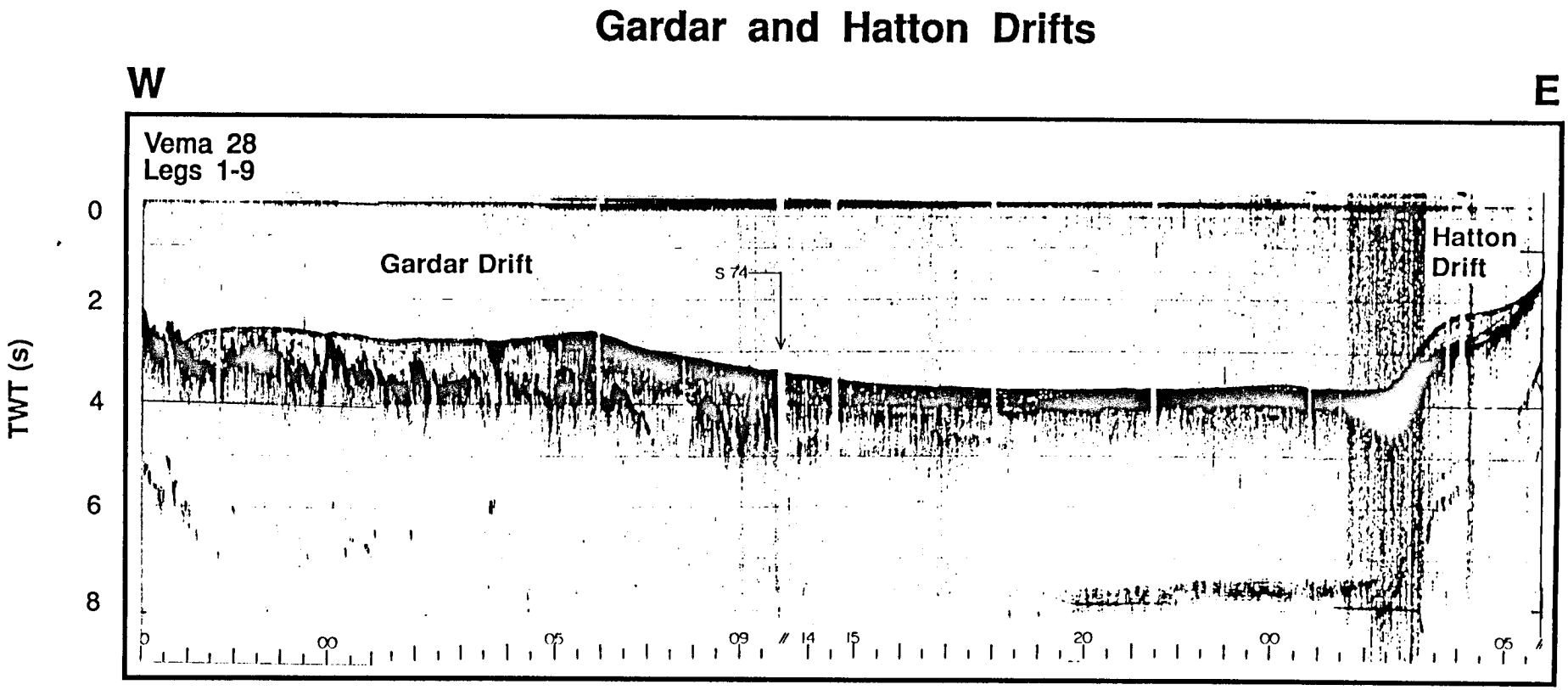
Gardar and Hatton Drifts
W
E
Vema 28
Legs 1-9
TWT (s)
0
2
4
6
8
Gardar Drift
S 74
Hatton
Drift
00
05
09
14
15
20
00
05

Figure 4.6

Gardar Drift

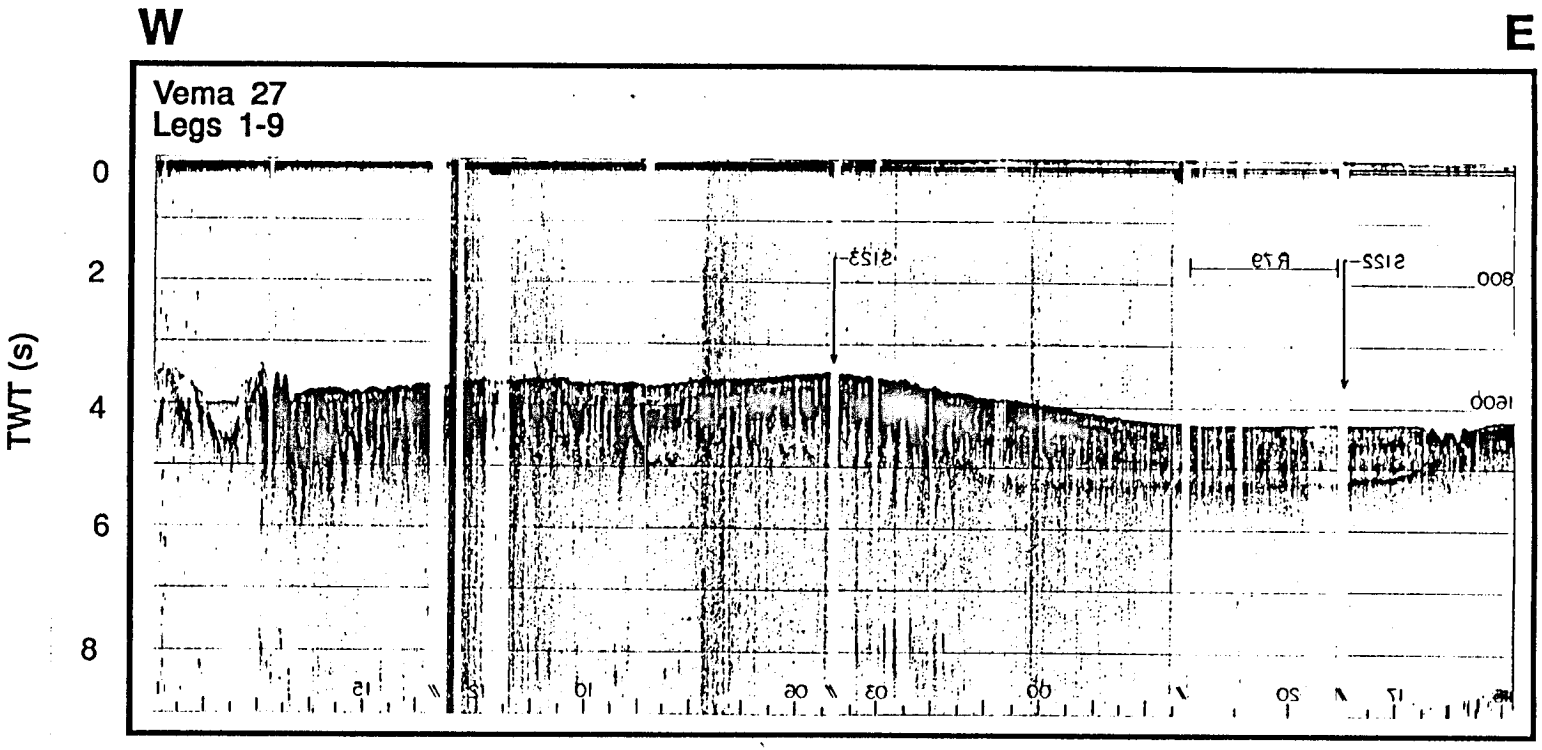

Figure 4.7

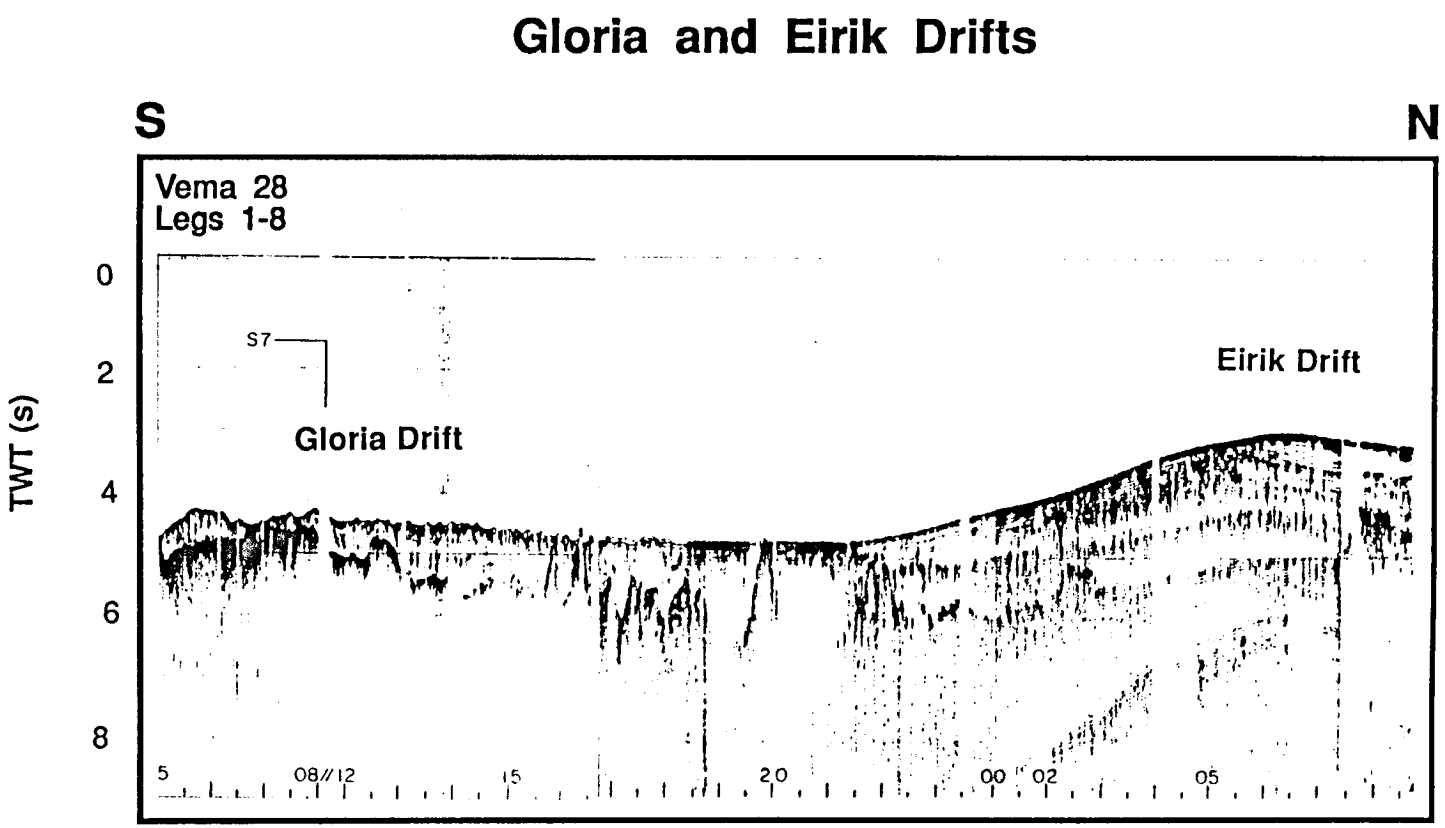
Gloria and Eirik Drifts
S
N
Vema 28
Legs 1-8
TWT (s)
0
2
4
6
8
S7
Gloria Drift
Eirik Drift
5
08//12
15
20
00
02
05

Figure 4.8

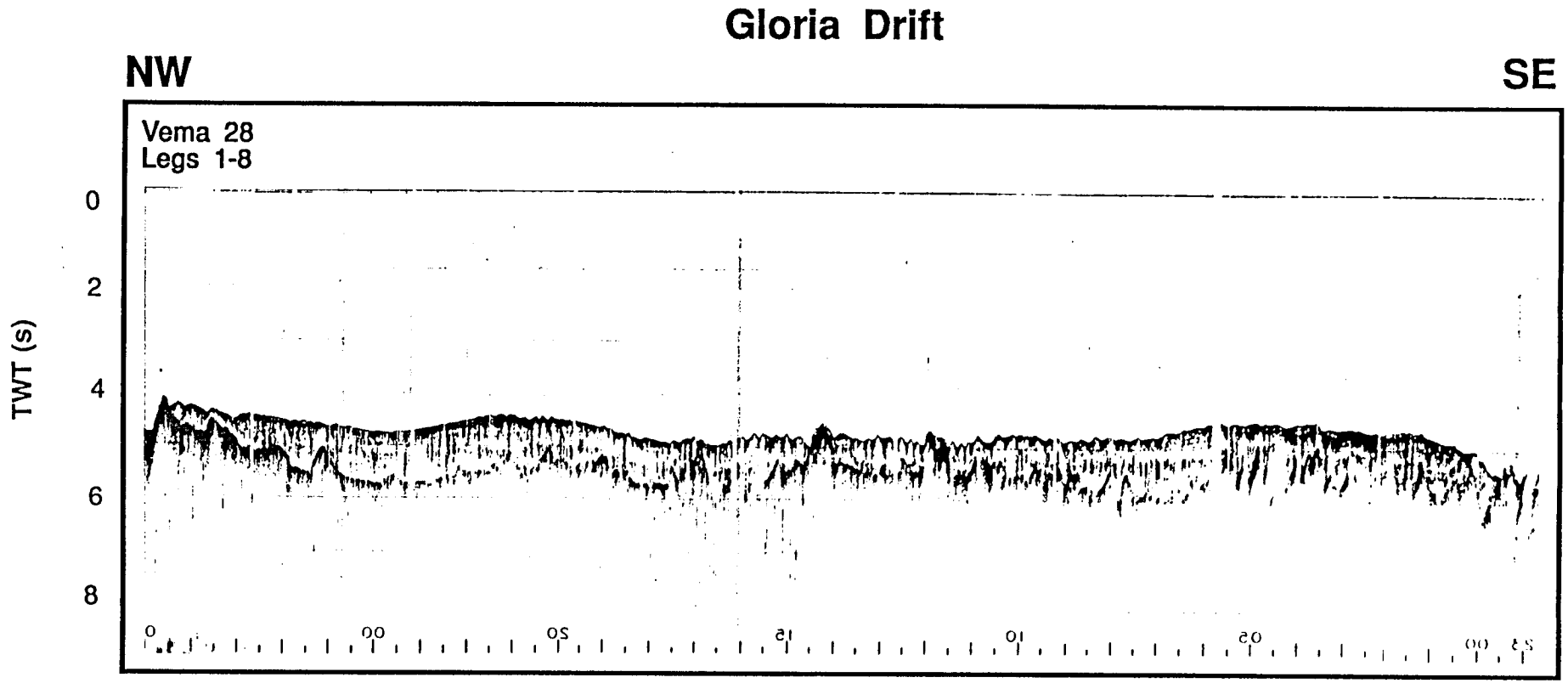

Figure 4.9

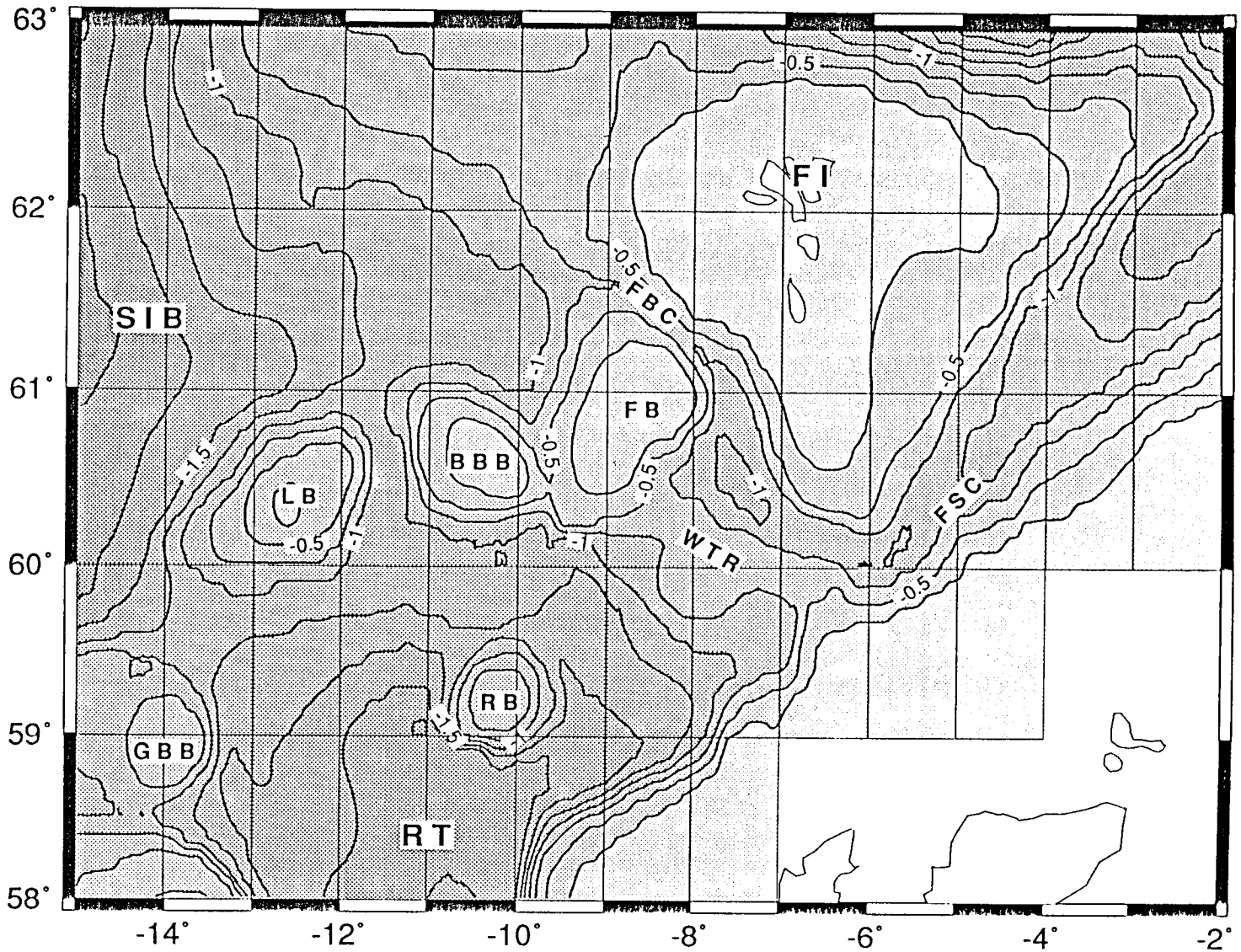
63°
62°
61°
60°
59°
58°
-14°
-12°
-10°
-8°
-6°
-4°
-2°
SIB
FI
FBC
FB
BBB
LB
GBB
RB
RT
WTR
FSC
-0.5
-1
-1.5

Figure 4.10

Sediment Drifts - 5 Ma

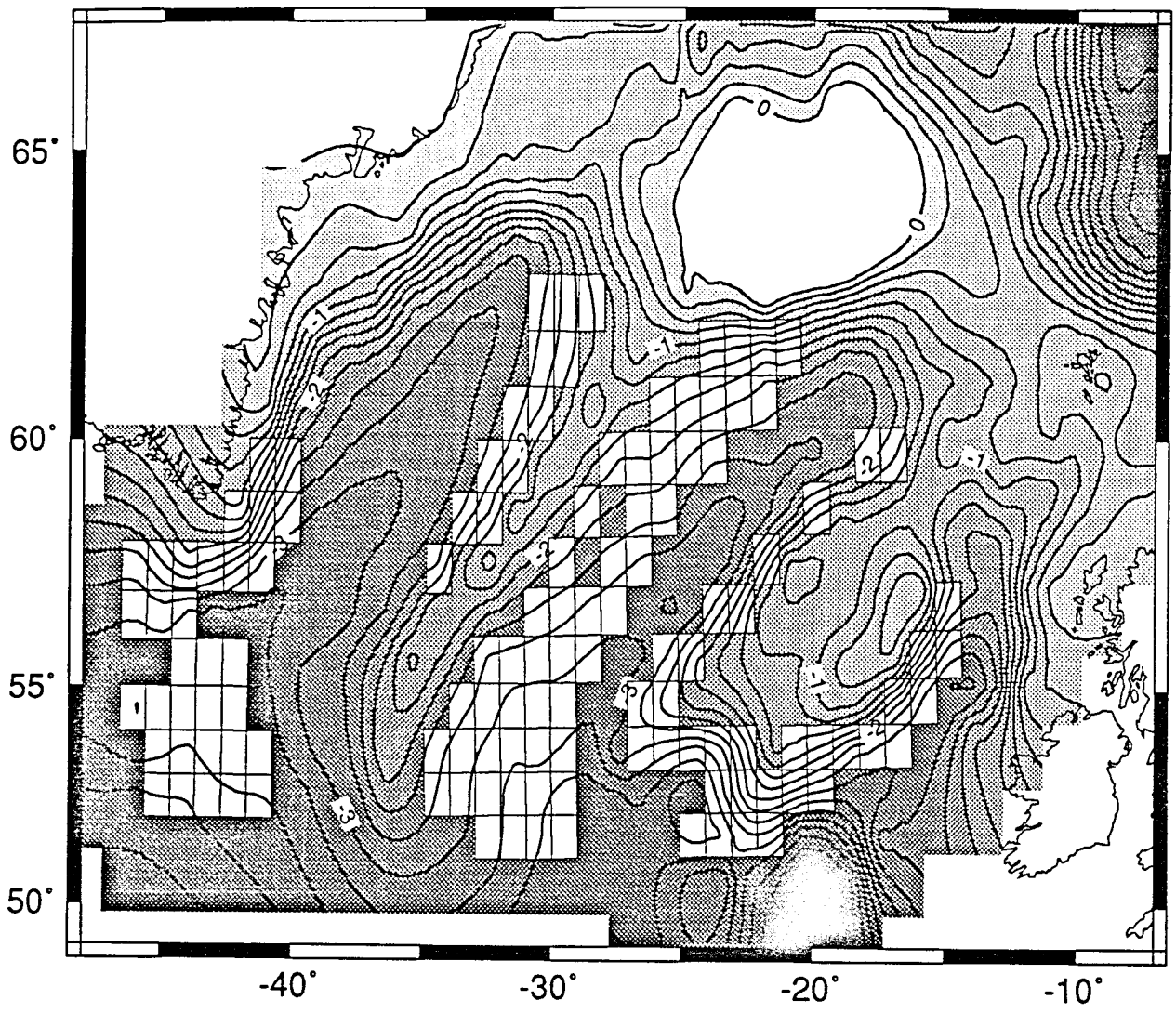

Figure 4.11

Sediment Drifts - 10 Ma

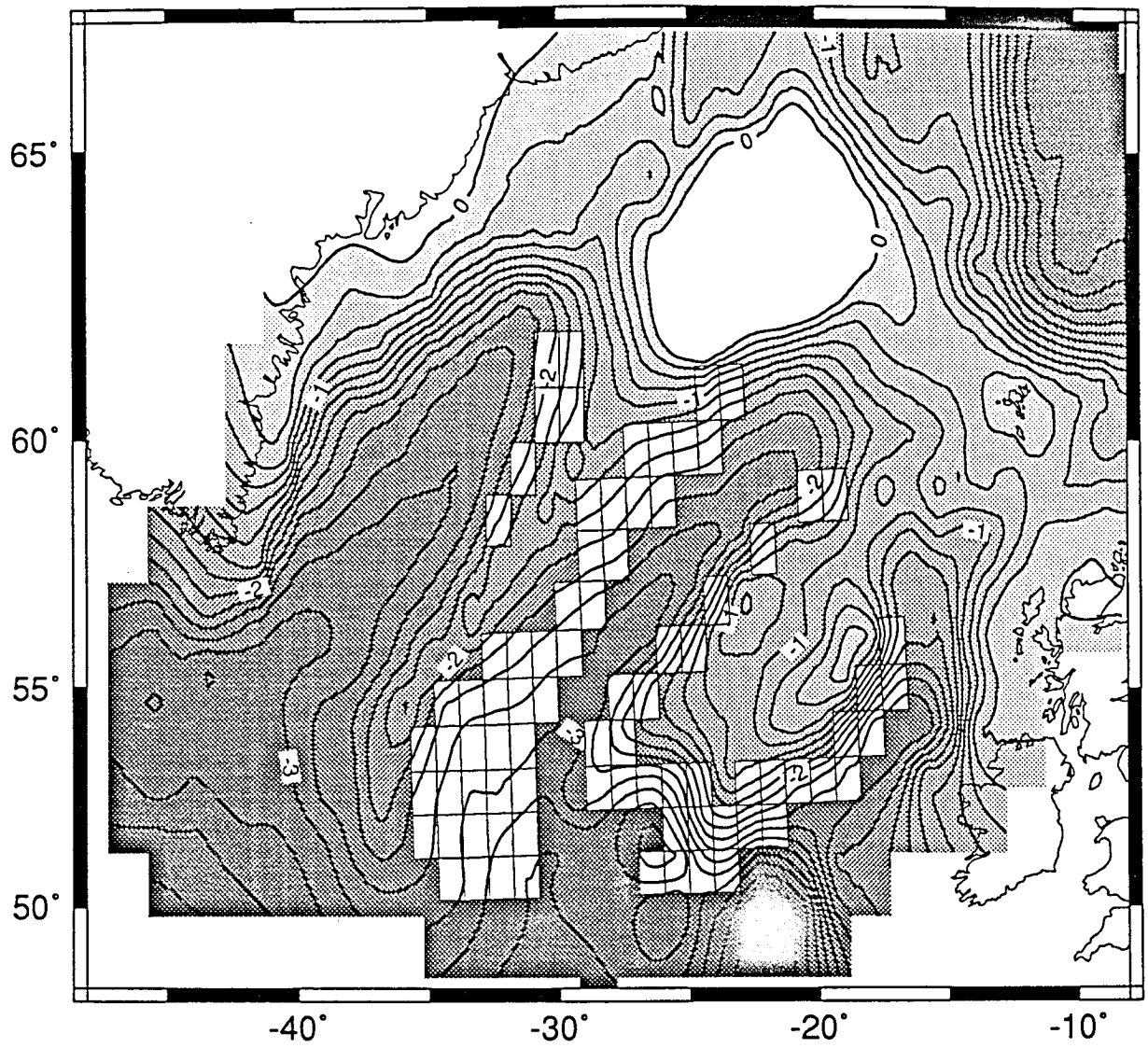

Figure 4.12

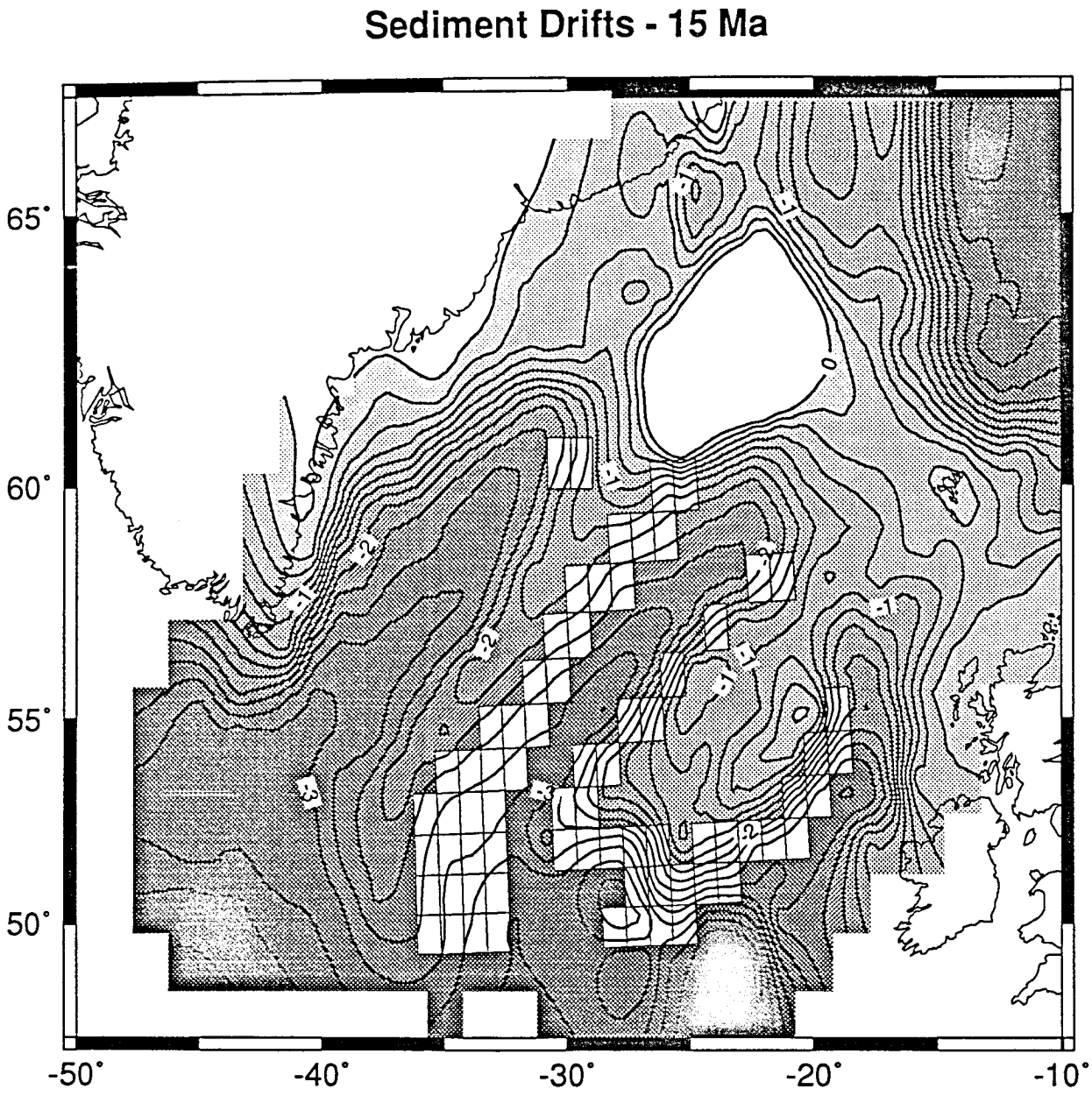

Figure 4.13

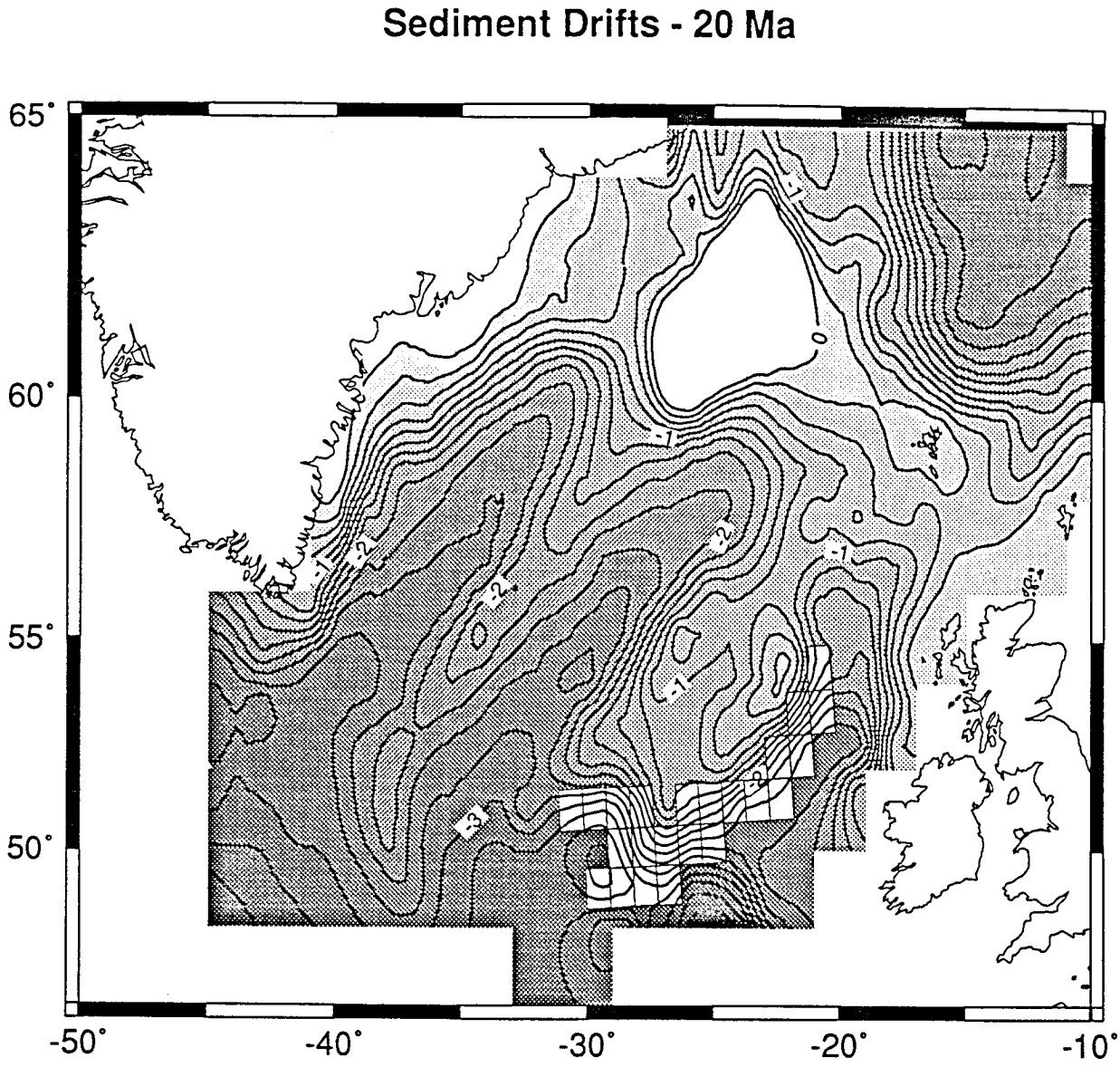

Figure 4.14

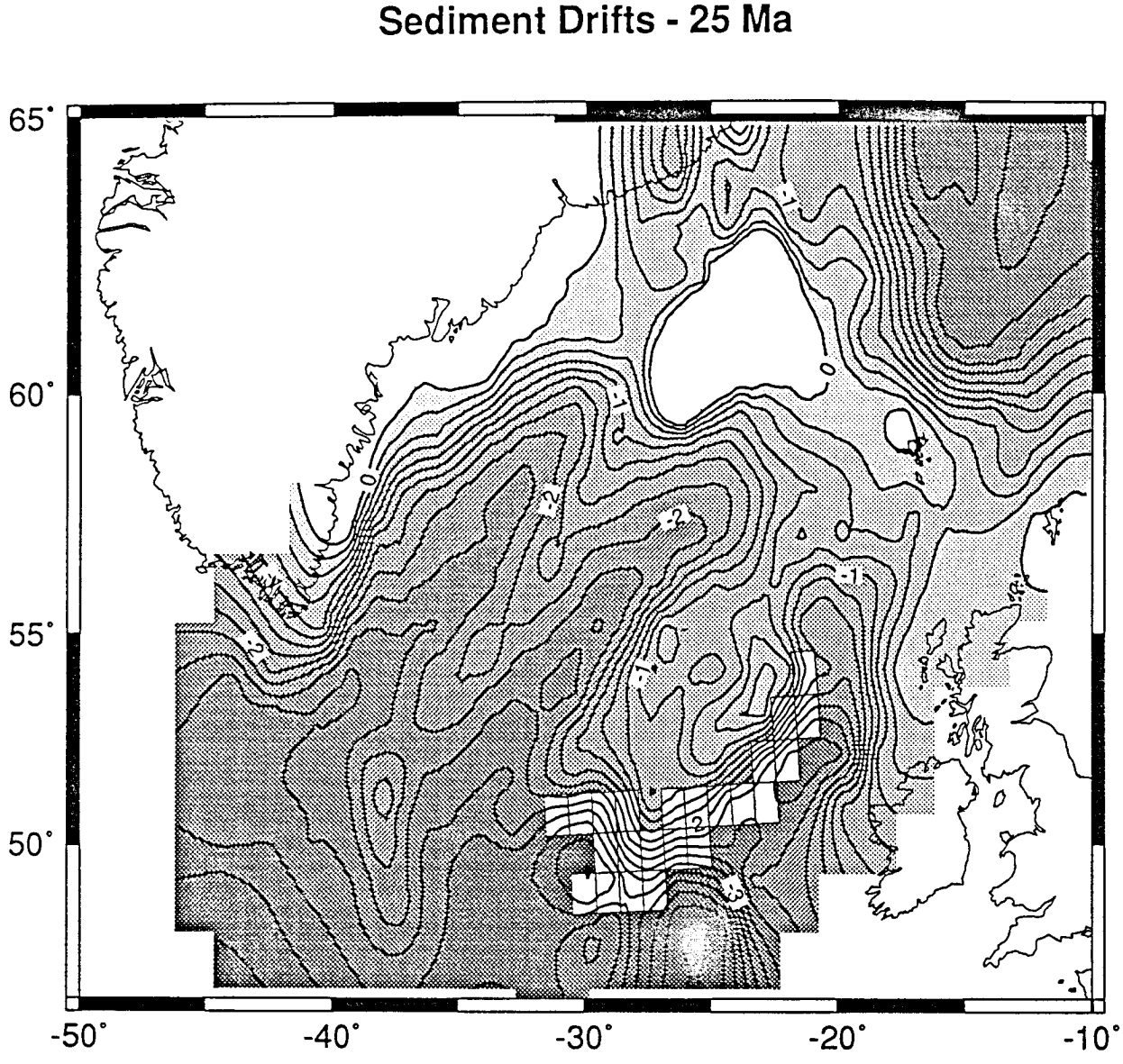

Figure 4.15

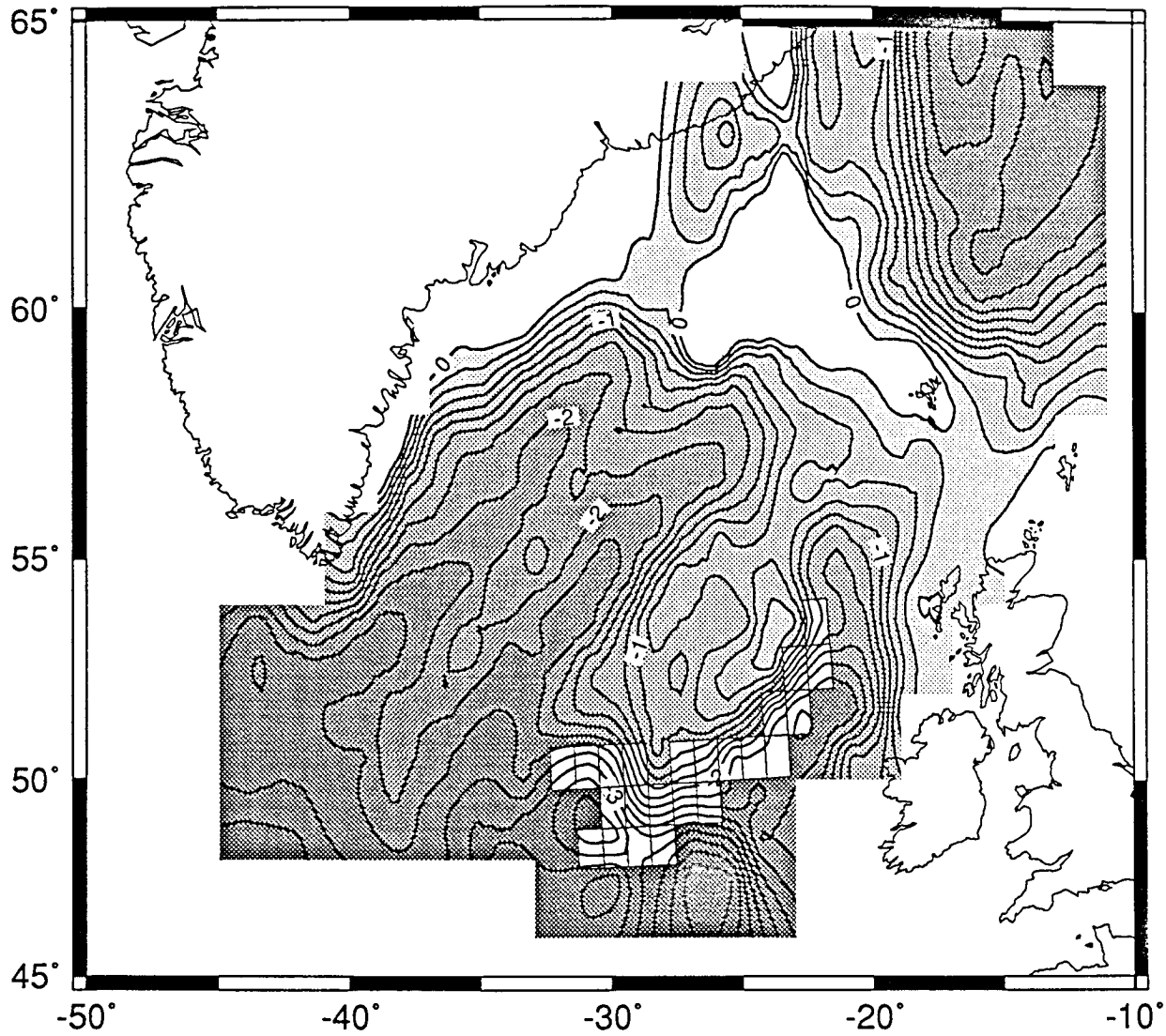

Figure 4.16

Sediment Drifts - 35 Ma

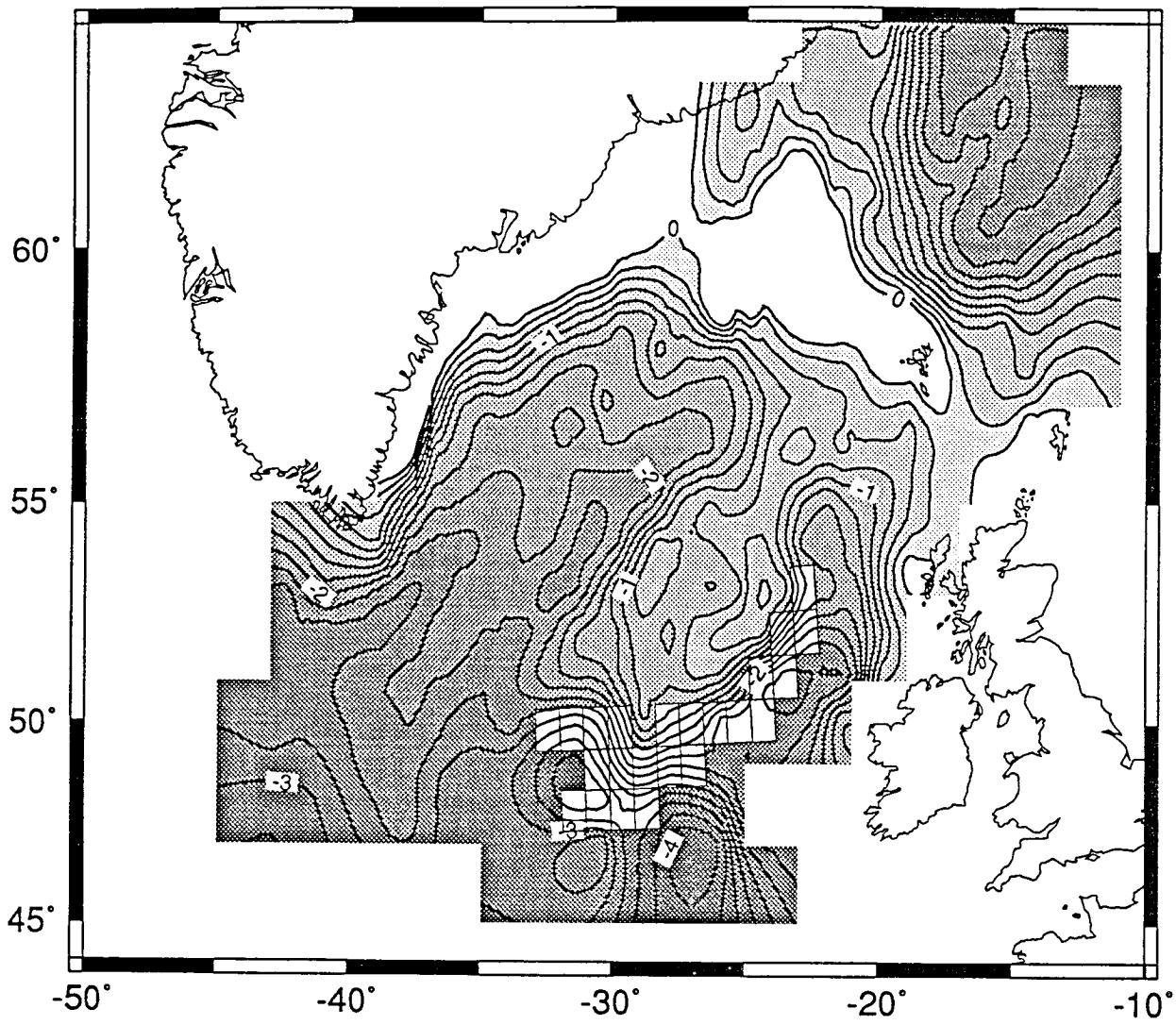

Figure 4.17

Figure 4.18

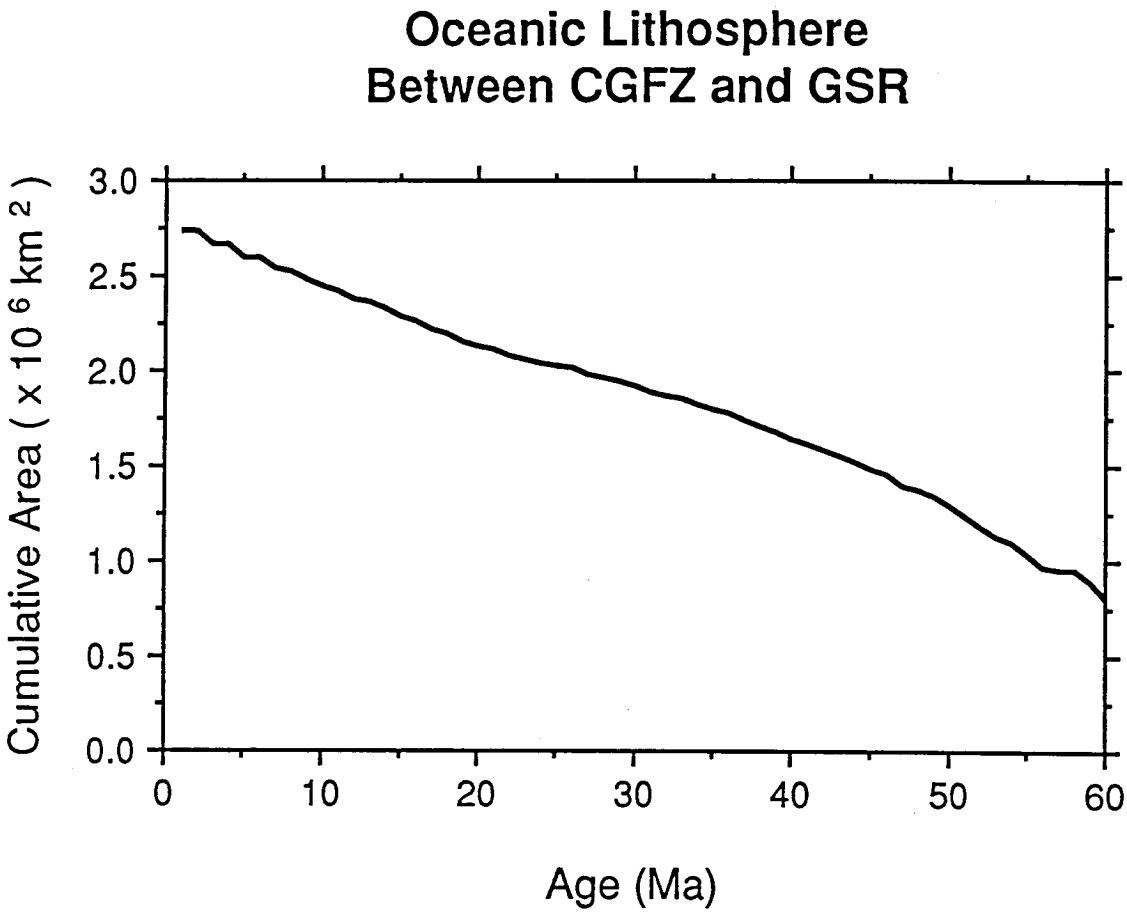
Oceanic Lithosphere
Between CGFZ and GSR
Cumulative Area (x 10 6 km 2)
3.0
2.5
2.0
1.5
1.0
0.5
0.0
0
10
20
30
40
50
60
Age (Ma)

Figure 4.19

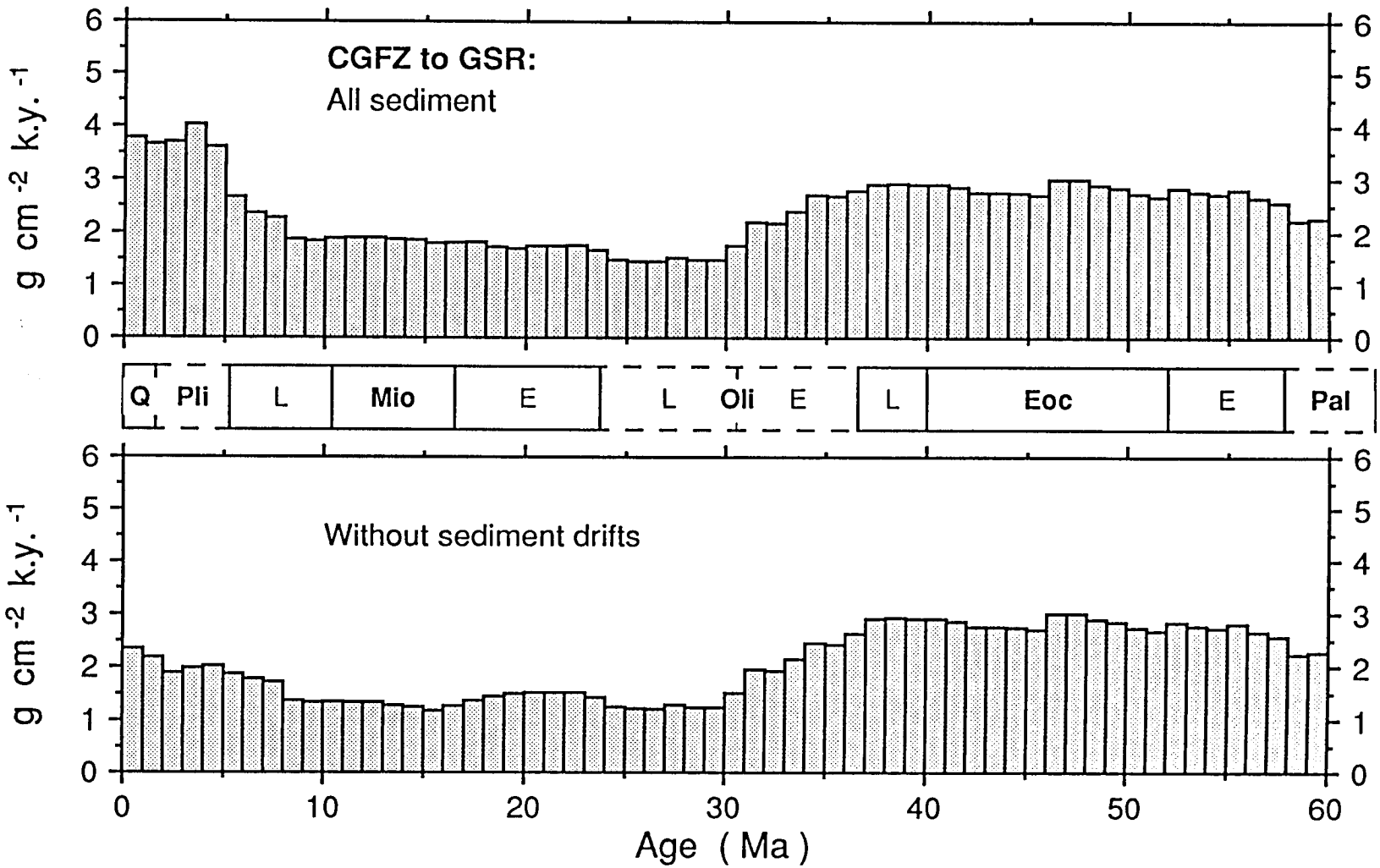
CGFZ to GSR:
All sediment
g cm -2 k.y. -1
Q
Pli
L
Mio
E
L
Oli
E
L
Eoc
E
Pal
Without sediment drifts
g cm -2 k.y. -1
0
10
20
30
40
50
60
Age (Ma)

Figure 4.20

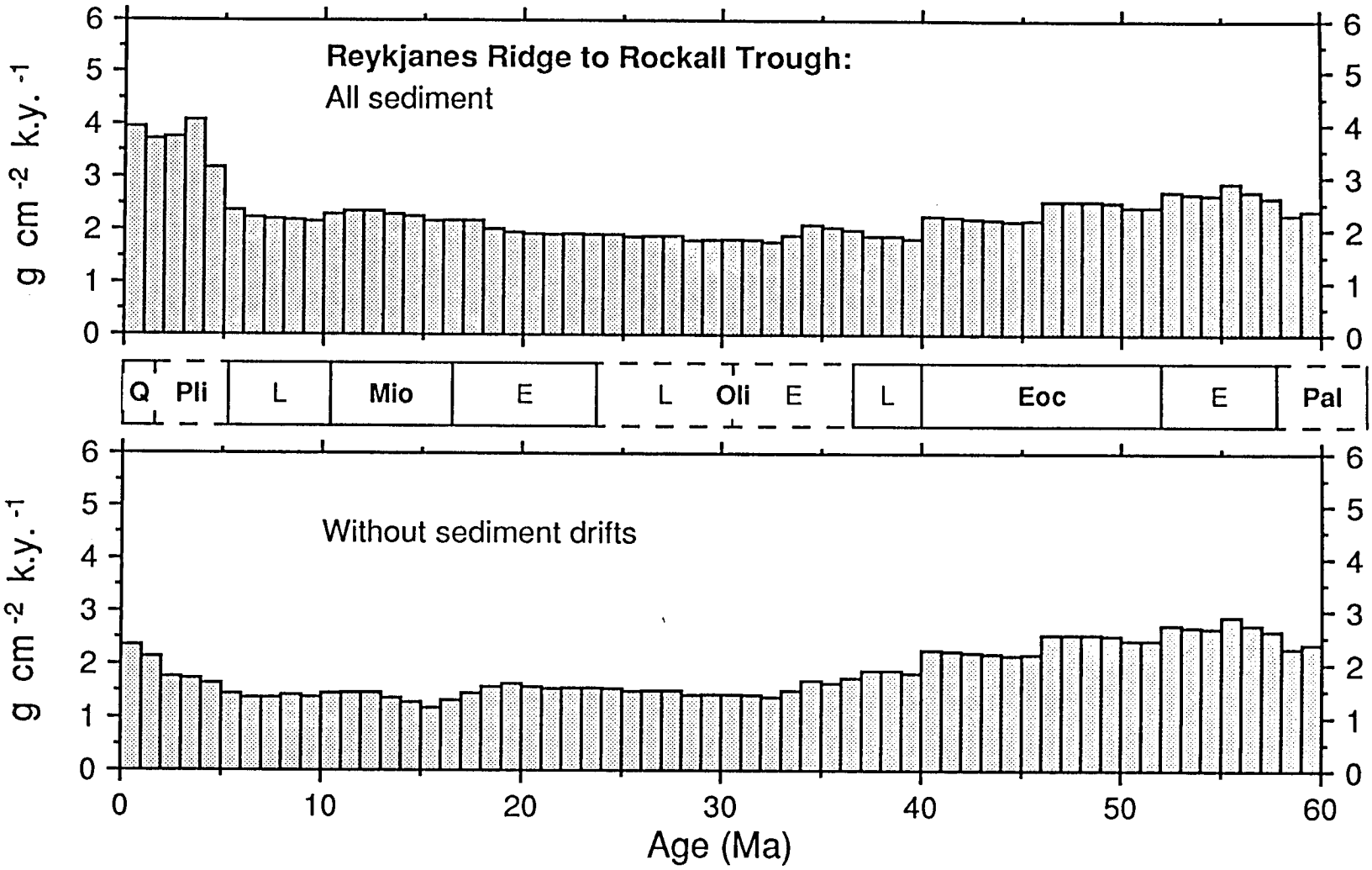
Reykjanes Ridge to Rockall Trough:
All sediment
Without sediment drifts
g cm -2 k.y. -1
Q
Pli
L
Mio
E
L
Oli
E
L
Eoc
E
Pal
0
10
20
30
40
50
60
Age (Ma)

Figure 4.21

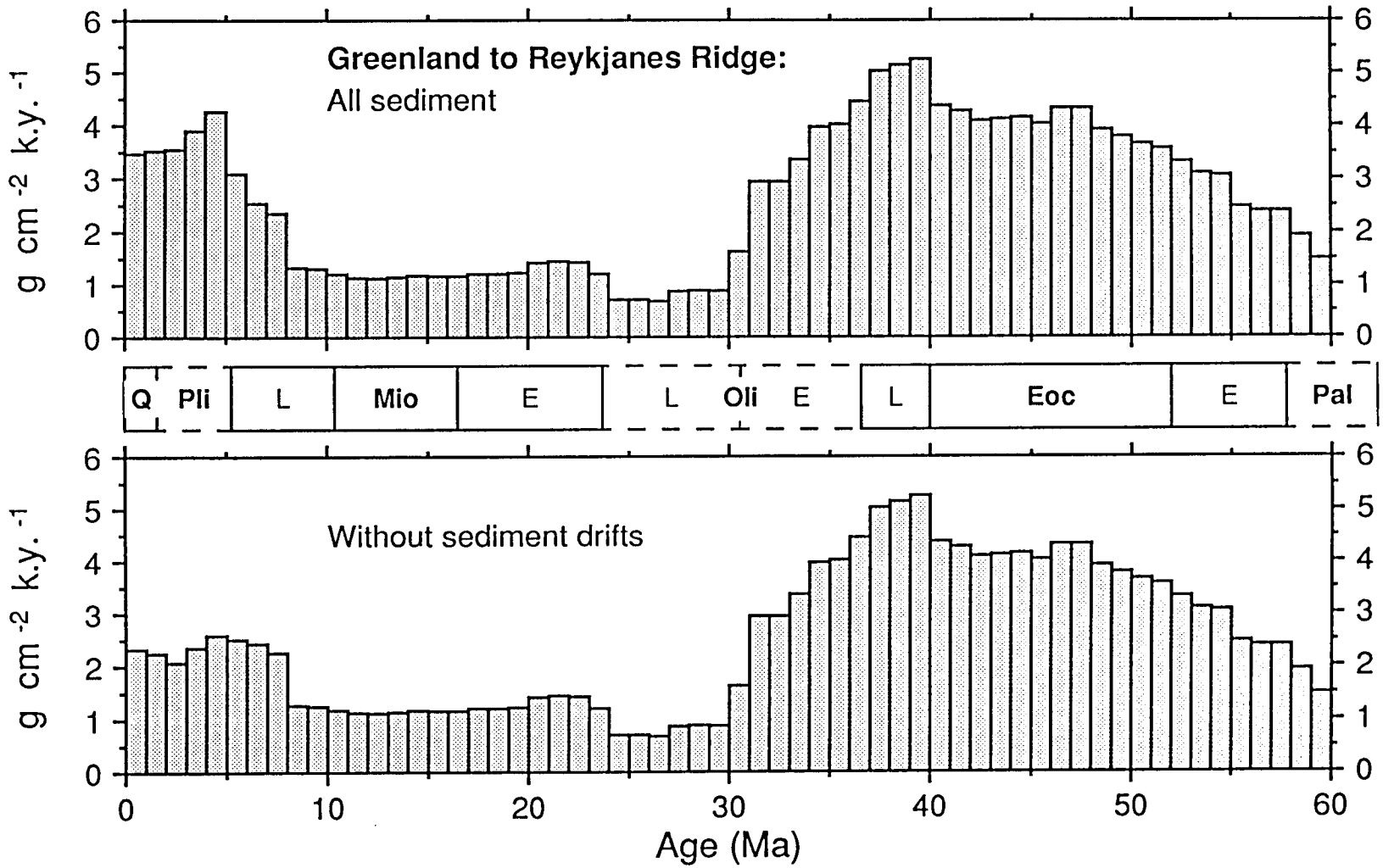
Greenland to Reykjanes Ridge:
All sediment
Without sediment drifts
g cm -2 k.y. -1
Q
Pli
L
Mio
E
L
Oli
E
L
Eoc
E
Pal
0
10
20
30
40
50
60
Age (Ma)

Figure 4.22

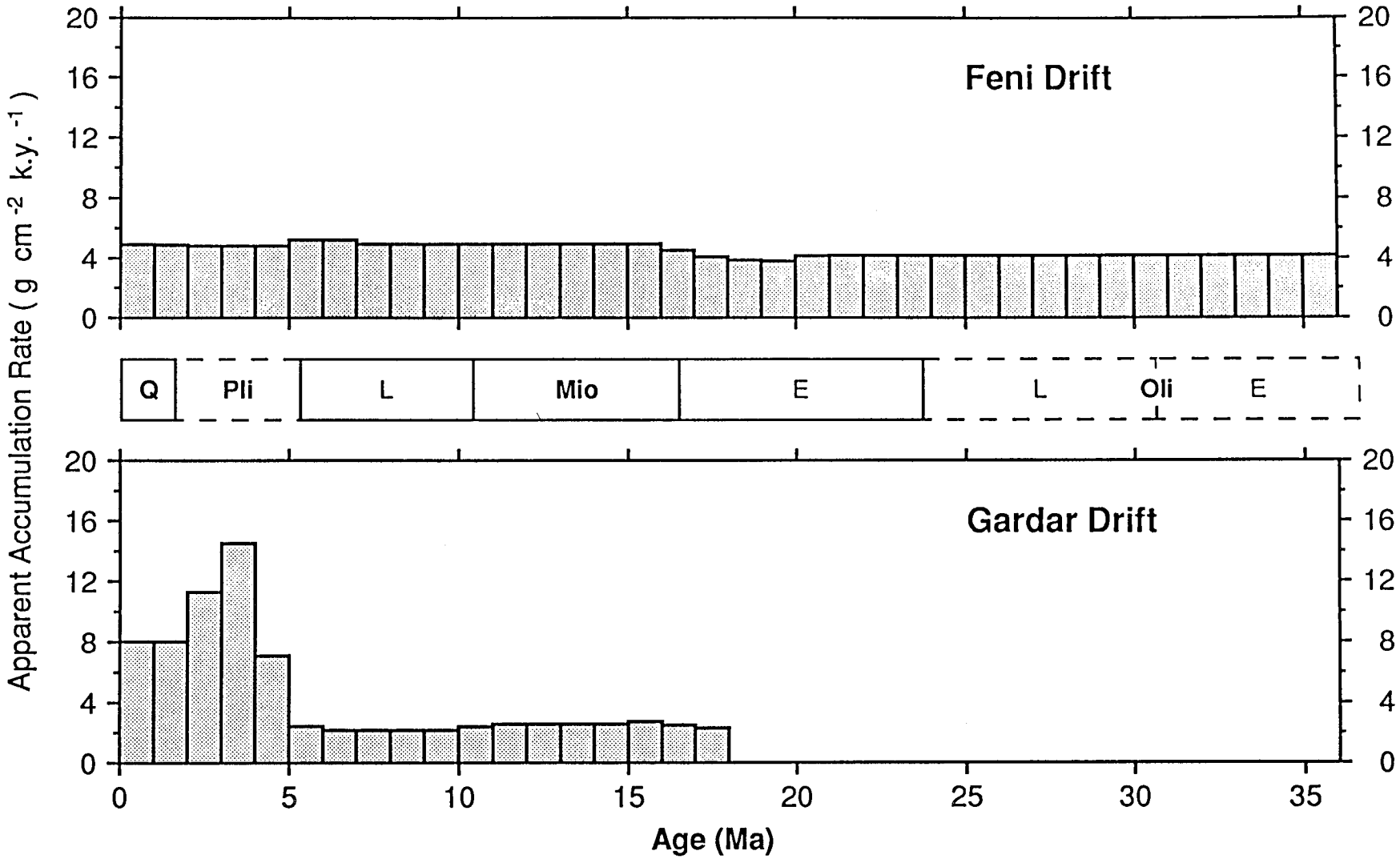
Feni Drift
Gardar Drift
Apparent Accumulation Rate (g cm -2 k.y. -1)
Age (Ma)
Q
Pli
L
Mio
E
L
Oli
E
0
4
8
12
16
20
0
5
10
15
20
25
30
35

Figure 4.23

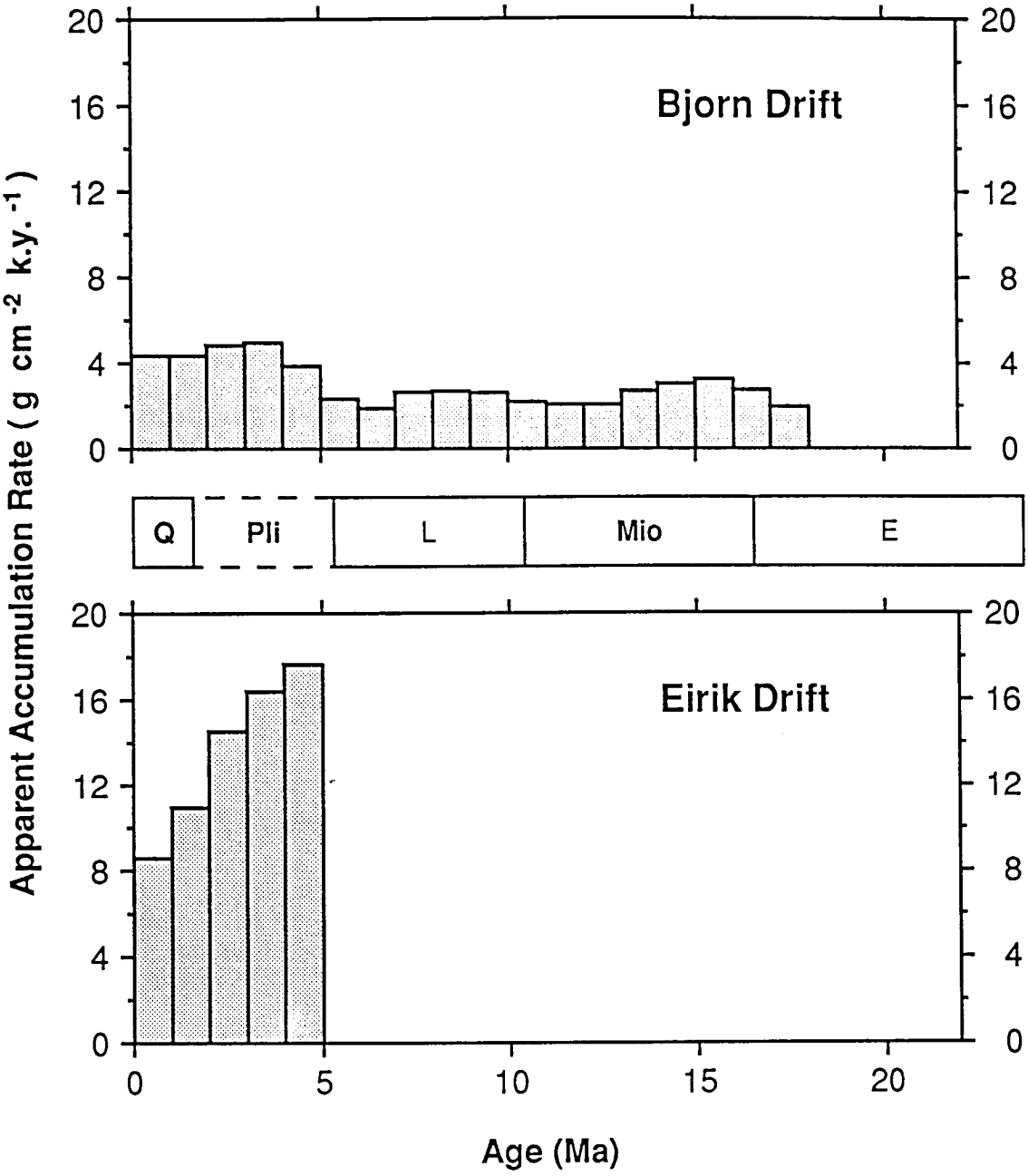
Bjorn Drift
Eirik Drift
Q
Pli
L
Mio
E
Apparent Accumulation Rate (g cm -2 k.y. -1)
Age (Ma)
0
4
8
12
16
20
0
5
10
15
20

Figure 4.24

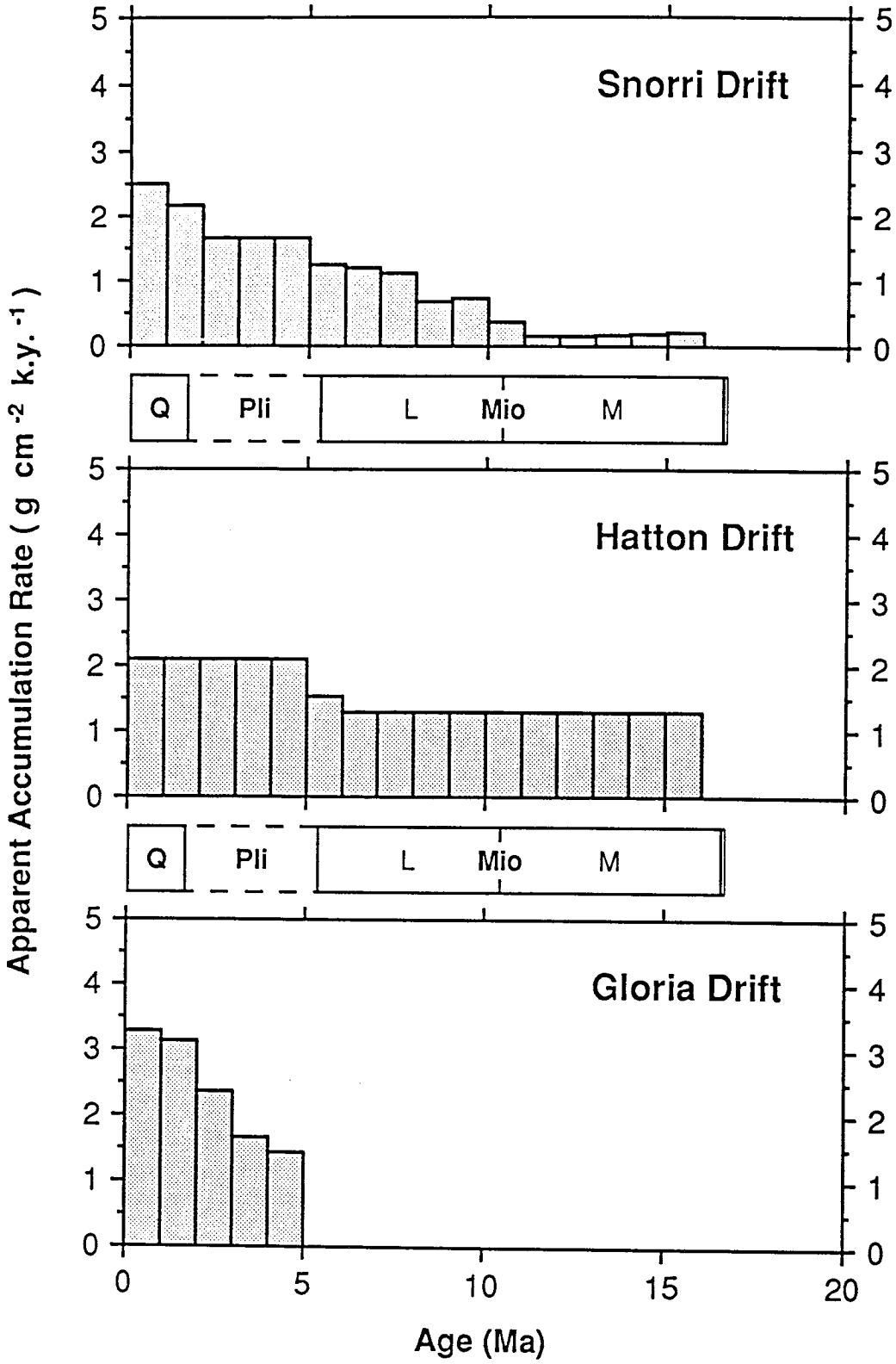
Snorri Drift
Hatton Drift
Gloria Drift
Q
Pli
L
Mio
M
Apparent Accumulation Rate (g cm -2 k.y. -1)
Age (Ma)
0
5
10
15
20
0
1
2
3
4
5

Figure 4.25

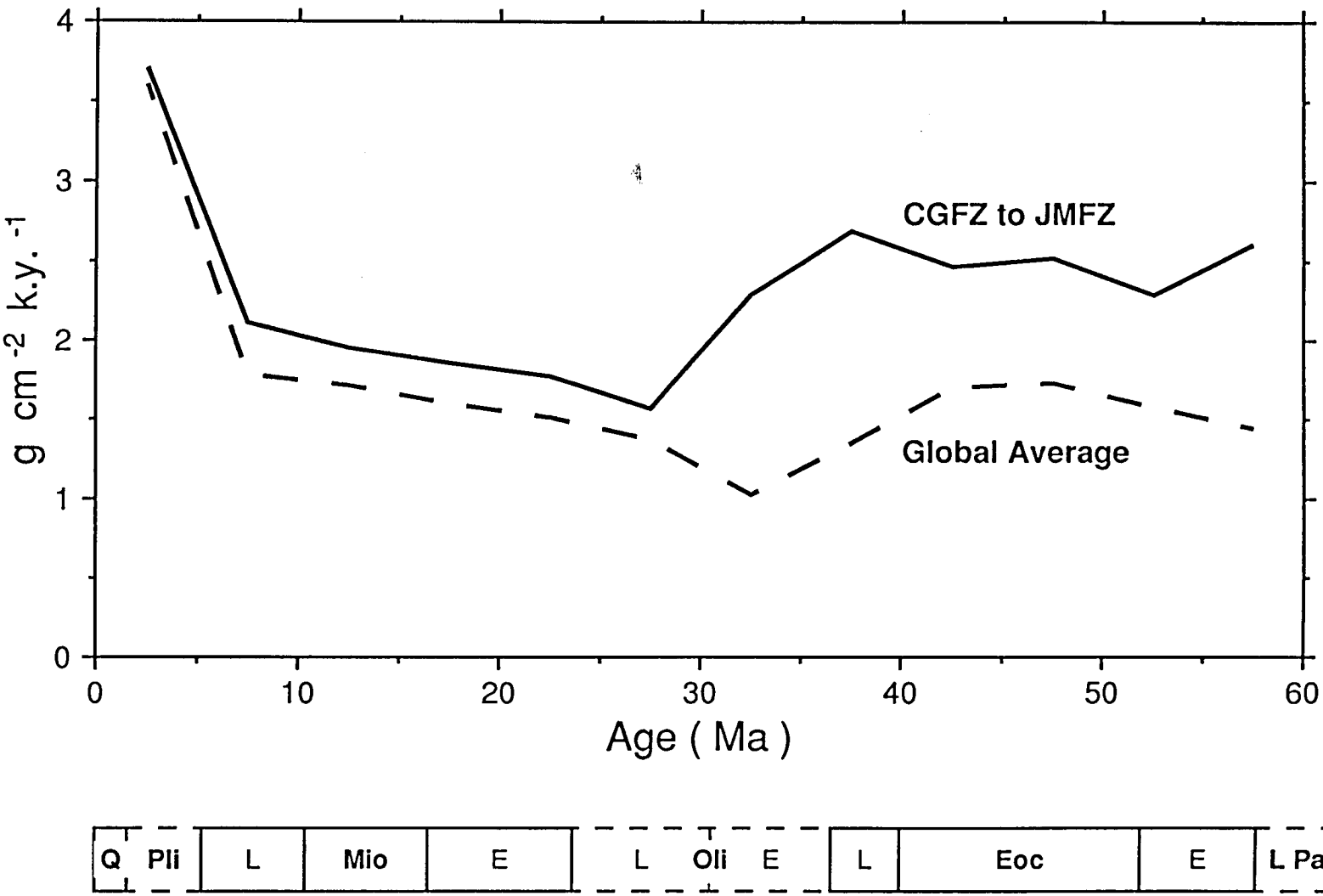
4
3
2
1
0
g cm -2 k.y. -1
CGFZ to JMFZ
Global Average
0
10
20
30
40
50
60
Age (Ma)
Q
Pli
L
Mio
E
L
Oli
E
L
Eoc
E
L Pal

Figure 4.26

0 to 1 Ma - Accumulation Rates

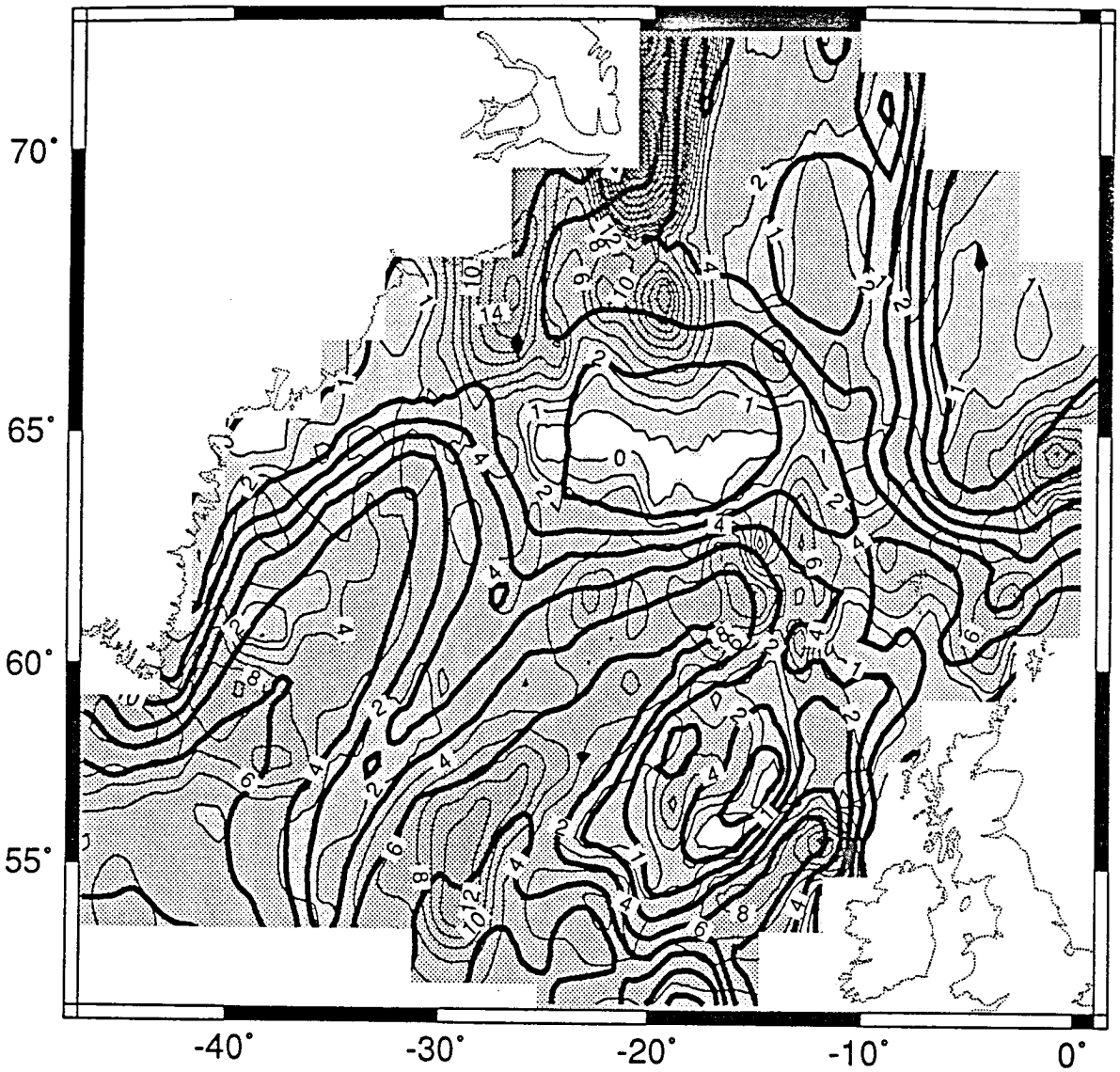

Figure 4.27

3 to 4 Ma - Accumulation Ra

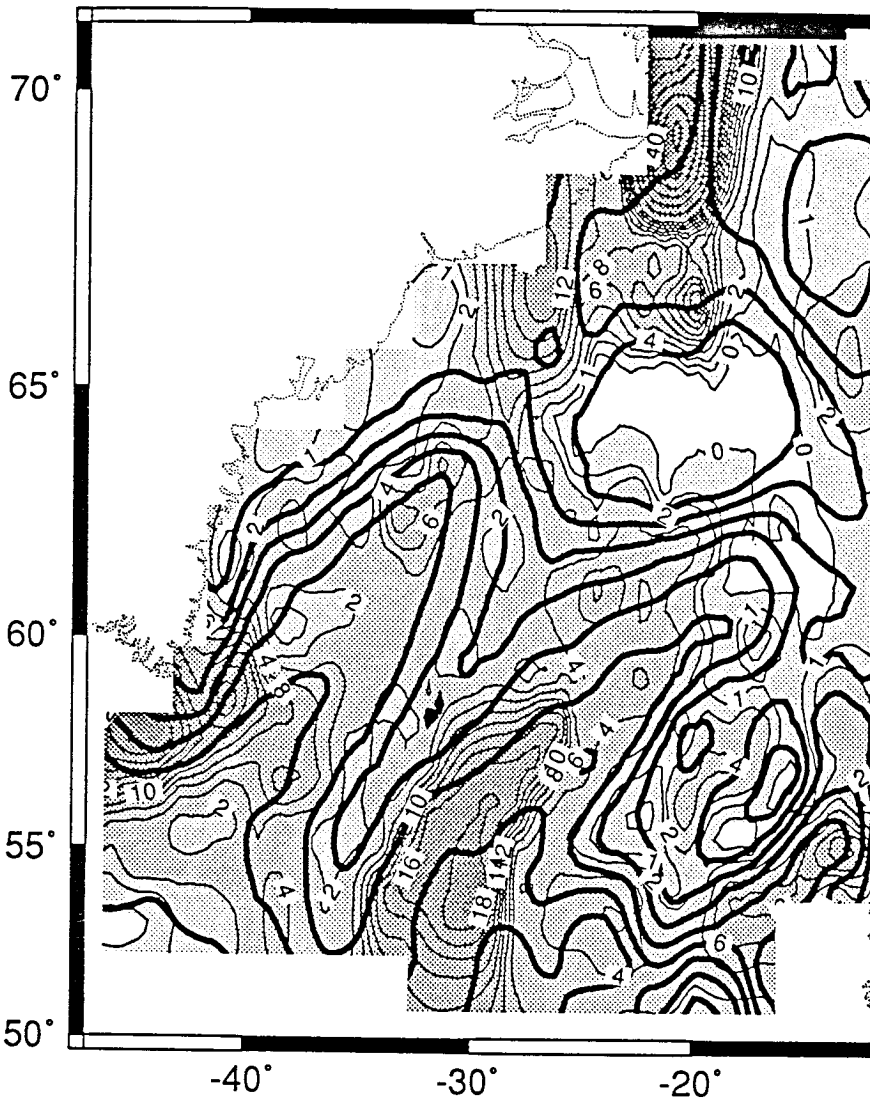

9 to 10 Ma - Accumulation Rates

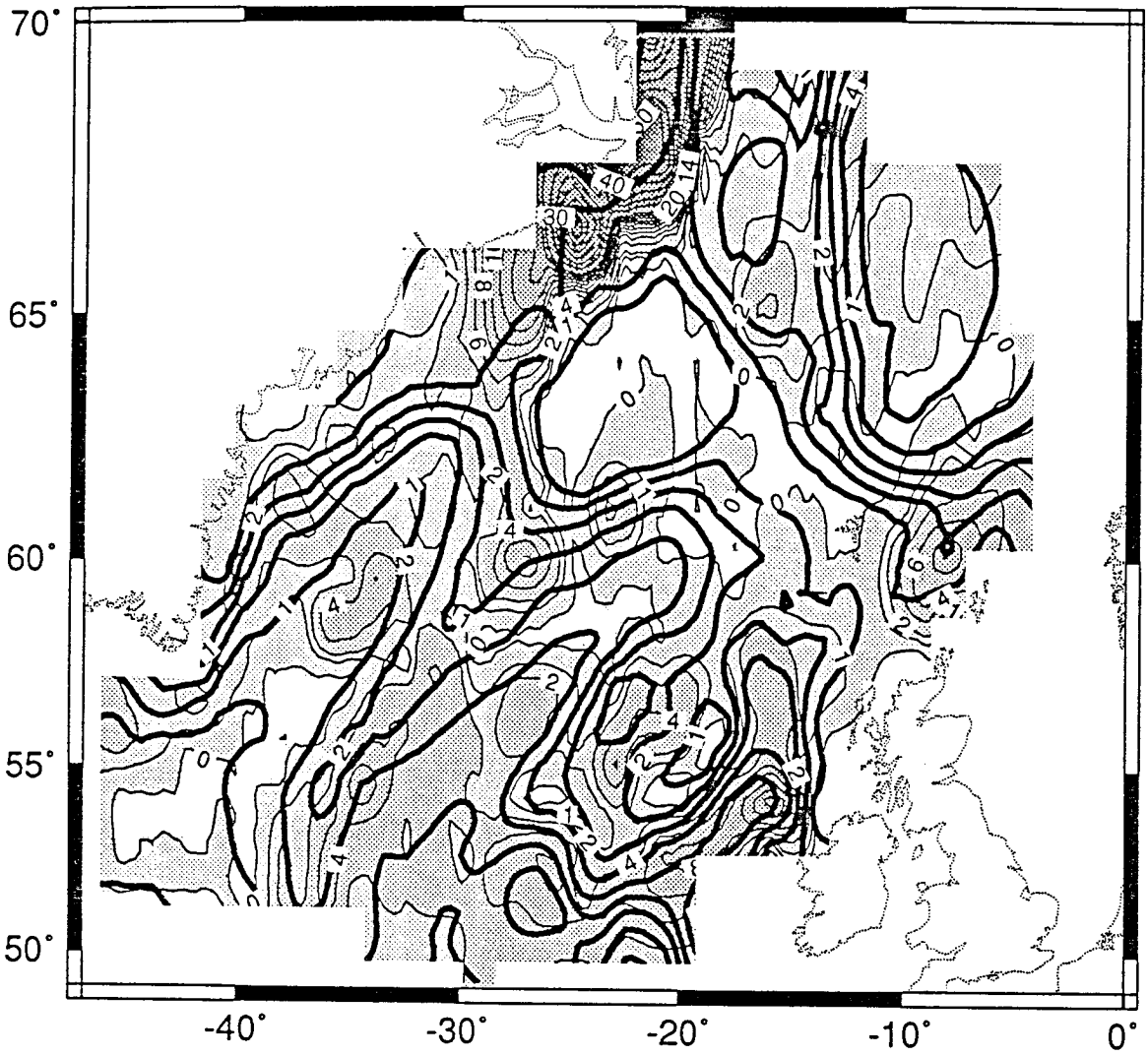

Figure 4.29

19 to 20 Ma - Accumulation Rates

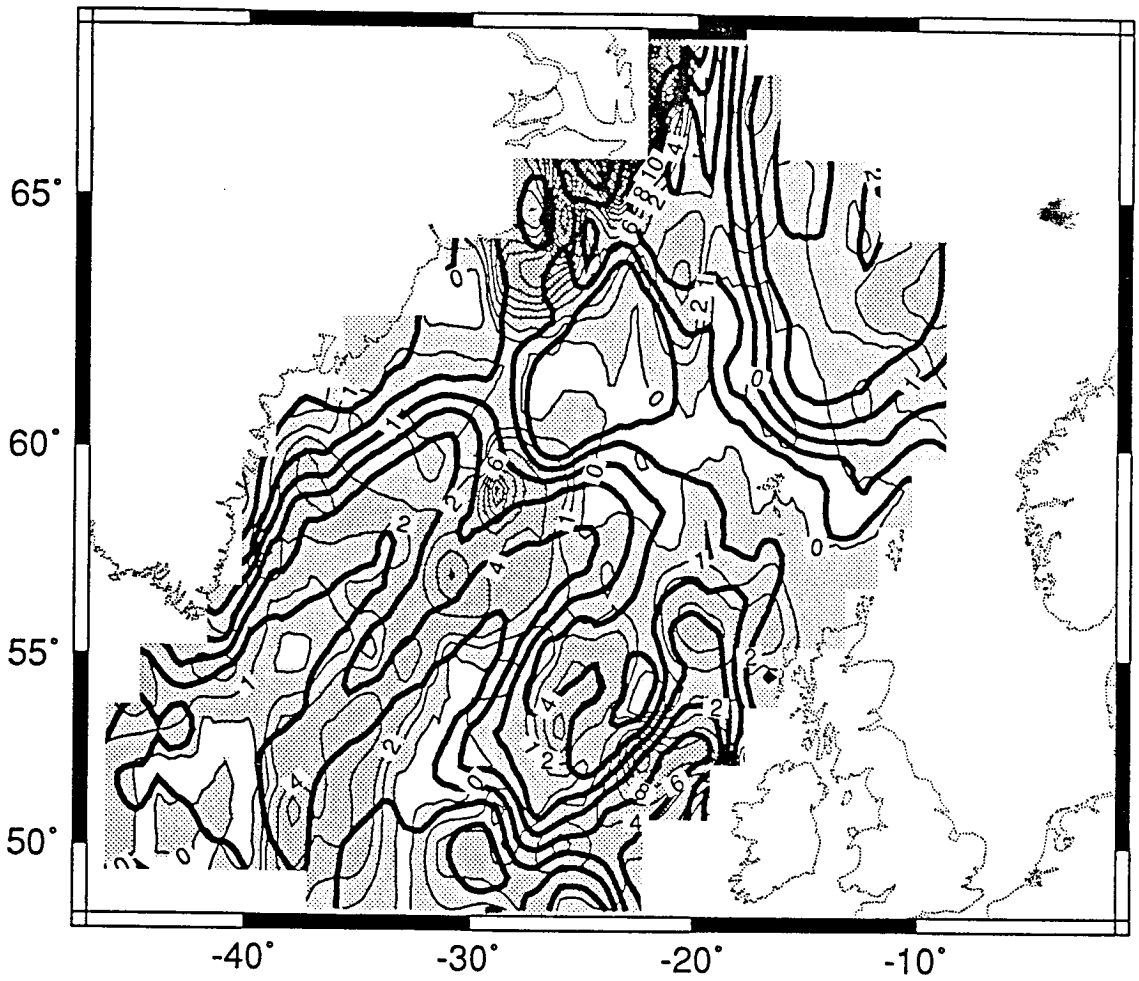

Figure 4.30

29 to 30 Ma - Accumulation Rates

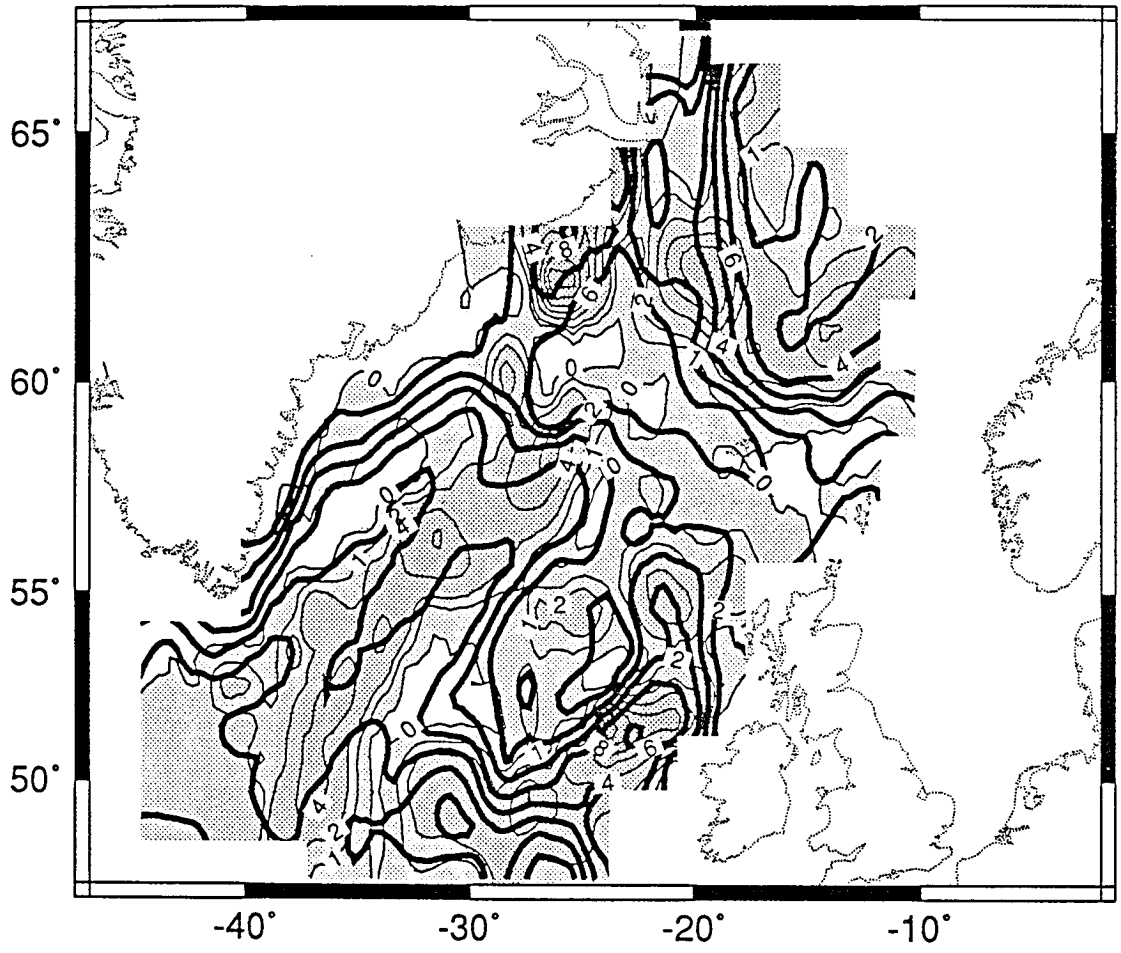

Figure 4.31

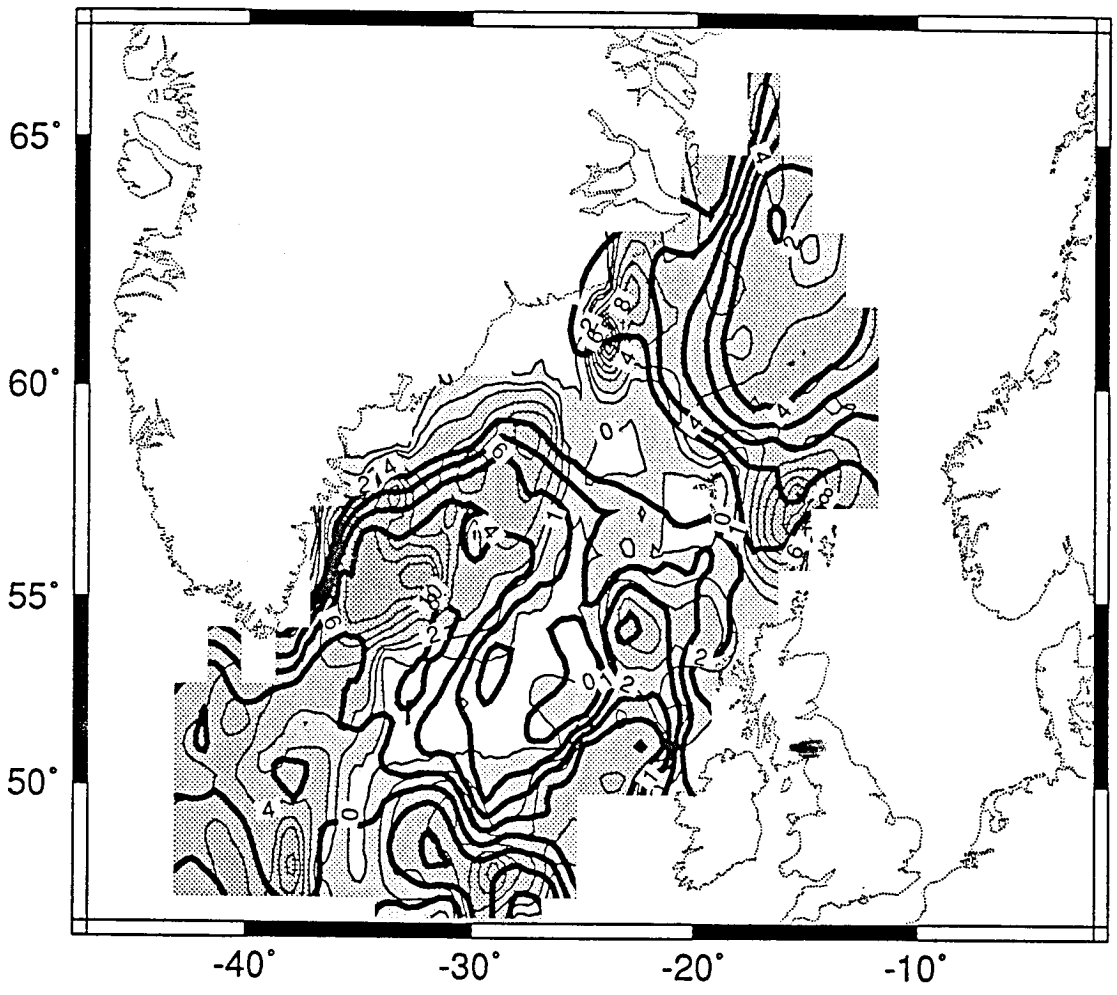

Figure 4.32

49 to 50 Ma - Accumulation Rates

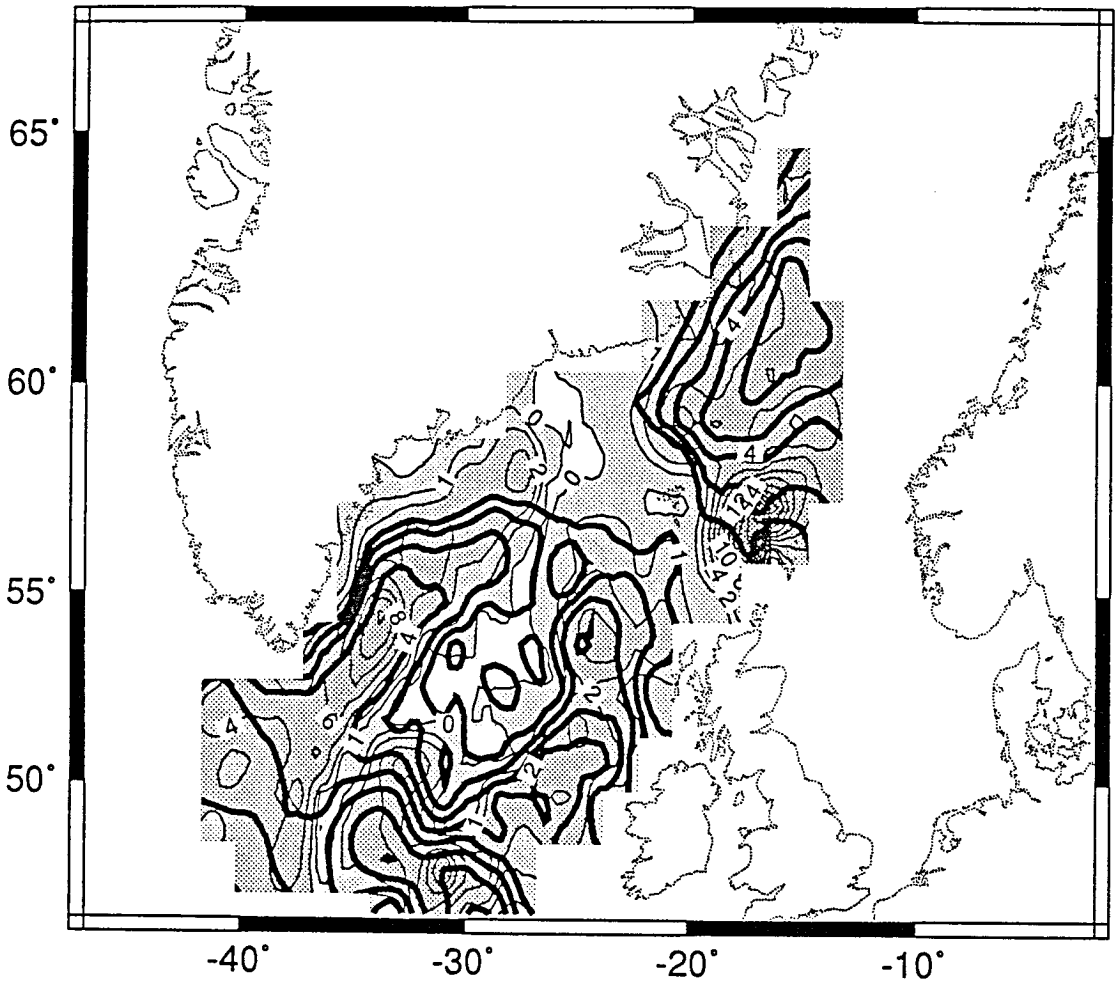

Figure 4.33

0 to 1 Ma - Relative Accumulation Rates

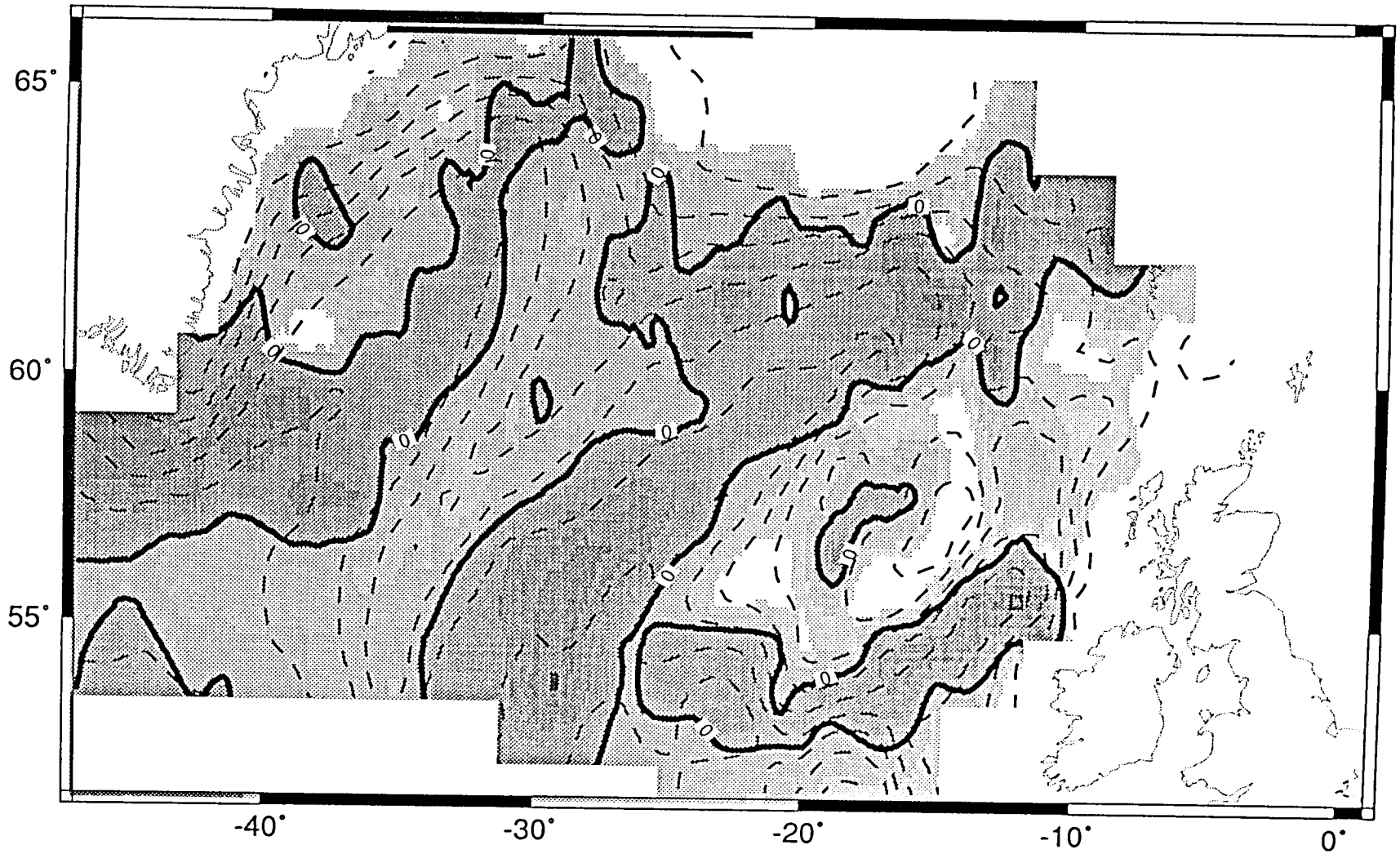

Figure 4.34

3 to 4 Ma - Relative Accumulation Rates

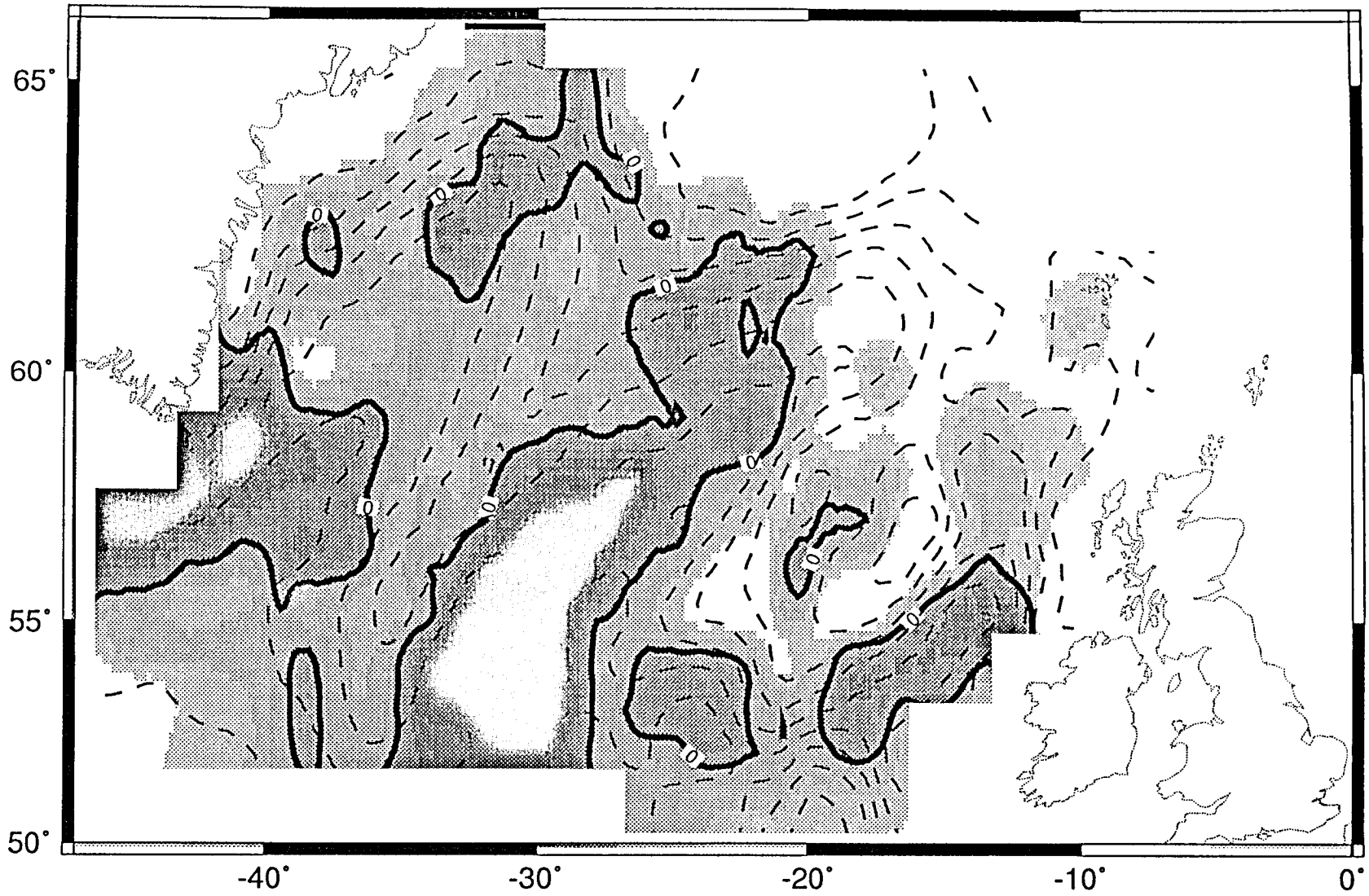

Figure 4.35

9 to 10 Ma - Relative Accumulation Rates

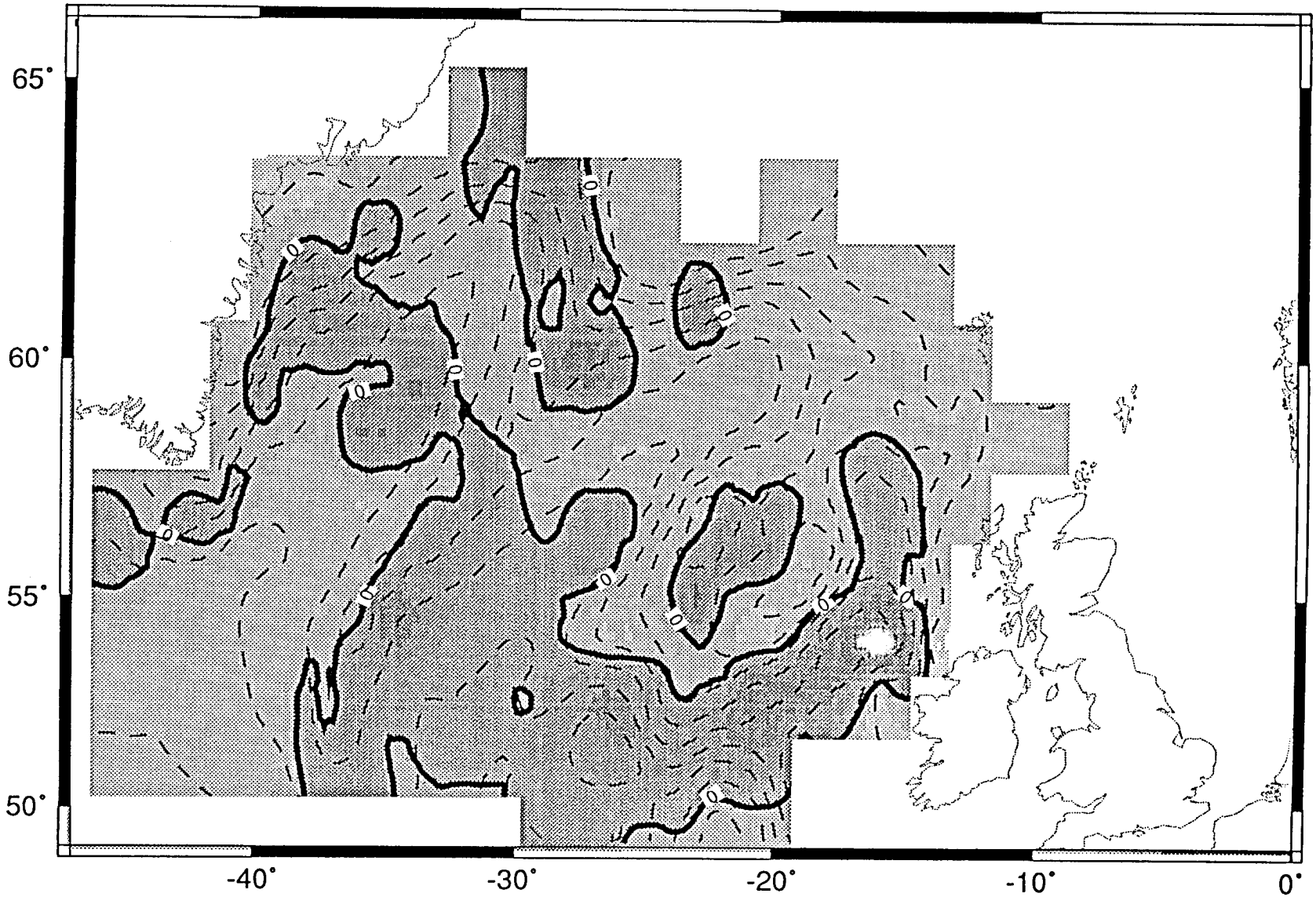

Figure 4.36

19 to 20 Ma - Relative Accumulation Rates

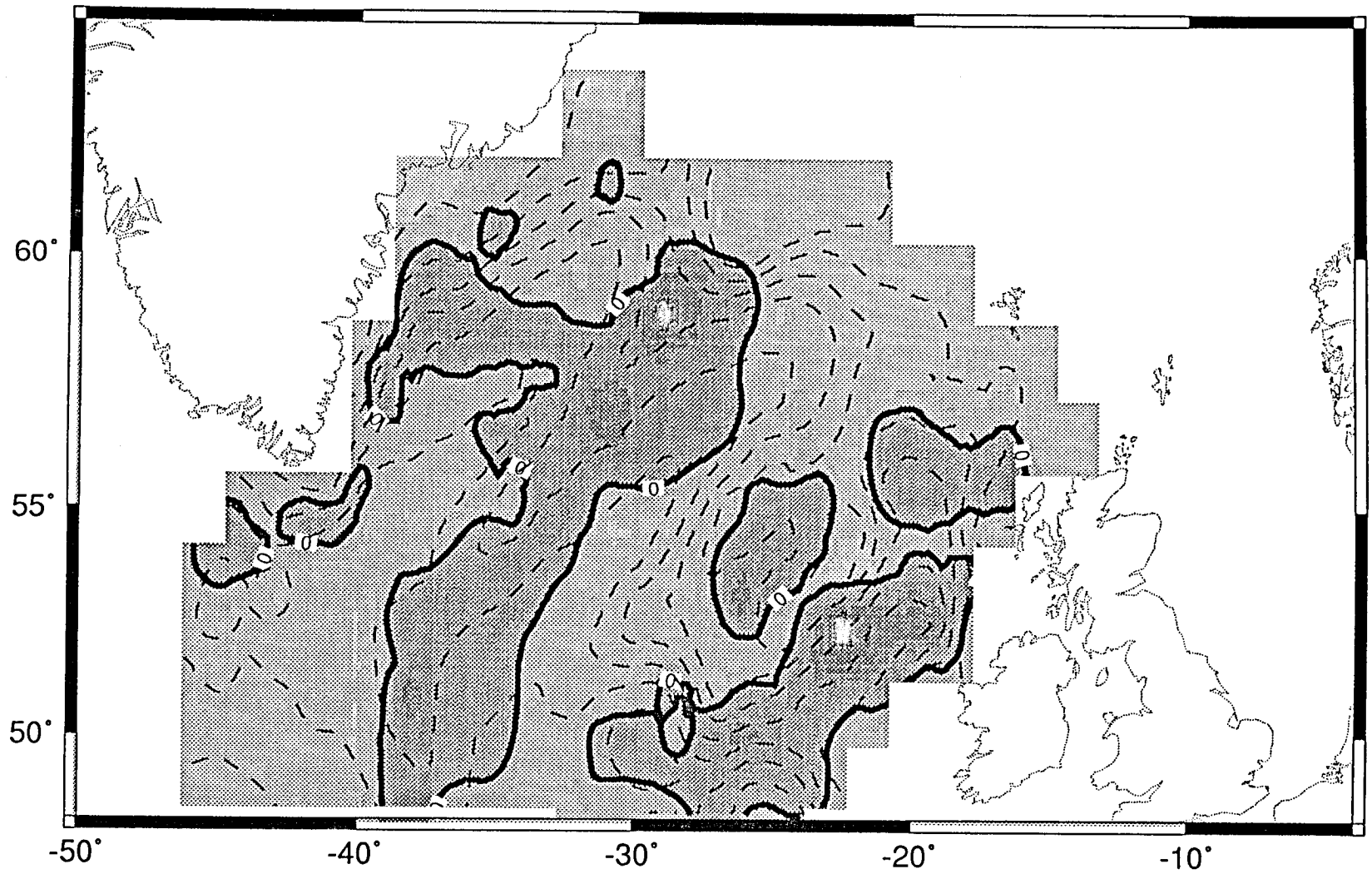

Figure 4.37

29 to 30 Ma - Relative Accumulation Rates

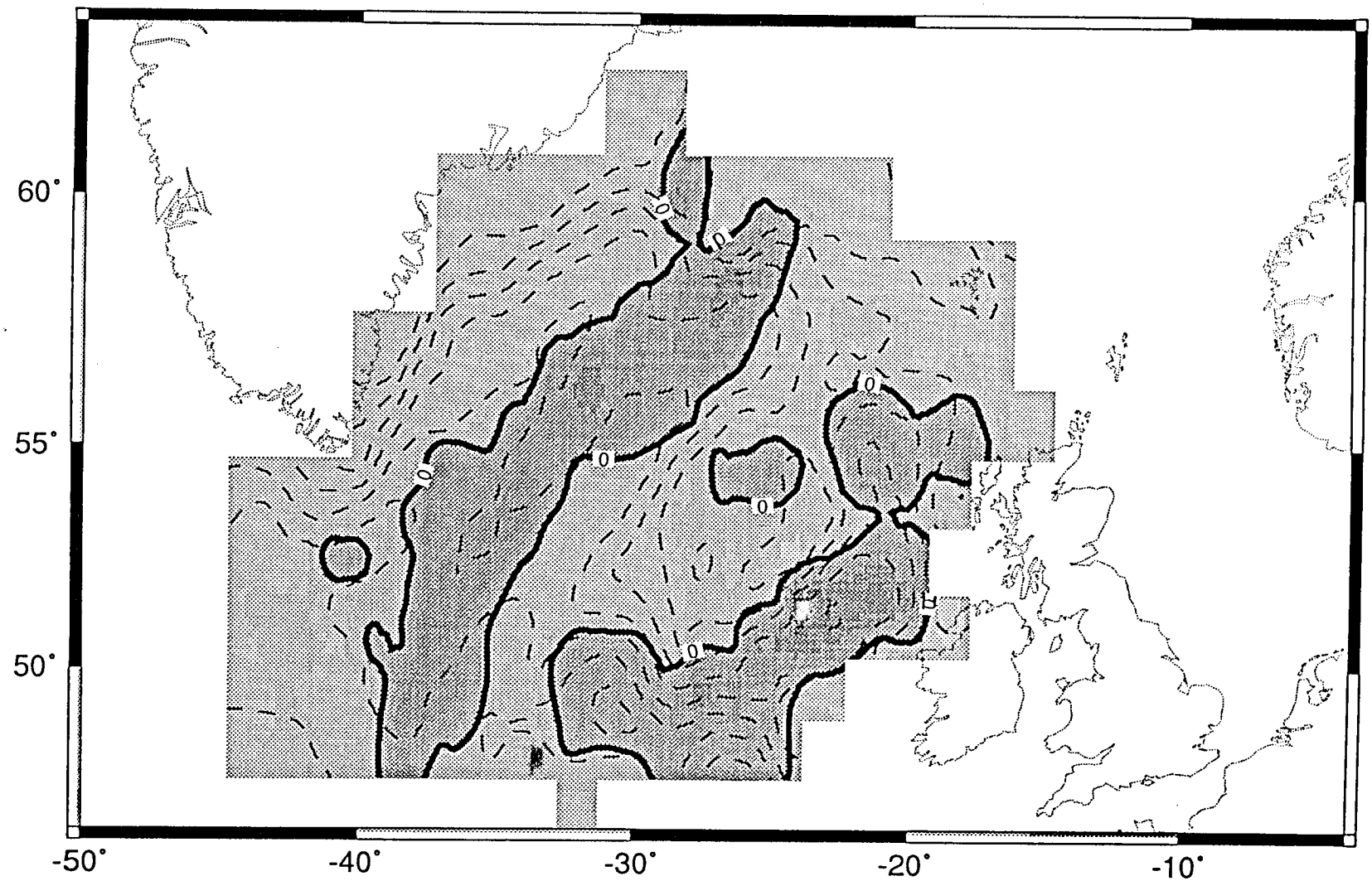

Figure 4.38

39 to 40 Ma - Relative Accumulation Rates

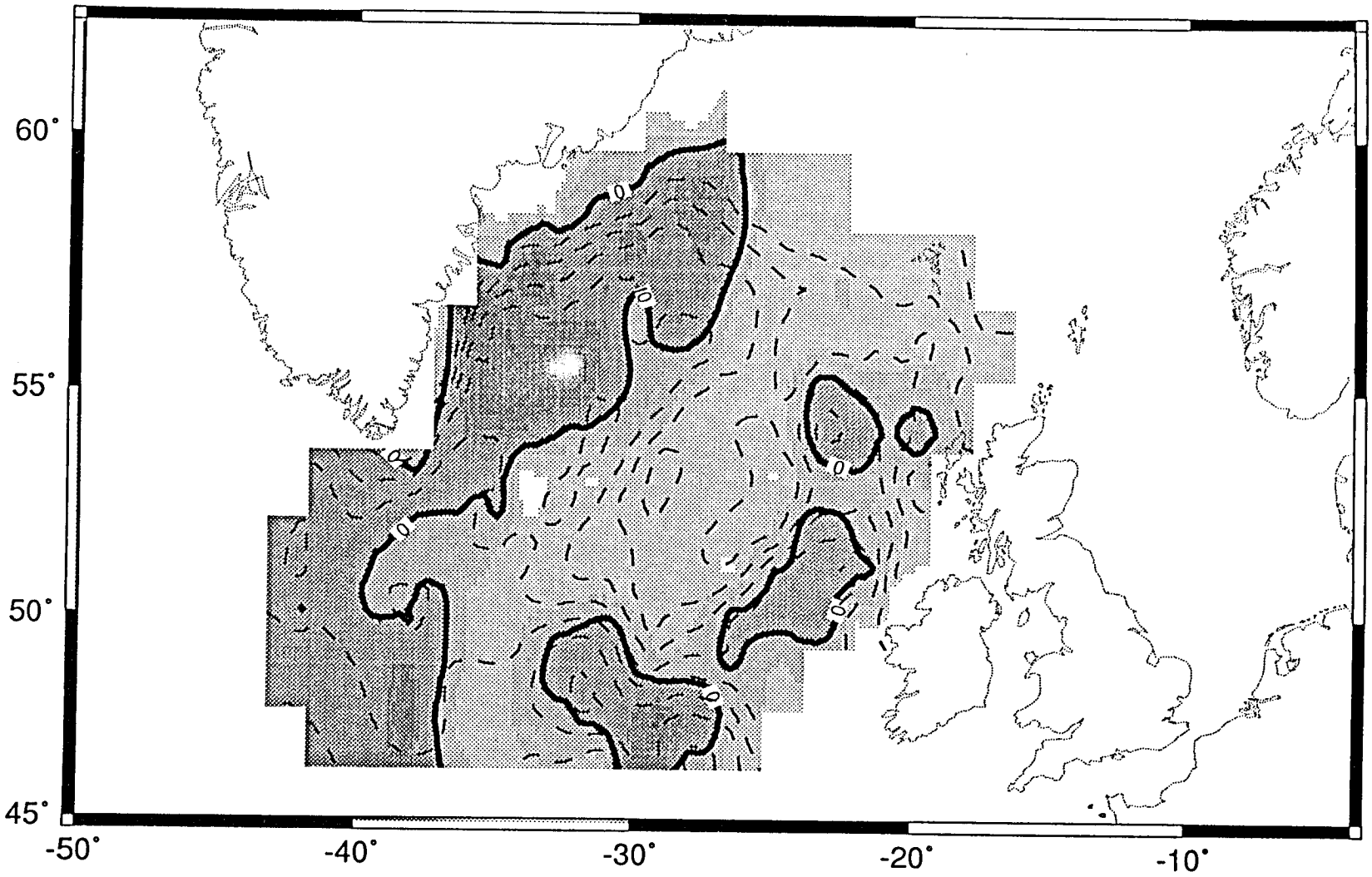

Figure 4.39

49 to 50 Ma - Relative Accumulation Rates

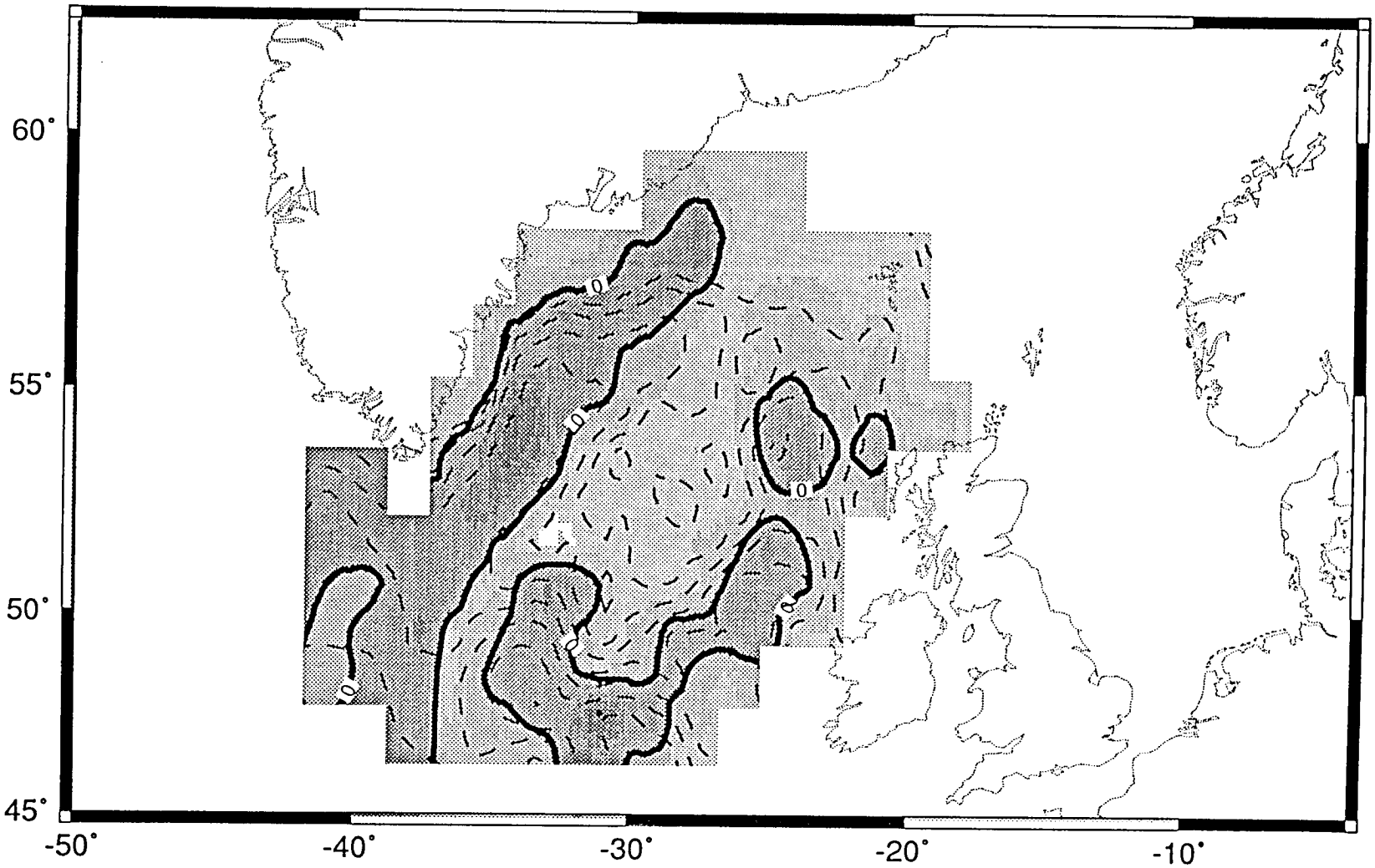

Figure 4.40

SEDIMENT DRIFTS

Drift Name	Area ($\times 10^4$ km^2)	Volume ($\times 10^7$ km^3)	Mass ($\times 10^{19}$ g)
Feni	11.7	11.4	19.3
Gardar	18.0	10.9	14.5
Bjorn	12.5	5.53	6.48
Eirik	8.23	5.36	6.05
Snorri	10.7	1.43	1.60
Hatton	6.21	1.30	1.59
Gloria	9.30	1.32	1.14
TOTAL:	76.6	37.2	50.7

Table 4.1. The compiled area, volume and total mass of sediment drifts between the Charlie Gibbs Fracture Zone and Greenland-Scotland Ridge.

Interval (Ma)	Global Apparent Accumulation Rates (g cm^{-2} $k.y.^{-1}$) Carbonate	Opaline Silica	Red Clay	Total Pelagic
0-5	0.88	0.20	0.25	1.3
5-10	0.69	0.16 (?)	0.23 (?)	1.1
10-15	0.62	0.11 (?)	0.20 (?)	0.93
15-20	0.56	0.042	0.14	0.74
20-25	0.56	0.040	0.14	0.74
25-30	0.61	0.018	0.14	0.77
30-35	0.37	0.017	0.088	0.48
35-40	0.30	0.019	0.074	0.39
40-45	0.41	0.018	0.10	0.53
45-50	0.38	0.021	0.093	0.49
50-55	0.31	0.020	0.076	0.41
55-60	0.30	0.0047	0.070	0.37

Table 4.2. Global apparent accumulation rates of pelagic sediment on ocean floor calculated from Tables 1 and 2 of Hay et al. (1988). The masses of opaline silica and red clay from 5 to 15 Ma were not given by Hay et al. (1988). The apparent accumulation rates for opaline silica and red clay from 5 to 15 Ma were calculated by interpolating the masses for these two components given at 0-5 and 15-20 Ma and then dividing the interpolated masses by the cumulative area of sea-floor at the midpoint of each interval.

Greenland-Scotland Ridge Overflow Water

Overflow	Potential Temperature (° C)	Salinity	σ_t	Flow Rate (Sv)
NS to RT over WTR	6	35.1	27.632	0.3
NS to SIB via FBC	3	35.1	27.965	1 - 1.1
NS to SIB via IFR	5	35.1	27.775	1
IS to IB vis DS	1 - 2	34.9	28.025	2.5 - 4

Table 4.3. Greenland-Scotland Ridge overflow waters. NS = Norwegian Sea, RT = Rockall Trough, WTR = Wyville-Thompson Ridge, SIB = South Iceland Basin, FBC = Faeroe Bank Channel, IFR = Iceland-Faeroe Ridge, IS = Iceland Sea, IB = Irminger Basin and DS = Denmark Strait. σ_t is the estimated water density (kg m^{-3}) minus 1000 kg m^{-3}.

Acknowledgements

I want to thank Prof. William W. Hay who has guided my research and education over the last six years. Our work and travels together have given me a new perspective on the world. His example has inspired me to strive for new and creative research. I also want to thank Prof. Jörn Thiede for making GEOMAR a great place to work and for his helpful comments on this manuscript. I thank Pompeyo Bajar for helping me learn how to program computers and for his initial help in writing the software for geological modelling (BalPal). I am especially grateful to my father, Dr. Richard J. Wold, who invited me to come to California and work with computer specialists at his company to develop the initial version of the software.

There are a large number of friends and colleagues in the United States and at GEOMAR who I thank for their help and discussions. It would be difficult to name all of the people who have contributed to this disseration, but I would especially like to thank: Dr. C. A. Shaw, Dr. K. M. Wilson, Dr. W. Weinrebe, M. Schulz, Prof. W. -C. Dullo, Dr. T. C. W. Wolf, Prof. E. Suess, Prof. O. Eldholm, Dr. M. Loughridge, R. Warnkin, K. Nowak, Dr. P. Hempel, T. Dickmann, Prof. R. Meissner, Prof. R. von Heune, Dr. T. Reston, N. Rosenthal, C. Hansen, Dr. W. Brückmann, Dr. M. Weinelt, K. Mehl, J. Welling and C. Hoffmann.

My wife Adrienne deserves special thanks for her patience and support. She has worked over-time taking care of our son Gustav, and the house so I could finish my dissertation.

References Cited

Anderson, D. L. (1982) Hotspots, polar wander, Mesozoic convection and the geoid. Nature, 297, 391-393

Arthaud, F., and Matte, P. (1975) Late Hercynian wrench faults in southwestern Europe: Geometry and nature of deformation. Tectonophysics, 25, 139-171

Arthur, M. A., Srivastava, S. P., Kaminski, M., Jarrard, R., and Osler, J. (1989) Seismic stratigraphy and history of deep circulation and sediment drift development in Baffin Bay and the Labrador Sea. In Proceedings of the Ocean Drilling Program, Scientific Results, V. 105, eds. Srivastava, S. P., Arthur, M. A., and Clement, B., College Station, TX: Ocean Drilling Program, 957-988

Athy, L. F. (1930) Density, porosity, and compaction of sedimentary rocks. Am. Assoc. Petrol. Geol. Bull., 14, 1-24

Baldwin, B. (1971) Ways of deciphering compacted sediments. J. Sed.Petrol., 41, 293-301

Baldwin, B., and Butler, C. O. (1985) Compaction curves. Am. Assoc. Petrol. Geol. Bull., 69, 622-626

Barrell, J. (1917) Rhythms and the measurement of geological time. Geol. Soc. Am. Bull., 28, 745-904

Barron, E. J. (1985) Numerical climate modelling, a frontier in petroleum source rock prediction: Results based on Cretaceous simulations. Am. Assoc. Petrol. Geol. Bull., 69, 448-459

Baumgartner, A., and Reichel, E. (1975) The World Water Balance: Mean Annual Global Continental and Maritime Precipitation, Evaporation and Runoff, Amsterdam: Elsevier. 176 pp

Berggren, W. A., and Hollister, C. D. (1977) Plate tectonics and paleocirculation, commotion in the ocean. Tectonophysics, 38, 11-48

Berggren, W. A., Kent, D. V., Flynn, J. J., and van Couvering, J. A. (1985) Cenozoic geochronology. Geol. Soc. Am. Bull., 96, 1406-1418

Berggren, W. A., and Schnitker, D. (1983) Cenozoic marine environments in the North Atlantic and Norwegian-Greenland Sea. In NATO Conference Series, Series IV: Marine Sciences, V. 8, Structure and Development of the Greenland-Scotland Ridge: New Methods and Concepts, eds. Bott, M. H. P., Saxov, S., Talwani, M., and Thiede, J., New York: Plenum Press, 495-548

Bott, M. H. P. (1983) The crust beneath the Iceland-Faeroe Ridge. In NATO Conference Series, Series IV: Marine Sciences, V. 8, Structure and Development of the Greenland-Scotland Ridge: New Methods and Concepts, eds. Bott, M. H. P., Saxov, S., Talwani, M., and Thiede, J., New York: Plenum Press, 63-76

Bott, M. H. P. (1985) Plate tectonic evolution of the Icelandic transverse ridge and adjacent regions. J. Geophys. Res., 90, 9953-9960

Bott, M. H. P., and Gunnarsson, K. (1980) Crustal structure of the Iceland-Faeroe Ridge. J. Geophys., 47, 221-227

Bott, M. H. P., Nielsen, P. H., and Sunderland, J. (1976) Converted P-waves originating at the continental margin between the Iceland-Faeroe Ridge and the Faeroe Bank. J. R. Astr. Soc., 44, 229-238

Boulton, G. S., Thors, K., and Jarvis, J. (1988) Dispersal of glacially derived sediment over part of the continental shelf of South Iceland and the geometry of the resultant sediment bodies. Marine Geol., 83, 193-233

Budyko, M. I., Ronov, A. B., and Yanshin, A. L. (1987) History of the Earth's Atmosphere. New York: Springer-Verlag. 139 pp

Bullard, E. C., Everett, J. E., and Smith, A. G. (1965) The fit of the continents around the Atlantic. Phil. Trans. R. Soc. London, Ser. A, 258, 41-51

Cande, S. C., LaBrecque, J. L., Larson, R. L., Pitman, W. C., III, Golovchenko, X., and Haxby, W. F. (1989) Magnetic lineations of the world's ocean basins. American Association of Petroleum Geologists, map

Cavelier, C., Labourguigne, J., Mégnien, F., Mégnien, C. Pomerol, C., and Wyns, R. (1980) Synthse Géologique du Bassin de Paris: 1, Stratigraphie et Paléogéographie. In Mémoires du Bureau de Recherches Géologiques et Miniéres, 101, eds. Mégnien, C., and Mégnien, F., 379-399

Coachman, L. K., and Aagaard, K. (1974) Physical oceanography of Arctic and Subarctic seas. In Marine Geology and Oceanography of the Arctic Seas, ed. Herman, Y., Berlin: Springer-Verlag, 1-72

Corliss, B. C., and Keigwin, L. D., Jr. (1986) Eocene-Oligocene paleoceanography. In Geodynamics Series, V. 15: Mesozoic and Cenozoic Oceans. ed. Hsü, K. J., Washington, D.C.: American Geophysical Union, 101-118

Courtillot, V. (1982) Propagating rifts and continental breakup. Tectonics, 1, 239-250

Courtillot, V., and Besse, J. (1987) Magnetic field reversals, polar wander, and core-mantle coupling. Science, 237, 1140-1147

Cox, A., and Hart, R. B. (1986) Plate Tectonics: How It Works. Palo Alto, CA: Blackwell Scientific Publications, Inc. 392 pp

Dagley, P., Wilson, R. L., Ade-Hall, J. M., Walker, G. P. L., Haggerty, S. E., Sigurgeirsson, T., Watkins, N. D., Smith, P. J., Edwards, J., and Grasty, R. L. (1967) Geomagnetic polarity zones for Icelandic lavas. Nature, 216, 25-29

Davis, E. E., and Lister, C. R. B. (1974) Fundamentals of ridge crest topography. Earth and Planet. Sci. Lett., 13, 405-413

Detrick, R. S., Sclater, J. G., and Thiede, J. (1977) Subsidence of aseismic ridges. Earth and Planet. Sci. Lett., 34, 185-196

Dickin, A. P. (1988) The North Atlantic Tertiary Province. In Continental Flood Basalts, ed. Macdougall, J. D., Dordrecht: Kluwer Academic Publishers, 111-149

Dickinson, W. R. (1953) Geological aspects of abnormal reservoir pressures in Gulf Coast Louisiana. Am. Assoc. Petrol. Geol. Bull., 37, 410-432

Dietrich, G. (1969) Atlas of the Hydrography of the Northern Atlantic Ocean Based on the Polar Front Survey of the International Geophysical Year, Winter and Summer, 1958. Copenhagen, Denmark: International Council for the Exploration of the Sea

Dingle, R.V., Megson, J.B., and Scrutton, R.A. (1982) Acoustic stratigraphy of the sedimentary succession west of Porcupine Bank, N. E. Atlantic Ocean: A preliminary account. Marine Geol., 47, 17-35

Durmishyan, A. G. (1974) Compaction of argillaceous sediments. Int. Geol. Rev., 16, 650-653

Egloff, J., and Johnson, G. L. (1975) Morphology and structure of the southern Labrador Sea. Can. J. Earth Sci., 12, 2111-2133

Egloff, J., and Johnson, G. L. (1979) Erosional and depositional structures of the southwest Iceland insular margin: Thirteen geophysical profiles. In American Association of Petroleum Geologists Memoir 29: Geological and Geophysical Investigations of Continental Margins, eds. Watkins, J. S., Montadert, L., and Dickerson, P. W., 43-64

Eldholm, O. (1991) Magmatic-tectonic evolution of a volcanic rifted margin. Marine Geol., 102, 43-61

Eldholm, O., Thiede, J., and Taylor, E., eds. (1987) Proceedings of the Ocean Drilling Program, Part A - Initial Reports, V. 104. College Station, TX: Ocean Drilling Program. 783 pp

Eldholm, O., and Windisch, C. C. (1974) Sediment distribution in the Norwegian-Greenland Sea. Geol. Soc. Am. Bull. , 85, 1661-1676

Ellett, D. J., and Martin, J. H. A. (1973) The physical and chemical oceanography of the Rockall Channel. Deep-Sea Res., 20, 585-625

Emery, K. O., and Uchupi, E. (1984) The Geology of the Atlantic Ocean. New York: Springer Verlag. 1050 pp

ETOPO5 (1986) Relief map of the earth's surface. EOS, 67, 121

Ewing, M., Carpenter, G., Windisch, C., and Ewing, J. (1973) Sediment distribution in the oceans: The Atlantic. Geol. Soc. Am. Bull., 84, 71-88

Featherstone, P. S., Bott, M. H. P. and Peacock, J. H. (1977) Structure of the continental margin of south-eastern Greenland. Geophys. J. R. Astr. Soc., 48, 15-27

Garrels, R. M., and Mackenzie, F. T. (1971a) Evolution of Sedimentary Rocks. New York: Norton. 397 pp

Garrels, R. M., and Mackenzie, F. T. (1971b) Gregor's denudation of the continents. Nature, 231, 382-383

GEBCO (1982) General Bathymetric Chart of the Oceans, 1:35 000 000 with Polar Regions at 1:25 000 000. 5th edition. Ottawa: Canadian Department of Fisheries and Oceans. 18 sheets

Gilluly, J. (1949) Distribution of mountain building in geologic time. Geol. Soc. Am. Bull., 60, 561-590

Goll, R. M. (1989) A synthesis of Norwegian Sea biostratigraphies: ODP Leg 104 on the Vøring Plateau. In Proceedings of the Ocean Drilling Program, Scientific Results, V. 104, eds. Eldholm, O., Thiede, J., and Taylor, E., College Station, TX: Ocean Drilling Program, 777-826

Gorshkov, S. G. (1977) Atlas Okeanov V. 2: Atlanticheskiy I Indiyskiy Okean'i. Leningrad: Ministerstvo Oboronyi SSSR, Voenno-Morskoe Flot, 306 + 27 pp

Gregor, C. B. (1968) The rate of denudation in Post-Algonkian time. Koninkl. Nederl. Akad. Wetenschap., Proc. Ser. B, Phys. Sci., 71, 22-30

Gregor, C. B. (1970) Denudation of the continents. Nature, 228, 273-275

Gregor, C. B. (1985) The mass-age distribution of Phanerozoic sediments. In Geological Society Memoir 10: The Chronology of the Geological Record. ed. Snelling, N. J., Oxford: Blackwell Scientific Publications, 284-289

Grønlie, G., and Talwani, M. (1978) Vema Research Series, V. 4: Geophysical Atlas Norwegian-Greenland Sea. Palisades, NY: Lamont-Doherty Geological Observatory, 26 pp

Gudlaugsson, S. T., Gunnarsson, K., Sand, M. and Skogseid, J. (1988) Tectonic and volcanic events at the Jan Mayen Ridge microcontinent. In Geological Society Special Publication No. 39: Early Tertiary Volcanism and the Opening of the NE Atlantic. , eds. Morton, A. C. and Parson, L. M., Oxford: Blackwell Scientific Publications, 85-93

Gurnis, M. (1990a) Ridge spreading, subduction and sea level fluctuations. Science, 250, 970-972

Gurnis, M. (1990b) Plate-mantle coupling and continental flooding. Geophys. Res. Lett., 17, 623-626

Gurnis, M. (1992) Long-term controls on eustatic and epeirogenic motions by mantle convection. GSA Today, 2, 141, 144-145, 156-157.

Hanisch, J. (1984) The Cretaceous opening of the northeast Atlantic. Tectonophysics, 101, 1-23

Haq, B. U. (1989) Sequence stratigraphy, sea level change, and significance for the deep sea. In International Association of Sedimentologists Special Publication 12: Sedimentation, Tectonics and Eustasy: Sea Level Change at Active Margins. ed. Macdonald, D. I. M., 3-39

Haq, B. U., Hardenbol, J., and Vail, P. R. (1987) Chronology of fluctuating sea levels since the Triassic. Science, 235, 1156-1167

Harrison, C. G. A., and Lindh, T. (1982) A polar wandering curve for North America during the Mesozoic and Cenozoic. J. Geophys. Res., 87, 1903-1920

Hay, W. W. (1981) Sedimentological and geochemical trends resulting from the breakup of Pangaea. Oceanol. Acta, 4 Supplement, 135-147

Hay, W. W. (1993, in press) Pleistocene-Holocene fluxes are not the Earth's norm. Washington, D.C. National Academy of Sciences Press

Hay, W. W., and Behensky, J. F. (1981) The northern Gulf of Mexico as an anomalous passive margin. Gulf Coast Assoc. Geol. Socs., Trans., 31, 309-313

Hay, W. W., Shaw, C. A., and Wold, C. N. (1989) Mass-balanced paleogeographic reconstructions. Geol. Rundschau, 78, 207-242

Hay, W. W., and Wold, C. N. (1986) A 150 MY cycle in erosion and sedimentation rates. Geol. Soc. Am., Abs. w. Prog., 18, 632

Hay, W. W., and Wold, C. N. (1990) Relation of selected mineral deposits to the mass/age distribution of Phanerozoic sediments. Geol. Rundschau, 79, 495-512

Hay, W. W., and Wold, C. N. (in press) Mass-balanced reconstruction of paleogeology.In Computerized Basin Analysis: The Prognosis of Energy and Mineral Resources, eds. Harff, J., and Merriam, D., New York: Plenum Press

Hay, W. W., Wold, C. N., and Shaw, C. A. (1989) Mass-balanced paleogeographic maps: Background and input requirements. In Quantitative Dynamic Stratigraphy, ed. Cross, T. A., Englewood Cliffs, NJ: Prentice-Hall, Inc., 261-275

Hay, W. W., Wold, C. N., and Wilson, K. M. (1988) Reconstructed sedimentary fluxes during the Phanerozoic. EOS, 69, 253

Heestand, R. L., and Crough, S. T. (1981) The effects of hot spots on the oceanic age-depth relation. J. Geophys. Res., 86, 6107-6114

Henrich, R., Wolf, T., Bohrmann, G., and Thiede, J. (1989) Cenozoic paleoclimatic and paleoceanographic changes in the northern hemisphere revealed by variability of coarse-fraction composition in sediments from the Vϕring Plateau - ODP Leg 104 drill sites. In Proceedings of the Ocean Drilling Program, Scientific Results, V. 104, eds. Eldholm, O., Thiede, J., and Taylor, E., College Station, TX: Ocean Drilling Program, 75-188

Hinz, K. (1981) A hypothesis on terrestrial catastrophies: Wedges of very thick oceanward dipping layers beneath passive margins - Their origin and paleoenvironmental significance. Geol. Jb., E, 22, 3-28

Holmes, A. (1965) Principles of Physical Geology. Edinburgh: Nelson. 1025 pp

Huang, Z., and Gradstein, F. M. (1990) Depth-porosity relationship from deep sea sediments. Scientific Drilling, 1, 157-162

Hunt, J. M. (1979) Petroleum Geochemistry and Geology. San Francisco: W. H. Freeman and Co., 617 pp

Johannessen, O. M. (1986) Brief overview of the physical oceanography. In The Nordic Seas, ed. Hurdle, B. G., New York: Springer-Verlag, 103-127

Johnson, G. L., and Schneider, E. D. (1969) Depositional ridges in the North Atlantic. Earth and Planet. Sci. Lett., 6, 416-422

Jones, E. J. W., Ewing, M, Ewing, J. I., and Eittreim, S. L. (1970) Influences of Norwegian Sea overflow water on sedimentation in the northern North Atlantic and Labrador Sea. J. Geophys. Res., 75, 1655-1680

Jurdy, D. M.Stefanick, M. (1991) Are plumes fixed? Or do they go with the flow? EOS, 72, 445

Keigwin, L. D., Jr. (1980) Paleoceanographic change in the Pacific at the Eocene-Oligocene boundary. Nature, 287, 722-725

Kellogg, T. B. (1987) Glacial-interglacial changes in global deepwater circulation. Paleoceanography, 2, 259-271

Kennett, J. P., and Shackleton, N. J. (1976) Oxygen isotopic evidence for the development of the psychrosphere 38 m.y. ago. Nature, 260, 513-515

Kent, D. V., and Gradstein, F. M. (1986) A Jurassic to Recent chronology. In The Geology of North America, V. M: The Western North Atlantic Region, eds. Vogt, P. R., and Tucholke, B. E., Boulder, CO: Geological Society of America, 45-50

Kidd, R. B., and Hill, P. R. (1986) Sedimentation on mid-ocean sediment drifts. In Geological Society Special Publication No. 21: North Atlantic Palaeoceanography, eds. Summerhayes, C. P., and Shackleton, N. J., Oxford: Blackwell Scientific Publications, 87-102

Kidd, R. B., and Hill, P. R. (1987) Sedimentation on Feni and Gardar sediment drifts. In Initial Reports of the Deep Sea Drilling Project, V. 94 , eds. Ruddiman, W. F., Kidd, R. B., and Thomas, E., Washington, D.C.: U.S. Government Printing Office, 1217-1244

Killworth, P. D. (1983) Deep convection in the world ocean. Rev. Geophys. Space Phys., 21, 1-26

Kominz, M. (1984) Oceanic ridge volumes and sealevel change - an error analysis. In American Association of Petroleum Geologists Memoir 36: Interregional Unconformities and Hydrocarbon Accumulation. ed. Schlee, J. S., 109-127

Krawczyk, C. (1990) Die Nordflanke Des Island-Faeroer Rückens - Eine Hochauflösende Reflexionsseismische Vermessung. In Diplomarbeit, Institut Für Geophysik der Christian-Albrecht-Universität Zu Kiel. 108 pp

Kristjansson, L. (1976) A marine magnetic survey off southern Iceland. Marine Geophys. Res., 2, 315-326

Kristoffersen, Y. (1978) Sea-floor spreading and the early opening of the North Atlantic. Earth and Planet. Sci. Lett., 38, 273-290

Larsen, H. C. (1984) Geology of the East Greenland shelf. In Petroleum Geology of the North European Margin, ed. Spencer, A. M., London: Graham & Trotman, 329-339

Larsen, H. C. (1990) The East Greenland shelf. In The Geology of North America, V. L: The Arctic Ocean Region, eds. Grantz, A., Johnson, L., and Sweeny, J. F., Boulder, CO: Geological Society of America, 185-210

Larson, R. L. (1991) Latest pulse of Earth: Evidence for a mid-Cretaceous superplume. Geology, 19, 547-550

Larson, R. L., and Olson, P. (1991) Mantle plumes control magnetic reversal frequency. Earth and Planet. Sci. Lett., 107, 437-447

Larson, R. L. (In press) Geological consequences of superplumes. Geology

Laughton, A. S., Berggren, W. A., et al. (1972) Initial Reports of the Deep Sea Drilling Project, V. 12. Washington, D.C.: U.S. Government Printing Office. 1243 pp

Laughton, A. S., Matthews, D. W., and Fisher, R. L. (1970) The structure of the Indian Ocean. In The Sea, V. 4, Pt. 2: New Concepts of Sea Floor Evolution. ed. Maxwell, A. E., New York: John Wiley & Sons, 543-586

Lawver, L. A., Müller, R. D., Srivastava, S. P., and Roest W. (1990) The opening of the Arctic Ocean. In NATO Advanced Studies Institutes Series C: Mathematical and Physical Sciences, V. 308: Geological History of the Polar Oceans: Arctic Versus Antarctic, eds. Bleil, U., and Thiede, J., Dordrecht: Kluwer Academic Publishers, 29-62

Le Pichon, X., Sibuet, J.-C., and Francheteau, J. (1977) The fit of the continents around the North Atlantic Ocean. Tectonophysics, 38, 169-209

Locker, S., and Martini, E. (1989) Cenozoic silicoflagellates, ebridians, and actiniscidians from the Vφring Plateau (ODP Leg 104). In Proceedings of the Ocean Drilling Program, Scientific Results, V. 104, eds. Eldholm, O., Thiede, J., and Taylor, E., College Station, TX: Ocean Drilling Program, 543-585

Lonsdale, P. F., Hollister, C. D. (1979) A near bottom traverse of Rockall Trough: Hydrographic and geologic inferences. Oceanol. Acta, 2, 91-105

Magara, K. (1976) Thickness of removed sedimentary rocks, paleopore pressure, and paleotemperature, southwestern part of Western Canada basin. Am. Assoc.Petrol. Geol. Bull., 48, 554-565

Masson, D. G., and Kidd, R. B. (1987) Revised Tertiary seismic stratigraphy of the southern Rockall Trough. In Initial Reports of the Deep Sea Drilling Project, V. 94, eds. Ruddimann, W. F., Kidd, R. B., and Thomas, E., Washington, D.C.: U.S. Government Printing Office, 1117-1126

Matthews, R. K., and Poore. R. Z. (1980) Tertiary $\delta^{18}O$ record and glacio-eustatic sea-level fluctuations. Geology, 8, 501-504

Maxwell, J. C. (1964) Influence of depth, temperature, and geologic age on porosity of quartzose sandstone. Am. Assoc. Petrol. Geol. Bull., 48, 697-709

McCave, I. N., Lonsdale, P. F., Hollister, C. D., and Gardner, W. D. (1980) Sediment transport over the Hatton and Gardar contourite drifts. J. Sed. Pet., 50, 1049-1062

McCave, I. N., and Tucholke, B. E. (1986) Deep current-controlled sedimentation in the western North Atlantic. In The Geology of North America, V. M: The Western North Atlantic Region, eds. Vogt, P. R., and Tucholke, B. E., Boulder, CO: Geological Society of America, 451-468

McKerrow, W. S., Lambert, R. St. J., and Cocks, L. R. M. (1985) The Ordovician, Silurian and Devonian periods. In Geological Society (London) Memoir 10: Chronology of the Geological Record. ed. Snelling, N. J., Oxford: Blackwell Scientific Publications, 73-80

Meincke, J. (1983) The modern current regime across the Greenland-Scotland Ridge. In Structure and Development of the Greenland Scotland Ridge: New Methods and Concepts. eds. Bott, M. H. P., Saxov, S., Talwani, M., and Thiede, J., New York: Plenum Press, 637-650

Menard, H. W. (1969) Elevation and subsidence of oceanic crust. Earth and Planet. Sci. Lett., 6, 275-284

Miller, K. G., and Tucholke, B. E. (1983) Development of Cenozoic abyssal circulation south of the Greenland-Scotland Ridge. In NATO Conference Series, Series IV: Marine Sciences, V. 8: Structure and Development of the Greenland-Scotland Ridge: New Methods and Concepts. eds. Bott, M. H. P., Svend S., Talwani, M., and Thiede, J., New York: Plenum Press, 549-589

Millero, F. J., and Poisson, A. (1981) International one-atmosphere equation of state of sea-water. Deep-Sea Res., 28A, 625-629

Molostovsky, E. A., and Khramov, A. N. (1984) Paleomagnetic scale for the Phanerozoic and magnetostratigraphic problems. In Proc. 27th Int. Geol. Congr., V. 1, Stratigraphy, Amsterdam: VNU Science Press, 31-46

Montadert, L., Roberts, D. G., de Charpal, O., and Guennoc, P. (1979) Rifting and subsidence of the northern continental margin of the Bay of Biscay. In Initial Reports of the Deep Sea Drilling Project, 48, eds. Montadert, L., Roberts, D. G., Washington, D.C.: U.S. Government Printing Office, 1025-1060

Montadert, L., Roberts, D. G., et al., (1979) Initial Reports of the Deep Sea Drilling Project, V. 48. Washington, D.C.: U.S. Government Printing Office. 1183 pp

Moorbath, S., Sigurdsson, H., and Goodwin, R. (1968) K-Ar ages of the oldest exposed rocks in Iceland. Earth and Planet. Sci. Lett., 4, 197-205

Morgan, W. J. (1983) Hotspot tracks and the early rifting of the Atlantic. Tectonophysics, 94, 123-139

Morgan, J. V., Barton, P. J. and White, R. S. (1989) The Hatton Bank continental margin-III. Structure from wide-angle OBS and multichannel seismic refraction profiles. Geophys. J. Int., 98, 367-384

Müller, C. (1976) Tertiary and Quaternary calcareous nannoplankton in the Norwegian-Greenland Sea, DSDP, Leg 38. In Initial Reports of the Deep Sea Drilling Project, V. 38, eds. Talwani, Udintsev et al., Washington, D.C.: U.S. Government Printing Office, 823-828

Müller, R. D., Roest, W. R. (1992) Fracture zones in the North Atlantic from combined Geosat and Seasat data. J. Geophys. Res., 97, 3337-3350

Murray, J. W. (1992) Palaeogene and Neogene. In Geological Society Memoir No. 13: Atlas of Palaeogeography and Lithofacies, eds. Cope, J. C. W., Ingham, J. K., and Rawson, P. F., Bath, UK: The Geological Society Publishing House, 141-147

Mutter, J. C., Talwani, M., and Stoffa, P. L. (1982) Origin of seaward-dipping reflectors in oceanic crust off the Norwegian margin by "subaerial sea-floor spreading" Geology, 10, 353-357

Nilsen, T. (1978) Lower Tertiary laterite on the Iceland-Faeroe Ridge and the Thulean land bridge. Nature, 274, 786-788

Nilsen, T. H. (1983) Influence of the Greenland-Scotland Ridge on the geological history of the North Atlantic and Norwegian-Greenland Sea areas. In NATO Conference Series, Series IV: Marine Sciences, V. 8, Structure and Development of the Greenland-Scotland Ridge: New Methods and Concepts, eds. Bott, M. H. P., Saxov, S., Talwani, M., and and Thiede, J., New York: Plenum Press, 457-478

Nunns, A. G. (1982) The structure and evolution of the Jan Mayen Ridge and the surrounding regions. In American Association of Petroleum Geologists Memoir 34: Studies in Continental Margin Geology, eds. Watkins, J.S., and Drake, C.L., 193-208

Nunns, A. G. (1983) Plate tectonic evolution of the Greenland Scotland Ridge and surrounding regions. In NATO Conference Series, Series IV: Marine Sciences, V. 8: Structure and Development of the Greenland Scotland Ridge: New Methods and Concepts, eds. Bott, M. H. P., Saxov, S., Talwani, M., and Thiede, J., New York: Plenum Press, 11-30

Nunns, A. G., Talwani, M., Lorentzen, G. R., Vogt, P. R., Sigurgeirsson, T., Kristjansson, L., Larsen, H. C., and Voppel, D. (1983) Magnetic anomalies over Iceland and surrounding areas. In NATO Conference Series, Series IV: Marine Sciences, V. 8: Structure and Development of the Greenland-Scotland Ridge: New Methods and Concepts, eds. Bott, M. H. P., Saxov, S., Talwani, M., and Thiede, J., New York: Plenum Press, 661-678

Palmason, G. (1974) The insular margin of Iceland. In The Geology of Continental Margins, eds. Burk, C. A., and Drake, C. L., New York: Springer-Verlag, 375-379

Park, C-H., Tamaki, K., and Kobayashi, K. (1990) Age-depth correlation of the Phillipine Sea back-arc basins and other marginal basins in the world. Tectonophysics, 181, 351-371

Parson, L. M., and the ODP Leg 104 Scientific Party. (1988) Dipping reflector styles in the NE Atlantic Ocean. In Geological Society Special Publication No. 39: Early Tertiary Volcanism and the Opening of the NE Atlantic, eds. Morton, A. C. and Parson, L. M., London, 57-68

Parsons, B., and Sclater, J. G. (1977) An analysis of the variation of ocean floor bathymetry and heat flow with age. J. Geophys. Res., 82, 803-827

Pearson, I., and Jenkins, D. G. (1986) Unconformities in the Cenozoic of the North-East Atlantic. In Geological Society Special Publication No. 21: North Atlantic Palaeoceanography, eds. Summerhayes, C. P., and Shackleton, N. J., Oxford: Blackwell Scientific Publications, 79-86

Peterson, W. H. (1979) A Steady State Thermohaline Convection Model [Ph.D. Thesis]. Miami: Rosenstiel School of Marine and Atmospheric Sciences, University of Miami. 160 pp

Peterson, W. H., and Rooth, C. (1976) Formation and exchange of deep water in the Greenland and Norwegian seas. Deep-Sea Res., 23, 273-283

Pflug, R. (1982) Bau und Entwicklung Des Oberrheingrabens. Erträge der Forsching. Darmstadt: Wissenschaftliche Buchgesellschaft, 145 pp

Philander, S. G. H., and Pacanowski, R. C. (1986) The mass and heat budget in a model of the tropical Atlantic Ocean. J. Geophys. Res., 91, 14212-14220

Pitman, W. C., III, and Talwani, M. (1972) Sea floor spreading in the North Atlantic. Geol. Soc. Am. Bull., 83, 619-646

Ramsay, J. G. (1969) The measurement of strain and displacement in orogenic belts. In Geological Society Special Publication No. 3: Time and Place in Orogeny, 43-79

Ridd, M. F. (1981) Petroleum geology west of the Shetlands. In Petroleum Geology of the Continental Shelf of Northwest Europe, ed. Illing, L. V., and Hobson, G. D., London: Heyden, 414-425

Ridd, M. F. (1983) Aspects of the Tertiary geology of the Faeroe-Shetland Channel. In NATO Conference Series, Series IV: Marine Sciences, V. 8: Structure and Development of the Greenland-Scotland Ridge: New Methods and Concepts, eds. Bott, M. H. P., Saxov, S., Talwani, M., and Thiede, J., New York: Plenum Press, 91-108

Roberts, D. G. (1975) Tectonic and stratigraphic evolution of the Rockall Plateau and Trough. In Petroleum and the Continental Shelf of North-west Europe. V. 1, Geology, ed. Woodland, A. W., Essex, U.K.: Applied Science Publishers, 77-89

Roberts, D. G., Backman, J., Morton, A. C., Murray, J. W., and Keene, J. B. (1984) Evolution of volcanic rifted margins: Synthesis of Leg 81 results on the west margin of Rockall Plateau. In Initial Reports of the Deep Sea Drilling Project, V. 81, eds. Roberts, D. G., and Schnitker, D., Washington, D. C.: U.S. Government Printing Office, 883-911

Roberts, D. G., Bott, M. H. P., and Uruski, C. (1983) Structure and origin of the Wyville-Thompson Ridge. In NATO Conference Series, Series IV: Marine Sciences, V. 8 Structure and Development of the Greenland-Scotland Ridge: New Methods and Concepts, eds. Bott, M. H. P., Saxov, S., Talwani, M., and Thiede, J., New York: Plenum Press, 133-158

Roberts, D. G., Ginzberg, A., Nunn, K., and McQuillin, R. (1988) The structure of the Rockall Trough from seismic refraction and wide-angle reflection measurements. Nature, 332, 632-635

Roberts, D. G., Montadert, L., and Searle, R. C. (1979) The western Rockall Plateau: Stratigraphy and stuctural evolution. In Inital Reports of the Deep Sea Drilling Project, 48, eds. Montadert, L., Roberts, D. G., Washington, D.C.: U.S. Government Printing Office, 1061-1088

Roberts, D. G., Masson, D. G., and Miles, P. R. (1981) Age and structure of the southern Rockall Trough: New evidence. Earth and Planet. Sci. Lett., 52, 115-128

Roest, W. R., and Srivastava, S. P. (1989) Seafloor spreading in the Labrador Sea: A new reconstruction, Geology, 17, 1000-1003

Ronov, A. B. (1968) Probable changes in the composition of sea water during the course of geologic time. Sedimentology, 10, 25-43

Ronov, A. B. (1982) The earth's sedimentary shell (quantitative patterns of its structure, compositions, and evolution). Int. Geol. Rev., 24(12), 1365-1388

Rowley, D. B., and Lottes, A. L. (1988) Plate-kinematic reconstructions of the North Atlantic and Arctic: Late Jurassic to Present. Tectonophysics, 155, 73-120

Ruddiman, W. F. (1972) Sediment redistribution on the Reykjanes Ridge: Seismic evidence. Geol. Soc. Am. Bull. , 83, 2039-2062

Ruddimann, W. F., Kidd, R. B., Thomas, E., et al. (1987) Initial Reports of the Deep Sea Drilling Project, V. 94 . Washington, D.C.: U.S. Government Printing Office. 1261 pp

Saemundsson, K. (1974) Evolution of the axial rifting zone in northern Iceland and the Tjornes Fracture Zone. Geol. Soc. Am. Bull. , 85, 495-504

Schnitker, D. (1980) North Atlantic oceanography as a possible cause of Antarctic glaciation and eutrophication. Nature, 284, 615-616

Schrader, H.-J., Bjørklund, R. R., Manum, S., Martini, E., and van Hinte, J. (1976) Cenozoic biostratigraphy, physical stratigraphy and paleoceanography in the Norwegian-Greenland Sea, DSDP Leg 38, paleontological synthesis. In Initial Reports of the Deep Sea Drilling Project, V. 38, eds. Talwani, M., and Udintsev, G., Washington, D.C.: U.S. Government Printing Office, 1197-1211

Schroeder, W. (1984) The empirical age-depth relation and depth anomalies in the Pacific Ocean Basin. J. Geophys. Res., 89, 9873-9883

Schuchert, C. (1931) Geochronology, or the age of the earth on the basis of sediments and life. In Bulletin 80: Physics of the Earth, 4. The Age of the Earth, Washington: National Research Council, 10-64

Schweitzer, H. M. (1980) Environment and climate in the Early Tertiary of Spitsbergen. Palaeogeog., Palaeoclimtaol., Palaeoecol., 30, 297-311

Sclater, J. G., Hellinger, S. and Tapscott, C. (1977) Paleobathymetry of the Atlantic Ocean. The Journal of Geology, 76, 509-522.

Sclater, J. G., Anderson, R. N., and Bell, M. L. (1971) The elevation of ridges and the evolution of the central Eastern Pacific. J. Geophys. Res., 76, 7883-7915

Sclater, J. G., and Christie, P. A. F. (1980) Continental stretching: An explanation of the post mid-Cretaceous subsidence of the central North Sea Basin. J. Geophys. Res., 85, 3711-3739

Sclater, J. G., and Francheteau, J. (1970) The implications of terrestrial heat flow observations on current tectonic and geochemical models of the crust and upper mantle of the earth. Geophys. J. R. Astr. Soc, 20, 509-542

Sclater, J. G., Meinke, L., Bennett, A., and Murphy, C. (1985) The depth of the ocean through the Neogene. In Geological Society of America Memoir 163: The Miocene Ocean, ed. Kennett, J. P., 1-19

Scrutton, R. A. (1985) Modelling of magnetic and gravity anomalies at Goban Spur, Northeast Atlantic. In Initial Reports of the Deep Sea Drilling Project, V. 80, eds. de Graciansky, P. C., Poag, C. W., Washington, D.C.: U.S. Government Printing Office, 1141-1151

Scrutton, R. A., Stow, D. A. V. (1984) Seismic evidence for Early Tertiary bottom-current controlled deposition in the Charlie Gibbs Fracture Zone. Marine Geol., 56, 325-334

Shaw, C. A. (1989) Mass Balanced Paleogeographic Modeling: Examples from the Western North Atlantic Ocean and Gulf of Mexico. Boulder, CO: Ph.D. Thesis, University of Colorado. 381 pp

Shaw, C. A., and Hay, W. W. (1989) Mass-balanced paleogeographic maps: Modeling program and results. In Quantitative Dynamic Stratigraphy, ed. Cross, T.A., Englewood Cliffs, N.J.: Prentice-Hall, Inc., 277-291

Shor, A. N., and Poore, R. Z. (1979) Bottom currents and ice rafting in the North Atlantic: Interpretation of Neogene depositional environments of Leg 49 cores. In Initial Reports of the Deep Sea Drilling Project, V. 49:, eds. Luyendyk, B. P., Cann, J. R., Washington, DC: U.S. Government Printing Office, 859-872

Skogseid, J., and Eldholm, O. (1987) Early Cenozoic crust at the Norwegian continental margin and the conjugate Jan Mayen Ridge. J. Geophys. Res., 92, 11471-11491

Smythe, D. K. (1983) Færoe-Shetland escarpment and continental margin north of the Færoes. In NATO Conference Series, Series IV: Marine Sciences, V. 8 Structure and Development of the Greenland Scotland Ridge: New Methods and Concepts, eds. Bott, M. H. P., Saxov, S., Talwani, M., and Thiede, J., New York: Plenum Press. 109-120

Snelling, N. J. (1985) An interim time-scale. In Geological Society (London) Memoir 10: The Chronology of the Geological Record, ed. Snelling, N.J., Oxford: Blackwell Scientific Publications, 261-265

Southam, J. R., and Hay, W. W. (1981) Global sedimentary mass balance and sea level changes. In The Sea, V. 7, The Oceanic Lithosphere, ed. Emiliani, C., New York: Wiley-Interscience, 1617-1684

Spiegler, D., Jansen, E. (1989) Planktonic foraminifer biostratigraphy of Norwegian Sea sediments: ODP Leg 104. In Proceedings of the Ocean Drilling Program, Scientific Results, V. 104, eds. Eldholm, O., Thiede, J., and Taylor, E., College Station, TX: Ocean Drilling Program, 681-737

Srivastava, S. P. (1978) Evolution of the Labrador Sea and its bearing on the early evolution of the North Atlantic. Geophys. J. R. Astr. Soc, 52, 313-357

Srivastava, S. P. (1985) Evolution of the Eurasian Basin and its implications to the motion of Greenland along the Nares Strait. Tectonophysics, 114, 29-53

Srivastava, S. P., and Arthur, M. A. (1989) Tectonic evolution of the Labrador Sea and Baffin Bay: Constraints imposed by regional geophysics and drilling results from Leg 105. In Proceedings of the Ocean Driling Program, Scientific Results, V. 105, eds. Srivastava, S. P., Arthur, M. A., and Clement, B., College Station, TX: Ocean Drilling Program, 989-1009

Srivastava, S. P., Arthur, M. A., Clement, B., et al., (1987) Proceedings of the Ocean Drilling Program, Part A - Initial Report, V. 105. College Station, TX: Ocean Drilling Program. 917 pp

Srivastava, S. P., and Tapscott, C. R. (1986) Plate kinematics of the North Atlantic. In Geology of North America, V. M: The Western North Atlantic Region, eds. Vogt, P. R., and Tucholke, B. E., Boulder, CO: Geological Society of America, 379-404

Srivastava, S. P., Verhoef, J., and Macnab, R. (1988a) Results from a detailed aeromagnetic survey across the northeast Newfoundland margin, Part I: Spreading anomalies and relationship between magnetic anomalies and the ocean-continent boundary. Marine and Petrol. Geol., 5, 306-323

Srivastava, S. P., Verhoef, J., and Macnab, R. (1988b) Results from a detailed aeromagnetic survey across the northeast Newfoundland margin, Part II: Early opening of the North Atlantic between the British Isles and Newfoundland. Marine and Petrol. Geol., 5, 324-337

Steckler, M. S., and Watts, A. B. (1978) Subsidence of the Atlantic-type continental margin off New York. Earth and Planet. Sci. Lett., 41, 1-13

Steele, J. H., Barrett, J. R., and Worthington, L. V. (1962) Deep currents south of Iceland. Deep-Sea Res., 9, 465-474

Stow, D. A. V., and Holbrook, J. A. (1984) Hatton Drift contourites, northeast Atlantic, Deep Sea Drilling Project Leg 81. In Initial Reports of the Deep Sea Drilling Project, V. 81, eds. Roberts, D. G., Schnitker, D., Washington, D.C.: U.S. Government Printing Office, 1217-1244

Stow, D. A. V., and Piper, D. J. W. (1984) Deep-water fine-grained sediments: Facies models. In Geological Society of America Special Publication 15: Fine-Grained Sediments: Deep-Water Processes and Facies. eds. Stow, D. A. V., and Piper, D. J. W., 611-647

Surlyk, F., Clemmensen, L. B. and Larsen, H. C. (1981) Post-Paleozoic evolution of the east Greenland continental margin. In Canadian Society of Petroleum Geologists Memoir 7In Geology of the North Atlantic Borderlands, 611-645

Swift, J. H., Aagaard, K., and Malmberg, S.-A. (1980) The contribution of the Denmanrk Strait overflow to the deep North Atlantic. Deep-Sea Res., 27, 29-42

Talwani, M., and Eldholm, O. (1977) Evolution of the Norwegian-Greenland Sea. Geol. Soc. Am. Bull., 88, 969-999

Talwani, M., Udintsev, G., et al., (1976) Initial Reports of the Deep Sea Drilling Project, V. 38. Washington, D.C.: U.S. Government Printing Office. 1256 pp

Thiede, J. (1978) Pelagic sedimentation in immature ocean basins. In NATO Advanced Study Institutes Series C: Mathematical and Physical Sciences, V. 37: Tectonics and Geophysics of Continental Rifts, ed. Ramberg, I. B., and Neumann, E.-R.,Dordrecht, Holland: D. Riedel Publishing Co., 237-248

Thiede, J. (1980) Palaeo-oceanography, margin stratigraphy and palaeophysiography of the Tertiary North Atlantic and Norwegian-Greenland Seas . Phil. Trans. R. Soc. London, Ser. A, 294, 177-185

Thiede, J., and Eldholm, O. (1983) Speculations about the paleodepth of the Greenland-Scotland Ridge during the Late Mesozoic and Cenozoic times. In NATO Conference Series, Series IV: Marine Geology, V. 8: Structure and Development of the Greenland-Scotland Ridge. eds. Bott, M. H. P., Saxov, S., Talwani, M., and Thiede, J., New York: Plenum Press, 445-456

Thiede, J., Eldholm, O., and Taylor, E. (1989) Variability of Cenozoic Norwegian-Greenland Sea paleoceanography and northern hemisphere paleoclimate. In Proceedings of the Ocean Drilling Program, Scientific Results, V. 104, eds. Eldholm, O., Thiede, J., and Taylor, E. College Station, TX: Ocean Drilling Program, 1067-1118

Tucholke, B. E. (1988) Sediment distribution. In Geophysical Atlas of the North Atlantic Between 50° to 72° N and 0° to 65° W, eds. Srivastava, S. P., Voppel, D., and Tucholke, B., Hamburg: Deutsches Hydrographisches Institut, 9-12

Tucholke, B. E., and McCoy, F. W. (1986) Paleogeographic and paleobathymetric evolution of the North Atlantic Ocean. In The Geology of North America, V. M: The Western North Atlantic Region. eds. Vogt, P. R., and Tucholke, B. E., Boulder, CO: Geological Society of America, 589-602

Tucholke, B. E., and Vogt, P. R. (1979) Western North Atlantic: Sedimentary evolution and aspects of tectonic history. In Initial Reports of the Deep Sea Drilling Project, eds. Tucholke, B. E., and Vogt, P. R., Washington, D. C.: U. S. Government Printing Office, 791-825

Unternehr, P. (1982) Étude structurale et cinématique de la mer de Norvege et du Groenland. Évolution du microcontinent de Jan Mayen. Thése 3éme Cycle, Université de Bretagne Occidentale, Brest, France, 228 pp

Vail, P. R., Mitchum, R. M., Jr., and Thompson, S., III. (1977) Global cycles of relative changes of sea level. American Association of Petroleum Geologists Memoir 26: Seismic Stratigraphy - Applications to Hydrocarbon Exploration, ed. Payton, C. E., 83-97

Veizer, J., and Jansen, S. L. (1979) Basement and sedimentary recycling and continental evolution. J. Geol., 87, 341-370

Veizer, J., and Jansen, S. L. (1985) Basement and sedimentary cycling - 2: Time dimension to global tectonics. J. Geol., 93, 625-664

Verhoef, J., Roest, W. R., and Srivastava, S. P. (1989) Plate reconstructions and gridded data: A new tool in deciphering correlations across oceans. EOS, 70(21), 614, 618

Verhoef, J., Usow, K. H., and Roest, W. R. (1990) A new method for plate reconstructions: The use of gridded data. Computers & Geosciences, 16(1), 51-74

Vink, G. E. (1982) Continental rifting and the implications for the plate tectonic reconstructions. J. Geophys. Res., 87, 10677-10688

Vogt, P. R. (1972) The Faeroe-Iceland-Greenland aseismic ridge and the western boundary undercurrent. Nature, 239. 79-81

Vogt, P. R. (1986) Geophysical and geochemical signatures and plate tectonics. In The Nordic Seas, ed. Hurdle, B. G., Berlin: Springer-Verlag, 413-662

Vogt, P. R., Avery, O. E. (1974) Detailed magnetic surveys in the Northeast Atlantic and Labrador Sea. J. Geophys. Res., 79, 9949-9959

Vogt, P. R., Johnson, G. L., and Kristjansson, L. (1980) Morphology and magnetic anomalies north of Iceland. J. Geophys., 47, 67-80

Wajsprych, B. (1992) The Late Devonian - Early Carboniferous mantle superplume concept: Its lithotectonic and tectonostratigraphic evidence in the Sudetes Mountains. In GEOMAR Report 15, Berichte - Reports, Geologisch-Paläontologisches Institut Universität Kiel, Nr. 57: Fourth International Conference on Paleoceanography, Short and Long-Term Global Cahnge: Records and Modelling, 21-25 September 1992, Kiel/Germany, Program & Abstracts. eds. Sarnthein, M., Thiede, J., and Zahn, R., Kiel, Germany: GEOMAR, 293

Warren, B. A. (1981) Deep circulation of the world ocean. In Evolution of Physical Oceanography, eds. Warren, B. A., and Wunsch, C., Cambridge, MA: M.I.T. Press, 6-41

Weber, J. R. (1990) The structures of the Alpha Ridge, Arctic Ocean and Iceland-Faeroe Ridge, North Atlantic: Comparisons and implications for the evolution of the Canada Basin. Marine Geol., 93, 43-68

Wessel, P., and Smith, W. H. F. (1991) Free software helps map and display data. EOS Trans. AGU, 72, 441, 445-446

White, R. S. (1988) A hot-spot model for early Tertiary volcanism in the N Atlantic. In Geological Society Special Publication No. 39: Early Tertiary Volcanism and the Opening of the NE Atlantic. eds. Morton, A. C., and Parson, L. M., Oxford: Blackwell Scientific Publications, 3-13

White, R. S. (1989) Initiation of the Iceland Plume and Opening of the North Atlantic. In American Association of Petroleum Geologists Memoir 46: Extensional Tectonics and Stratigraphy of the North Atlantic Margins. eds. Tankard, A. J., and Balkwill, H. R., 149-154

White, R. S. (1992) Crustal structure and magmatism of North Atlantic continental margins. J. Geol. Soc., 149, 841-854

White, R. S., Spence, G. D., Fowler, S. R., McKenzie, D. P., Westbrook, G. K., and Bowen, A. N. (1987) Magmatism at rifted continental margins. Nature, 330, 439-444

Wold, C. N., and Hay, W. W. (1990) Estimating ancient sediment fluxes. Am. J. Sci., 290, 1069-1089

Wold, C. N., Hay, W. W., and Wilson, K. W. (1987) Reconstructed mass-age distributions of young sediment through the Phanerozoic. Geol. Soc. Am. Abstr. w. Prog., 19, 895

Wold, C. N., Shaw, C. A., DeConto, R. M., and Hay, W. W. (in press) Mass-balanced reconstruction of overburden. In Computerized Basin Analysis: The Prognosis of Energy and Mineral Resources, eds. Harff, J., and Merriam, D., New York: Plenum Press

Wold, C. N., Southam, J. R., and Hay, W. W. (1986) A global sedimentary systems function. EOS, 67, 959

Wolf, T. C. W., and Thiede, J. (1991) History of terrigenous sedimentation during the past 10 m.y. in the North Atlantic (ODP Legs 104 and 105 and DSDP Leg 81). Marine Geol., 101, 83-102

Woodruff, F., and Savin, S. M. (1989) Miocene deepwater oceanography. Paleoceanography, 87-140

Worthington, L. V. (1976) Johns Hopkins Series in Oceanography No. 6: On the North Atlantic Circulation. Baltimore, MD: Johns Hopkins University Press. 110 pp

Worthington, L. V., and Volkmann, G. H. (1965) The volume transport of the Norwegian Sea overflow water in the North Atlantic. Deep-Sea Res., 12, 667-676

Ziegler, P. A. (1982) Geological Atlas of Western and Central Europe. Amsterdam. Elsevier. 130 pp

Ziegler, P. A. (1988) Am. Assoc.Petrol. Geol. Memoir 43, Evolution of the Arctic-North Atlantic and the Western Tethys. 198 pp